

2010-04-29

Modification of Surfaces for Biological Applications

Eftim Milkani

Worcester Polytechnic Institute

Follow this and additional works at: <https://digitalcommons.wpi.edu/etd-dissertations>

Repository Citation

Milkani, E. (2010). *Modification of Surfaces for Biological Applications*. Retrieved from <https://digitalcommons.wpi.edu/etd-dissertations/216>

This dissertation is brought to you for free and open access by [Digital WPI](#). It has been accepted for inclusion in Doctoral Dissertations (All Dissertations, All Years) by an authorized administrator of Digital WPI. For more information, please contact wpi-etd@wpi.edu.

Modification of Surfaces for Biological Applications

By

Eftim Milkani

A Dissertation

Submitted to the Faculty of

WORCESTER POLYTECHNIC INSTITUTE

in fulfillment of the requirements for the

Degree of Doctor of Philosophy

in

Chemistry

March 26, 2010

APPROVED:

Dr. W. Grant McGimpsey,
Advisor

Dr. George A. Kaminski,
Committee Member

Dr. Christopher R. Lambert,
Committee Member

Dr. Tanja Dominko,
Committee Member

Dr. Kristin K. Wobbe,
Committee Member and
Head of Department

Dr. Stephen Lambert,
External Examiner

Abstract

Understanding and controlling the nature of interactions at interfaces between various materials and systems has always been of interest, but with the fast development and need of new technologies it has become crucial to employ these interactions for various applications that range from biosensing of analytes in bodily fluids and the environment, to the development of bio-compatible and bio-mimicking surfaces that can be used to successfully couple biological systems to artificial materials and also build models for understanding biological systems better. Self-assembled monolayers (SAMs) are organized molecular assemblies that are formed by spontaneous adsorption of a compound in solution to a surface. They can change the surface properties without the need of changing the physical properties of the bulk material. Formation of SAMs on different substrates was investigated and performed in the work described in the thesis to be used in the detection of nucleic acids and enzyme inhibitors, development of surfaces with anti-adhesive and anti-microbial properties, development of surfaces for directed and patterned cell adhesion, and the construction of artificial membranes that can be used for studying the interaction of membrane proteins and the discovery of new pharmaceuticals.

The surface of gold substrates was modified with alkanethiol compounds in order to attach biomolecules such as nucleic acids and proteins which allowed the modified surface to be used as a biosensor. Binding interactions were detected by electrochemical impedance spectroscopy and surface plasmon resonance. A surface resonance sensor provided a platform for the detection of DNA and RNA oligonucleotide sequences and also the detection of one-nucleotide mismatches from the hybridization these oligonucleotides. The same sensor platform, but with a different surface modification, was used to covalently attach an enzyme whose inhibitors are

used as therapeutic drugs and also as pesticides and nerve agents. The sensor was able to detect two of these inhibitors, which are used in the treatments of Alzheimer's disease, at a range of concentrations. This allowed the determination of binding affinity constants for the two inhibitors.

The surface of gold was modified with functional groups in order to obtain inert surfaces with anti-adhesive properties with regard to the attachment of proteins. These surfaces are of interest in generating bio-compatible medical implants that can resist rejection from the host's immune system and/or the formation of bacterial biofilms. The inert property was combined with anti-bacterial properties by attaching an antibiotic which is known to kill bacteria by binding to the cell membrane. Following characterization of gold surfaces by contact angle measurements, ellipsometry, grazing angle FT-IR, cyclic voltammetry and electrochemical impedance spectroscopy, the surface of glass substrates was modified with similar functional groups, by switching to a different coupling ligand for the substrate. Alkoxysilanes were used to modify the surface of glass, which can also be used to modify other materials, such as polymers and stainless steel.

Gold and glass surfaces were also modified with antibodies, other proteins, and other functional groups which favored or prevented cell adhesion. This led to the ability for patterned and directed adhesion, and differentiation of several cell lines. Preparation and chemical modification of magnetic beads and the ability to modify the bead surface created the possibility to grow and trap cells in a flow-through magnetic bioreactor, which will be used for the continuous production of metabolites and growth of tissue in a three-dimensional construct.

Modification of gold substrates also led to the construction of artificial phospholipid membranes, whose composition can be controlled and most importantly can be used for the insertion and characterization of membrane proteins on a two-dimensional platform. This will allow for characterization of ligand-protein and protein-protein interactions with surface characterization techniques such as surface plasmon resonance and electrochemical impedance spectroscopy.

The various surface modifications and applications described in this work underscore a general theme that the surface of many different materials can be modified by using the correct functional groups for the formation of the self-assembled monolayer on the substrate surface, thus obtaining the same surface properties without the need to change the physical and chemical properties of the bulk material.

Acknowledgements

I would like to sincerely thank my advisor, Professor W. Grant McGimpsey for his encouragement and opportunity in starting and pursuing my degree from the first time we met and thereafter. I have been very lucky to work in his lab and gain experience in various areas of research. I will always be grateful for this opportunity and the enduring support he has given me.

I would also like to thank Professor Christopher Lambert who has been my guidance in my research on a daily basis since he came to WPI. He has always been available to help me with anything and he has continuously challenged me to be a better and more thoughtful researcher. His inventiveness and excitement for new research ideas has been an inspiration. I would like to specifically thank him for his help and patience during the writing of manuscripts and this thesis.

I would also like to thank my previous colleague and friend in Professor McGimpsey's lab, now Dr. Peter Driscoll. He was always eager to teach me what he knew and help me if I had any questions or concerns. I'd like to thank previous members of Professor McGimpsey's lab that I worked closely with, Man Phewluangdee, Dr Nantanit Wanichacheva, Eugene Douglass, and Dr. Ernesto Soto. I would also like to thank particularly three new members of the lab, Aung Khaing, Fei Huang, and Morgan Stanton, who have helped me enormously with several parts of my research projects. In addition many thanks to the undergraduate students that have helped me with some of the projects described in this work, especially Anna Maziarz, John Blatton, Oljora Rezhdo and Roseann Gammal, whose help has been exceptional.

I would like to thank Dr. Sergi Morais for sharing his experience on immobilization of biomolecules on surfaces. He set in motion the biosensing projects in our lab.

Special thanks go to Dr. Yatao Liu who initiated my research experience on the biofilm project and was glad to share with me all his knowledge on bacterial studies.

I also deeply appreciate the priceless help and the collaboration I have received from Professors Tanja Dominko and Raymond Page, together with Mrs. Lucy Vilner on anything related to cell biology. It has been a wonderful and rewarding experience.

I am very grateful to Professor Terri Camesano for allowing me to use her lab space and equipment. Many thanks to Professors Marsha Rolle and George Pins for allowing me to use their fluorescent microscopes.

And last but not least, I would like to give thanks to the Department of Chemistry at Worcester Polytechnic Institute for their financial support for my degree through teaching assistantships. Especially I would like to thank Professors John MacDonald and Venkat Thalladi for always being eager to share their knowledge and experience whenever I ran into them with questions.

I gratefully acknowledge financial support my research throughout my time at WPI from the U.S. Army Medical Research and Materiel Command (USAMRMC) and the Telemedicine and Advanced Technology Research Center (TATRC).

Table of Contents

ABSTRACT	2
ACKNOWLEDGEMENTS	5
TABLE OF CONTENTS	7
LIST OF FIGURES	13
LIST OF TABLES	18
LIST OF SCHEMES	20
1. MAIN INTRODUCTION	21
1.1. Surface Chemistry.....	21
1.2. Controlling Surface Chemistry with Self-Assembled Monolayers.....	23
2. GENERAL EXPERIMENTAL METHODS.....	28
2.1. Materials	28
2.1.1. Reagents.....	28
2.1.2. Oligonucleotides.....	29
2.1.3. Proteins.....	29
2.1.4. Buffer solutions.....	29
2.1.5. Substrates	30
2.1.6. Cell lines and culture media	31
2.2. Modification of Gold Surfaces.....	31
2.2.1. Surface cleaning of gold slides.....	31
2.2.2. Alkanethiol SAMs	32
2.2.3. Carboxyl terminated alkanethiol SAMs.....	32
2.2.3. Amino terminated alkanethiol SAMs.....	32
2.3. Modification of Indium Tin Oxide, Glass and Polymer Surfaces	33
2.3.1. Indium tin oxide (ITO)	33
2.3.2. Glass	33
2.3.3. Polydimethylsiloxane (PDMS) and polyurethane (PU)	34

2.3.4. Polytetrafluoroethylene (PTFE)	34
2.4. Surface Reactions	35
2.4.1. Modification of terminal amines to carboxyl groups.....	35
2.4.2. Modification of terminal hydroxyls to carboxyl groups	35
2.4.3. Amide bond linkage on COOH-terminated surfaces.....	35
2.4.4. Amide bond linkage on NH ₂ -terminated surfaces.....	36
2.4.5. Covalent attachment of amines on hydroxyl terminated surfaces	36
2.4.6. Covalent immobilization of proteins on COOH-terminated surfaces.....	36
2.5. Surface Characterization.....	37
2.5.1. Contact angle goniometry.....	37
2.5.2. Ellipsometry	38
2.5.3. Grazing incidence infrared spectroscopy.....	38
2.5.4. Cyclic voltammetry	39
2.5.5. Electrochemical impedance spectroscopy.....	39
2.5.6. Surface plasmon resonance.....	40
2.5.7. Microscopy	40
2.6. Cell Culture.....	41
2.6.1. Jurkat cells	41
2.6.2. PC-12 cells	41
2.6.3. Neuroscreen-1 cells.....	42
2.6.4. SHSY5-Y cells.....	42
2.6.5. Mouse neo-natal fibroblasts	43
3. NUCLEIC ACID BIOSENSOR.....	44
3.1. Introduction	44
3.2. Experimental Details	52
3.2.1. Surface modification of gold slides with probe DNA	52
3.2.2. Modification of SPR sensing surface with probe DNA.....	53
3.2.3. Electrochemical characterization of gold slides	53
3.2.4. Surface plasmon resonance.....	55

3.3.	Results and Discussion	57
3.3.1.	Electrochemical characterization	57
3.3.2.	Surface plasmon resonance	64
3.3.3.	Effect of hybridization buffer on sensor performance	68
3.3.4.	Effect of flow rate and temperature on sensor performance	70
3.3.5.	Effect of mismatch site on sensor response	73
3.3.6.	DNA concentration	75
3.3.7.	RNA oligonucleotide detection	78
3.3.8.	Surface coverage of probe DNA.....	79
3.4.	Summary and Conclusions	82
3.5.	Practical Implementations and Future Work	84
4.	ENZYME-BASED BIOSENSOR.....	88
4.1.	Introduction.....	88
4.2.	Experimental Details	92
4.2.1.	Surface modification of gold surface on SPR sensing modules	92
4.2.2.	Immobilization of AChE	93
4.2.3.	AChE activity assay.....	93
4.2.4.	Imaging of AChE activity assay	94
4.2.5.	Surface plasmon resonance.....	94
4.3.	Results and Discussion	95
4.3.1.	Immobilization of AChE onto the COOH terminated SAM.....	95
4.3.2.	Enzyme activity and surface coverage	98
4.3.3.	Surface plasmon resonance.....	101
4.4.	Summary and Conclusions	104
4.5.	Practical Implementations and Future Work	106
5.	BIOFILM RESISTANT SURFACES	109
5.1.	Introduction	109
5.2.	Experimental Details	118
5.2.1.	Preparation of Dabco-C16.....	118

5.2.2.	Bacterial culture.....	118
5.2.3.	Bacterial attachment assay	119
5.2.4.	Biofilm assay	120
5.2.5.	Live/Dead staining.....	120
5.2.6.	Imaging with fluorescence microscopy	121
5.3.	Results and Discussion	124
5.3.1.	Surface characterization SAM-modified gold slides.....	124
5.3.2.	Surface characterization of SAM-modified glass slides.....	130
5.3.3.	Protein adhesion assay	130
5.3.4.	Bacterial attachment and biofilm assays	132
5.3.5.	Covalent attachment of daptomycin	136
5.4.	Summary and Conclusions	141
5.5.	Practical Implementations and Future Work	141
6.	INTERFACING SURFACES WITH BIOLOGICAL SYSTEMS.....	149
6.1.	Introduction	149
6.2.	Experimental Details	152
6.2.1.	Microcontact printing (μ CP).....	152
6.2.2.	Preparation of magnetic fluid.....	153
6.2.3.	Preparation of magnetic agarose beads.....	153
6.2.4.	Chemical modification of magnetic agarose beads	154
6.2.5.	Coating of agarose magnetic beads with protein.....	155
6.3.	Results and Discussion Part I: Modification of Substrates	156
6.3.1.	Gold.....	156
6.3.2.	Indium tin oxide	157
6.3.3.	Glass	164
6.3.4.	Stainless steel	164
6.3.5.	Polymer substrates.....	166
6.3.6.	PTFE (Teflon).....	166
6.4.	Result and Discussion Part II: Differentiation of Neuronal Cells on Modified Surfaces	168

6.4.1. Microcontact printing	168
6.4.2. Differentiation of Neuroscreen-1 on a surface pattern	169
6.5. Result and Discussion Part III: Trapping Cells in Suspension with Magnetic Agarose Beads	172
6.5.1. Preparation of the magnetic agarose beads.....	172
6.5.2. Surface modification of agarose beads	173
6.5.3. Using antibodies for cell immobilization.....	175
6.5.4. Attaching cells to agarose beads.....	178
6.5.5. Trapping cells in a magnetic flow-through bioreactor	181
6.5.6. Growing tissue in suspension on a magnetically stabilized support	184
6.6. Summary and Conclusions	187
6.7. Practical Implementations and Future Work	189
7. HYBRID AND BILAYER MEMBRANES	193
7.1. Introduction	193
7.2. Experimental Details	200
7.2.1. Preparation of lipid vesicles.....	200
7.2.2. Transmission electron microscopy (TEM) imaging	201
7.2.3. Amide bond linkage on COOH and NH ₂ terminated surfaces	201
7.2.4. Electrochemical characterization of hybrid and bilayer membranes	202
7.2.5. Formation of hybrid and bilayer membranes and protein incorporation.....	203
7.2.6. Assessment of protein activity	204
7.3. Results and Discussion	205
7.3.1. Hydrophobic alkanethiol monolayer characterization	205
7.3.2. Lipid vesicles	207
7.3.3. Formation of hybrid membrane on hydrophobic alkanethiol SAMs	208
7.3.4. Formation of bilayer membrane on COOH terminated SAM	213
7.3.5. Incorporation of a lipid-anchored protein into the membrane	215
7.3.6. Determination of AChE coverage on the hybrid membrane	222
7.4. Summary and Conclusions	223

7.5. Practical Implementations and Future Work	224
8. FINAL CONCLUSIONS	236
9. REFERENCES	239

List of Figures

Figure 1.1. Schematic representation of biosensors	22
Figure 1.2. Schematic diagram of an ideal self-assembled monolayer	25
Figure 3.1. Surface plasmon resonance	46
Figure 3.2. Surface plasmon resonance curve	47
Figure 3.3. Depiction of the SPR sensing surface.....	51
Figure 3.4. Diagram of the equivalent circuit used to fit the impedance spectroscopy data	54
Figure 3.5. Schematic drawing of the SPR experimental set-up	56
Figure 3.6. Cyclic voltammograms of bare gold and modified gold slides	58
Figure 3.7. Electrochemical impedance spectra of gold slides recorded in the form of Nyquist plots	61
Figure 3.8. Depiction of the changes on the gold surface after each modification step.....	63
Figure 3.9. Comparison of SPR response when running solutions of 1 μM non-complementary (control) and 1 μM complementary (FM) target DNA strands over the sensor	65
Figure 3.10. Hybridization/denaturation steps for the FM oligonucleotide at different cycles...67	67
Figure 3.11. Refractive index change after hybridization of 1 μM P11 (hollow bars) and FM (full bars) target DNA strands at different hybridization buffer concentrations (corresponding to 0.15, 0.30, 0.45, 0.60, and 0.75 M NaCl concentration, respectively)	68
Figure 3.12. Refractive index change after hybridization of 1 μM P11 (hollow bars) and FM (full bars) target DNA strands as a function of (A) flow rate; (B) temperature	71
Figure 3.13. Overlapped SPR sensorgrams obtained after flowing 1 μM P11, P1, P21, and FM target DNA oligonucleotides over the sensor surface	73
Figure 3.14. Hybridization of the target DNA strands (blue) to the probe strand (black) on the sensor surface.....	75
Figure 3.15. Refractive index change after hybridization of P11, P1, P21, and FM target DNA strands at different concentrations	76

Figure 3.16. Refractive index change after hybridization of the full complementary RNA strand at different concentrations	78
Figure 3.17. Refractive index change after hybridization of the full complementary Let 7a DNA strand at different concentrations	87
Figure 4.1. Hydrolysis of acetylcholine by acetylcholinesterase	88
Figure 4.2. The chemical structures of the reversible carbamate AChE inhibitors used in this study	90
Figure 4.3. Method used for immobilization of AChE on the surface	96
Figure 4.4. Measuring acetylcholinesterase activity on the surface.....	99
Figure 4.5. Calibration plot of absorbance at 410 nm for different amounts of AChE enzyme diluted in the activity assay solution (1 mM acetylthiocholine iodide and 500 μ M DTNB in PB, pH 8.0).....	100
Figure 4.6. Schematic drawing of the ideal hexagonal packing of AChE molecules on the surface	101
Figure 4.7. Normalized refractive index change obtained for different neostigmine and eserine concentrations	102
Figure 4.8. Schematic drawing of inhibition of the AChE active site by neostigmine	103
Figure 5.1. Images of bacterial biofilms. (Top) Scanning electron micrograph of a staphylococcal biofilm on an indwelling medical device. Bar, 20 μ m. (Bottom) Fluorescent image of a propidium iodide stained <i>Staphylococcus epidermidis</i> biofilm	113
Figure 5.2. Chemical structures of Dabco-C16 and ODMA	116
Figure 5.3. Chemical structure of daptomycin	117
Figure 5.4. Chemical structures of a cyanine dye and propidium iodide.....	121
Figure 5.5. <i>Staphylococcus epidermidis</i> bacterial cells stained with the Live/Dead kit.....	122
Figure 5.6. Bacterial cells adhered to DDT SAM stained for different time periods	123
Figure 5.7. Titration of Live/Dead kit	123
Figure 5.8. Conformation of the formation of COOH on NH ₂ -terminated surface treated with succinic anhydride by grazing IR spectroscopy	126

Figure 5.9. Grazing IR spectra showing the attachment of a PEG tether on the carboxyl terminated surface, followed by attachment of an amino containing compound, butylamine ...	129
Figure 5.10. Fluorescent microscope images of <i>Staphylococcus epidermidis</i> biofilms grown on SAMs that favor cell attachment and biofilm formation	134
Figure 5.11. Fluorescent microscope images of <i>Staphylococcus epidermidis</i> biofilms grown on SAMs that do not favor cell attachment and slow or block biofilm formation.....	135
Figure 5.12. Viability of suspended cells to daptomycin in solution by (top) live/dead assay and (bottom) agar plating	137
Figure 5.13. Viability of adhered cells to daptomycin in solution by (top) live/dead assay and (bottom) agar plating	139
Figure 5.14. Fluorescent microscope images of <i>Staphylococcus epidermidis</i> biofilms grown on glass, APTMS, and daptomycin crosslinked to APTMS through a PEG spacer	140
Figure 5.15. The different antimicrobial compounds that will be attached to the surface	143
Figure 5.16. Chemical structure of Amphotericin B	144
Figure 5.17. Several bacterial quorum sensing molecules	146
Figure 5.18. Depiction of the model that will be used to study biofilm formation in a microfluidic channel	148
Figure 6.1. Chemical structure of a trialkoxysilane	158
Figure 6.2. Cyclic voltammograms of bare and ITO coated with a decyltrimethoxy silane SAM	160
Figure 6.3. Grazing IR spectra of dodecanethiol SAM on gold and decyl trimethoxysilane SAM on ITO	161
Figure 6.4. Receding contact angle of PTFE; before (left) and after (right) surface modification	167
Figure 6.5. Microcontact printed pattern of a COOH-terminated alkanethiol on gold visualized with a fluorescent antibody.....	169
Figure 6.6. Grazing IR spectra of mixed SAMs of MUA and MUO at a 1 to 10 molar ratio in solution, prepared by solution deposition and microcontact printing	170

Figure 6.7. AUTMS coating (right) mimics collagen coating (left), which is typically used as substrate for growing and differentiating neuronal cell lines	171
Figure 6.8. Neuroscreen-1 cells differentiated on an amino-terminated surface pattern on gold.....	171
Figure 6.9. Neuroscreen-1 cells differentiated on AUTMS surface pattern on glass	172
Figure 6.10. Phase contrast image of the magnetic agarose beads	173
Figure 6.11. Agarose beads coated with a fluorescent antibody	174
Figure 6.12. Immobilized Jurkat cells on ITO slides.....	176
Figure 6.13. Immobilization of jurkat cells on gold slides. Gold slides were derivatized with 11-mercapto undecanoic acid (MUA) and 11-mercapto-1-undecanol (MUO) at different ratios: (A) 100% MUA; (B) 100% MUO; (C) 1:10 MUA:MUO; (D) 1:100 MUA:MUO	177
Figure 6.14. Phase contrast images at (A) 100X and (B) 400X magnification, showing the immobilization of Jurkat cells on magnetic agarose beads	178
Figure 6.15. Schematic diagram of the flow-through bioreactor system.....	181
Figure 6.16. Continuous flow-through magnetic bioreactor system assembled in the incubator (left) and detailed drawing of continuous flow-through magnetic bioreactor chamber (right).....	182
Figure 6.17. Phase contrast images showing the immobilization of Jurkat cells on magnetic agarose beads after 6 days incubation in the flow-through bioreactor.....	183
Figure 6.18. Schematic diagram of the beads suspended in a glass tube used for growing ECM	186
Figure 6.19. Phase contrast images at (A) 40X and (B) 400X magnification, showing the gel-like membrane grown on the magnetic bead ring	186
Figure 6.20. Histology staining of the fibroblast tissue grown in the test tube with a magnet.....	187
Figure 6.21. The chemical structures of the different trialkoxysilanes that will be used for coating glass coverslips	191
Figure 7.1. Schematic drawing of (A) a phospholipid and (B) a phospholipid vesicle	194

Figure 7.2. Schematic drawing of the formation of a hybrid membrane (left) or a bilayer membrane (right)	197
Figure 7.3. Diagram of lipid-anchored proteins on a hybrid membrane (left) and trans-membrane proteins on a bilayer membrane (right)	199
Figure 7.4. Chemical structure of DMPC (1,2-dimyristol-rac-glycero-3-phosphocholine)	200
Figure 7.5. Diagram of the equivalent circuit used to fit the impedance spectroscopy data	202
Figure 7.6. TEM image of the DMPC lipid vesicles	208
Figure 7.7. Capacitance of an octadecanethiol self-assembled monolayer (SAM) on the gold slide monitored sequentially over time	209
Figure 7.8. Alkanethiol chain length dependence of capacitance before and after the formation of the hybrid membrane	212
Figure 7.9. Capacitance of an 11-mercapto undecanoic acid (MUA) SAM on the gold slide monitored sequentially over time	214
Figure 7.10. Calibration of GPI-anchored AChE (from human red blood cells) activity in solution with or without 0.1% (v/v) Triton X-100 detergent.....	216
Figure 7.11. Strategy for insertion of a lipid-anchored AChE enzyme on a hybrid membrane and confirmation of the presence on the surface using an AChE activity assay	218
Figure 7.12. Insertion of AChE on a bilayer membrane	219
Figure 7.13. Red blood cell AChE activity assay on the surface	223
Figure 7.14. Activation of insulin receptor tyrosine kinase.....	226
Figure 7.15. Strategies for incorporation of tyrosine kinase (TK) construct on a planar bilayer membrane	227
Figure 7.16. The tyrosine assay activity determined with the free protein (K only), vesicles with no protein (V only), and protein incorporated in vesicles (V+K)	228
Figure 7.17. The tyrosine assay activity determined with the free protein (concentrations given on the x-axis), vesicles with no protein (V only), and protein incorporated in vesicles (V+K).....	229
Figure 7.18. The tyrosine assay activity determined with the free protein (K only)	231

Figure 7.19. The tyrosine assay activity determined with no kinase in solution (V only), the free protein (K only) and the protein incorporated in vesicles (V+K) at different temperatures.....	232
Figure 7.20. Strategy for the formation of a phospholipid self-assembled monolayer on gold.....	234

List of Tables

Table 3.1. Sequence of oligonucleotides used with the biosensor described in this work	51
Table 3.2. The hybridization buffer concentrations used in this study and the corresponding NaCl concentration in each of them	57
Table 3.3. Charge-transfer resistance (R_{CT}) of the gold slides after each surface modification step	62
Table 3.4. Charge-transfer resistance (R_{CT}) obtained after hybridization of probe DNA with the target oligonucleotides on the gold slides	64
Table 3.5. Binding rates of target oligonucleotides at 1 μ M concentration, obtained from Figure 3.13.....	74
Table 3.6. Binding affinities and maximum coverage of target oligonucleotides obtained from Figure 3.15, using the Hanes-Woolf equation.....	77
Table 4.1. Contact angles after each surface modification step. Solutions of 0.01 M H_2SO_4 and 0.01 M NaOH were used as pH 2 and pH 12 solutions, respectively	96
Table 4.2. Reversible acetylcholinesterase inhibitors used as medications	107
Table 5.1. Worldwide usage of medical implants in 2004	110
Table 5.2. Contact angle and ellipsometry thickness of alkanethiol SAMs with various terminal groups on gold	124
Table 5.3. Contact angles of an amino-terminated surface before and after incubating with an aqueous solution of succinic anhydride overnight at room temperature	125
Table 5.4. Contact angles on gold after each modification step during the covalent attachment of daptomycin.....	129

Table 5.5. Compounds and respective structures used for the modification of glass slides and contact angles of deionized water measured after the surface modification.....	131
Table 5.6. Ellipsometry thickness of SAM modified gold slides before and after incubation in 15% fetal bovine serum in DMEM cell culture growth medium	132
Table 5.7. Surface cell density on modified gold surfaces after exposing to a 2×10^7 bacteria/mL suspension of bacterial cells in Tris buffer at 37 °C for 1 hour	133
Table 5.8. Surface cell density after exposing modified glass surfaces to a 2×10^7 cells/mL suspension of bacteria in Tris buffer for 1 hour at 37 °C.....	136
Table 6.1. Contact angles of treated ITO substrates	159
Table 6.2. Contact angles of treated ITO substrates incubated at different times in a 1% (v/v) solution of decyl trimethoxysilane in anhydrous toluene containing 5 μ L/mL butylamine as catalyst	160
Table 6.3. Chemical structures of alkoxysilanes with simple functional groups	162
Table 6.4. Chemical structures of alkoxysilanes with complex functional groups	163
Table 6.5. Contact angles of ITO and glass substrates coated with a number of alkoxysilanes.....	165
Table 6.6. Contact angles of PDMS, polyurethane and polystyrene coated with APTMS	166
Table 6.7. Contact angles of PTFE surfaces before and after surface modification.....	167
Table 6.8. Jurkat cell immobilized on magnetic agarose beads in cell culture flasks.....	180
Table 6.9. Jurkat cells in the flow-through bioreactor	184
Table 7.1. Average water contact angles of dodecanethiol (DDT), tetradecanethiol (TDT) and octadecanethiol SAMs.....	206
Table 7.2. Average film thickness measured by ellipsometry of dodecanethiol (DDT), tetradecanethiol (TDT) and octadecanethiol SAMs.....	206
Table 7.3. Average capacitance values for dodecanethiol (DDT), tetradecanethiol (TDT) and octadecanethiol SAMs measured in sequence before and after formation of the hybrid bilayer membrane as shown in Figure 7.4.....	211

Table 7.4. Capacitance of the alkanethiol monolayer ($C_{S_{AM}}$), hybrid membrane (C_{HB}) and the calculated capacitance (C_{Lipid}) and thickness of the lipid monolayer 213

Table 7.5. Luminescence decrease and ATP consumption for the kinase concentrations used in Figure 7.17 (from 100 – 3.3 $\mu\text{g/mL}$) 230

List of Schemes

Scheme 5.1. Modification of terminal amines to carboxyl groups on the surface 125

Scheme 5.2. Covalent attachment of Dabco-C16 on OH-terminated surface..... 127

Scheme 5.3. Covalent attachment of daptomycin on the surface 128

Scheme 6.1. Modification of glass surface by piranha cleaning 164

Scheme 6.2. Modification of hydroxyls to carboxyl groups on agarose beads 174

1. Main Introduction

1.1. Surface chemistry

Nanotechnology, or the study of materials on the molecular scale, is a broad research field with numerous applications that range from energy production and storage, to new types of electronic devices, to healthcare. One area of nanotechnology that has received considerable interest in the past two decades is molecular level surface functionalization. Chemical surface modification, where a chemical bond is formed between the underlying material and the functionalizing unit, can be used to control surface properties and provide surface utility that the initial substrate does not possess. This allows for the engineering of materials which already have the desired bulk properties (*e.g.* density, strength, flexibility, cost) to be combined with desirable surface properties (*e.g.* hydrophobicity, biocompatibility, electrical conductivity, chemical reactivity or inertness). The development of a chemical ‘toolbox’, that allows for a single substrate to be modified with a large selection of different functionalities, offers many important and far ranging advantages in this field.

Surface chemistry refers to the chemical properties and reactivity of the surface on any substrate. Surfaces or interfaces between different media are the site of many interactions which can be employed for biosensing applications and also are essential for living organisms. Biosensing applications involve the use of biomolecules such as DNA and proteins, and even microorganisms as a substrate for detection of inorganic and organic analytes of interest including other DNA, proteins, and microorganisms. The definition for a biosensor is generally accepted in the literature as a self contained integrated device consisting of a biological

recognition element which is interfaced with a chemical sensor.¹ A schematic representation of biosensors is shown in Figure 1.1. Biosensors exploit the interaction properties of biomolecules

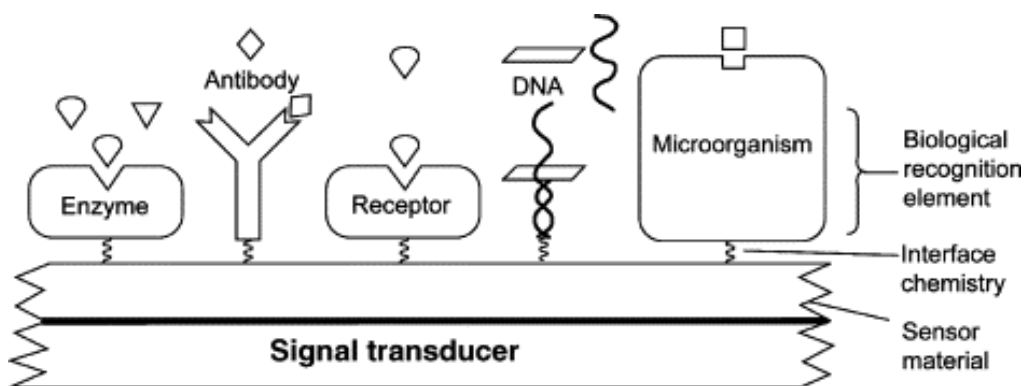


Figure 1.1. Schematic representation of biosensors.

which have specific and vital roles for many organisms. However, in their natural environment, these potential biosensing elements are not attached to a substrate material as those used in biosensors. Prior to using biomolecules as biosensors, it is important to know the substrate surface properties and their effect on the function of the biomolecules once they are attached to the surface. In addition, the attachment or immobilization of biomolecules needs to be done in ways that do not denature them and destabilize their function. Therefore, the knowledge of the surface chemical properties of the substrate and the ability to control or change the surface chemistry is crucial to provide a suitable environment for the function of the biomolecules bound to the surface.

Interactions at the surface or interface are essential to living organisms and their survival in their environments. Interfaces, such as cell membranes provide protection from the outside environment, but at the same time they control the flow of nutrients and metabolites, and host

proteins responsible for cell signaling and communication. Some of these cell membrane proteins also allow the cells to adhere to a solid surface, such as extra-cellular matrix or a synthetic material. In patients with medical implants, surface attachment is a survival mechanism for pathogenic microorganisms, where synthetic materials provide a substrate for the microorganisms to escape the host immune system and cause infections. However, the host organism immune system can also respond to these surfaces in a defensive way resulting in rejection of a medical implant. In these cases the implant surface needs to be an inert surface that does not allow attachment of microorganisms or other biomolecules, and does not trigger the response of the immune system. In other cases, the implant is required to interact with specific cells, tissue, or organs in the host organisms. This means that the surface of the medical implant has to present itself to the cells it is in contact with as part of the extra-cellular matrix, or even cause a desired response on the host's cells. Therefore, by controlling the surface chemistry of medical implant materials, the response or non-response of the tissue surrounding it can be controlled as well. Most importantly, surface chemistry allows for changing of the chemistry of the most outer layer of a material, thus having no impact on the physical properties of the bulk material.

1.2. Controlling surface chemistry with self-assembled monolayers

The organization of components into patterns or structures without human intervention is known as self-assembly.² Molecular self-assembly is a strategy for structure building and modification at the atomic level, which involves designing molecules so that specific interactions cause them

to aggregate into desired structures. One example is the self-assembly of molecules on bulk surfaces, which is easily achieved, and has been extensively studied in the recent years. Atoms or molecules at the surface of a material experience a different environment from those in the bulk and thus have different free energies, electronic states, and reactivities.³ Bare surfaces of metals and metal oxides tend to adsorb organic materials readily, because these adsorbents lower the surface energy of the interface between the metal or metal oxide and the outer medium.⁴ Surface energy refers to the disruption of intermolecular or interatomic forces on the surface, thus bare surfaces are less energetically stable. The adsorption and/or bonding of molecules from the outer medium to the surface layer of atoms lowers the surface energy, by creating an environment similar to the bulk material for these atoms. If molecules with ligands or head groups that have specific affinities or reactivities for the substrate are present in the medium, they will spontaneously form a self-assembled monolayer (SAM) on the substrate surface. SAMs are organic assemblies formed by the adsorption of molecular constituents from solution or the gas phase onto the surface of solids.⁴ The higher the affinity of the head group of the SAM constituent, the more it is able to displace nonspecifically-adsorbed molecules, the more ordered the structure of the SAM will be. After the SAM has formed, the surface properties of the bulk material are substituted by those of the terminal functional group of the SAM (Figure 1.2). The ability of SAMs to modify the surface properties of solids can be potentially used in the study and development of surfaces with various properties and functions.

SAMs of alkanethiols on transition metal elements have been studied since the initial report of organic disulfide monolayers on gold by Nuzzo and Allara in 1983.⁵ Thiol compounds are well known to readily form monolayers on metals including gold, silver, platinum, copper, and

mercury.⁶ A typical monolayer preparation involves cleaning the substrate, exposure to a dilute alkanethiol solution in a common organic solvent, incubation of the substrate in the monolayer solution to allow for SAM organization, and film characterization. Compounds with alkyl chains of 10 to 16 carbons in length are often desired to maximize inter chain Van der Waals forces that

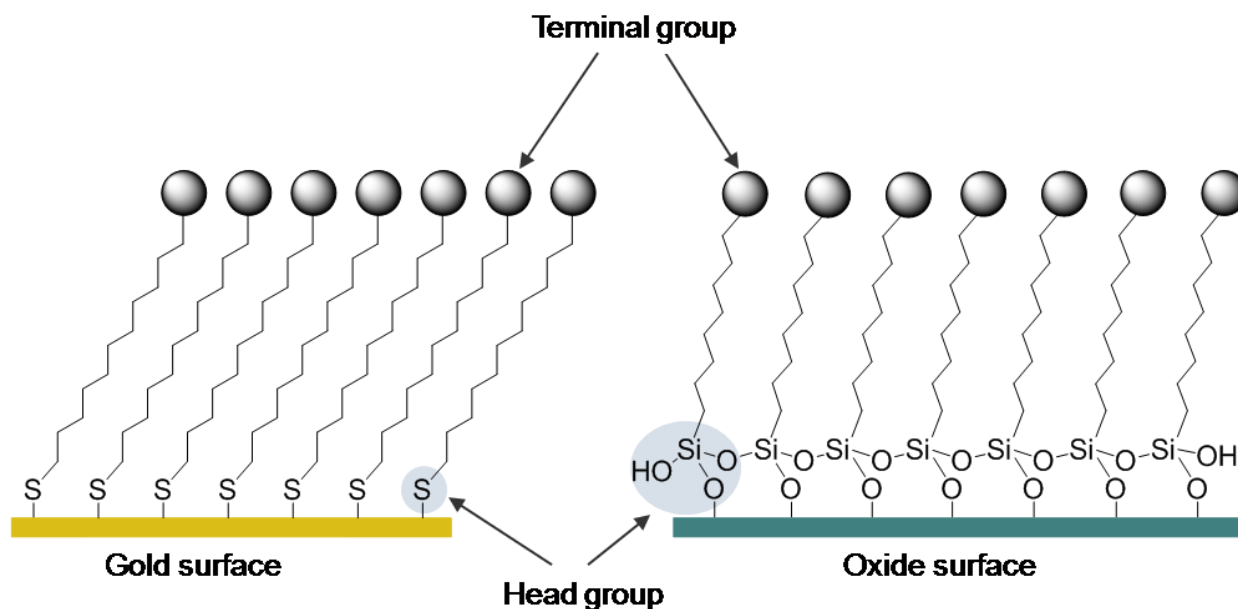


Figure 1.2. Schematic diagram of an ideal self-assembled monolayer (SAM) of an alkanethiol on the gold surface (left) and a trialkoxysilane on an oxide surface, such as indium tin oxide, silica, glass, or oxidized polymer surface (right).

organize and stabilize the film. Alkanethiols on gold are one of the most commonly studied SAMs due to their ease of preparation, high degree of stability, and unique level of control over surface properties. Planar gold substrates for monolayer preparation can either be obtained commercially or prepared by standard evaporation methods. Typically an adhesion layer of chromium or titanium is first deposited on a glass substrate to promote subsequent gold adhesion, as gold does not adhere well directly on glass, because it does not form an oxide layer

on its surface.⁶

Proper substrate pretreatment is essential in order to subsequently form a highly ordered monolayer with minimal defects. Gold is an inherently easily-contaminated substrate by organics and other contaminants which will readily adsorb to the surface when exposed to the atmosphere even for a short period of time. Since thiols have a very high affinity for gold, monolayers will form on contaminated gold surfaces as the thiols will displace, at least to some degree, impurities on the substrate. However, resulting films fail to possess the same degree of order and reproducibility as those prepared on properly pretreated substrates. Piranha etching is a standard method of pretreatment of metal substrates prior to monolayer deposition as piranha is an extremely strong oxidant and will remove any organic contaminants present on the surface (piranha is a mixture of 70 % (18 M) sulfuric acid and 30 % (35 % w/v) hydrogen peroxide). Following pretreatment monolayer deposition is accomplished through exposure of the pretreated substrate to a 1 to 5 mM solution of an alkanethiol in a common organic solvent (typically ethanol) overnight.

Alkoxysilanes form SAMs on oxide surface by covalent bonding with the free hydroxyl groups on the surface. One advantage of using alkoxysilanes is the variety of functional groups that can be incorporated into the molecule without affecting its overall stability. Formation of ordered alkoxysilane monolayers is more difficult to achieve due to the covalent nature of surface binding. However, they can modify a variety of substrates, such as glass, silica, indium tin oxide, polymers and theoretically any substrate that presents hydroxyl groups on the surface. Therefore, similar to gold, surface treatment is very important.

In the work described in this thesis the goal has been the modification of the surface of substrates and understanding of the surface chemistry that allows for the modification, with the final goal being the employment of the modified surface either for a biosensing application by coupling with surface characterization techniques or for direct use in applications where surface coatings with specific properties are required.

2. General Experimental Methods

2.1. Materials

2.1.1. Reagents

All chemicals and solvents were reagent grade or better and used as received. Potassium ferricyanide, 1,2-dimyristol-rac-glycero-3-phosphocholine (DMPC), acetylcholine chloride, neostigmine bromide, eserine, 6-mercapto-1-hexanol, 11-mercaptoundecanoic acid, 11-mercaptoundecanol, and triethylene glycol mono-11-mercaptoundecyl ether were purchased from Sigma-Aldrich (St. Louis, MO). 11-Amino-1-undecanethiol hydrochloride was purchased from Dojindo Molecular Technologies (Rockville, MD); SeaKem® LE agarose from Lonza (Walkersville, MD); polysorbate 80 from Mallinckrodt Baker (Phillipsburg NJ); soybean oil from Spectrum Ingredients (Petaluma, CA); NH₂-PEG-COOH (MW 2k Da) and mPEG-SH (MW 2k Da) and mPEG alkoxy silane (MW 2k Da) were obtained from Creative PEGWorks (Winston Salem, NC).

All alkoxy silane compounds (unless specified otherwise) were obtained from Gelest, Inc. (Morrisville, PA). Dodecanethiol, tetradecanethiol, octadecanethiol, N-hydroxysuccinimide (NHS), succinic anhydride, 1-ethyl-3-(3-dimethylaminopropyl) carbodiimide hydrochloride (EDC), sodium citrate, 5'-dithiobis-(2-nitrobenzoic acid) (DTNB), guanidine hydrochloride, choline chloride, tetra-n-propylammonium chloride, acetylthiocholine iodide, adenosine-5'-triphosphate (ATP) disodium salt and all other chemicals were purchased from Alfa Aesar (Ward Hill, MA). All aqueous solutions were prepared in deionized water which was obtained from a Millipore Synergy UV system (Billerica, MA).

2.1.2. Oligonucleotides

The thiol modified probe DNA oligonucleotide was obtained from Fidelity Systems, Inc. (Gaithersburg, MD). Unmodified target DNA and RNA oligonucleotides were purchased from Sigma Genosys (The Woodlands, TX). The target DNA and RNA oligonucleotides consisted of one full complementary strand, one non-complementary strand, and three one-mismatch complementary strands containing a single-nucleotide mismatch in the 5' end (P1), 3' end (P21), or middle of the sequence (P11). The non-complementary strand served as a non-thiolated control probe. The oligonucleotides were reconstituted in autoclaved DI water, at 1 mM concentration for the thiol-modified strand and 100 μ M for the unmodified target strands. RNA oligonucleotides were stored at -80 °C, whereas DNA oligonucleotides were stored at -20 °C.

2.1.3. Proteins

Acetylcholinesterase from electric eel (EC 3.1.1.7, type VI-S, 288 units/mg solid, MW 70 kDa), acetylcholinesterase from human erythrocytes (EC 3.1.1.7, amphiphilic form, 523 units/mg protein, 0.22 mg/mL, MW 80 kDa), and horseradish peroxidase (EC 1.11.1.7, type I, 113 units/mg solid, MW 44 kDa) were purchased from Sigma-Aldrich. Mouse monoclonal antibody to the human CD3 gene (CD3 antibody), mouse IgG_{2a} isotype control antibody (IgG_{2a} antibody), and Alexa Fluor 488 goat anti-mouse IgG antibody were obtained from Invitrogen (Carlsbad, CA).

2.1.4. Buffer solutions

Phosphate buffer (PB) was prepared at pH 7.0, 7.4, or 8.0 as a mixture of 10 mM sodium dihydrogenphosphate (NaH₂PO₄) and 10 mM sodium hydrogen phosphate (Na₂HPO₄) in

deionized water. The pH values of the phosphate buffer was set by mixing the 10 mM NaH_2PO_4 and 10 mM Na_2HPO_4 solutions while monitoring the pH of the mixture with a Model 225 pH meter from Denver Instruments (Bohemia, NY) until the desired pH value was reached.

Phosphate buffered saline (PBS) was prepared as a 138 mM sodium chloride (NaCl) and 2.7 mM potassium chloride (KCl) solution in 10 mM phosphate buffer at pH 7.4. Tris buffered saline (TBS) was prepared as a 150 mM NaCl and 20 mM Tris solution, pH 7.0 or 7.5. Hybridization buffer was prepared as a 20x concentrated stock solution (3.0 M NaCl, 0.3 M sodium citrate, pH 7.0). The pH of the hybridization buffer and TBS was adjusted by adding 5 M sodium hydroxide (NaOH) or 5 M hydrochloric acid (HCl), respectively, while monitoring the pH of the buffer. Carbonate buffer, pH 9.6, was prepared as a mixture of 100 mM sodium bicarbonate (NaHCO_3) and 100 mM sodium carbonate (Na_2CO_3) solutions.

2.1.5. Substrates

Gold substrates were purchased from Evaporated Metal Films (Ithaca, NY). They consisted of 1 mm thick float glass (75 mm \times 25 mm) coated on one side with 50 Å of a chromium layer followed by 1000 Å of gold. Indium tin oxide (ITO) substrates were obtained from Delta Technologies, Ltd. (Stillwater, MN). They consist of 0.7 mm thick polished float glass (50 mm \times 25 mm) coated on one surface with a SiO_2 passivation layer (200 – 300 Å) followed by the ITO coating (1,200 – 1,600 Å) with a sheet resistance of 8 – 12 Ω . J. Melvin Freed Brand microscope glass slides (75 mm \times 25 mm \times 1 mm) were obtained from VWR (West Chester, PA). Polymer sheets, polyurethane (PU), silicone, polycarbonate (PC), polystyrene (PS), polymethylmethacrylate (PMMA) and polytetrafluoroethylene (PTFE or Teflon), were purchased from Goodfellow (Huntingdon, England).

Polydimethylsiloxane (PDMS) sheets were prepared by using Sylgard 184 Silicone Elastomer Kit from Dow Corning (Midland, MI). PDMS was mixed per manufacturer's instructions (10:1 base to curing agent by mass), placed under vacuum to remove all air pockets, cast into a mold (a 160 cm diameter plastic Petri dish) and cured for 2-3 hours at 70 °C.

2.1.6. Cell lines and culture media.

Staphylococcus epidermidis bacteria, strain 49461, were purchased from ATCC (Manassas, VA). Mammalian cells, Jurkat clone E6-1, PC-12 and SHSY5-Y were purchased from ATCC. Neuroscreen-1 cells were obtained from Cellomics (Pittsburgh, PA). Fetal bovine serum and horse serum were obtained from HyClone (Waltham, MA). RPMI, F12-K and DMEM/F12 growth media and Dulbecco's phosphate buffered saline (D-PBS) were purchased from Mediatech (Manassas, VA).

2.2. Modification of Gold Surfaces

2.2.1. Surface cleaning of gold slides

The gold slides were cut to size and cleaned in piranha solution (7:3, v/v H₂SO₄/35% H₂O₂) for 5 – 10 min, rinsed several times with deionized water and finally rinsed with anhydrous ethanol. Long exposures (>10 min) to piranha solution can destroy the gold layer. The slides were then dried under a stream of nitrogen gas and further cleaned in oxygen plasma for 45 seconds using a Plasma Prep II from SPI Supplies (West Chester, PA). The plasma cleaned slides were used immediately in the next step.

2.2.2. Alkanethiol SAMs

Most alkanethiol self-assembled monolayers on gold were prepared by immersion of plasma cleaned gold slides in 1 mM solution of alkanethiol in anhydrous ethanol overnight at room temperature. The slides were rinsed with ethanol, dried with nitrogen, and either used immediately or stored in a sealed Petri dish at 4 °C until further use.

2.2.3. Carboxyl terminated alkanethiol SAMs

The plasma cleaned gold slides were immersed in a 1 mM ethanolic solution of 11-mercaptoundecanoic acid (MUA) containing 2% (v/v) trifluoroacetic acid (TFA) and incubated overnight at room temperature. TFA prevents the formation of MUA dimers on the gold surface due to hydrogen bonding and ionization of the COOH group due to trace water amounts in ethanol, which in both cases would affect the quality of the SAM.⁷ Upon removal from the ethanol solution the slides were sequentially rinsed with ethanol, 10% (v/v) ammonium hydroxide (NH₄OH) in ethanol, and ethanol followed by drying with nitrogen.

2.2.4. Amino terminated alkanethiol SAMs

The plasma cleaned gold slides were immediately immersed in a 1mM ethanolic solution of amino alkanethiol containing 3% (v/v) triethylamine (TEA) and incubated overnight at room temperature. TEA is used for the deposition of amino alkanethiols to avoid protonation of the amino groups and hydrogen bonding between protonated and deprotonated amino groups.⁷ Upon removal from the ethanol solution the slides were sequentially rinsed with ethanol, 10% (v/v) acetic acid (CH₃COOH) in ethanol, and ethanol followed by drying in a stream of nitrogen.

2.3. Modification of Indium Tin Oxide, Glass and Polymer Surfaces

2.3.1. Indium tin oxide (ITO)

ITO slides were cut to size and cleaned by immersion in a 20 % (v/v) ethanolamine solution in DI water. The solution with the ITO slides was heated to 80 °C for 15 min with stirring.

Substrates were then sonicated with a Branson 1210 ultrasonicator (Danbury, CT) in the same ethanolamine solution for an additional 15 min. Following sonication, the ITO surfaces were rinsed several times with DI water, once with anhydrous ethanol and dried in a stream of nitrogen. The slides were placed in a glass Petri dish and further cleaned in oxygen plasma for 1 min. The plasma cleaned ITO slides were immersed in 1% (v/v) solution of the designated alkoxy silane in anhydrous toluene or ethanol, containing 0.5% (v/v) n-butylamine as catalyst, and incubated overnight in a dessicator at room temperature. Anhydrous toluene was used as solvent for hydrophobic (alkyl) alkoxy silanes, whereas anhydrous ethanol was used for all the other alkoxy silanes. Subsequently the ITO slides were rinsed several times with deposition solvent (toluene or ethanol) and then sonicated for 15 min in deposition solvent, followed by further rinsing with deposition solvent and drying with nitrogen. The derivatized slides were either stored in a closed container at room temperature for later use or incubated at 70 °C for 1 hour in a vacuum oven for immediate use.

2.3.2. Glass

Glass slides were cut to the desired size and cleaned by immersion in piranha solution for 1 hour. The slides were rinsed several times with DI water, followed by one rinse with anhydrous ethanol, and then dried with nitrogen. The dried slides were placed on a glass Petri dish and

further cleaned in oxygen plasma for 2 min. The glass slides next underwent the same surface modification procedure as the ITO slides (see Section 2.3.1).

2.3.3. *Polydimethylsiloxane (PDMS) and polyurethane (PU)*

The polymer sheets were cut to desired size and sonicated for 15 min in ethanol. After drying with nitrogen, they were treated with oxygen plasma for 60 sec. The oxidized surfaces were immersed in 1% (v/v) solution of alkoxy silane in anhydrous ethanol, containing 0.5% (v/v) n-butylamine as catalyst, and incubated in a dessicator overnight at room temperature.

Subsequently they were rinsed with ethanol, sonicated for 15 min in the same solvent, and dried with nitrogen.

2.3.4. *Polytetrafluoroethylene (PTFE)*

A PTFE sheet (1 mm thickness) was cut into smaller size samples (1 × 1 cm). The PTFE samples were immersed in acetone and sonicated for 30 min. The sonicated samples were placed in a mixture of toluene and elemental sodium and the mixture was refluxed overnight. The samples were then rinsed with acetone, dried with nitrogen, and immersed in a piranha solution at 90 °C for 8 hours. They were thoroughly rinsed with water, dried with nitrogen and further treated in oxygen plasma for 2 minutes. The samples then underwent the same deposition procedure as the PDMS and PU samples.

2.4. Surface Reactions

2.4.1. *Modification of terminal amines to carboxyl groups*

Amino group terminated surfaces were modified to carboxyl groups by reacting them with a cyclic acid anhydride (dicarboxylic acid anhydride). Acid anhydrides are known to be highly reactive with nucleophiles.⁸ Succinic anhydride (0.4 g) was dissolved in 1 mL of dimethyl sulfoxide (DMSO). The volume was brought to 20 mL volume using 50 mM aqueous solution of Na₂HPO₄ and the pH was adjusted to 6.5 using 5 M NaOH. Amino terminated surfaces were incubated in this solution overnight at room temperature. The surfaces were then rinsed with deionized water and dried with nitrogen.

2.4.2. *Modification of terminal hydroxyls to carboxyl groups*

Hydroxyl-terminated surfaces were modified to carboxyl groups by adapting a procedure which uses chloroacetic acid to modify polysaccharides or hydroxyl-containing polymers that contain no other nucleophilic groups.^{9,10} The hydroxyl-surfaces were immersed in a freshly prepared solution of 1 M chloroacetic acid in 3 M NaOH. The immersed samples were agitated for 70 min on a Thermo Scientific (Waltham, MA) Barnstead/Lab-line orbital shaker at 70 rpm at room temperature to facilitate the reaction. The samples were next rinsed several times with deionized water and dried with nitrogen.

2.4.3. *Amide bond linkage on COOH terminated surfaces*

Carboxyl terminated surfaces were activated by immersing in a freshly prepared 100 mM EDC and 20 mM NHS solution in deionized water and agitating on the orbital shaker for 15 min at room temperature. The samples were then rinsed with DI water, dried, and immediately placed

in a water or ethanol solution (1 – 100 mM) of the desired compound containing a primary amino group. Following overnight incubation at room temperature, the surfaces were rinsed with deposition solvent and were dried with nitrogen.

2.4.4. Amide bond linkage on NH₂-terminated surfaces

Amino terminated surfaces were immersed and incubated in an anhydrous ethanol solution of the carboxyl-containing compound (1 or 10 mM) and dicyclohexyl carbodiimide (DCC) (5 or 50 mM, respectively) overnight at room temperature. The surfaces were rinsed with ethanol and dried with nitrogen.

2.4.5. Covalent attachment of amines on hydroxyl terminated surfaces

Hydroxyl terminated surfaces were activated by immersing in a 0.2 g/mL solution of p-toluenesulfonyl chloride (tosyl chloride) in acetonitrile (CH₃CN), containing 1% (v/v) triethyl amine. The samples were agitated on an orbital shaker for 4 hours at room temperature and next were rinsed with acetonitrile and transferred to an amine-containing compound solution (1 – 100 mM) in acetonitrile. The surfaces were incubated overnight at room temperature under agitation on an orbital shaker. They were then rinsed with acetonitrile and dried with nitrogen.

2.4.6. Covalent immobilization of proteins on COOH-terminated surfaces

COOH-terminated surfaces were activated by immersing and agitating in a freshly prepared solution of 100 mM EDC and 20 mM NHS in deionized water for 15 min. Then the slides were rinsed with deionized water, dried with nitrogen gas, and immediately covered with a small volume (100 – 200 μ L) of protein solution in pH 9.6 carbonate buffer for 24 hours at 4 °C. The

protein coated surfaces were rinsed with PBS buffer and then stored dry in a sealed container at 4°C until further use.

2.5. Surface characterization

2.5.1. Contact Angle Goniometry

Sessile drop contact angle measurements were obtained with a manual Rame-Hart Model 100 goniometer or a computer-controlled Rame-Hart Model 300 goniometer (Netcong, NJ).

On the manual goniometer, contact angle measurements were obtained by dispensing 1 μL droplets of deionized water, pH 2, and pH 12 solutions on the sample surface using a calibrated automatic pipettor. The pH 2 and pH 12 solutions were prepared as 0.01 M H_2SO_4 and 0.01 M NaOH solutions, respectively. The contact angle was measured manually by using the ocular piece of the goniometer which contains a 10X magnification lens. Images were taken with a digital camera through the ocular piece of the goniometer.

On the computer-controlled goniometer, 1 μL droplets of deionized water, pH 2, and pH 12 solutions were deposited on the substrates using the Automated Dispensing System accessory coupled to the goniometer. Advancing and receding contact angles were obtained by dispensing and then retracting 10 μL of DI water on the substrate surface using the automated dispensing pump. Images were obtained by an integrated digital camera and the entire system was controlled using Rame-Hart's DROPimage Standard (v. 2.0.10) software package. The software automatically provides contact angle measurements once the liquid is dispensed.

For both goniometers, the contact angle measurements were taken immediately after each surface modification. The contact angle was measured within 60 seconds after dispensing the droplet on the surface. Six measurements were taken per surface for at least two different samples and the results were averaged.

2.5.2. Ellipsometry

Ellipsometric measurements were obtained with a manual photoelectric ellipsometer, series 439L633P, from Rudolph Instruments (Fairfield, NJ). The measurements were taken at a 70° angle of incidence using a He–Ne laser with a wavelength of 632.8 nm. The film thickness values were obtained by using the software package provided with the instrument which uses regression algorithms to calculate the thickness based on the optical constants of the film and substrate. The extinction coefficient and refractive index of the films were assumed to be 0 and 1.457, respectively.^{11, 12} Plasma cleaned, bare gold substrates were used to determine the optical constants of the gold film. The extinction coefficient of the gold slides was determined to be 3.4; whereas the determined refractive index varied from 0.15 – 0.20 and it was varied in that range in 0.01 increments for the thickness calculations. The reported thickness values for each film are the average of at least five measurements obtained per slide from three freshly prepared samples, measured after each surface modification step.

2.5.3. Grazing Incidence Infrared Spectroscopy

Grazing incidence infrared spectra were collected using a Thermo Electron (Waltham, MA) Nicolet FT–IR model 6700 spectrometer equipped with a Thermo Nicolet grazing angle accessory and a liquid nitrogen cooled mercury cadmium telluride (MCT) detector. The IR

beam was incident at 75 degrees to the substrate. The optical path was purged with nitrogen gas prior to (20 minutes) and during data acquisition. A clean, bare gold slide was used as the background, and a new background was collected before each spectrum measurement. For each spectrum, 64 scans were taken, with a wavelength scan range from 4000 to 600 cm^{-1} . The spectra were automatically corrected for H_2O and CO_2 .

2.5.4. Cyclic Voltammetry

Electrochemical measurements were taken with a Gamry Instruments Reference 600 Potentiostat/Galvanostat/ZRA (Warminster, PA). An electrochemical cell consisting of three electrodes was assembled. The modified gold or ITO slides were used as the working electrodes, an Accumet saturated calomel electrode (SCE) from Fisher Scientific (Pittsburgh, PA) as the reference electrode, and an Accumet platinum wire as the counter electrode. The slide was contacted with an alligator clip, while an area of 1 cm^2 was immersed in the electrolyte solution together with the SCE and counter electrode. The cyclic voltammetry (CV) curves were obtained at a 50 mV/s scan rate.

2.5.5. Electrochemical Impedance Spectroscopy

The electrochemical impedance spectroscopy (EIS) measurements were performed using the same setup and instrument as described for cyclic voltammetry experiments. The measurements were taken at a fixed DC potential versus the SCE electrode and a 10 mV AC perturbation within a 100 kHz to 0.1 Hz range. The impedance spectra were recorded in the form of Nyquist plots and they were fitted to equivalent circuit models that represent electrochemical transformations

occurring at the electrode/electrolyte interface. The modelling was done with Gamry Echem Analyst software, Version 5.10.

2.5.6. Surface Plasmon Resonance (SPR)

SPR measurements were performed with an SPR3, High Sensitivity Spreeta Evaluation Kit, from ICx Nomadics (Stillwater, OK). The kit includes parts to assemble a flow cell integrated with the sensor module and an electronic control box to process the signal. SPR sensing modules, model TSPR1K23, were purchased from ICx Nomadics. The modules contain a 0.12 mm thick borosilicate glass slide (16.9 mm × 5.6 mm) coated with 500 Å of gold as the sensing surface. The assembly of the flow cell creates three small parallel channels over the gold sensing surface. The dimensions of each of the flow channels are: 9 mm long, 0.8 mm wide and 0.1 mm deep, providing for a 0.72 µL volume per channel. The SPR experiments were performed while running buffered solutions over the sensor surface and the flow rate was controlled using a Manostat Carter 4/8 multi-channel peristaltic pump from Barnant Co. (Barrington, IL). The SPR signal was monitored and recorded using Spreeta 5 software, Version 21.14, from Texas Instruments, Inc. (Dallas, TX). The flow cell was thermally insulated and protected from light by enclosing it in a Styrofoam lined, light-tight box. Each SPR measurement was carried out in triplicate by monitoring the SPR response curve for all three channels simultaneously and the average change was reported. All aqueous solutions used for SPR experiments were filtered prior to use through a 1 µm PURADISC™ 25 GD filter from Whatman (Florham Park, NJ).

2.5.7. Microscopy

Brightfield, phase contrast and fluorescent images of surfaces and cells were obtained with either

an inverted Leica fluorescence microscope connected to a camera operated from Leica software or with a Nikon Eclipse E400 fluorescence microscope that uses a IN1820 Spot Insight model Diagnostic Instruments camera attached to the Nikon microscope and Spot Advanced 4.5 software. The Nikon microscope was used to obtain images at 1000X magnification using an oil immersion lens.

2.6. Cell Culture

2.6.1. Jurkat cells

Jurkat cells were grown in RPMI medium supplemented with 10% fetal bovine serum (FBS) and were maintained in an incubator at 37°C and 5% CO₂. For cell attachment experiments the cells were dispersed by pipetting aseptically, as they tend to form small aggregates during their growth, and then the cells were counted using a hemocytometer, diluted in growth medium and exposed to surfaces at a concentration of 1×10^5 cells/mL. The surfaces were incubated in the presence of the cells overnight, gently rinsed by adding fresh growth medium that had been warmed to 37 °C and then images were taken. If the substrates were gold slides then the cells were stained with Vybrant[®] DiO (Invitrogen) cell-labeling fluorescent dye and fluorescent images were taken.

2.6.2. PC-12 cells

PC-12 cells were cultured in F12-K medium with 15% horse serum and 2.5% FBS at 37 °C and 5% CO₂. The surface of the polystyrene dish where they were grown was pre-coated with collagen by covering the surface with a small film of collagen I solution (3 mg/mL) and rinsing

the surface with D-PBS after 5 min incubation at 37 °C. For cell attachment and differentiation experiments, the cells were seeded on the surface at a concentration of 1×10^4 cells /mL in F12-K growth medium with 15% horse serum and 2.5% FBS over 2 – 3 days. The cells were differentiated in F12-K containing 10% HS, 5% FBS and 100 μ g/mL nerve growth factor (NGF). The differentiating medium was changed every 2 days and images were taken after at least 7 days.

2.6.3. Neuroscreen-1 cells

Neuroscreen-1 (a subclone of PC-12 cells) cells were cultured in RPMI medium supplemented with 10% horse serum and 5% FBS in an incubator at 37 °C and 5% CO₂. For cell attachment and differentiation experiments, the cells were plated on the surface at a concentration of 1×10^4 cells/mL and allowed to attach and grow for 2 – 3 days. The cells were differentiated by replacing the growth medium with RPMI containing 10% horse serum, 5% FBS and 100 μ g/mL NGF. The differentiating medium was changed every 2 days and images were taken after at least 4 days.

2.6.4. SHSY5-Y cells

SHSY5-Y cells were cultured in DMEM /F12 with 10% FBS in 37 °C at 5% CO₂. They were seeded on surfaces at 1×10^4 cells/mL and after 2 – 3 days they were differentiated by exposing to 10 μ g/ml retinoic acid in the growth medium for 7 days, followed by 2 ng/mL brain-derived neurotrophic factor (BDNF) for another 7 days. The differentiating medium was changed every 2 – 3 days. Images were taken after at least 2 weeks.

2.6.5. Mouse neo-natal fibroblasts

Mouse fibroblasts were cultured in DMEM/F12 with 10% FBS in 37 °C at 5% CO₂. They were treated 4 ng/mL fibroblast growth factor (FGF) in DMEM/F12 with 10 % FBS for a period of two weeks in order to generate extra-cellular matrix. The medium with FGF was replaced every 3 days.

3. Nucleic Acid Biosensor

3.1. Introduction

Nucleic acids play an important role in storing and transferring genetic information in nature. Hybridization of oligonucleotides with immobilized DNA has become increasingly important as a probe for use in biosensing applications in many fields, including bioengineering and homeland security. These applications involve detection of single-nucleotide polymorphisms (SNPs) and genetically modified organisms (GMOs). An SNP is a single nucleotide mutation in the genome of an organism. There are approximately 10 million variance sites or SNPs in the world's human population and they make up most of the 0.1% genetic variance observed in the human population.¹³ Common diseases, including cancer, are known to be caused by combinations of multiple genetic and environmental factors.¹⁴ Large-scale surveys have already associated certain common diseases with specific genes and variations in their sequence.¹⁵ There is an international effort underway to create a map of all human SNPs and determine their connections to many diseases,¹⁶ and at the same time their link to differences in response to therapeutic agents.¹⁷ GMOs are organisms whose genome has been altered by using genetic engineering, usually through the introduction of a gene from another organism. The extensive recent use of GMOs in agriculture and their increased use in the manufacture of food products, require the detection of GMOs in these products for labeling and regulation purposes.¹⁸

Detection of RNA is also important, particularly for studying and monitoring gene expression. In addition, with the discovery of RNA interference (RNAi), a new form of RNA, micro RNA (miRNA), has been added to the other known RNA sequences. These RNAs are small, non-coding, 18 to 24-nucleotide single-stranded sequences that are involved in gene regulation,

affecting essential processes such as cell proliferation, cell death, tumor genesis, and mammalian cell development.¹⁹⁻²¹ Due to their small size, miRNAs are difficult to detect using conventional methods²² and there is a pressing need for rapid, label-free detection methods. This would speed ongoing research in understanding their role in gene regulation, and potentially lead to the development of new medical therapeutic technologies which will be based on the ability of miRNAs to block and /or control gene expression.

The detection of nucleic acids requires a platform which is able to sense the hybridization process, and which also facilitates the immobilization of single-stranded (ss) probe DNA, while maintaining its ability to efficiently hybridize with the target sequence. Surface plasmon resonance (SPR) is a surface characterization technique that can be employed to report changes on a metal-coated surface based on alterations occurring in the dielectric medium within a very short distance (100 – 500 nm) from the metal surface.²³ SPR provides non-invasive, real time, label-free detection of biomolecular binding interactions, such as ligand-receptor coupling, antibody-antigen binding, protein-DNA interactions, and DNA-DNA hybridizations.^{23, 24}

SPR is an optical-electronic phenomenon that occurs during the reflection of light on an optical substrate, such as glass, coated with a thin metal film (~50 nm) that is semitransparent, under conditions of total internal reflection (Figure 3.1). Total internal reflection happens when light passes from a higher refractive index medium (such as glass) to a lower refractive index one (such as water) and strikes the medium boundary at an incident angle that is larger than the critical angle (θ_c); at larger angles the light beam is partially transmitted as refracted light. As

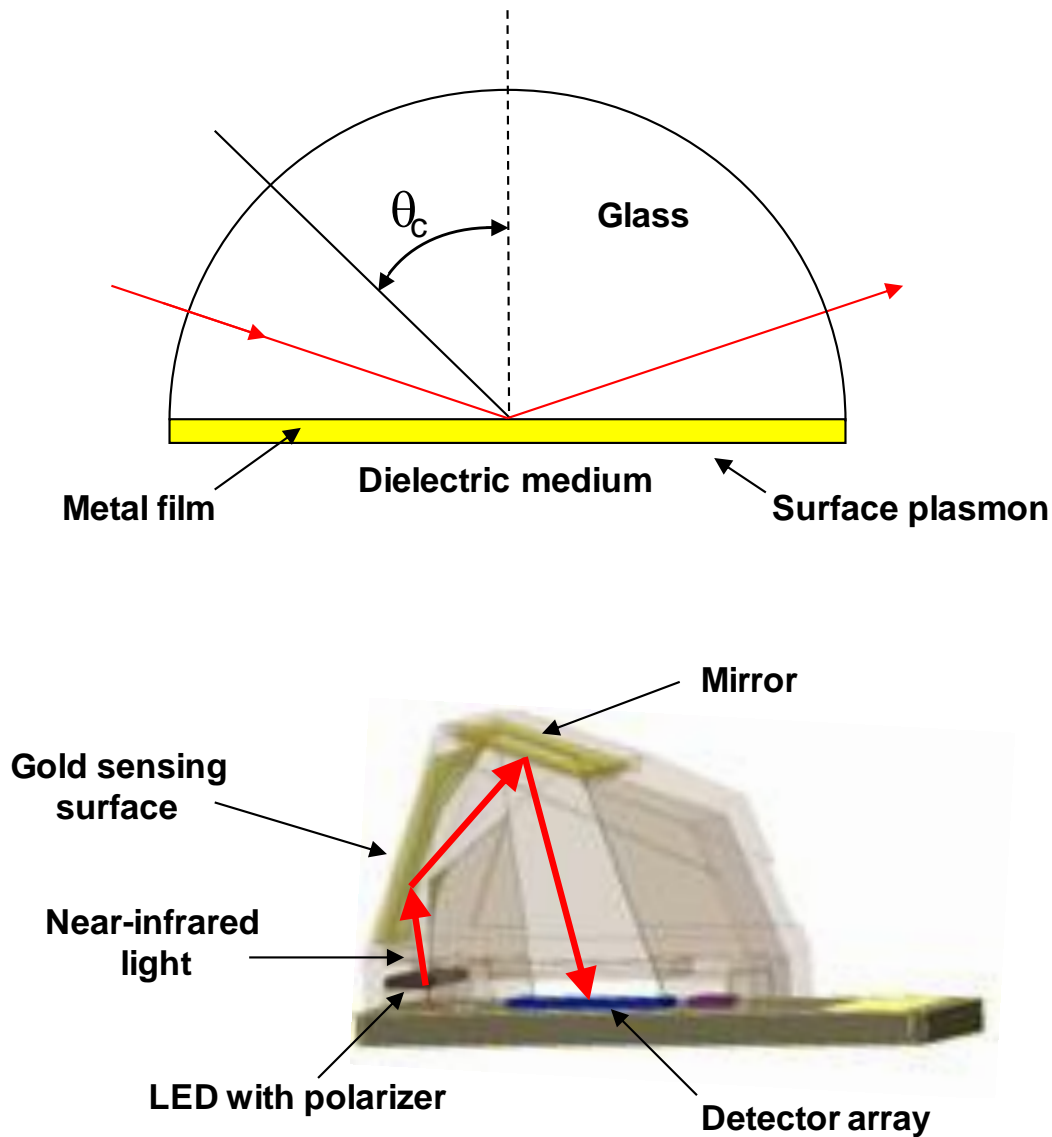


Figure 3.1. Surface plasmon resonance. (Top) Diagram of the surface plasmon resonance according to the Kretschman configuration. If the light beam travelling through the glass medium has an incident angle (with respect to the normal of the surface) larger than the critical angle (θ_c), it is reflected at 100%. The presence of a semitransparent metal film allows for the generation of surface plasmons or plasma waves that propagate alongside the metal-dielectric medium. (Bottom) Sketch of the Spreeta SPR sensing module. Near-infrared light (840 nm) from a light emitting diode (LED) is polarized and reflected off the gold sensing surface. The light is then directed by the mirror into a linear array of silicon photodiodes. The entire assembly is embedded in an optically clear material, and on the outside the surface is coated with an opaque material to block external light (except the sensing surface which is coated with a semitransparent gold film).

light is reflected under these conditions, evanescent waves are generated and propagated across the interface. When a semitransparent metal film is present at the medium boundary, surface plasmons are generated, and they propagate along the metal/dielectric (or metal/water) interface as surface electromagnetic waves. There is a drop in the intensity of the reflected light as a consequence of the oscillation of mobile electrons (or plasma) at the surface of the metal film in response to the evanescent waves. These oscillating surface electrons are the surface plasmons mentioned above and they are located on the gold side facing the dielectric medium (or water).

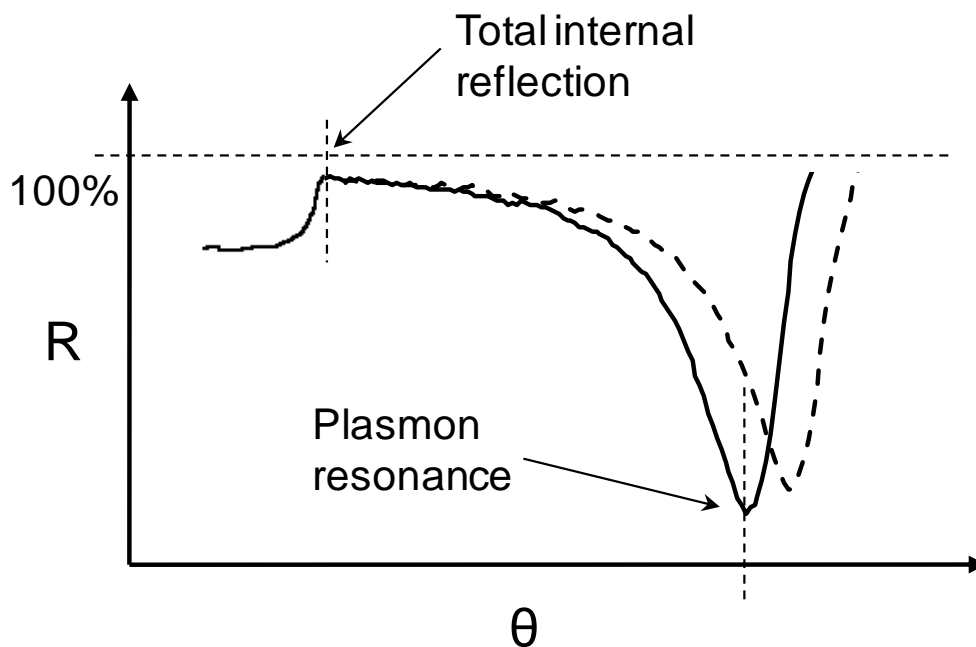


Figure 3.2. Surface plasmon resonance curve. If monochromatic light is reflected from the surface at a range of incident angles, then a SPR curve can be obtained, which is a plot of the intensity of the reflected light versus the angle of incidence. The minimum occurs when the vector of the incident light matches that of electron oscillations on the metal-dielectric interface. The dotted line represents a shift of the SPR peak due to the presence of a coating on the gold surface.

There is an incident angle at which this loss in light is greatest and at which the intensity of reflected light reaches a minimum (Figure 3.2). The intensity minimum occurs when the wave vector of the incident light matches the value of the wave vector of the surface plasmons, causing the surface electrons to resonate, hence the term *surface plasmon resonance*.²⁵ The resonance frequency of the surface plasmons is directly related to the refractive index of the dielectric medium; thus changes in the position of the SPR curve minimum are proportional to the refractive index of the dielectric medium adjacent to the gold surface.

The Spreeta SPR sensor is arranged in a similar way to the Kretschman configuration described in Figure 3.1. SPR based technology has been used for the real time and label-free detection of various biomolecular binding events, antibody-antigen interactions, protein-DNA interactions, and DNA-DNA hybridizations. In addition, SPR allows measurements of kinetic rates and equilibrium affinity constants for the analyte-receptor interaction which it monitors.²⁶ Consequentially, SPR biosensors have been developed that are capable of detecting analytes ranging in size from relatively small molecules, such as morphine²⁷ and atrazine,²⁸ to the larger size oligonucleotides and proteins, and even whole organisms, such as intact bacteria.²⁹ SPR sensor surfaces usually consist of a conductive substrate or chip on whose surface a protein ligand or DNA probe is immobilized. After running the analyte-free buffer continuously over the modified surface, the binding analyte or target DNA strand is dissolved or diluted in the same buffer and the sample is injected over the sensor surface and the change in signal is monitored in real time. Biosensing technology that monitors DNA hybridization is useful in the development of dense arrays of nucleotides for DNA profiling of large sample numbers, and in the rapid detection of single-nucleotide polymorphisms (SNP). Electrochemical DNA sensors make up a

large part of the current technology. Some of these methods have been reported to detect femtomoles of target.³⁰ However, they have disadvantages such as high background signals, sample destruction, chemical labelling steps, and rather complex constructs of the sensing surface.³⁰

SPR is an indirect detection method for DNA hybridization. The sensor reports changes in refractive index based within 500 nm from the gold surface³¹ and thereby makes possible real time, label-free detection of hybridization including DNA-DNA and DNA-RNA interactions.³¹⁻³⁴ SPR does not destroy the sample and does not require labeling of the target DNA sequences. Usually, the SPR systems used to detect DNA hybridization consist of sensing surfaces that consist of three-dimensional, 100 nm thick carboxymethylated dextran polymers, to which the probe DNA is anchored with biotin-streptavidin.^{23, 35-37} The sensitivity of this kind of probe surfaces is dependent on the diffusion of the analyte. Mark *et al.* monitored DNA hybridization reactions with dendrimer-functionalized self-assembled monolayers (SAMs) with a detection limit of 3.9 nM,³⁸ while Vaisocherova *et al.* used streptavidin-functionalized SAMs to reach a similar detection limit.³⁹ Other researchers have monitored DNA hybridization by covalently attaching DNA probes to an amino terminated SAM.⁴⁰ Lower detection limits have been reported, but they involve the usage of DNA-capped gold nanoparticles.⁴¹ Another label-free optical technique is Total Internal Reflection Ellipsometry, which has been shown to detect both genomic DNA and DNA oligonucleotides.^{42, 43}

Detection of SNPs or single nucleotide mismatches by SPR has been reported by Nakatani *et al.* who reported detection of guanine-guanine mismatches by using a mismatch specific ligand.⁴⁴

They were able to detect these mismatches at 1 nM oligonucleotide concentrations. The same group was also able to detect guanine-adenine mismatches down to 100 nM concentrations using a synthetic aromatic molecule which stabilized the mismatch.⁴⁵ Others were able to detect mismatches using a thiolated DNA probe with a detection limit of 500 nM.⁴⁶ Tawa and Knoll used fluorescent labeled target DNA sequences to distinguish for SNPs using surface plasmon fluorescence spectroscopy.⁴⁷ Dell'Atti *et al* reported a piezoelectric biosensor with a 100 nM detection limit with regard to detection of SNPs.⁴⁸

In the present work, the surface of a commercially available SPR sensor was modified by self-assembly to create a mixed monolayer of a hexanethiol-modified 21-base long probe DNA and 6-mercapto-1-hexanol, which has the same length as the thiol terminated tether of the probe DNA (Figure 3.3). 6-Mercapto-1-hexanol was used to avoid non-specific adsorption and to facilitate hybridization of target DNA by spacing the probe oligonucleotides, as described previously.⁴⁹⁻⁵² The 21-base probe DNA strand was modified with a hexane thiol tether [HS-(CH₂)₆-] at the 5' end. The 21-base target oligonucleotides were not modified. The DNAtarget strands consisted of one full complementary strand, one non-complementary strand, and three one-mismatch complementary strands containing a single nucleotide mismatch in the 5' end (P1), 3' end (P21), or middle of the sequence (P11) (Table 3.1). The non-complementary strand served as a non-thiolated control probe DNA. The RNA strands consisted of a non-complementary and a full complementary strand. Hybridization was characterized and detected by electrochemistry and SPR. Hybridization was monitored by SPR under a variety of conditions (flow rate, buffer concentration and temperature) to determine the optimum conditions for sensing. It was possible to use the sensor to detect SNPs and the signal response

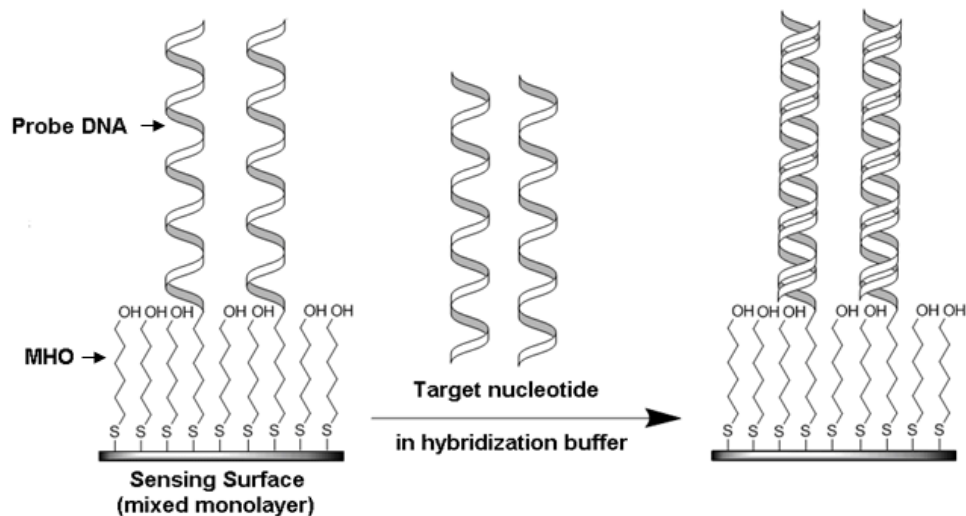


Figure 3.3. Depiction of the SPR sensing surface. The sensing surface consists of a mixed monolayer of hexanethiol-modified probe DNA oligonucleotide (probe DNA) and 6-mercapto-1-hexanol (MHO) chemisorbed on the gold surface of the SPR sensor through the sulphur of the thiol group. Upon target DNA exposure the hybridization of probe to target strands occurs resulting in a detectable change in the SPR signal.

Table 3.1. Sequence of oligonucleotides used with the biosensor described in this work. The mismatch positions are labeled with respect to the full match target DNA sequence. Mismatched nucleotides are given in underlined bold.

Oligonucleotide	Sequence (5' – 3')
probe DNA (DNA-SH)	HS-(CH ₂) ₆ -CCCGATTGACCAGCTAGCATT
full match (FM)	AATGCTAGCTGGTCAATCGGG
middle mismatch (P11)	AATGCTAGCT <u>A</u> GTCAATCGGG
5' end mismatch (P1)	<u>G</u> ATGCTAGCTGGTCAATCGGG
3' end mismatch (P21)	AATGCTAGCTGGTCAATCGGG <u>C</u>
control (full mismatch)	CCCGATTGACCAGCTAGCATT
RNA full match	AAUGCUAGCUGGUCAAUCGGG
RNA control (full mismatch)	CCCGAUUGACCAGCUAGCAUU

was found to be sensitive to the position of the mismatch. The sensor surface could be regenerated by washing the surface *in situ* with a denaturing solution. The response of the sensor remained the same after at least 20 cycles of hybridization/denaturation steps, allowing for the sensor surface to be reused for subsequent hybridization measurements.

3.2. Experimental Details

3.2.1. Surface modification of gold slides with probe DNA

The surface modification strategy was based on the high affinity of thiols for the gold surface and their ability to replace other functional groups.⁶ Immediately after plasma cleaning, the gold slides were covered with a 10 μM solution of thiol-modified probe DNA (DNA-SH) in 10 mM phosphate buffer (PB), pH 7.0. Since the clean gold surface is hydrophilic, only a small volume ($\sim 100 \mu\text{L}$) of the probe DNA solution was required to completely wet the surface. The 10 μM probe DNA concentration was chosen in order to maximize the surface density as previously reported in the literature.^{46, 49-51, 53, 54} The gold substrates were incubated in a closed container for approximately 48 hours at room temperature and finally rinsed with PB, pH 7.0, and dried with nitrogen.

The DNA-derivatized gold slides were incubated in a 1 mM aqueous solution of 6-mercapto-1-hexanol (MHO) at room temperature for 1 hour in a closed container, rinsed with deionized water and dried with nitrogen. Hybridization with the target strands was carried out in 3x hybridization buffer (HB) (Table 3.2). The slides were covered with a 1 μM solution of target DNA strands in HB for 1 hour at room temperature, rinsed with 3x HB,

deionized water and dried with a stream of nitrogen. Control experiments included the incubation of bare gold slides in an unmodified control probe DNA solution with the same sequence as the thiol-modified probe and incubation of bare gold slides in MHO solution. At least three samples were prepared for each modification.

3.2.2. Modification of SPR sensing surface with probe DNA

The gold film on the SPR sensing surface was rinsed with deionized water and anhydrous ethanol. The sensor surface was dried with a stream of nitrogen and the sensor was cleaned in oxygen plasma for 45 seconds prior to surface modification. Oxygen plasma exposure was found not to affect the performance of the sensor.

SPR sensing modules were modified by wetting the gold sensor surface with 50 μL of 10 μM DNA-SH solution in PB, pH 7.0, and incubating in a closed container for 48 hours at room temperature. The gold surface was rinsed with PB, pH 7.0, and dried with nitrogen. The DNA-derivatized gold surface was incubated with 100 μL of 1 mM MHO in deionized water, and stored for 1 hour in a closed container. The surface was rinsed with deionized water, dried with nitrogen, and then stored in a sealed Petri dish at 4°C until further use.

3.2.3. Electrochemical characterization of gold slides

Electrochemical measurements were performed as described in Section 2.8.4. The electrolyte solution was prepared in 10 mM phosphate buffer, pH 7.0, containing 1 mM potassium ferricyanide [$\text{K}_3\text{Fe}(\text{CN})_6$] (as redox probe) and 100 mM KCl (as supporting electrolyte). The cyclic voltammetry (CV) curves were obtained in the range of -0.3 V to 0.7 V . The

electrochemical impedance spectroscopy (EIS) measurements were performed at a fixed potential of 0.18 V *vs* SCE (the redox potential of ferricyanide ions) and in the frequency range of 0.1 Hz to 100 kHz. The impedance spectra were recorded in the form of Nyquist plots and they were fitted to an equivalent circuit, shown in Figure 3.4, based on the Randles and Ershler model.⁵⁵⁻⁵⁷

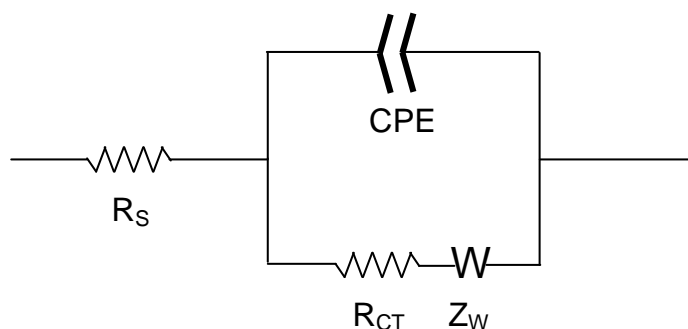


Figure 3.4. Diagram of the equivalent circuit used to fit the impedance spectroscopy data.

In the presence of a redox probe the model circuit consists of the resistance of the electrolyte solution (R_S), the Warburg resistance (Z_W) resulting from the diffusion of the redox probe, the charge-transfer resistance (R_{CT}) of the electrode/electrolyte interface on the surface of the working electrode, and a non-ideal capacitance represented by the constant phase element (CPE) due to the non-homogeneity of the interface on the working electrode surface.⁵⁷⁻⁵⁹ The last two elements represent parameters that are dependent on the solution-electrode interface, thus the nature of the film covering the gold surface. For non-homogeneous films and rough surfaces the impedance data do not fit the theoretical behaviour predicted by the equivalent circuit made of ideally behaving components.^{56, 60} For such cases, the capacitance can be replaced by the constant phase element (CPE)⁵⁷⁻⁵⁹ and any changes in surface coverage are determined by observing changes in the R_{CT} values.^{49, 57, 61-65} When molecules with hydrophobic parts adhere to

the gold surface, they form an insulation layer which perturbs the interfacial electron transfer between the electrode and the electroactive species in solution, thereby increasing the charge-transfer resistance. The same effect is observed when charged molecules, such as DNA oligonucleotides, are deposited on the electrode surface. This is attributed to the electrostatic repulsion between the negatively charged DNA layer and the ferricyanide ion, $[\text{Fe}(\text{CN})_6]^{3-}$.

3.2.4. Surface plasmon resonance

SPR experiments were performed by using the set-up shown in Figure 3.5. The Spreeta Evaluation kit includes parts to assemble a flow cell integrated with the sensor module and the electronic control box that processes the signal. The flow cell was thermally insulated and protected from light by enclosing it in a Styrofoam lined, light-tight box. The modules contain a 0.12 mm thick borosilicate glass slide (16.9 mm × 5.6 mm) coated with 500 Å of gold as the sensing surface and there are three active sensing regions 4.5 mm long and 0.1 mm wide on the sensor surface. The assembly of the flow cell creates a small flow channel directly above each of the active sensing region. The dimensions of the flow channels are: 9 mm long, 0.8 mm wide and 0.1 mm deep, providing for a 0.72 μL volume per channel. The sensing area is significantly smaller than the flow channel and is completely covered by the flowing buffer solution during the measurements. The refractive index was monitored while running hybridization buffer in order to determine the background signal and then oligonucleotide samples in hybridization buffer were pumped over the sensor surface. Each SPR measurement was carried out in triplicate by monitoring the SPR response curve for all three channels simultaneously and the average change was reported. The relative amount of target DNA bound to the surface was determined by measuring the net increase of the refractive index over time, compared to that of

running buffer alone.

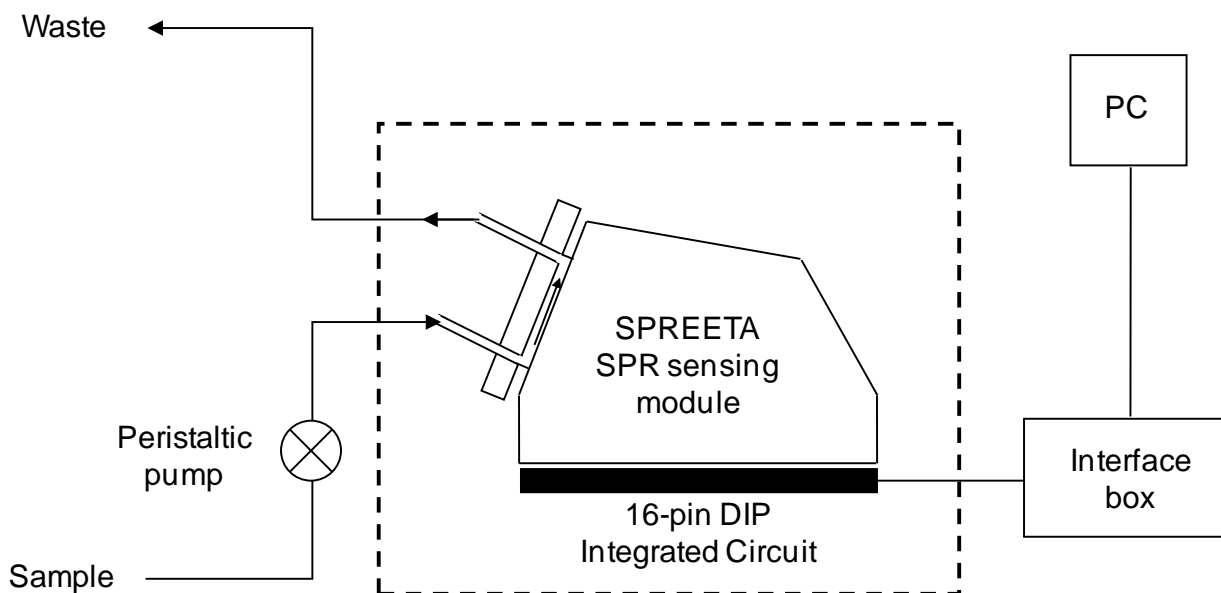


Figure 3.5. Schematic drawing of the SPR experimental set-up. The dashed line represents the black box fitted with Styrofoam.

Following hybridization, the sensor surface was regenerated by washing it *in situ* with a 7 M guanidinium chloride aqueous solution for 10 min. Experiments were carried out to determine the effect of the mismatch site on the SPR signal (i.e. 5', 3', and middle) at target DNA concentrations ranging from 10 pM to 1 μ M. A series of experiments were performed at various HB concentrations (1x, 2x, 3x, 4x, and 5x) (see Table 3.2), flow rates (20, 50, 100, 200, 400, and 800 μ L/min), and temperatures (20, 25, 30, 40, 50, and 60 $^{\circ}$ C). The temperature was controlled by immersing the sample tubing in a temperature controlled water bath before it entered the flow cell. The temperature of running buffer was monitored by inserting a 0.25 mm diameter thermocouple probe, OMEGA Engineering, Inc. (Stamford, CT), inside the lumen of

the tube at the closest point possible to the liquid input port on the SPR flow cell. When the temperature of the in-flowing buffer solution reached the desired temperature the target strand sample was pumped through the system. For the experiments investigating different HB concentrations, flow rates, and temperatures, the flow time of target DNA was 5 minutes, whereas for the DNA concentration titration the flow time was 30 minutes, since target binding happens at a slower rate for low DNA concentrations.

Table 3.2. The hybridization buffer concentrations used in this study and the corresponding NaCl concentration in each of them. Hybridization buffer was prepared as a 20x concentrated stock solution (3.0 M NaCl, 0.3 M sodium citrate, pH 7.0).

Hybridization buffer	NaCl concentration (M)
1x	0.15
2x	0.30
3x	0.45
4x	0.60
5x	0.75

3.3. Results and Discussion

3.3.1. *Electrochemical characterization*

Cyclic voltammetry is an electrochemical technique that measures the current response of the working electrode to a cyclic linear scan in potential. The presence of an electroactive ion, such

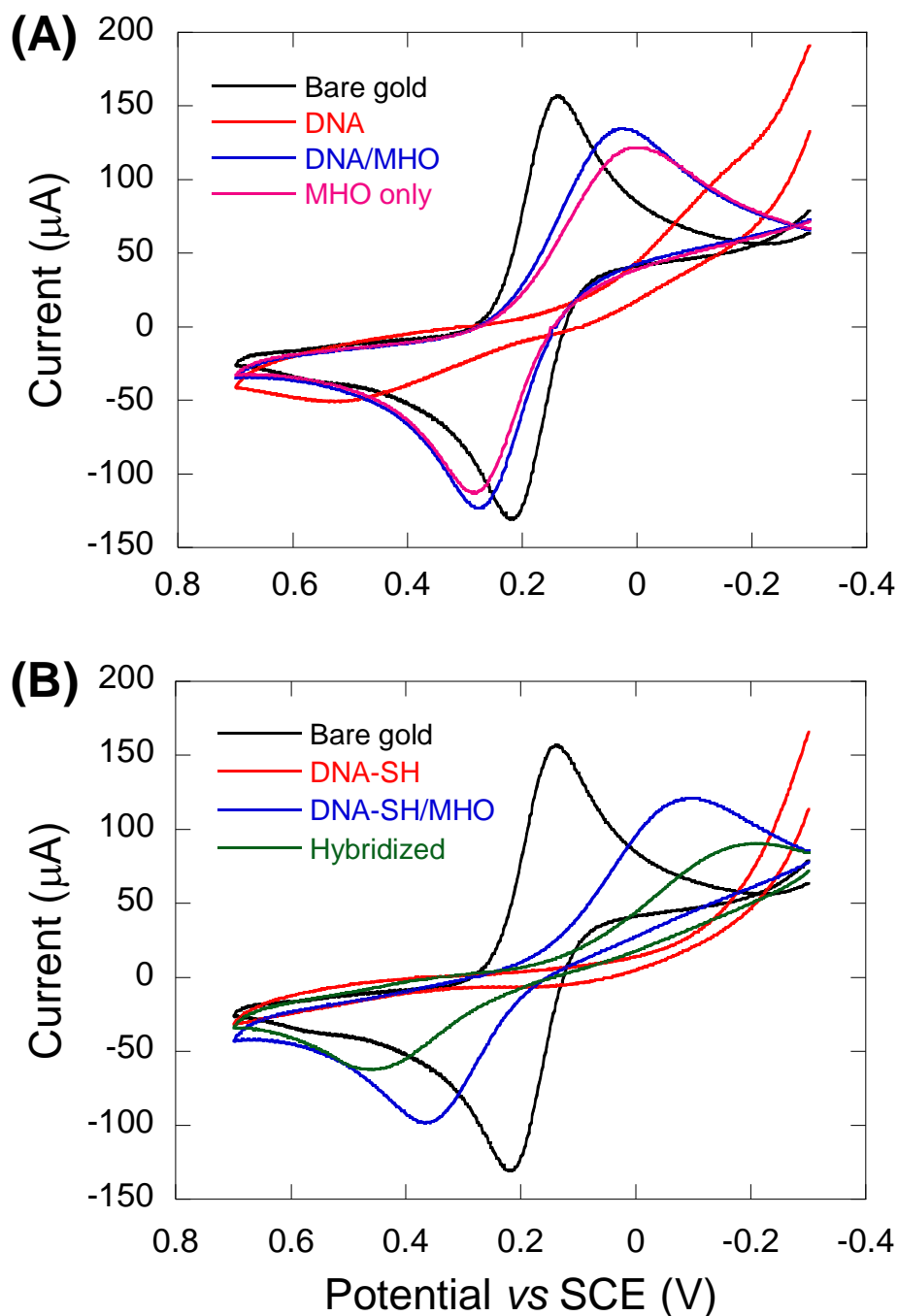


Figure 3.6. Cyclic voltammograms of bare gold and modified gold slides. (A) Bare gold; gold surface incubated in 10 μM non-thiolated control probe oligonucleotide (DNA); DNA surface incubated in 1 mM 6-mercapto-1-hexanol (MHO) (DNA-SH/MHO); and gold incubated in 1 mM MHO (MHO only). (B) Bare gold; gold surface incubated in 10 μM thiolated probe oligonucleotide (DNA-SH); DNA-SH surface incubated in 1 mM MHO (DNA-SH/MHO); and DNA-SH/MHO surface incubated in 1 μM full match target oligonucleotide (hybridized).

as $[\text{Fe}(\text{CN})_6]^{3-}$, in solution allows for charge or electron transfer to occur between the electrode/electrolyte interface due to oxidation or reduction of the $[\text{Fe}(\text{CN})_6]^{3-}$ ion. If the gold surface is unmodified, thus conductive, then two redox current peaks will be observed, whereas the opposite is observed (no redox current peaks) when the gold surface is coated with a film that blocks electron transfer. The cyclic voltammetry (CV) curves of the modified gold electrodes showed no conductivity after the deposition of both thiol-modified (DNA-SH) and non-thiolated (DNA) probe oligonucleotide, but they became conductive again after incubation in 6-mercapto-1-hexanol (MHO) solution (Figure 3.6). The lack of redox peaks after modification with DNA-SH or DNA is interpreted as the inability of the $[\text{Fe}(\text{CN})_6]^{3-}$ ion to penetrate the chemisorbed and physisorbed DNA film. Physisorption of DNA refers to non-specific binding of other functional groups due to the high surface energy of gold.⁶⁶ The reappearance of the redox peaks after incubation in MHO solution shows the opposite; i.e. the $[\text{Fe}(\text{CN})_6]^{3-}$ ion is able to penetrate the mixed monolayer formed on the gold electrode. However, there is an outwards shift of the redox peaks compared to the CV of bare gold. This happens as a result of the resistivity, although relatively small, of the DNA-SH/MHO mixed monolayer. In support of this view, bare gold slides incubated only in MHO solution for 1 hour provided the same CV curve as the DNA-SH/MHO samples (see Figure 3.6A). The result for the MHO only coated slides is expected as SAMs formed by alkanethiol chains shorter than nine carbons are known not to provide blocking CVs.⁶

These results appear to show that MHO molecules replace the physisorbed DNA, resulting in the formation of a mixed monolayer of DNA-SH and MHO, which would be suitable for DNA hybridization. After incubation in hybridization buffer with the full match (FM) target strand,

the redox peaks of the CV shift outwards (Figure 3.6B), showing higher resistivity of the surface towards the $[\text{Fe}(\text{CN})_6]^{3-}$ ions. This would be expected if the DNA-SH was still bound to the surface so that it can hybridize with the full match target strand. Hybridization of probe DNA results in an increase in the amount of negative charges on the gold surface, thus there would be stronger repulsion towards the negatively charged ferricyanide ions. The resistivity of the DNA nucleotide layer can also be observed by impedance spectroscopy, and as it will be discussed below, the CV data are in agreement with the impedance spectra.

The impedance spectra were recorded in the form of Nyquist plots and the data were fitted to a general equivalent circuit model that contained a CPE parameter instead of capacitance, as shown in Figure 3.4, since it provided a better fit for the experimental impedance spectra. As mentioned earlier, deposition of negatively charged molecules on the electrode surface results in an increase of the charge-transfer resistance (R_{CT}), due to the electrostatic repulsion between the negatively charged DNA layer and the ferricyanide ion, $[\text{Fe}(\text{CN})_6]^{3-}$. Transformations in the interface or changes in surface coverage were determined by observing changes in the R_{CT} values.

Typical impedance spectra expressed in the form of Nyquist plots before and after hybridization are shown in Figure 3.7. The charge-transfer resistance of the gold slides after each deposition step are given in Table 3.3. Slides derivatized with DNA-SH or DNA yielded R_{CT} values at least 100-fold larger than those of bare gold. However, the R_{CT} was reduced after the subsequent

incubation in MHO solution. Similar to the result obtained with cyclic voltammetry, this is caused by the removal of physisorbed DNA oligonucleotides and the physisorbed portion of DNA-SH oligonucleotides due to the chemisorption of the MHO to the gold surface through its thiol group. The high surface energy of plasma cleaned gold increases the affinity of other functional groups in DNA to the surface causing random binding and orientation of the nucleotide strand to the surface. Besides causing the high R_{CT} values, random physisorption of oligonucleotides also results in their wide range of R_{CT} values for both DNA-SH and DNA

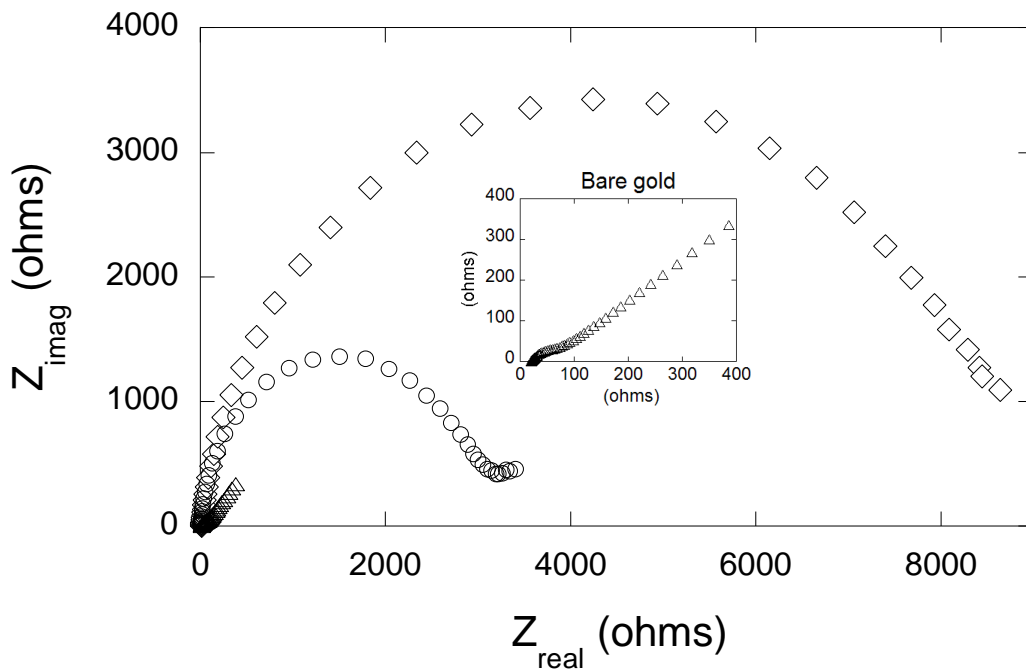


Figure 3.7. Electrochemical impedance spectra of gold slides recorded in the form of Nyquist plots prior to surface modification (Δ bare gold); after surface modification with the mixed monolayer of thiolated probe and 1 mM 6-mercapto-1-hexanol (\circ DNA-SH/MHO); and after hybridization with 1 μ M full match target oligonucleotide (\diamond DNA-SH/MHO+FM). Impedance measurements were performed in 1 mM $K_3Fe(CN)_6$ and 100 mM KCl solution prepared in 10 mM phosphate buffer, pH 7.0. The spectra were obtained in the frequency range from 100 kHz to 0.1 Hz at a fixed DC potential of 0.18 V. Inset: impedance spectrum of the bare gold slide at a smaller scale.

surfaces (Table 3.3). Following incubation in mercapto hexanol solution, the R_{CT} values for the DNA-SH/MHO samples decreased, as also observed for the DNA/MHO surfaces. In both cases incubation in MHO solution provided for consistent R_{CT} values between the samples, while the DNA-SH/MHO surfaces had a larger R_{CT} value compared to the DNA/MHO surfaces.

In addition the DNA/MHO slides had the same resistance as the MHO monolayer, showing that the DNA layer was completely replaced by mercapto hexanol. These results further support the

Table 3.3. Charge-transfer resistance (R_{CT}) of the gold slides after each surface modification step. The standard deviation was obtained from triplicate measurements on three samples. When the relative standard deviation was larger than the 50%, the range of the R_{CT} values obtained is given.

Surface modification	Average R_{CT} ($k\Omega$)	Standard deviation (n = 9)
Bare gold	0.06	0.02
DNA	7.0 – 31	—
DNA-SH	7.2 – 37	—
MHO	0.9	0.2
DNA/MHO	0.8	0.3
DNA-SH/MHO	2.6	0.5
DNA-SH + FM	9.8 – 25	—
MHO + FM	1.4	0.5
DNA/MHO + FM	1.5	0.4
DNA-SH/MHO + FM	8.5	1.0

view that MHO molecules replace the physisorbed DNA, resulting in the formation of a mixed monolayer of DNA-SH and MHO (Figure 3.8).

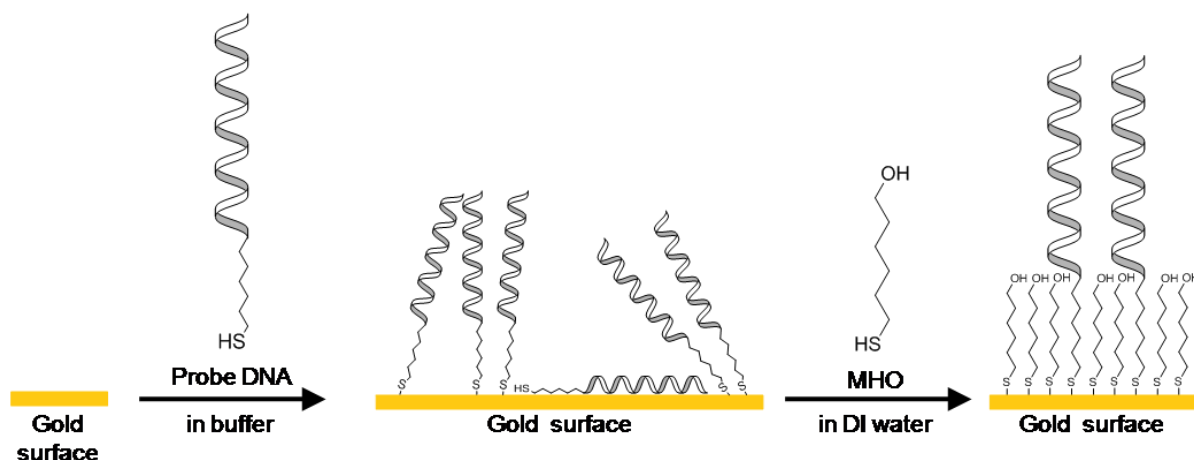


Figure 3.8. Depiction of the changes on the gold surface after each modification step. Incubation of gold in the thiolated probe DNA solution coats the gold surface with a mixture of physisorbed and chemisorbed DNA. The CV and impedance results support the view that only after incubation in MHO solution, the probe DNA is available for hybridization due to physisorption and random orientation prior to incubation in MHO solution.

After the hybridization step by incubation in 1 μM full match (FM) target oligonucleotide, the charge-transfer resistance of the DNA-SH/MHO surfaces increased three-fold, whereas the DNA/MHO slides showed no significant change. In addition, hybridization performed on MHO and DNA-SH surfaces (no incubation in MHO) did not show any changes in R_{CT} values. The increase in R_{CT} only for the DNA-SH/MHO surfaces strongly supports the idea that the thiolated probe DNA strands are attached to the surface as part of a mixed monolayer with MHO molecules and they are capable to hybridize with full match target DNA as shown by the increase the resistivity of the surface towards the negatively charged $[\text{Fe}(\text{CN})_6]^{3-}$ ions.

In a separate experiment, hybridization of DNA-SH/MHO modified slides with each of the four target DNA strands clearly caused a higher charge transfer resistance than the R_{CT} of the samples exposed to the control target DNA. Exposure to the middle mismatch target strand (P11) yielded the lowest average R_{CT} value compared to the full match strand and the other two one-mismatch strands. In addition, the R_{CT} values for the P11 strand were consistently lower than the R_{CT} of the full match strand. However, the other mismatched target nucleotides did not have significantly different average values from the full match strand (Table 3.4).

Table 3.4. Charge-transfer resistance (R_{CT}) obtained after hybridization of probe DNA with the target oligonucleotides on the gold slides. Concentration of target DNA was 1 μ M. The standard deviation was obtained from triplicate measurements on three samples.

Target oligonucleotide	Average R_{CT} ($k\Omega$)	Standard deviation (n = 9)
Control	2.1	± 0.3
FM	4.9	± 0.7
P11	3.1	± 0.8
P1	4.0	± 0.5
P21	3.9	± 0.5

3.3.2. Surface plasmon resonance

The SPR experiments were performed by monitoring the refractive index over time while running the target DNA samples over the sensing surface. Binding of target DNA to the sensor

surface is associated with a proportional increase in the refractive index. This change is usually reported in response units (RU) where 1 RU is equivalent to 1×10^{-6} change in the refractive index. When a 1 μM solution of full match strand (FM) in 3x hybridization buffer was run, the response curve increased by more than 100 RU within one minute and did not return to baseline after rinsing with hybridization buffer (HB) (Figure 3.9). Hybridization of the full match strand is shown by the rapid initial linear increase of the response curve. This is due to a higher concentration of binding sites on the sensor surface compared to concentration of target DNA in solution. After the initial rapid increase, the response curve increases slowly, as the binding sites are nearing the saturation point. At first, the slow phase represents the saturation of the binding

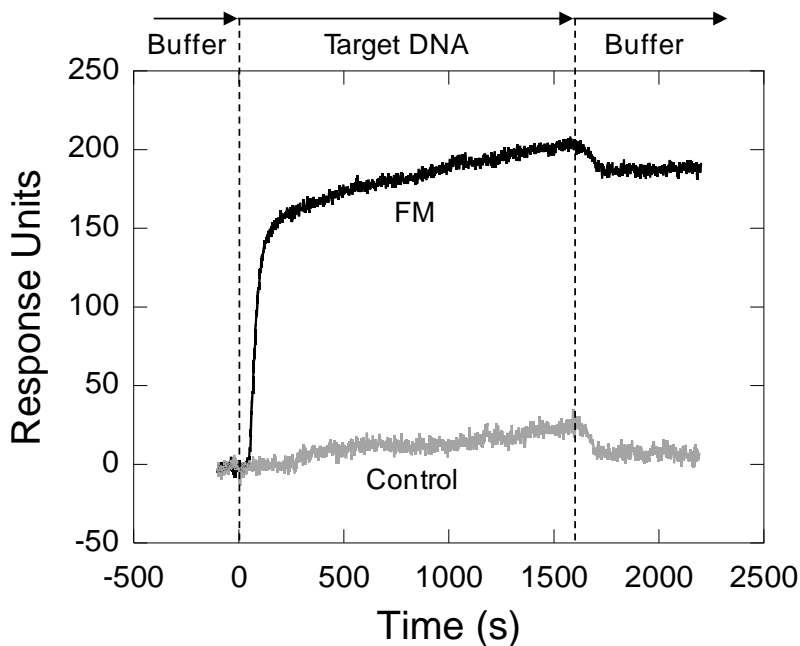


Figure 3.9. Comparison of SPR response when running solutions of 1 μM non-complementary (control) and 1 μM complementary (FM) target DNA strands over the sensor. The SPR experiment was performed in 3x hybridization buffer, using 100 $\mu\text{L}/\text{min}$ flow rate at room temperature. Each sensorgram represents the average of three runs.

sites with target DNA strands, whereas afterwards, as the SPR signal slowly rises, it is caused by the accumulation of target DNA on the solution/surface interface as explained by the model of indirect hybridization.⁶⁷ This theoretical model suggests that prior to hybridization on the surface, the target oligonucleotides must first be non-specifically adsorbed on the surface (i.e. in the solution/surface interface), from where they can diffuse laterally until they find a binding site. According to this model there is equilibrium between oligonucleotides in solution and surface oligonucleotides (non-specifically adsorbed oligonucleotides), which is established only after the binding sites are saturated, as hybridization happens faster than surface adsorption. Therefore, as the binding sites are saturated, the concentration of non-specifically adsorbed DNA on the solution/sensor surface interface slowly increases, resulting in a slow increase of the response curve.

A 1 μ M solution of non-complementary oligonucleotide (control) caused a change in the response curve similar to that of the slow phase of the FM target strand when it flowed over the sensor surface (Figure 3.9). After switching to buffer, the response curve returned back to the baseline level. Following buffer rinse there is a drop in the response curve for the FM strand, too. Therefore, it appears that the slow phase is partially caused by the non-specific adsorption and lateral diffusion of target oligonucleotides on the sensor surface. All RU values reported in this work represent the change in signal with respect to the baseline after the buffer rinse. The sensor surface could be regenerated by washing the surface *in situ* with a denaturing solution (7 M guanidinium chloride). It was found that the response of the sensor remained the same after at least 20 cycles of hybridization/denaturation steps (Figure 3.10), allowing for the sensor surface to be reused for subsequent hybridization measurements. In addition, the sensors were

shown to be stable for at least one year. After storing dry in a sealed container for one month at 4 °C, the sensor was still able to detect the FM target oligonucleotide with the same magnitude as prior to storage.

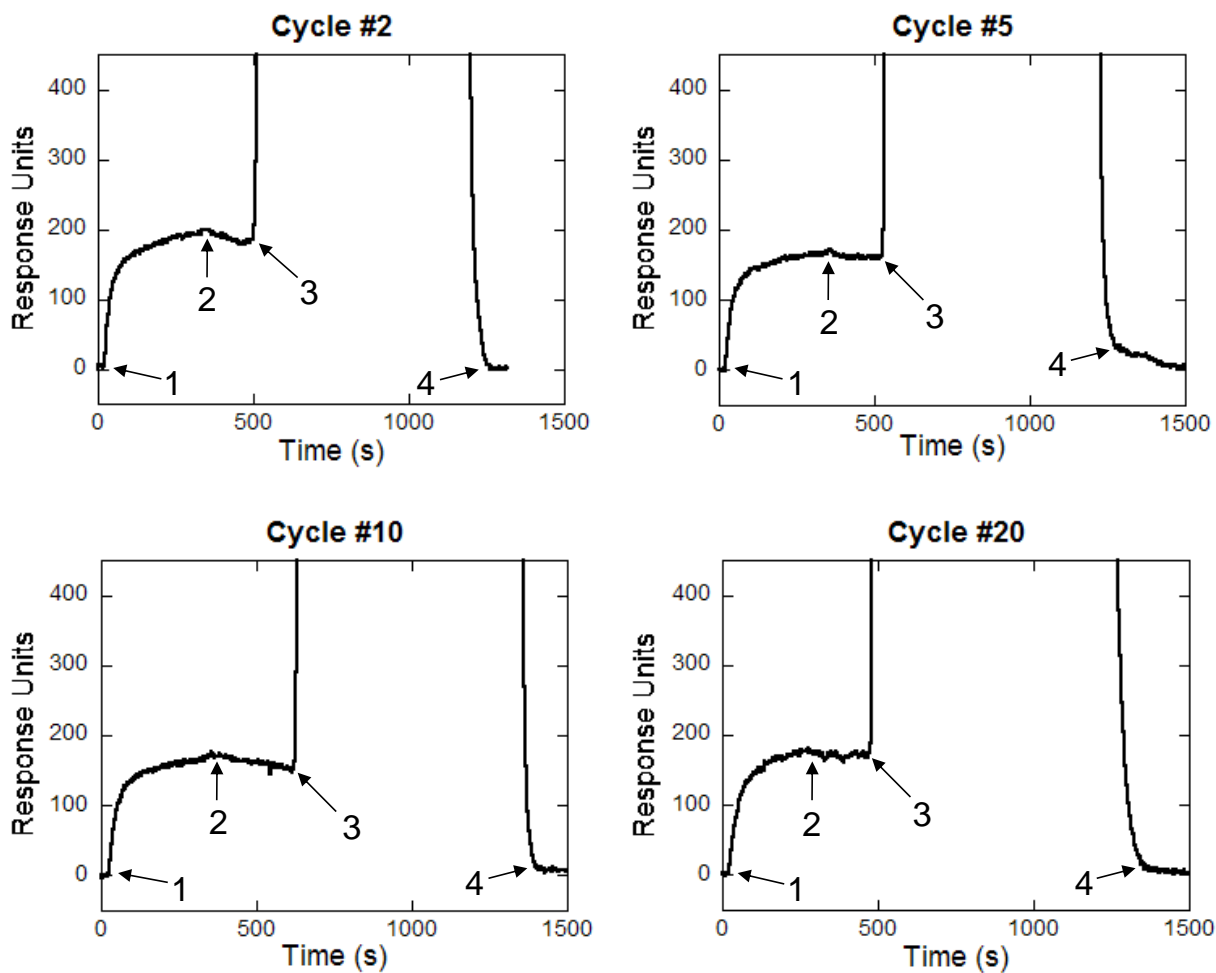


Figure 3.10. Hybridization/denaturation steps for the FM oligonucleotide at different cycles. Each sensorgram starts with the background signal of the hybridization buffer. The numbers indicate time points where different solutions are flowed over the sensor surface: 1 – full match (FM) target oligonucleotide; 2 – hybridization buffer; 3 – denaturing solution; 4 – hybridization buffer. The SPR experiments were carried out in 3x hybridization buffer and 7 M guanidinium chloride as denaturing solution, using 1 μ M target oligonucleotide, with 100 μ L/min flow rate at room temperature. The denaturing solution causes the refractive index to increase from 1.3 to 1.7 (or approximately 40,000 RU) due to its high concentration. Each SPR sensorgram represents the average of three runs.

3.3.3. Effect of hybridization buffer on sensor performance

The change in the SPR response curve upon hybridization was compared between the middle mismatch (P11) and full match (FM) target strands under a range of hybridization buffer concentrations (Figure 3.11). The sensorgrams obtained in 2x, 3x, and 4x hybridization buffer showed a significant difference between the hybridization of the P11 and FM target oligonucleotides. The 3x buffer was selected for the subsequent experiments, since it appeared to give the largest difference between the response curve of the FM and P11 strands. In 5x buffer the refractive index change for P11 and FM target strands is almost identical. This is

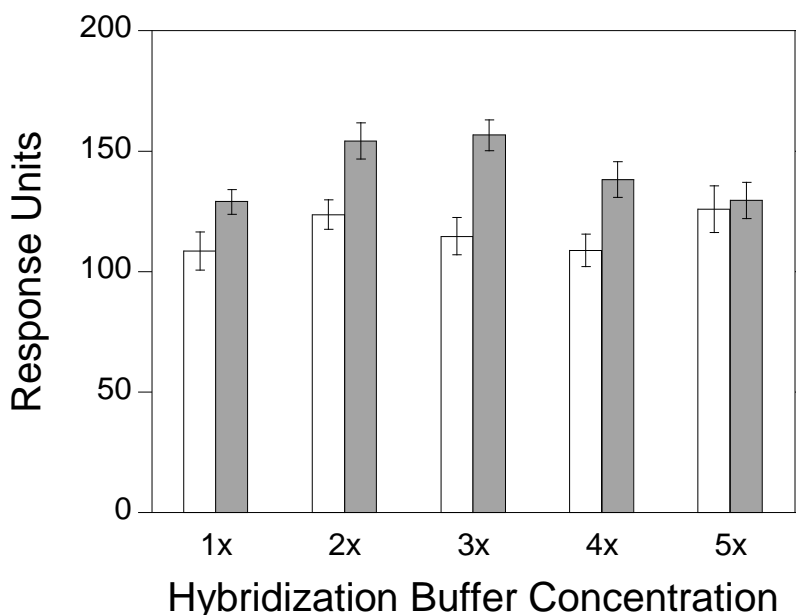


Figure 3.11. Refractive index change after hybridization of 1 μ M P11 (hollow bars) and FM (full bars) target DNA strands at different hybridization buffer concentrations (corresponding to 0.15, 0.30, 0.45, 0.60, and 0.75 M NaCl concentration, respectively). The hybridization experiments were performed using 100 μ L/min flow rate at room temperature with 5 min flow time for the target oligonucleotides. Error bars represent the standard deviation between the sensorgrams obtained from the three sensing areas on the SPR module.

interpreted to mean that the amount of DNA binding to the surface is the same for both oligonucleotides.

The difference in binding affinity between the P11 and FM strands (due to one base mismatch), that is observed for the other HB concentrations, is not obtained at the higher ionic strength of the 5x buffer (see Table 3.2). This result is consistent with known effects of ionic strength on DNA hybridizations.⁶⁸⁻⁷⁰ Since DNA is a highly negatively charged biopolymer due to its phosphate-deoxyribose backbone, the positive ions present in solution neutralize the negative charges of the DNA backbone, thus facilitating the hybridization of DNA strands. This ionic strength dependence of DNA/DNA interactions is observed in several ways on sensor surfaces, such as: the degree of single-strand DNA (ssDNA) stretching; reduction of negative charge repulsion between probe and target due to the presence of positive ions; and, by the same effect, the reduction of repulsion among probe strands on the surface before and after hybridization. As a result, the higher ionic strength of the 5x buffer reduces the electrostatic repulsion between the DNA backbones on the sensor surface caused by the unpaired base and facilitates hybridization for the one-mismatch P11 strand so that it has the same change in magnitude as the FM strand.

At relatively low ionic strength or 1x hybridization buffer, the difference in the response curve between P11 and FM was also reduced. This is in accordance with the ionic strength effect. At low ionic strength hybridization is not as efficient as in higher salt concentrations, therefore fewer FM strands hybridize. Most importantly, Figure 3.11 shows that with regard to detecting single nucleotide mismatches, this sensor is capable of detecting single nucleotide mismatches in a wide range of buffer or salt concentrations (0.30 – 0.60 M NaCl). Thereby, from a practical

implementation aspect, this sensor would not be affected by fluctuations in buffer or salt concentration between different DNA sample solutions, with regard to detecting single nucleotide mismatches.

3.3.4. Effect of flow rate and temperature on sensor performance

The rate of analyte delivered to the sensor matrix on the surface, also known as the mass transport of analyte, has been reported to affect the binding or hybridization rate.^{26, 71-73} In order to detect DNA, these SPR systems usually contain sensing surfaces that consist of 100 nm thick carboxymethylated dextran polymers, which provide many anchoring sites for attaching probe DNA using biotin-streptavidin. However, for our sensor, the flow rate was not expected to affect the response signal for binding of analyte to the surface, since the sensor surface is planar. The results in Figure 3.12A show the change in RU for FM and P11 target at different flow rates. The results show that the flow rate had no significant influence on the SPR response between the P11 and FM strands.

With an approximate 0.08 mm² cross sectional area and 0.72 μ L total volume of the flow channel, the actual liquid velocity on the sensor surface varies from 4 mm/s (for 20 μ L/min) to 167 mm/s (for 800 μ L/min). These liquid velocities should have the same effect on the DNA hybridization, since mass transport is not the rate limiting step, (i.e. it is not a factor for this sensor).⁷⁴ Fluctuations in flow rate are therefore not expected to influence the response of the sensor and its ability to detect single nucleotide mismatches, an important consideration in designing a practical analytical instrument. The 100 μ L/min flow rate was preferred in this study for practical reasons, because it allowed for a larger number of hybridizations to be carried out,

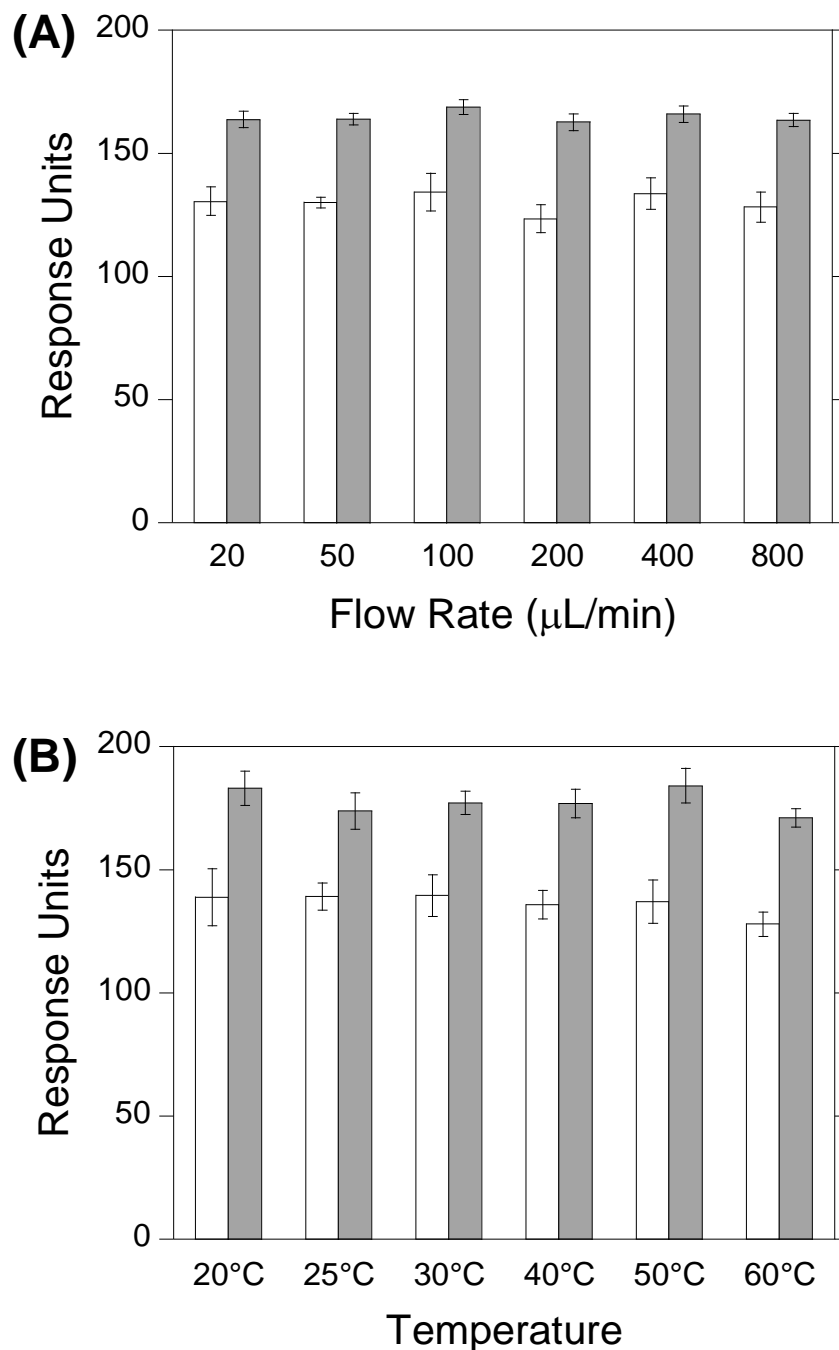


Figure 3.12. Refractive index change after hybridization of 1 μM P11 (hollow bars) and FM (full bars) target DNA strands as a function of (A) flow rate; (B) temperature. The hybridization experiments were carried out in 3x buffer using 100 $\mu\text{L}/\text{min}$ flow rate at room temperature (unless specified otherwise) with 5 min flow time for the target oligonucleotides. Error bars represent the standard deviation between the sensorgrams obtained from the three sensing areas on the SPR module.

while using a relatively small sample volume (0.5 – 3.0 mL). However, if only a small volume of sample is available (< 1 mL), a lower flow rate would be more advantageous, since it will allow time for binding equilibrium to be reached before the entire sample is consumed. Nevertheless, the time parameter can be removed, if the sample is re-circulated, (i.e. if the output from the sensor goes back to the sample container).⁷⁴ We note that there are small, but statistically significant variances between measurements for the same oligo. However, no systematic changes were observed.

The binding affinity for DNA hybridization in solution is also known to be affected by temperature.^{68, 75, 76} In our experiments the *change* in the SPR response upon target oligonucleotide hybridization was not affected in the range 20°C – 60°C. The melting temperatures of the FM and P11 oligonucleotides were 67.1 and 61.0 °C, respectively. Even though it was expected that at higher temperatures would increase the gap between the FM and P11 strands this was not observed. This indicates that hybridization on the surface is not affected by temperature unlike hybridization in solution. In addition, it has been reported that for long oligonucleotide sequences (more than 20 bases) the melting point is affected by the dispersion or availability of the probe DNA on the surface.⁷⁷ Performing hybridization on the surface at higher temperatures (which was not done due to experimental set-up limitations) could increase the gap in signal between the FM and P11 target strands. The difference in SPR response as a function of temperature between P11 and FM was also not affected by temperature (Figure 3.12B). It is noted that provided the temperature of the sensor and flow rate are kept constant (± 0.5 °C and ± 60 μ L/min, respectively) during the measurement, then these parameters do not change our ability to monitor hybridization and detect single nucleotide mismatches.

3.3.5. Effect of mismatch site on sensor response

The effect of the mismatch site on the SPR response was investigated in 3x buffer, using 100 $\mu\text{L}/\text{min}$ flow rate at room temperature. Hybridization of the P11 strand resulted in the smallest change in amplitude, followed by the 3' end mismatch (P21) and then the 5' mismatch (P1) target strands (Figure 3.13). The rate of hybridization was highest for the FM strand (4.85 RU/s), decreasing for the P1 strand (2.60 RU/s), while the P11 and P21 strands were similar and had the lowest rates (1.66 and 1.52 RU/s, respectively). The hybridization rates (Table 3.5) were obtained from the slope of the linear phase of the SPR sensorgrams shown in Figure 3.13. The difference in binding between the one-mismatch target strands may be explained in terms of the effects of ionic strength on DNA hybridizations or the proximity of the mismatch to the solution.

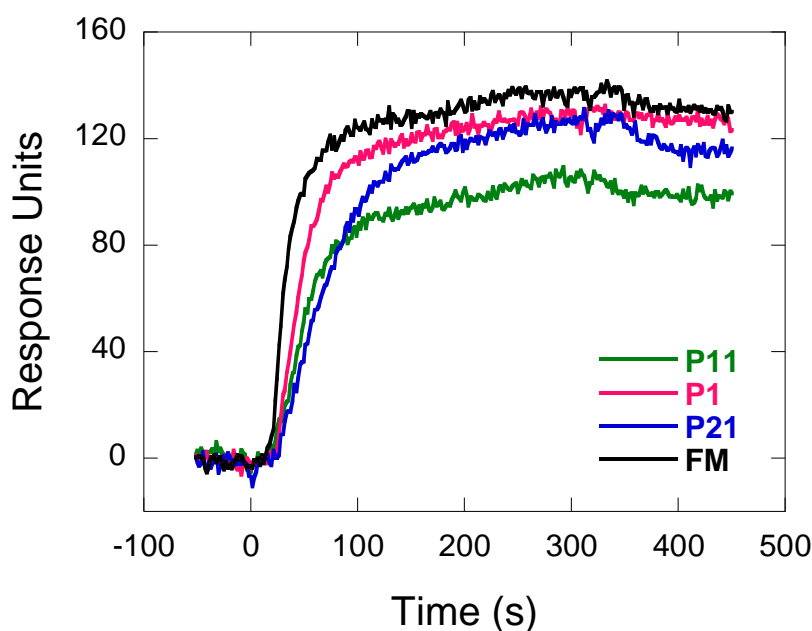


Figure 3.13. Overlapped SPR sensorgrams obtained after flowing 1 μM P11, P1, P21, and FM target DNA oligonucleotides over the sensor surface. The effect of the mismatch site on the SPR response was investigated in 3x hybridization buffer, using 100 $\mu\text{L}/\text{min}$ flow rate at room temperature for 5 min. Each sensorgram represents the average of three runs.

Table 3.5. Binding rates of target oligonucleotides at 1 μM concentration, obtained from Figure 3.13. The binding or hybridization rates represent the slope of the linear region of each sensorgram. The error was obtained by performing a regression analysis of each plot using Excel spreadsheet.

Target oligonucleotide	Binding rate (RU/s)
FM	4.85 \pm 0.44
P11	1.66 \pm 0.08
P1	2.60 \pm 0.10
P21	1.52 \pm 0.08

Following hybridization of the P1 strand the mismatch is formed on the distal end of the duplex or at the DNA monolayer/solution interface, whereas for the P21 strand the mismatch is formed at the proximal end, i.e. closer to the gold surface and away from the DNA monolayer/solution interface. As both mismatches cause the unpaired ends of the target strands to occupy more space than if they were hybridized, it is the proximal mismatch that is more restrained and feels stronger repulsions from neighboring probe strands, thus reducing the rate of formation of the duplex and its stability. The unpaired base of the P1 strand on the distal end is more flexible and it is more accessible by positive ions and the electrostatic repulsion among DNA strands is reduced by the presence of positive ions. As for the P11 strand it could hybridize with the probe through one half or it can fully hybridize and form a small bulge in the middle of the sequence. The middle position of the mismatch could also allow cross-hybridization between two neighboring probes, as suggested by Levicky and Horgan.⁷⁸ The P11 strand appears to have the lowest change in magnitude of the refractive index after hybridization thus the smallest number

of target DNA oligonucleotides bound to the surface. Therefore, it is more likely that cross-hybridization between two probes is the most common scenario. A depiction of this explanation is shown in Figure 3.14.

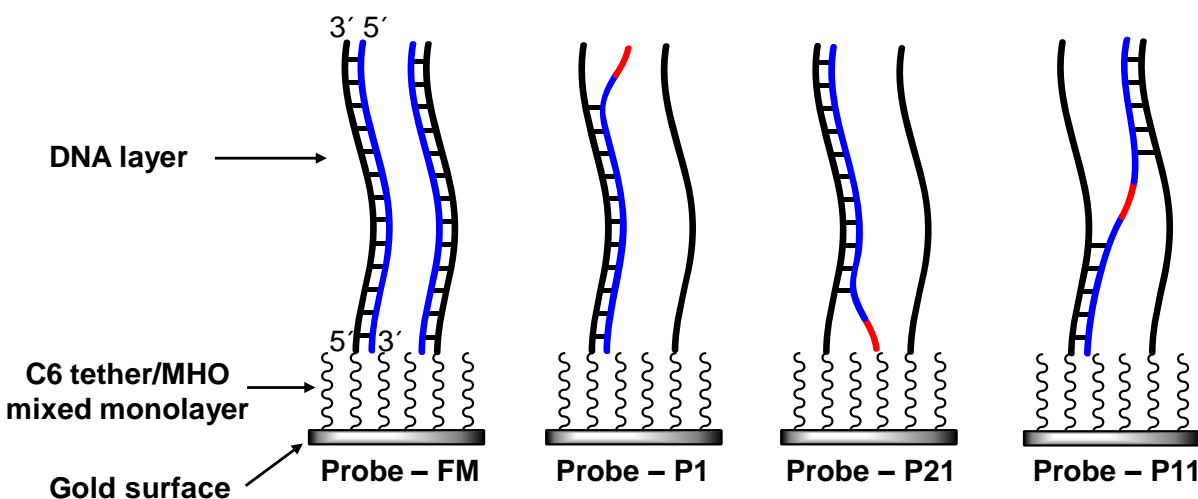


Figure 3.14. Hybridization of the target DNA strands (blue) to the probe strand (black) on the sensor surface. The mismatched base is shown in red. C6 tether and MHO refer to the hexane thiol tether of the DNA probe and 6-mercapto-1-hexanol, respectively. The P11 strand could also bind to one probe, resulting in the formation of a small bulge.

3.3.6. DNA concentration

A series of hybridization experiments was performed to test the influence of target DNA concentrations for both the FM and the one mismatch strands. As can be seen from Figure 3.15, the signal response was 20% or larger for the hybridization of the FM strand at all concentrations when compared to the P11 strand. The response magnitude of the P21 strand was also lower in magnitude compared to the FM strand at all concentrations. This demonstrates the ability of the sensor to distinguish single nucleotide mismatches in the middle and 3' position of the target strand over several orders of magnitude in concentration. The P1 strand showed no

significant difference with the FM strand. The smallest concentration measured was 100 pM. Accounting for the baseline noise, the detection limit of the oligonucleotides was determined to be 20 pM, calculated as a triple of baseline noise standard deviations. Assuming a working sample volume of 500 μL and the flow rate to be 20 $\mu\text{L}/\text{min}$, the detection limit was calculated to be 10 femtomoles.

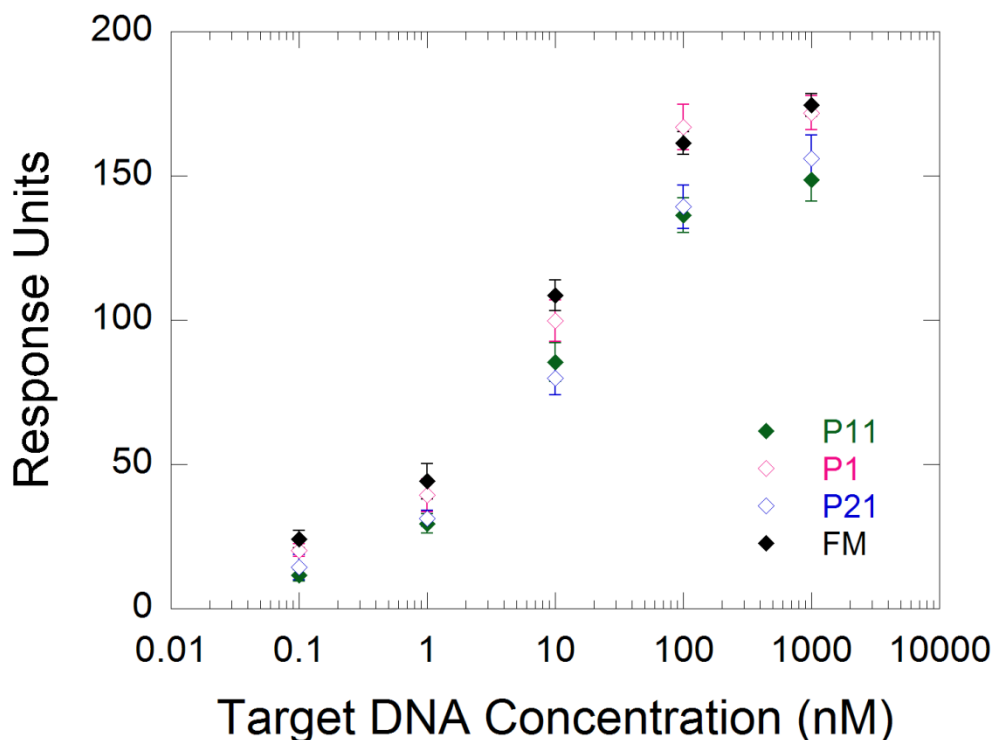


Figure 3.15. Refractive index change after hybridization of P11, P1, P21, and FM target DNA strands at different concentrations. The hybridization experiments were conducted in 3x hybridization buffer, using 100 $\mu\text{L}/\text{min}$ flow rate at room temperature for 30 min. The differences in RU are statistically significant at all concentrations between the FM and P11 and FM and P21 target strands. Error bars represent the standard deviation between the sensorgrams obtained from the three sensing areas on the SPR module.

The concentration dependant data were fit to different linearized forms of the Langmuir equation (equation 3.1), and the best fit was provided from the Hanes-Woolf linearization (equation 3.2):

$$S = S_{max} \frac{KC}{1 + KC} \quad (3.1)$$

$$\frac{C}{S} = \frac{1}{S_{max}K} + \frac{C}{S_{max}} \quad (3.2)$$

where C is the concentration of target DNA, S is the change in refractive index at each target DNA concentration, S_{max} is the maximum binding of target DNA or maximum increase in the refractive index, and K is the binding affinity. The Langmuir equation shows the dependence of analyte coverage or adsorption on a solid surface from the solution concentration of the analyte in the medium adjacent to the surface. The Hanes-Woolf linearized equation which is derived from the Langmuir equation provides an easier way for fitting experimental data than the Langmuir equation which requires more sophisticated computer programs. The fits were done with Microsoft Excel. The fits resulted in binding affinities that show the FM and P1 strands to have the highest affinities, whereas the P11 and P21 strands had relatively lower affinities (Table 3.6). These values match the order of the binding rates observed in Figure 3.13.

Table 3.6. Binding affinities and maximum coverage of target oligonucleotides obtained from Figure 3.15, using the Hanes-Woolf equation.

Target oligonucleotide	Binding affinity (K) ($\times 10^8 \text{ M}^{-1}$)	Maximum coverage (S_{max})
FM	2.4	175.4
P11	1.7	149.5
P1	2.4	172.7
P21	1.5	157.2

3.3.7. RNA oligonucleotide detection

The detection of a full match RNA oligonucleotide was also monitored as a function of concentration, as shown in Figure 3.16. The sensor yielded a very similar SPR response and detection limit as those observed for DNA sensing. These results demonstrate the potential use of this sensing system to rapidly detect short RNA sequences using the DNA probe oligonucleotide. The use of a probe RNA oligonucleotide is not practical owing to the instability of RNA compared to DNA.⁷⁵ The results show that our DNA-based sensor is capable of detecting or binding RNA oligonucleotides with the same efficiency as DNA oligonucleotides. Therefore, this sensor has the potential to be used for detection of RNA directly from biological samples.

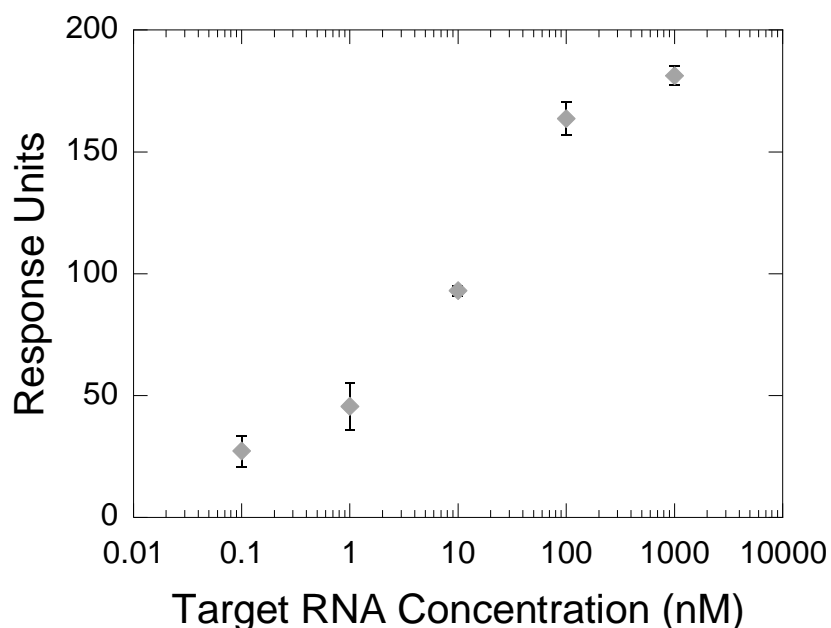


Figure 3.16. Refractive index change after hybridization of the full complementary RNA strand at different concentrations. The hybridization experiments were conducted in 3x hybridization buffer, using 100 $\mu\text{L}/\text{min}$ flow rate at room temperature for 30 min. Error bars represent the standard deviation between the sensorgrams obtained from the three sensing areas on the SPR module.

3.3.8. Surface coverage of probe DNA

The electrochemistry data demonstrated that incubation of probe DNA coated gold surfaces in 6-mercapto-1-hexanol (MHO) removed the physisorbed DNA and allowed for spacing of thiolated DNA probe. No change in the charge transfer resistance (or hybridization) was observed, when DNA-SH or MHO only surfaces were exposed to the FM strand (Table 3.3). Thiolated probe DNA oligonucleotide surface densities after incubation in MHO solutions have been shown to be in the range of $2.0 \times 10^{12} - 3.8 \times 10^{13}$ molecules/cm²,^{50,51} while the highest target hybridization density (7.0×10^{12} molecules/cm²) was obtained after 1 hour incubation in MHO.⁵⁰

As it will be explained below, we believe our probe density is within the range above, which would allow space for efficient target hybridization. SPR experiments involving hybridization of target DNA oligonucleotides to probe on the surface have shown that an increase of 1 Response Unit corresponds to 1.2 pg/mm² surface-bound DNA (regardless of oligonucleotide length).⁷⁹ For the FM strand (MW 6,486 g/mol), since the average change in refractive index was 174.7 and each sensing region of the SPR module has a 0.45 mm² surface area, the average amount of oligonucleotide on the surface after hybridization was calculated to be 7.2×10^{-12} moles/cm². Dividing by Avogadro's number provides for a target surface density of 4.3×10^{12} molecules/cm². This means that the density of our probe DNA is equal to or higher than 4.3×10^{12} molecules/cm². Interestingly, it has been reported that maximum hybridization of probe DNA (with 70 – 100% hybridization efficiency) is obtained only when the probe DNA density is lower than 4×10^{12} molecules/cm².⁵⁰ In addition, surface attachment of a duplexed

probe DNA (hybridized prior to immobilization) produced a surface density of 2.8×10^{12} molecules/cm².⁵¹

These experimental results are approximately 10-fold smaller than the theoretical maximum coverage of double stranded (duplexed) DNA based on the diameter of the duplex. Double stranded DNA has a diameter of 2.4 nm and if oriented perpendicular to the surface, each duplex would cover a circle with a surface area of 4.5 nm². Assuming maximum surface coverage by hexagonal packing the surface density is calculated to be 2.2×10^{13} molecules/cm². This implies that steric hindrance is not the only factor that needs to be considered when calculating maximum double strand DNA surface coverage. The electrostatic repulsion among the phosphate DNA backbones causes them to require more space than the one calculated by geometric impediments in order for the DNA strands to pack tightly. This is confirmed by the fact that the immobilization of duplexed DNA probe achieved a surface density of only 2.8×10^{12} molecules/cm², even though it was deposited in 1 M NaCl, which has a relatively high ionic strength and would be able to repress some of the electrostatic repulsion.

Vainrub and Pettitt modelled the effect of electrostatic repulsion forces upon hybridization of 25-base target oligonucleotides and determined that suppression of hybridization begins at surface densities as low as 10^{12} molecules/cm².^{80,81} This could mean that in our sensor surface the hybridized probes are already feeling the presence of neighboring hybridized probes. In our sensor the spacing of probe DNA appears to be sufficient enough to see a difference in binding between the proximal (3') and distal (5') mismatch in the target DNA.

We did a further calculation to determine the average spacing of hybridized probes on our SPR sensor based on the surface density of bound full match target (or hybridized probes) calculated earlier to be 4.3×10^{12} molecules/cm². This was done from two different considerations: (1) assuming a random packing of probe DNA on the surface, then the square root of the surface density unit would give the average number of probes per unit length (2.1×10^6 molecules/cm), meaning the average distance or spacing between the hybridized probes would be 4.8 nm. Since duplexed DNA has a diameter of 2.4 nm, then the edge to edge separation between the hybridized probes would be 2.8 nm; (2) assuming ordered packing of the duplexed probes and since their footprint on the surface would be a circle, then they would pack hexagonally and cover only 90.7 % of the available surface (see Section 4.2.2). Thus a surface density of 4.3×10^{12} molecules/cm² corresponds to a surface area of each hybridized probe of 2.1×10^{-13} cm²/molecule, resulting in a distance of 5.2 nm between two hybridized probes. The edge to edge distance would be 2.8 nm.

In both considerations of probe DNA packing, the spacing between hybridized DNA probes is theoretically sufficient to fit another probe-target DNA pair, but as both experimental and modelling studies have shown, the sensing surface is already saturated with duplexed DNA. Most likely the overall probe density for our sensor is higher than 4.3×10^{12} molecules/cm², meaning there are single-stranded probe oligonucleotides between the hybridized ones. And it is the presence of these un-hybridized probes that is probably causing the discrepancy in binding between the one-mismatch target oligonucleotides, depending on the location of the mismatch. Therefore, these results show that by controlling probe DNA spacing, one could potentially control the ability of the sensor to distinguish between full match and single nucleotide mismatch

target, including the magnitude of difference in signal, as a larger (approximately more than 50%) change in signal upon hybridization would be easier to detect.

3.4. Summary and Conclusions

The electrochemistry data showed that incubation in 6-mercapto-1-hexanol (MHO) removed the physisorbed DNA and allowed for spacing of the thiolated DNA probe. No change in the charge transfer resistance (or hybridization) was observed, when DNA-SH or MHO only surfaces were exposed to the FM strand (Table 3.3). Thiolated probe DNA oligonucleotide surface densities after incubation in MHO solutions have been shown to be in the range of $2.0 \times 10^{12} - 3.8 \times 10^{13}$ molecules/cm², while the highest target hybridization density (7.0×10^{12} molecules/cm²) was obtained after 1 hour incubation in MHO. It is estimated that the probe densities in our experiment are within the range above, which would allow space for efficient target hybridization.

To our knowledge this is the only work where a comparison is performed between 3', 5', and middle mismatches and the effect of three hybridization parameters (buffer concentration, flow rate, and temperature) is studied with regard the detection of single oligonucleotide mismatches. The results showed that fluctuations in buffer concentrations, flow rate and temperature should not impede the sensor's ability to detect single nucleotide mismatches. Compared to other SPR-based SNP sensors, our system was able to detect mismatches at much lower DNA concentrations (100 pM). The sensor was shown to be reproducible over at least 20 cycles of hybridization/denaturation. In addition, the sensors were shown to be stable for at least one

month. After storing in a sealed container dry for one month at 4 °C the sensor was still able to detect DNA hybridization and distinguish between the FM and P11 target oligonucleotides.

In this work, the surface of a commercially available SPR sensor was modified by self-assembly to create a mixed monolayer of a thiol modified 21-base long DNA probe and 1-mercapto-6-hexanol, in order to avoid non-specific adsorption and to facilitate hybridization of target DNA. The detection limit was 20 pM or 10 femtomoles, while single-nucleotide mismatches could be detected over five orders of magnitude in concentration. RNA was also detected with the same detection limit as DNA. The site of the mismatch affected the SPR response. The P11 (middle) and P21 (3' mismatch) DNA strands caused a decrease in the magnitude of the SPR response compared to the full match strand. The observed response for P1 (5' mismatch) hybridization was similar to that of the full match strand. This shows that single mismatches at the proximal end of the probe result in a less efficient hybridization of target to probe compared to the mismatch being on the distal end of the probe, which is closer to the solution. Most importantly, with regard to detecting single nucleotide mismatches, this sensor is not affected by fluctuations in buffer concentration or salt concentration of the DNA sample solution.

Flow rate and temperature did not affect either the hybridization efficiency of target oligonucleotides to the probe or sensor performance. The concentration of the hybridization buffer did not affect the response of the sensor over a wide range (0.30 – 0.60 M NaCl) with regard to the detection of single-nucleotide middle mismatch. Therefore any fluctuations in these parameters should not affect the read-out of the sensor. In addition, the detection time of this sensor was five minutes or less. This opens the way for a practical sensing system. By using

microfluidic platforms, this sensing system could be employed to construct parallel sensing channels for rapid and label-free multiple sample analysis. In addition, this system could potentially be paired with other detection methods, such as impedance spectroscopy, in order to obtain a dual read-out biosensor.

3.5. Practical Implementations and Future Work

As mentioned in the introduction, there are three major field applications for the nucleic acid sensor described and assayed in this work; (1) medicine, where it can be used for detection of single nucleotide polymorphisms (SNPs) and micro RNAs (miRNAs); (2) bioengineering for the detection of genetically modified organisms (GMOs); and (3) homeland security, where it can be used as a detector of pathogenic microbes and viruses. Detection of SNPs and miRNAs has a direct application of our sensor in the current format. However in each case, there are obstacles that need to be addressed. For detection of SNPs, sample preparation is required from blood or mouth swab samples, starting with amplification of genomic DNA or messenger RNA (mRNA) by using polymerase chain reaction (PCR). Amplification of the genomic DNA sequence containing the SNP will provide the genetic imprint of the SNP, whereas mRNA amplification (which requires initially an additional step to convert RNA to complementary DNA or cDNA) will provide information about which SNP is being expressed if the individual is heterozygous. In both cases the PCR product is double-stranded with the size varying from 60 base-pairs (bp) to usually 300 bp. This means that the product is longer than the synthetic target oligonucleotides used in this study. In addition, prior to analysis of the PCR products, it will be

necessary to denature the dsDNA either chemically or physically as it is done for common DNA sensing assays, such as Southern blots.

With respect to using PCR, denaturation of duplexed DNA in the presence of a chemical reagent, such as guanidinium chloride or formamide, would have to be done *in situ*. This would impede hybridization with the probe DNA and most likely increase the detection limit of the sensor considerably, while some of the reagent could damage the sensor surface or the flow cell assembly. Generation of single-stranded DNA can be achieved without the use of denaturing agents. Asymmetric PCR allows for amplification of one strand for more cycles than the complementary strand by using unequal primer concentrations (increasing the concentration of the primer whose elongation results in the desired sequence).⁸² At the end of the PCR process there will be a mixture of double and single strands of amplified DNA. The single stranded DNA provides the target sequence that can hybridize with the probe DNA.

The asymmetric PCR method will be employed in constructing a DNA sensor for detection the mutations that are a cause of Alzheimer's disease in 50% of the cases. Two polymorphisms that occur within 46 base pairs are responsible, and either one can be used for the mismatch detection.⁸³ Detection of the mutations will be done by using asymmetric amplification of DNA to obtain a mixture of single and double stranded genomic sequences that contains the polymorphic sites. Restriction enzymes (which have been previously selected) will be used to cut a 21-30 base pair long sequence containing the polymorphic sites from the longer double stranded PCR product. After running one denaturing step by heating the sample, the short

double strand sequences will denature and then rehybridize randomly resulting in enough single stranded 21-30 base long single stranded sequences to be detected by our SPR sensor.

The results also showed that the sensor can be used to detect RNA oligonucleotides. RNA samples are typically single stranded, but could have secondary structures or form partial double helix structures. Similar to DNA samples, chemical or physical methods such as temperature can be used to disrupt the double helix or secondary structures. Another way to detect RNA would be to use RNA as a template for cDNA prior to sensing, which would also amplify the amount of the target sequence. Our goal will be to increase the change in signal between the full match and single mismatch in order to make the sensor useful in many more applications.

As mentioned in the Introduction, detection of miRNAs has become very important in understanding gene expression and controlling the gene expression pathways when they are the cause of the disease. In order to address this area of research, we selected a miRNA sequence that is known to be involved in many pathways. In fact this miRNA exists in several sequences that vary by 1- 3 nucleotides comprising a family. Using a DNA probe with matching sequence and the synthetic RNA sequence a titration curve was obtained. Interestingly the 22-base target sequence showed a higher binding signal compared to the 21-target sequences (Figure 3.17). The detection limit was similar to the 21-base RNA. RNA from Jurkat cells was isolated and small RNA sequences (less 100 bases) were purified with an RNA purification kit. However, our sensor was not able to detect the specific miRNA from the purified RNA sample. This means the sensitivity of the DNA sensor has to be increased. For the detection of RNA from pathogenic

microorganisms this can be done by using a longer DNA probe. A larger mass of the binding analyte is expected to provide a larger change in the refractive index signal.

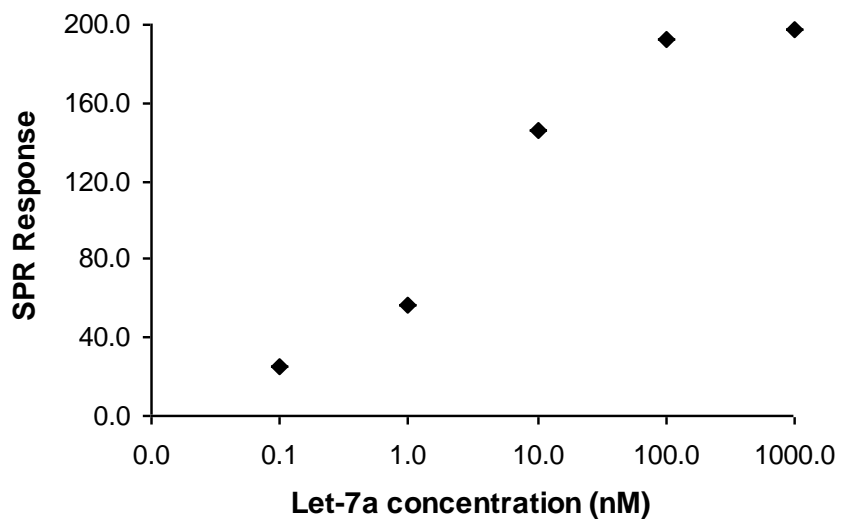


Figure 3.17. Refractive index change after hybridization of the full complementary Let 7a DNA strand at different concentrations. The hybridization experiments were conducted in 3x hybridization buffer, using 100 $\mu\text{L}/\text{min}$ flow rate at room temperature for 30 min.

4. Enzyme-based Biosensor

4.1. Introduction

Acetylcholinesterase (AChE) terminates impulse transmissions at cholinergic synapses in the nervous system by rapid hydrolysis of the neurotransmitter acetylcholine.^{84, 85} This is achieved by hydrolyzing acetylcholine in the postsynaptic neuron after the action potential has been transmitted (Figure 4.1A). Acetylcholine is the only neurotransmitter in neuro-muscular

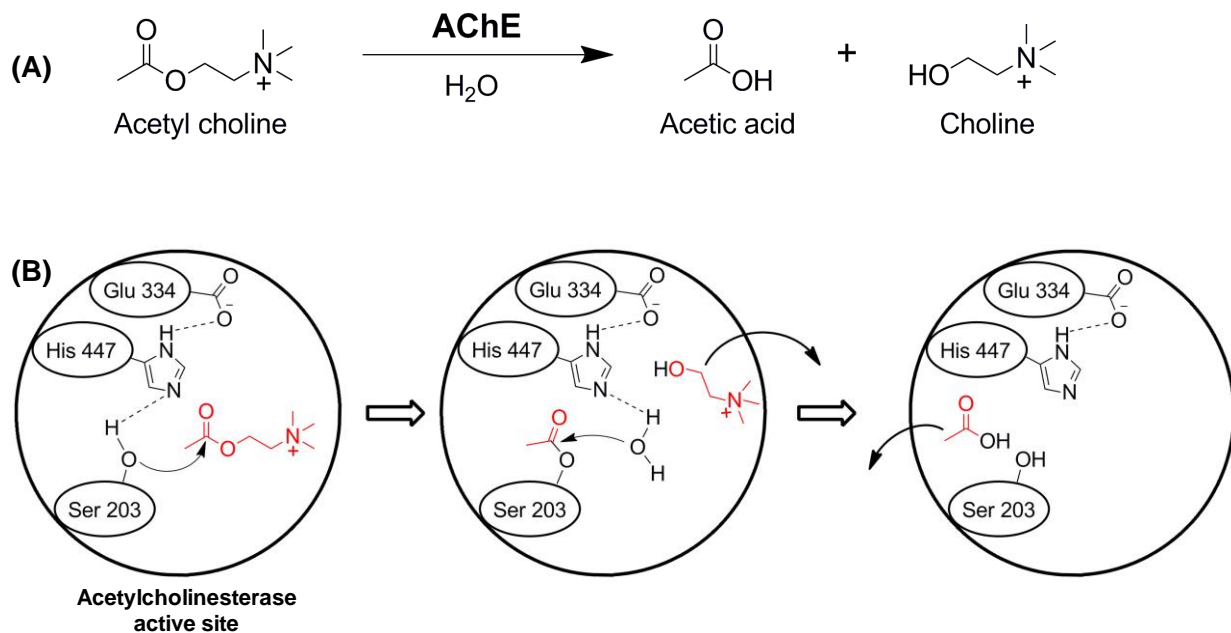


Figure 4.1. Hydrolysis of acetylcholine by acetylcholinesterase. (A) Hydrolyzation reaction of acetylcholine in the presence of AChE. (B) The steps involved in the hydrolysis of acetylcholine inside the AChE active site. The serine residue in the active site is rendered highly nucleophilic through a charge-relay system involving hydrogen bonding between the glutamate carboxyl, the histidine imidazole and the hydroxyl of the serine. Upon acetylcholine entering the active site, the hydroxyl attacks the carbonyl carbon, resulting in the formation and loss of choline and acylation of the serine residue. This is immediately followed by deacylation of the serine residue from the nucleophilic attack by a water molecule, resulting in the formation of acetic acid and regeneration of the active site.

junctions, while it is also found in the autonomous nervous system and central nervous system. The presence and normal function of AChE ensures blocking of continuous and uncontrolled generation of action potentials in the postsynaptic neuron.

Acetylcholinesterase is a serine esterase that belongs to the hydrolase category of enzymes. It is a globular protein with an ellipsoidal shape that has approximate dimensions of $45 \times 60 \times 65$ angstroms.⁸⁶ AChE's active site contains two regions: the catalytic region where the ester bond is hydrolyzed, and the anionic region that accommodates the positively charged portion of acetylcholine. The first region contains the catalytic triad of Ser 203, His 447, and Glu 334. This catalytic triad is similar to other serine esterases. The mechanism of this type of enzyme involves the nucleophilic attack of the hydroxyl group of the serine residue on the carbonyl carbon of the ester bond. The serine residue is temporarily acylated, as choline is formed and diffuses out of the active site. Next, the acylated hydroxyl of the serine residue is hydrolyzed and acetate is formed and diffuses out of the active site, which is ready again to hydrolyze another acetylcholine (Figure 4.1B).

Due to its function, AChE is the target of many neurotoxins and drugs, which bind specifically to its active site. Total inactivation of this enzyme by irreversible inhibitors results in excessive stimulation of nerve impulses followed by uncontrolled convulsions and eventually, death.⁸⁷ These inhibitors have found application as pesticides, such as carbofuran and parathion, and nerve agents, such as Sarin and VX. Controlled or "reversible" inhibition of AChE has therapeutic uses, including in Alzheimer's disease therapy.^{84, 88, 89} Reversible inhibitors include tetraalkylammonium ions and carbamate compounds, whereas irreversible inhibitors consist of

organophosphate compounds. Neostigmine and eserine (Figure 4.2) are reversible carbamate AChE inhibitors that are used as treatments in conditions where the activity of the AChE enzyme needs to be lowered. Neostigmine is used to treat people with myasthenia gravis, a neuromuscular disease that results in muscle weakness.⁹⁰ Eserine is used to treat myasthenia gravis and Alzheimer's disease symptoms.⁹¹

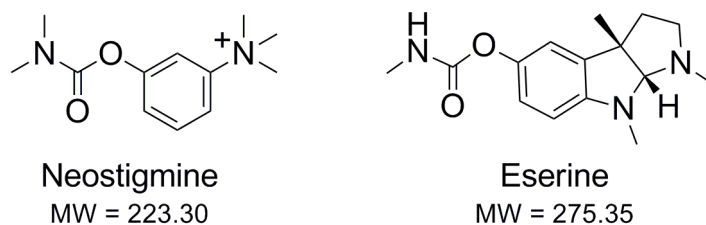


Figure 4.2. The chemical structures of the reversible carbamate AChE inhibitors used in this study.

AChE provides a probe in developing biosensors capable of detecting these types of therapeutic drugs and possibly neurotoxins. Several biochemical detection methods have been developed and proposed for AChE inhibitors. Most of them rely on the photometric sensing of AChE activity by employing acetylthiocholine and 5,5'-dithiobis-(2-nitrobenzoic acid) (DTNB) also known as Ellman's reagent.⁹² A few other methods have also been reported, that use chemiluminescence^{93,94} and electrochemical detection.^{95,96} Coupled with surface plasmon resonance, AChE immobilized on the sensor surface can be used to detect and screen for inhibitory drugs. Surface plasmon resonance (SPR) is an optical technique which reports changes in refractive index based on alterations occurring in the dielectric medium within 500 nm from a metal surface.³¹ SPR makes possible real time, label-free detection of

biomolecular binding event, such as, antibody-antigen interactions, and protein-DNA interactions (see Section 3.1).

In this study, AChE was covalently attached to a self-assembled monolayer on the surface of a Spreeta SPR sensor (ICX Nomadics) using amide coupling chemistry *via* EDC/NHS activation. Protein immobilization and activity on the surface was confirmed with several surface characterization techniques and a standard photometric AChE activity assay. Binding of AChE inhibitors was monitored by SPR at different concentrations of neostigmine and eserine by observing the change in the SPR response signal. The sensor was able to detect both inhibitors at micromolar concentrations and provide binding affinity constants for both inhibitors; therefore it can be used to monitor drug concentration in patients and also to directly study the binding of different AChE inhibitors.

This enzyme-based sensor has the potential to be used in the detection and screening of new inhibitor drug candidates, which could be more effective for the treatment of the diseases mentioned above. In addition, by binding different AChEs on the surface, the different enzymes can be screened in order to obtain those that provide the largest change in the SPR signal upon binding of neurotoxin inhibitors such as pesticides and nerve agents. This will increase the detection limit, so the sensor can potentially be used for the detection of the neurotoxins.

The relatively large change in refractive index compared to the relatively small molecular weight of the inhibitors, indicates that the change in SPR signal is due to a shift in conformation of the enzyme as a result of inhibitor binding in the active site. Therefore, other proteins of interest,

which are targets of therapeutic drugs, can be immobilized on the surface and after determining that changes in conformation upon drug binding can be observed by SPR, the sensors can be used for high-throughput screening of potential pharmaceutical drug candidates. In addition, this type of enzyme-based sensor will require further investigation in order to find out whether the change in conformation can be determined by other methods, such as electrochemistry, so that the sensing system is applied for high-throughput screening of drug candidates under stationary conditions.

4.2. Experimental Details

4.2.1. Surface modification of gold surface on SPR sensing modules

The gold film on the SPR sensing surface was rinsed with deionized water and anhydrous ethanol. The sensor surface was dried with a stream of nitrogen and the sensor was cleaned in oxygen plasma for 45 seconds prior to surface modification.

The 11-mercaptoundecanoic acid SAM on the SPR module surface was formed by using microcontact printing with a flat polydimethylsiloxane (PDMS) stamp.⁹⁷ The SAM was formed by stamping rather than immersion in solution because the SPR module is not resistant to prolonged exposures to organic solvents. The PDMS stamp was soaked in a 10 mM ethanolic solution of MUA containing 2% TFA. The stamp was subsequently dried with nitrogen and gently placed on the sensor surface, while making sure that the PDMS made contact with the gold surface. After 1 minute the PDMS stamp was carefully peeled off. The gold surface was

then sequentially rinsed with ethanol, 10% (v/v) NH_4OH in ethanol, and ethanol followed by drying with nitrogen.

4.2.2. Immobilization of AChE

COOH terminated gold slides were activated with EDC/NHS as described in Section 2.4.6.

Acetylcholinesterase was covalently immobilized by covering the EDC/NHS treated slides with a small volume (100 – 200 μL) of 0.5 mg/mL AChE (electric eel) solution for 24 hours at 4°C.

The AChE solution was prepared in pH 9.6 carbonate buffer (100 mM $\text{Na}_2\text{CO}_3/\text{NaHCO}_3$). The enzyme coated slides were rinsed several times with PBS, and then stored in a sealed container at 4°C until further use.

The surface of the SPR module was modified with a procedure similar to the modification of gold slides. The COOH terminated gold sensor surface was covered with a freshly prepared aqueous solution of 100 mM EDC and 20 mM NHS in deionized water for 15 min. Then the sensor surface was rinsed with deionized water, dried with nitrogen. AChE immobilization followed using the same procedure as for the gold slides described in the paragraph above.

4.2.3. AChE activity assay

AChE activity was calibrated using Ellman's reagent. Stock solutions of 100mM acetylthiocholine iodide and 500 μM 5,5'-dithiobis-(2-nitrobenzoic acid) (DTNB) were prepared in 10 mM phosphate buffer, pH 8.0. The AChE enzyme stock solution (0.4 pmol/ μL) was prepared in the 500 μM DTNB solution. Different volumes of AChE enzyme stock solution and 30 μL of acetylthiocholine iodide were added to the DTNB solution in a quartz cuvette for a final

volume of 3.0 mL. The absorbance was measured at 410 nm after 2 min with a Perkin Elmer Lambda 35 UV-Vis double beam spectrophotometer (Waltham, MA). In order to determine the activity of immobilized enzyme, the gold slides with covalently attached AChE were immersed in 3.0 mL solution containing 500 μ M DTNB and 1 mM acetylthiocholine iodide in PB, pH 8.0, inside a quartz cuvette. Following 2 min incubation at room temperature, the solution was mixed using a pipettor, the slide was removed and the solution absorbance was measured at 410 nm.

4.2.4. Imaging of AChE activity assay

The manual Rame-Hart goniometer contains an ocular piece with a 10X magnification lens, which is used for viewing the water droplet on the substrate and determination of its contact angle with the substrate surface. To image the formation of the yellow product on the gold surface, a gold slide was placed standing up in a quartz cuvette with the activity assay solution and after 2 minute incubation a side-view digital image of the gold slide inside the quartz cuvette was obtained through the ocular piece of the goniometer using a digital camera.

4.2.5. Surface plasmon resonance

For the AChE experiments, the relative amount of inhibitor bound to the AChE was determined by measuring the net increase of the refractive index over time, compared to that of running buffer alone. Each measurement was carried out in triplicate by monitoring the SPR response curve for all three channels simultaneously and the average change was reported. PBS was used as running buffer and the analytes were diluted in PBS, before flowing them on the sensor. The experiments were carried out in PBS for 10 min using a constant flow rate of 50 μ L/min at room temperature.

4.3. Results and Discussion

4.3.1. Immobilization of AChE onto the COOH-terminated SAM

The surface modification strategy was based on the self-assembly of a carboxyl-terminated thiol, 11-mercapto undecanoic acid, on the gold surface. The presence of functional groups, such as carboxyl acids, at the terminal end of the alkanethiol molecule allows for further modification of the surface using various covalent coupling reactions.⁹⁸ Carboxyl acid-terminated SAMs, are activated with N-hydroxy succinimide (NHS) in the presence of a coupling reagent such as, 1-ethyl-3-(3-dimethylaminopropyl) carbodiimide hydrochloride (EDC).⁹⁹⁻¹⁰¹ The activated carboxyl acid groups on the surface then form amide bonds in the presence of primary amines.

AChE was covalently immobilized by using amide coupling chemistry *via* EDC/NHS activation. The gold surface allowed for characterization of the surface with different methods such as, ellipsometry and goniometry, in order to confirm the presence and activity of the enzyme on the surface. Derivatization of the gold surface with COOH groups was followed by activation with EDC/NHS and then exposure to the AChE solution in pH 9.6 buffer (100mM NaHCO₃/Na₂CO₃) (Figure 4.3). After formation of the self-assembled monolayer of 11-mercaptoundecanoic acid (MUA), the gold surface showed a hydrophilic contact angle of 17.3° for DI water, 22.4° for pH 2 and 7.9° for pH 12 as shown in Table 4.1. The low contact angle values and the difference in contact angle between the pH 2 and pH 12 solutions supports the presence of the carboxyl groups on the gold surface.^{102, 103}

Following activation with EDC/NHS, the contact angle increased to 35° and 30° for deionized water and pH 12, respectively. This implies the COOH groups have reacted with NHS, and the

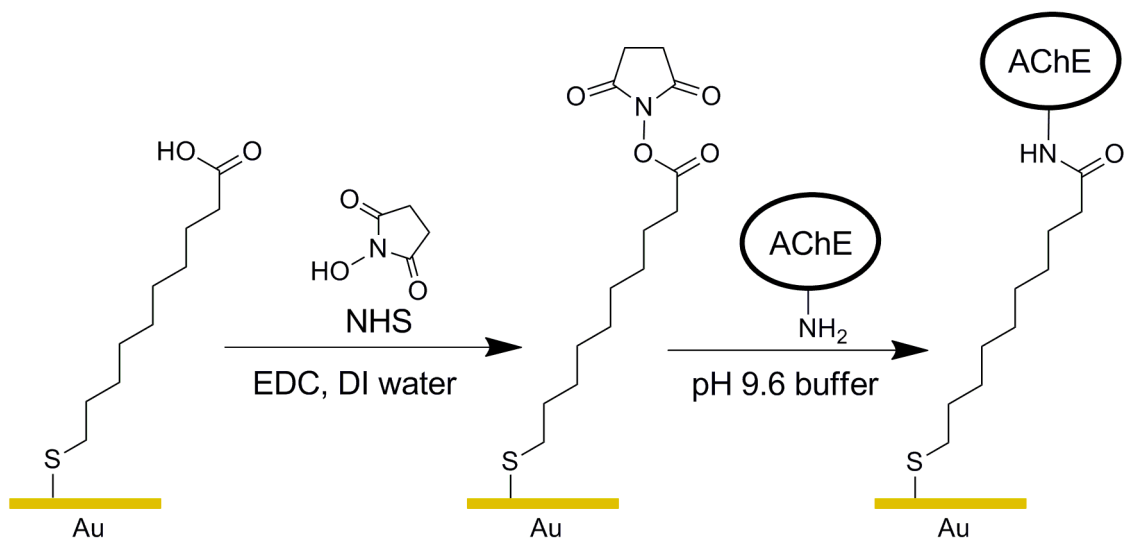


Figure 4.3. Method used for immobilization of AChE on the surface. Incubation in the aqueous EDC/NHS mixture, the COOH group reacts with the carbodiimide, which is then replaced by an NHS molecule, resulting in a more stable NHS ester. Incubation in the protein solution in pH 9.6 ensures that most amino groups of the lysine residues are deprotonated, so they can attack the carbonyl carbon removing the NHS molecule and forming an amide bond, which immobilizes the enzyme on the surface.

Table 4.1. Contact angles after each surface modification step. Solutions of 0.01 M H₂SO₄ and 0.01 M NaOH were used as pH 2 and pH 12 solutions, respectively.

Surface	Deionized water	pH 2	pH 12
MUA	17.3 (2.3)*	22.4 (1.3)	7.9 (0.9)
MUA – NHS	35.3 (3.1)	9.8 (2.1)	30.7 (2.0)
MUA – AChE	54.7 (1.6)	52.5 (2.7)	49.0 (1.1)

*Standard deviation determined after making six measurements per slide for two different samples for a total of twelve measurements.

surface is less hydrophilic due to capping of the COOH groups with NHS molecules.¹⁰⁴

However, the contact angle for the pH 2 solution decreased to 10°. This is due to hydrolyzation of NHS esters in acidic conditions. As a control, the MUA – NHS surface was rinsed with a 0.1 M HCl solution and following rinsing with deionized water and drying with nitrogen the

contact angle values returned to those of the MUA SAM, showing the instability of the NHS ester.

When proteins are immobilized on the activated esters, they are coupled to the activated carboxyl groups through the amino side groups of lysine residues, which are the only primary amine residues available for amide bond formation in proteins. Following incubation in the enzyme solution, the contact angle values increased, while at the same time they were similar for deionized water, pH 2, and pH 12 solutions. This implied that; (1) the gold surface or MUA SAM was fully covered with the protein layer, and (2) the AChE deposited on the surface had most likely formed a uniform layer, due to the relatively small deviation between the contact angle values measured.

Ellipsometry measurements appeared to confirm the deposition of a uniform protein monolayer following incubation in the enzyme solution. The MUA SAM thickness was found to be 1.0 ± 0.2 nm, whereas after incubation of the gold surfaces in AChE solution the overall thickness became 4.3 ± 0.3 nm. Subtracting the SAM thickness from the overall value provides with a calculated protein film thickness of 3.3 ± 0.5 nm. This thickness value is comparable with the reported dimensions of AChE which vary from 4.5 – 6.5 nM, assuming that the enzymes attach to the surface through their longer axis. Since the ellipsometry measurements were done on dry gold slides, it is possible that the structure of the immobilized AChE is more tightly packed and not as extended as it would be if it was in a water environment. The lower thickness determined by ellipsometry may also be explained by the thickness of hydration layer between the COOH and the protein terminated surface. The COOH-terminated surface is likely to have a thicker

hydration layer than the protein coated surface, due to higher wettability and surface energy as shown by the water contact angle values. Deposition of the AChE replaces the hydration layer of the MUA SAM and the hydration layer of the AChE film is not as thick, possibly causing a lower overall ellipsometry thickness.

4.3.2. Enzyme activity and surface coverage

The activity of the enzyme was tested with a photometric AChE assay which uses 5,5'-dithiobis-(2-nitrobenzoic acid) (DTNB) and acetylthiocholine. AChE catalyzes the hydrolysis of acetylthiocholine similar to acetylcholine, producing acetic acid and thiocholine. In the presence of DTNB any compounds containing a thiol functional group are oxidized to a disulfide byproduct, and DTNB is reduced to a yellow product with an absorbance peak of 410 nm and a molar extinction coefficient of $14,150 \text{ M}^{-1}\text{cm}^{-1}$. The enzyme activity can then be determined by visible spectroscopy (Figures 4.4A & B). Following calibration of AChE activity with known amounts of enzyme in solution, slides with immobilized enzyme were immersed in the same volume of reagent inside the quartz cuvette and incubated for the same time as the solution assay. Within a minute, the formation of the yellow product was observed, which slowly diffused from the gold surface, as the color intensity increased (Figures 4.4C & D). Prior to removing the slide, the product formed was mixed by pipetting, and the absorbance of the solution was measured. As a control, immersing a COOH terminated slide for at least 10 min in the activity assay solution did not result in the formation of the yellow product.

The maximum amount of active enzyme on the surface based on the calibration curve was calculated to be $1.4 \pm 0.3 \text{ pmol/cm}^2$ (Figure 4.5). This value is similar to published results on

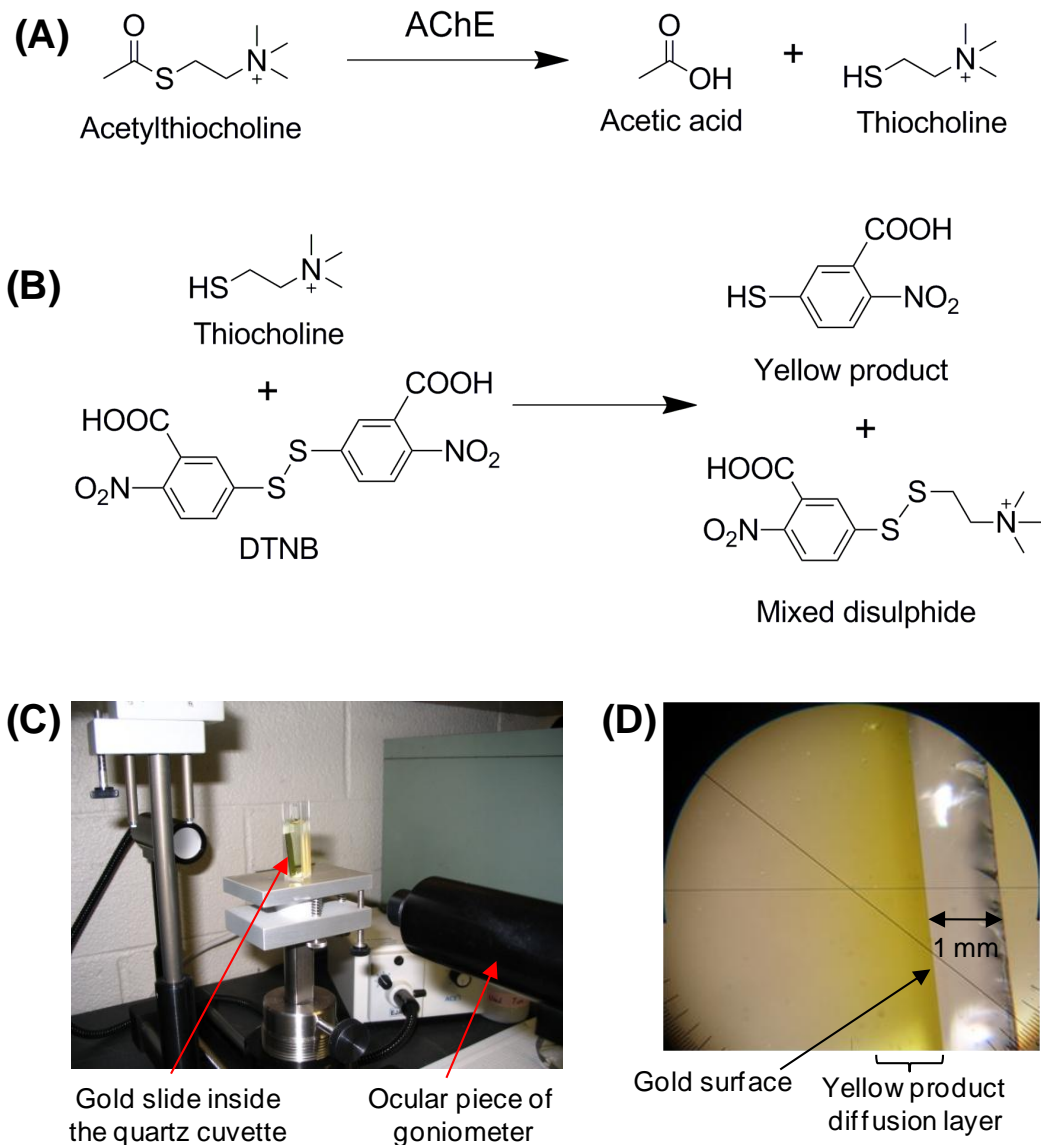


Figure 4.4. Measuring acetylcholinesterase activity on the surface. (A) Hydrolyzation of the acetylthiocholine substrate in the presence of AChE. (B) Reduction of DTNB in the presence of thiocholine results in the formation of a yellow-colored product (2-nitro-5-thiobenzoic acid). (C) The Rame-Hart goniometer set-up used to take a close up image of the AChE coated slide immersed in the activity assay solution in the quartz cuvette. (D) Side view image of the AChE coated slide taken with a digital camera through the ocular piece (10X magnification) of the goniometer. The image was taken 2 min after immersing the slide in the activity assay solution (1 mM acetylthiocholine iodide and 500 μ M DTNB in PBS, pH 8.0). The formation of the yellow diffusion layer next to the gold surface shows the presence and the activity of the immobilized AChE. Immersing a COOH terminated slide for at least 10 min in the activity assay solution did not result in the formation of the yellow product.

horseradish peroxidase immobilization on gold surfaces obtained by both a photometric activity assay and quartz crystal gravimetry.^{105, 106} This value was also compared to the maximum amount of enzyme that can be bound on the surface based on its dimensions and assuming it did not form multilayers. As mentioned earlier, AChE is an ellipsoidal molecule with dimensions of approximately $4.5 \times 6.0 \times 6.5$ nm. Assuming that AChE immobilized on the surface is a sphere with an average diameter of 6 nm, then the area that an enzyme would cover is a circle with a 3×10^{-13} cm² surface area. As the ideal maximum surface coverage would be achieved by hexagonal packing, the maximum surface area that AChE can occupy is calculated to be 91% of

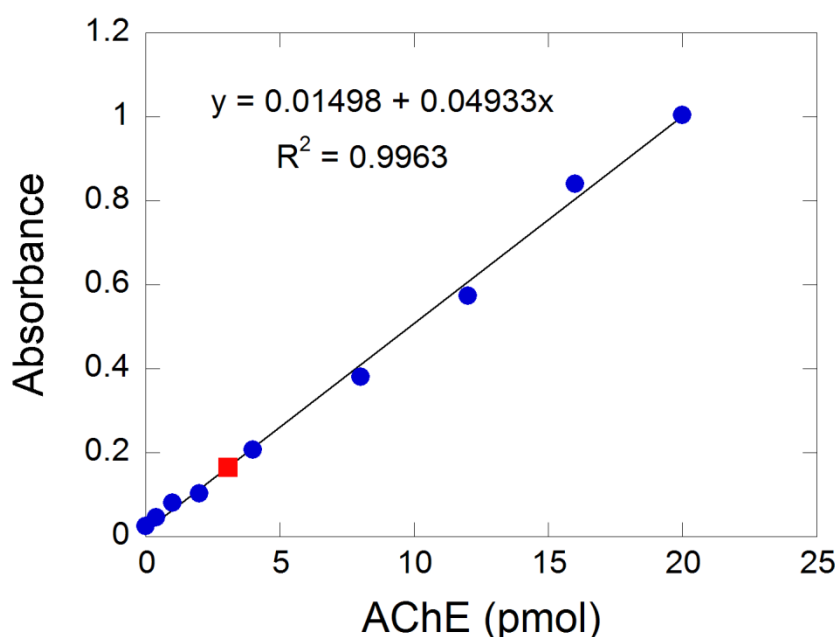


Figure 4.5. Calibration plot of absorbance at 410 nm for different amounts of AChE enzyme diluted in the activity assay solution (1 mM acetylthiocholine iodide and 500 μ M DTNB in PBS, pH 8.0). The absorbance was measured after 2 min reaction incubation time. The square represents the average value obtained for three AChE coated slides after the same incubation time and then mixing the diffusion layer and removing the slides from the activity assay solution. The absorbance values of the slides were 0.12627, 0.17277 and 0.20095 and each had a surface area of $0.9 \text{ cm} \times 2.5 \text{ cm} = 2.25 \text{ cm}^2$.

the available surface (Figure 4.6). That converts to a maximum AChE surface concentration of 3×10^{12} molecules/cm² or 5 pmol/cm². This is larger than the surface concentration of the enzyme obtained from the activity assay, although it is not unexpected. Some of the enzymes are not active when bound to the surface due to their orientation on the surface (their active site is inaccessible). In addition protein impurities that come with the enzyme sample could also deposit on the surface. Finally, the orientation of the enzymes with accessible active sites could also lower their turnover number and thus their activity and efficiency in hydrolyzing the substrate, compared to their counterparts in solution.

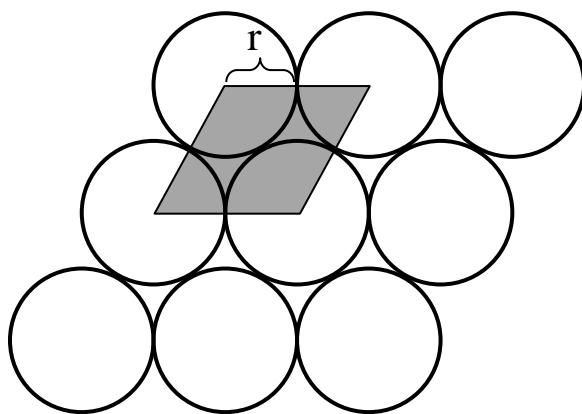


Figure 4.6. Schematic drawing of the ideal hexagonal packing of AChE molecules on the surface. The circles represent the average area, covered from each protein, while the grey parallelogram represents the unit cell, where r is the radius of each circle. The protein surface coverage area was calculated to be 91% of the total surface area after taking the ratio between the area occupied from the circles (πr^2) and the area of the unit cell ($3.46 r^2$).

4.3.3. Surface plasmon resonance

SPR monitors the change in refractive index of the medium immediately adjacent to the gold surface. Any analyte binding on the gold surface would be due to specific interaction with AChE

and would result in a change of the refractive index. Experiments were performed by monitoring the refractive index (RI) changes as a function of time under flow conditions. This change is usually reported in response units (RU) where 1 RU is equivalent to 1×10^{-6} RI units. The solution flowed over the surface or running buffer was PBS. All analyte stock solutions were prepared and then diluted in PBS, pH 7.4. Neostigmine was detected down to a concentration of 10 μM , and eserine was detectable at 50 μM . Neostigmine showed a higher response in the SPR signal at any concentration compared to eserine (Figure 4.7). Langmuir fits were used to fit the plots in Figure 6. The binding affinities (K_A) obtained from the fits were $4.7 \times 10^3 \text{ M}^{-1}$ for neostigmine and $2.1 \times 10^3 \text{ M}^{-1}$ for eserine, showing a higher affinity of the sensor for neostigmine. This is consistent with a published study on the reactivity of carbamate inhibitors

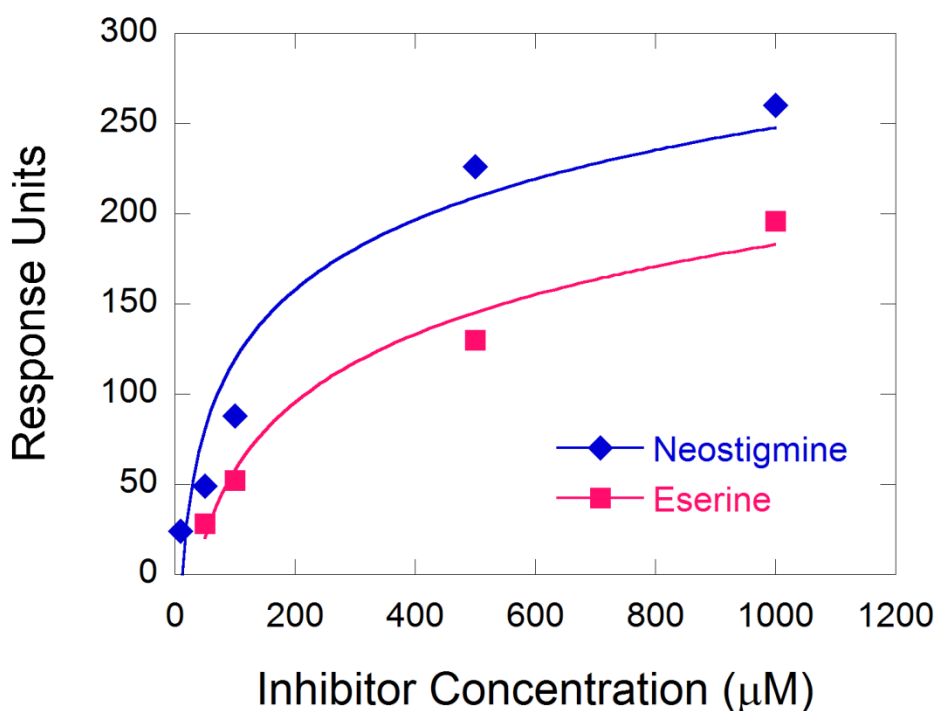


Figure 4.7. Normalized refractive index change obtained for different neostigmine and eserine concentrations. Langmuir fits provided binding affinities values of $4.7 \times 10^3 \text{ M}^{-1}$ and $2.1 \times 10^3 \text{ M}^{-1}$ for neostigmine and serine, respectively.

with AChE, which showed that the reaction rate of neostigmine with AChE was 15 times faster than the reaction of eserine with AChE.¹⁰⁷

A control experiment that was performed on an SPR sensor coated with a different enzyme (horseradish peroxidase) with the same immobilization method as AChE showed no response to a solution of 1 mM neostigmine, showing that the change in refractive index is due to specific binding of the inhibitor and not due to any changes in refractive index by the presence of the inhibitor in solution. Experiments with acetylcholine, choline, and tetra-n-propyl ammonium showed a small signal change for 1 mM solutions, but no change was observed for 100 μ M or lower concentrations.

AChE's active site is blocked by carbamate inhibitors. The mechanism of inhibition is initially similar to the acylation of the serine residue. Carbamates, such as neostigmine, are similar in structure and charge to acetylcholine. At the active site they covalently modify the serine residue by adding a carbamate group to the hydroxyl (Figure 4.8).

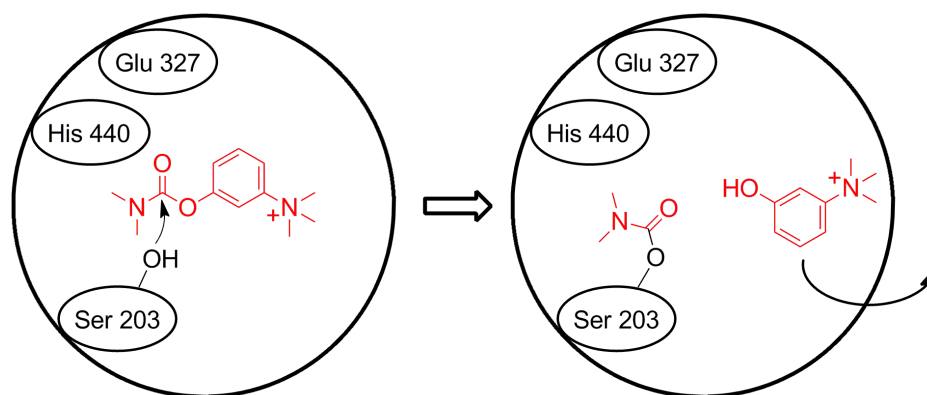


Figure 4.8. Schematic drawing of inhibition of the AChE active site by neostigmine.

Choline and tetra-n-propyl ammonium can only bind to the anionic region of AChE active site. However, the fact that acetylcholine causes a smaller change in refractive index than neostigmine point to the fact that neostigmine stays bound to AChE longer than acetylcholine. In addition, according to the amount of enzyme on the gold surface and the magnitude of change for inhibitor binding based only on its mass should be smaller, even if all the active sites are saturated with inhibitor. The reported change in the refractive index is approximately 1 RU for 1 pg of surface bound analyte.⁷⁹ Based on these assumptions, the change in refractive index should be approximately 5 RU upon inhibitor binding on all available sites. Therefore, the large change observed for neostigmine and eserine could be due to changes in conformation of AChE. Researchers have shown that upon binding of inhibitor there is a significant change in the conformation of AChE, which is likely to be larger in solution compared to known changes obtained from x-ray crystallography data.¹⁰⁸ It has also been reported that changes in conformation of adsorbed proteins on solid surfaces, affect the refractive index of the protein layer.¹⁰⁹ Combined with our results it can be assumed that the sensor is more likely detecting changes in protein conformation rather than mass binding of inhibitor.

4.4. Summary and Conclusions

The surface of gold was modified with a carboxyl terminated SAM and acetylcholinesterase was covalently immobilized by the formation of amide bonds. Enzyme immobilization was shown by an increase in thickness on top of the gold surface as measured by ellipsometry. The thickness values were in agreement with the known dimensions of the enzyme and also indicated that the immobilized AChE did not form a multilayer. Contact angle measurements also showed

a decrease in wettability of the surface due to the enzyme covering the highly hydrophilic carboxyl-terminated SAM. Physical attachment of a protein is not useful unless the enzyme is still active. To confirm the presence of enzyme on the surface and determine its activity, a standard photometric activity assay was used. By assuming that the activity of the immobilized enzyme is similar to the solution enzyme the amount of AChE on the surface was calculated to be 1.4 ± 0.3 pmol/cm². This value is significantly smaller than the maximum possible surface density of enzyme based on its average diameter. Since the contact angle and ellipsometry measurements showed that the surface was fully covered, then it was concluded that the activity of the enzyme on the surface is lower than when it is in solution. The lower activity may be caused by the random orientation of the enzyme on the surface, affecting the accessibility of the active site to the substrate.

The gold sensing surface of commercially available SPR sensor was modified by contact printing of the carboxyl-terminated SAM and the covalent attachment of AChE was achieved performing the same amide coupling chemistry that was used on gold slides. The enzyme coated surface was used as the sensing surface in SPR experiments to detect binding of two carbamate inhibitors, neostigmine and eserine, tetra-n-propyl ammonium chloride, acetyl choline, and choline. Only the carbamate inhibitors showed a response at concentrations lower than 1 mM. Neostigmine had the lowest detection limit, 10 μ M. Measuring the change in refractive index at different concentrations provided the affinity constants for both inhibitors by fitting the data to a Langmuir curve. The ability of this sensor to detect binding of AChE inhibitors showed that it can potentially be used for the detection and screening of new AChE inhibitors. In addition the sensor did not require the use of antibodies in order to detect the relatively small inhibitors. The

SPR signal generated upon binding of either neostigmine or eserine is not supported simply by their physical binding on the sensor surface due to their small molecular weight. The change in refractive index observed, can only be caused by relatively large shifts of the immobilized enzymes. Since it has been reported that there is a considerable change in conformation of AChE after inhibitor binding, it is this change in protein conformation (and local refractive index) that the SPR sensor is detecting. By immobilizing other enzymes or cell receptors of interest on the SPR sensor surface, their response upon exposure to inhibitors and ligands can be also be assessed, and if observed, it can be used for discovery and screening of new pharmaceuticals.

4.5. Practical Implementations and Future Work

A biosensor that can detect binding of AChE inhibitors has three major uses; it can be used as (1) detector of contamination in water, soil, and foods with pesticides or nerve gases; (2) detector/monitor the blood or urine level of AChE inhibitors used as drugs; and (3) a platform for the high-throughput screening of AChE inhibitors and the discovery of new ones. Detection of pesticides has to be possible at a concentration of 1 ng/mL or lower. Our current sensor is able to detect neostigmine at 10 μ M concentration or 2.2 μ g/mL. Similarly for the monitoring or detection of AChE inhibitors in blood or urine the detection capability of the sensor would have to be in the range of 0.2 – 10 ng/mL of blood (Table 4.2). The only exception is neostigmine which can be used at doses up to 375 mg. The third use is the most feasible one for the enzyme-based sensor described in this work. The format of SPR sensors allows for screening of multiple analytes in sequence and/or in parallel by using multiple channel SPR sensors. This will allow

for rapid and systematic high-throughput screening of large numbers of potential drug candidates and the discovery of new leads by simply running the analyte solutions over the sensor surface.

Table 4.2. Reversible acetylcholinesterase inhibitors used as medications.

Retail name	Chemical name	Dosage	Molecular weight	Clinical use
Vagostigmin	Neostigmine	15 to 375 mg	223.3	Myasthenia Gravis
Physostigmine	Eserine	1 mg	275.4	Alzheimer's, Glaucoma, Myasthenia Gravis
Cognex	Tacrine	10 to 50 mg	198.3	Alzheimer's
Aricept	Donepezil	5 or 10 mg	379.5	Alzheimer's
Exelon	Rivastigmine	10 mg	250.3	Alzheimer's
Razadyne	Galantamine	4, 8 or 12 mg	287.4	Alzheimer's

This system could be also applied to the discovery of new pesticides that will specifically target pests, but not humans and other mammals and birds. By coating the surface of the sensor with AChE enzymes from different animal groups, the high-throughput screening system can be used to score for pesticides that target a specific animal group, without affecting others. This could lead to the discovery of pesticides that for example would be toxic to some insects, but not bees, which are essential to agriculture and whose numbers have been in decline over the last decades, most likely due to the use of pesticides that indiscriminately target all insects.

Future work will focus on the ability of SPR to detect protein conformations that occur upon interactions, such as binding of inhibitors or ligands to enzymes or cell receptors of interest.

Immobilization of enzymes will be done either through amide coupling or, if they contain a lipid tail, through non-covalent anchoring *via* the lipid tail on modified surfaces that mimic cell membranes, as will be shown in Chapter 7. Some AChEs, such as those that reside on red blood cells, naturally contain a lipid tail. It will be interesting to see whether an AChE bound on the gold surface through a lipid tail, will provide a detectable SPR signal upon inhibitor binding, similar to the covalently bound AChE. Receptors are typically trans-membrane proteins and their immobilization can only be done by insertion on a planar lipid membrane. Once insertion of the receptor protein in the membrane is achieved and its activity is confirmed on regular gold slides, the construct will be build on the gold surface of the SPR sensor, and the refractive index will be monitored upon exposure to ligands and other analytes at different concentrations. As mentioned earlier, detection of protein conformation in response to interaction with analytes can be used for the high-throughput screening of pharmaceutical targeting that protein.

5. Biofim Resistant Surfaces

5.1. Introduction

Infections associated with medical implants can be devastating, especially for immuno-compromised patients. The common use of invasive technologies has made the development of antibacterial and anti-biofouling surfaces necessary. Bacteria attach to medical implants and grow on the surface while enclosing themselves in a matrix of extracellular material that is mainly composed of polysaccharides.^{110,111} This extracellular matrix provides bacteria with protection from the immune system and antibiotic treatments.¹¹² The aggregation of surface adhered bacteria and the extracellular matrix around them is known as biofilm. Once the biofilm forms, the proper function of the implant can be impeded, and infection of the tissue surrounding the implant may occur. Cells can detach and spread the infection to other parts of the body.¹¹³

Medical implants include everything from dental fillings to artificial hearts. Implants, such as catheters, contact lenses, knee and hip prosthesis, stents, or artificial heart valves, have become common, while many other medical devices are also being used (Table 5.1). As a result of their use improvement in healthcare has been considerable. Due to the various functions they need to perform, implants can be made of plastics (polymers), metals, ceramics, glasses, carbon, and composite materials. Substrates (natural or synthetic) that come into contact with biological systems are generally known as biomaterials.¹¹⁴ All biomaterial and medical devices, not only need to have the right physical properties to fulfill their performance requirements, but also have to be biocompatible with the host. Biocompatibility refers to the ability of the device to perform

Table 5.1. Worldwide usage of medical implants in 2004.¹¹⁴

Medical Device	Estimated usage
Heart valve	200,000
Pacemaker	200,000
Breast implant	300,000
Vascular graft	400,000
Dental implant	500,000
Hip and knee prostheses	1,000,000
Stent	2,000,000
Intraocular lens	7,000,000
Renal dialyzer	25,000,000
Contact lenses	75,000,000
Catheter	300,000,000

its intended function once incorporated in the host, without causing any undesirable local or systemic effects in that host. One accepted definition is: “Biocompatibility is the ability of a material to perform with an appropriate host response in a specific application.”¹¹⁵ For example, in medical implants that come into contact with blood, an “appropriate host response” includes lack of blood clotting, resistance to biofilm formation, and normal healing of any punctured or damaged tissue in the sewing or insertion site. Essentially, biocompatibility refers to the achieving the desired outcome upon interaction of the surface of the implant material with the biological system. In order to change the biocompatibility or surface properties of the implant, it is not necessary to change the chemical properties or composition of the entire material. Modification of the surface with chemical groups can impart the desired surface properties while maintaining the physical characteristics of the bulk material. Intravascular devices, such as

catheters, are usually made of synthetic polymers, such as silicone or polyurethane. Silicone is an inorganic polymer consisting of polysiloxane backbones ($-\text{SiR}_2-\text{O}-\text{SiR}_2-\text{O}-\text{SiR}_2-\text{O}-$) often cross linked via the side groups attached to the silicon atoms. Polyurethane consists of a chain of organic units joined by urethane links ($-\text{COO}-\text{NH}-\text{R}_1-\text{NH}-\text{COO}-\text{R}_2-$). Once antimicrobial and anti-biofouling surfaces are successfully developed on substrates such as gold or indium tin oxide, which allow a thorough examination of the surface, they can be applied to polymeric surfaces.

Biofilm formation and infection are the universal risks associated with any implant or medical device that comes into contact with bodily fluids. Medical implants provide a substrate for bacterial attachment and biofilm formation. The first stage of biofilm development is the binding of a few bacteria to the surface through their outer cell wall. This is done through hydrogen bonding, ionic interactions and hydrophobic between biomolecules on the cell wall and the surface^{116, 117} This process can be helped by the nonspecific adsorption of molecules from the hosting environment on the surface of the implant material, which results in the formation of conditioning films. The conditioning layer provides an array of chemical groups and structures for the attraction and adsorption of bacterial cells.¹¹⁸ Bacteria have also developed specific proteins, called adhesins, which are located on structures extending from the cell surface and have the function of docking bacteria on the surface. In the second stage, bacteria respond to surface adsorption by producing extracellular polysaccharides that complex with the surface and attach bacteria firmly and irreversibly to the surface.¹¹⁹ In the third stage bacteria replicate actively while making more extracellular material, and the overall density, complexity and mass of the biofilm increases.¹²⁰ This biofilm growth results in entrapment of other molecules and

proteins from the surrounding environment, including nutrients and proteins produced by the immune response of the host. In the fourth and final stage the outer layers of the biofilm becomes a source of free-floating bacteria that can initiate biofilm formation in other locations.

Biofilms can be formed by a single bacterial species (Figure 5.1), but more often they consist of many species of bacteria, as well as fungi. The main bacterial species found in medical implant biofilms are *Staphylococcus epidermidis*, *Staphylococcus aureus*, and *Pseudomonas aeruginosa*.^{121, 122} Bacteria present in biofilms are resistant to antibiotics and also to immune system responses such as antibodies and phagocytes. Biofilm bacteria have been found to tolerate antibiotics at 1000 times higher concentrations than those needed for their counterparts growing in suspension.^{113, 123} In addition to the biofilm matrix inhibiting penetration of antimicrobial agents due to slow diffusion rates, physiological changes in the local environment of the biofilm matrix also contribute to its resistance. For example, biofilms are known to vary the local pH,¹²⁴ and since most antibiotics are only effective at a narrow pH range, they can be ineffective in the biofilm environment.¹²⁵ Genotype expression and phenotype changes, including lower metabolic rates, occur as bacteria go from a suspended to a biofilm state. This can decrease a number of antibiotic targets in the cells and results in immunity against those antibiotics.^{126, 127}

Medical implant related infections can sometimes be lethal, especially for immuno-compromised patients. Infections caused by the insertion of central venous catheters (CVC) happen in 3-5% of patients.¹²¹ These catheters are inserted in the veins for the administration of fluids, blood products, medications, nutritional solutions, and hemodynamic monitoring. Studies have shown

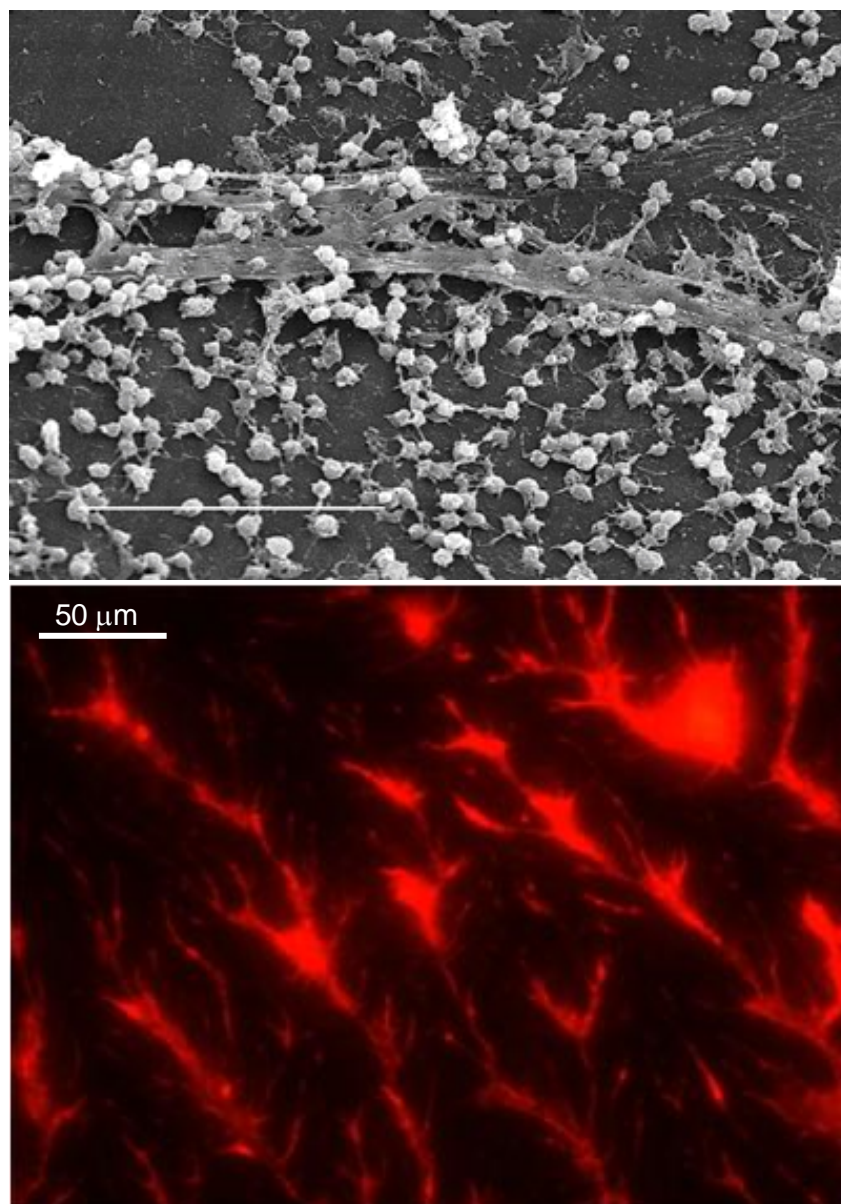


Figure 5.1. Images of bacterial biofilms. (Top) Scanning electron micrograph of a staphylococcal biofilm on an indwelling medical device. Bar, 20 μm .¹²⁸ (Bottom) Fluorescent image of a propidium iodide stained *Staphylococcus epidermidis* biofilm. The *Staphylococcus epidermidis* biofilm was grown by incubating a dodecanethiol SAM modified gold slide in a $2 \times 10^7/\text{mL}$ bacterial suspension in tryptic soy broth with 0.25% glucose for 24 hours at 37 °C.

that biofilm formation can happen within 3 days¹²⁹ and that biofilms appear to be always present on CVCs, whether it is in the outside or the lumen of the catheter.^{121, 130} One explanation for such rapid biofilm formation is the conditioning films formed on the surface of the catheter from

platelets and plasma proteins (albumin, fibrinogen, fibronectin, and laminin), which provide anchoring sites for bacteria.¹³⁰ The organisms originate either from the skin insertion site, migrating along the external surface, or from the catheter itself due to manipulation by the health care workers, migrating along the inner lumen. Urinary catheters are even more susceptible to infections. They are used in 13.2% of hospital patients and cause urinary tract infections 10-50% of the time in short-term catheterizations (up to 7 days), and essentially all patients undergoing long-term catheterizations (more than 28 days).¹³¹ They are commonly used to collect urine during surgery, and prevent urinary retention. Urinary catheter biofilms are known to result in mineral precipitation and encrustation due to the changes in the local pH through the production of urease, which hydrolyzes urea in urine to form ammonia.¹³² Other common medical devices that are susceptible to biofilm formation are prosthetic heart valves, intrauterine devices, and contact lenses.¹¹³ In all these cases the device is not only the support for biofilm formation, but potentially even the source of the infection.

Once it forms, the most effective way to neutralize the biofilm is to remove or replace the medical implant and administer an aggressive round of antibiotics.¹³³ Prevention of biofilm formation provides the best option in ensuring the health of patients and performance of medical implants. As bacterial attachment is the initial step for biofilm formation, the development of modified surfaces that minimize protein and bacterial adhesion, and/or surfaces that kill bacteria upon binding to the surface, would be of benefit. The approach so far has been to use implants with coatings that release by diffusion antibiotics or silver ions. This provides a short term antimicrobial protection depending on the retention time of the adsorbed antibacterial compounds.¹³⁴ Due to their antimicrobial properties, silver and its salts have been widely used to

coat medical equipment. Silver coated bandages have been used to cover burn wounds and traumatic injuries.¹³⁵ Acticoat and Silverlon, silver-coated polyethylene sheets and silver-coated polyamide fibers, respectively, are two commercial products that use silver as an antimicrobial coating. Silver coated heart valves and catheters have also been used. All these coatings work similarly, by releasing Ag^+ ions and/or silver nanoparticles that have antibacterial properties.¹³⁶ Medical implants can also be coated (impregnated) with antibiotics and other agents. However, the success of these coatings depends on the retention time of the adsorbed antibiotics. They can only retard biofilm formation.¹³⁴

Another approach in preventing bacterial attachment and biofilm formation has been to chemically incorporate molecules or functional groups on the surface of polymers that will prevent the adsorption of biomolecules and the formation of conditioning layers. Poly(ethylene glycol) (PEG) was incorporated by physisorption into poly(ethylene terephthalate) (PET) surfaces. PET is used for a variety of artificial implants which put it in contact with bodily fluids. PEG coverage showed a decrease in protein surface adsorbance.¹³⁷ This property of PEG was first studied on self-assembled monolayers containing PEG oligomers of varying molecular weight and density on gold substrates.^{138, 139} In aqueous solutions, PEG chains are highly solvated and it is thought that protein adsorption would require desolvation of the PEG, which would be energetically unfavorable. Another surface that could provide resistance to protein adsorption is fluorocarbon-terminated surface. Fluorocarbons are known to be both hydrophobic and lipophobic due to small intermolecular forces and low surface energies. These types of surfaces provide passive resistance to protein or bacterial adhesions, however a surface that also

contained antibacterial properties would be able to neutralize any bacteria that manage to attach. Ideally a surface that can both repel bacteria and kill them would be desired.

Some cationic surfactants, such as Dabco-C16 and octadecyldimethyl ammonium ions (ODMA) (Figure 5.2), are known to disrupt the cell membrane of bacterial cells, causing membrane depolarization, and eventual cell death. Dabco-C16 was immobilized on cotton fibers and was shown to have antibacterial properties.

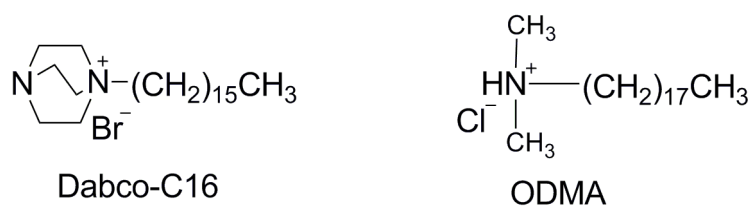


Figure 5.2. Chemical structures of Dabco-C16 and ODMA.

There is also a class of natural amphiphilic antibiotics which are known to kill bacteria by disrupting the cell membrane. Daptomycin is one of these antibiotics with potent antibacterial properties that was only recently approved by the FDA for the treatment of serious skin infections by certain gram-positive bacteria that are resistant to other antibiotics.¹⁴⁰ The structure of daptomycin consists of a cyclic decapeptide and a tail that starts with three amino acid residues and ends with a lipophilic chain (Figure 5.3). The exact mode of action is not well understood. Daptomycin is activated by Ca^{2+} ions. Upon binding to calcium ions, daptomycin binds to bacterial membranes through its lipophilic tail, and disrupts the membrane by allowing ions to flow in or out depending on their chemical gradients. This causes a rapid depolarization of membrane potential. The loss of membrane potential leads to inhibition of protein, DNA, and

RNA synthesis, and bacterial cell death within a few hours.¹⁴¹ This mechanism of action is distinct from other antibiotics. Its ability to kill bacteria by only interacting with the cell

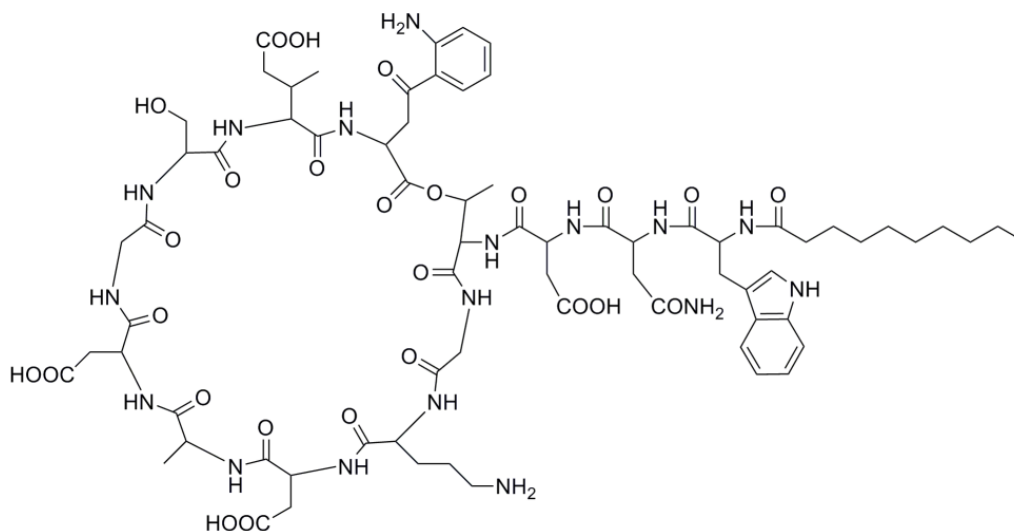


Figure 5.3. Chemical structure of daptomycin.

membrane makes daptomycin a good candidate for generating surfaces with antibacterial properties that can actively prevent biofilm formation. If daptomycin molecules were attached to a surface, then potentially any gram-positive bacterial cells attaching to that surface would be killed, thus preventing colonization and biofilm formation. One of the challenges stands on how to bind this antibacterial compound on the surface while still keeping its antibacterial properties. The approach in this work has been to attach daptomycin to the surface using a crosslinker, which would provide flexibility to daptomycin. The cross linker consisted of a bifunctional PEG molecule, $\text{NH}_2\text{-(PEG)-COOH}$, to allow for covalent attachment to the surface. Other surfaces, PEG, Dabco-C16, and ODMA were tested for their ability to resist biofilm growth of gram-positive bacteria, alongside daptomycin. Such surfaces can then be tested for their antibacterial activity against gram-negative bacteria and other microorganisms. The final goal is

to generate surfaces that prevent biofilms both passively and actively. The cross linker for daptomycin was chosen to be 40 units long so not only it provides flexibility for daptomycin, but also presents a passive anti-biofouling surface.

SAMs are easily formed on surfaces of gold, silver, indium tin oxide, or silica. Therefore, these substrates provide a practical working field for building, characterization, and testing of the antimicrobial activity of many molecules or functional groups. SAMs with terminal groups that allow for covalent bond formation can facilitate the attachment of antimicrobial compounds and antibiotics known to kill cells by interacting with the cell membrane. Binding these compounds to the surface of the implant could potentially kill any microbes that would try to attach to the implant.

5.2. Experimental Details

5.2.1. Preparation of Dabco-C16

Dabco (10 g) and 1-bromohexadecane (5.5 g) were mixed in 70 mL ethylacetate and the mixture was stirred overnight at room temperature. The white precipitate that was generated was filtered and was washed three times each with ethyl acetate and diethyl ether. The white precipitate that forms was the product, Dabco-C16, and the percent yield was 96%.

5.2.2. Bacterial culture

Staphylococcus epidermidis bacteria were cultured aerobically under agitation in tryptic soy broth growth medium at 37°C. For each experiment one bacterial colony was pre-cultured from

tryptic soy agar plates in 18 mL of TSB overnight for 18 hours. From this culture 1.0 mL was used to grow the bacterial cells in 50 mL of tryptic soy broth. After 1 hour incubation, the optical density was measured every 15 min using a spectrophotometer. When mid-log growth phase was reached (at an absorption of 0.5 at 600 nm, which corresponds to 2×10^9 cells/mL),¹⁴² the bacteria were either used for the biofilm assay or collected by centrifugation to be used for the attachment and viability assay, and then washed by suspending in Tris buffer (20mM Tris, 0.85% NaCl, pH 7.0) and spun again in the centrifuge. The bacterial cells were then resuspended in Tris buffer at the same volume that they were harvested from the growth medium. A 100x dilution of the suspension gives a 2×10^7 /mL bacterial concentration, which was used for the attachment assay.

5.2.3. Bacterial attachment assay

Surface samples (gold or glass slides) were immersed with the modified face up in 4 mL of 2×10^7 bacterial suspension in Tris buffer. The surfaces were incubated for 1 hour at 37 °C without agitation to allow adhesion of the cells. The bacterial suspension was replaced with fresh Tris buffer and the samples were incubated for an additional 1-2 hours to allow for the interaction of the bacteria with the modified surfaces. The slides were washed gently with 3-5 mL of Tris buffer using a plastic transfer pipette, and were stained by incubating in a diluted solution of SYTO 9 (1 μ M) and propidium iodide (20 μ M) in Tris buffer. The incubation time was 15 min at room temperature away from light. Using tweezers, each of the slides was removed from the staining solution, rinsed by dipping in Tris buffer, tilted to drain off most of the liquid and placed face up on a microscope slide. A glass cover slip was placed on top of the sample. Pictures of the stained bacteria attached to the surface were taken using an oil

immersion lens with an IN1820 Spot Insight model Diagnostic Instruments camera attached to a Nikon Eclipse E400 fluorescence microscope at 1000X magnification. Pictures were taken using FITC and Texas Red filter cubes. The green and red images were combined using Spot Advanced 4.5 computer software and the ratio of live cells was determined by counting.

5.2.4. Biofilm assay

Bacteria from the mid-log phase of the culture were directly diluted to 2×10^7 in tryptic soy broth supplemented with 0.25 % glucose. Samples were immersed in the bacterial suspension and incubated for 4 hours at 37 °C with no agitation. The surfaces were rinsed with Tris buffer, stained with the Live/Dead kit and then imaged as described above.

5.2.5. Live/Dead staining

The Live/Dead *BacLight* kit stain mixture (cat. nr. L-7012; Molecular Probes, Eugene, OR) distinguishes viable bacterial cells from dead ones on the basis of membrane integrity. The mixture was used to stain cells in the attachment and biofilm assay. The kit contains two nucleic acid stains; the green-fluorescent Syto 9[®] which can penetrate intact plasma membranes staining both live and dead cells, and the red-fluorescent propidium iodide which penetrates only compromised membranes staining only dead cells (Figure 5.4). Bacterial suspensions incubated in the presence of both stains simultaneously will fluoresce either green (i.e., live) or red (i.e., dead), depending on their viability. If both dyes are bound to DNA propidium iodide quenches the fluorescence of Syto 9[®]. The excitation and emission maxima for these dyes when bound to DNA are about 480 and 500 nm for Syto 9[®], and 530 and 635 nm for propidium iodide, respectively.¹⁴³

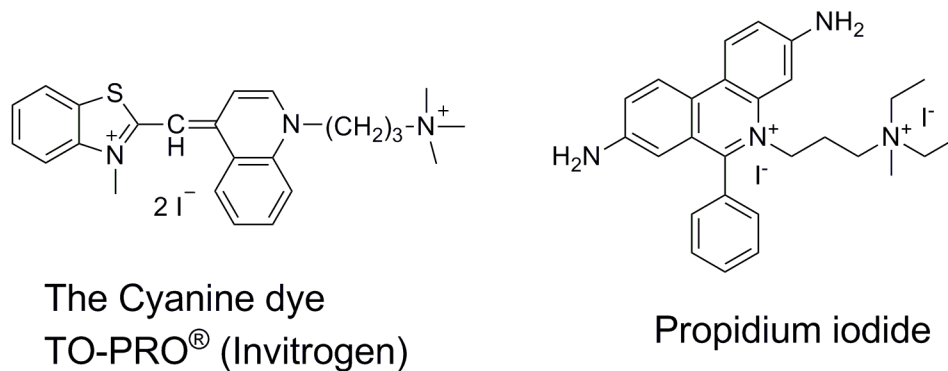


Figure 5.4. Chemical structures of a cyanine dye and propidium iodide. The cyanine nucleic acid dye shown here is cell membrane-impermeant. The proprietary Syto 9[®] is also a cyanine dye, but it is cell-permeable instead.

5.2.6. *Imaging with fluorescence microscopy*

Pictures were taken using oil immersion microscopy with a camera attached to a fluorescence microscope. Two pictures are obtained per field of view; one through a green (FITC) filter, which captures the fluorescence of SYTO 9 and the other through a red (Texas Red) which captures the fluorescence of propidium iodide. The two pictures are then combined to create a merged image (Figure 5.5). The ratio of live (green) cells can be determined by cell counting. Prior to performing attachment and viability experiments on the surface modified slides, the Live/Dead BacLight kit fluorescent dyes were tested first and a method for staining of bacterial cells on surfaces was devised. An optimal dilution of dye was determined to provide images with no background interference. Next, bacterial cells were incubated in 70% (v/v) isopropanol in 0.85% NaCl solution in order to obtain dead bacteria. Live and dead (isopropanol treated) cells were stained separately, and it was confirmed that propidium iodide stained red only dead cells and not the live ones, and that SYTO 9 stained both dead and live cells green, as expected.

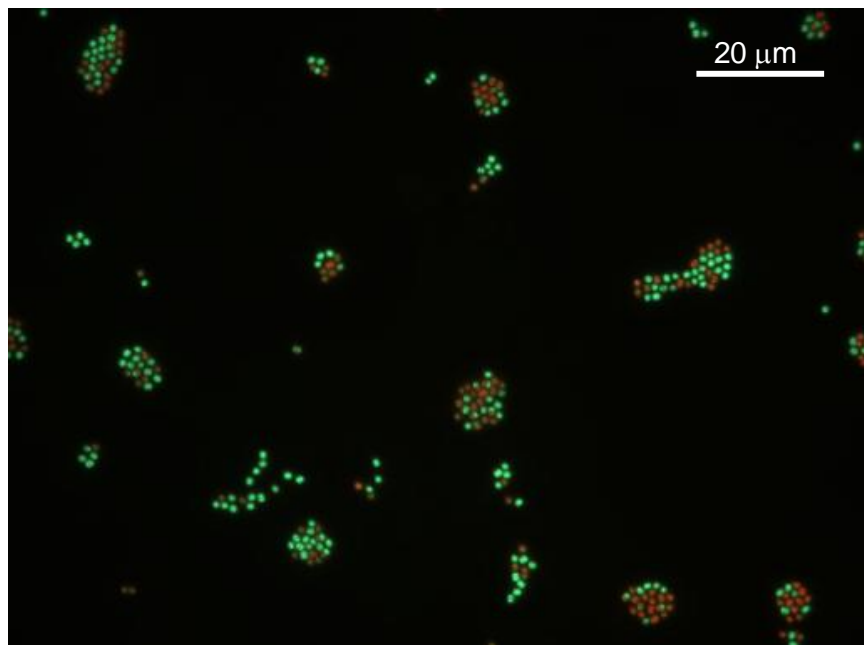


Figure 5.5. *Staphylococcus epidermidis* bacterial cells stained with the Live/Dead kit. The cells were attached to a gold slide coated with a dodecanethiol SAM that was incubated in 2×10^7 /mL bacterial suspension in Tris buffer at 37 °C for 1 hour.

Dodecanethiol (DDT) terminated gold slides were incubated in 2×10^7 /mL bacterial suspension in Tris buffer at 37 °C for 1 hour to allow for bacterial adhesion. The surface adhered bacteria were also stained at different times and then observed under the fluorescent microscope, to see whether leakage of the red dye (propidium iodide) could occur inside healthy cells or if the dye solution was toxic over that period of time. The results showed no variance in cell viability, up to one hour, between different staining times (Figure 5.6). Therefore, any variance in dye incubation time (15-30 min) among different samples would not be the cause of any different viability results. In order to complete the test of the Live/Dead viability assay, bacterial cells attached on gold slides coated with dodecanethiol SAM were incubated for 1 hour at 37°C with different ratios of isopropanol in 0.85% NaCl solutions. The percentage of live cells was plotted vs the percentage (v/v) of isopropanol in solution (Figure 5.7). After three trials, the results

showed that more than 50% of cells had died in 10% isopropanol and almost all of them at 20% or more isopropanol. Most importantly the expected gradual death of bacteria is observed by using the live/dead staining assay method.

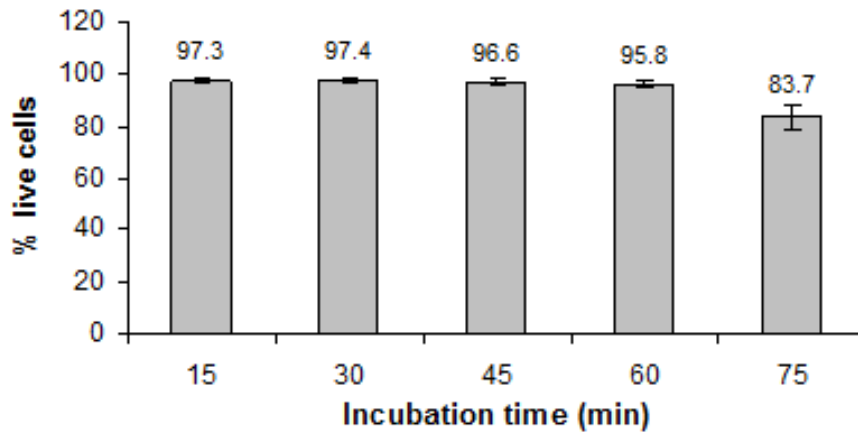


Figure 5.6. Bacterial cells adhered to DDT SAM stained for different time periods.

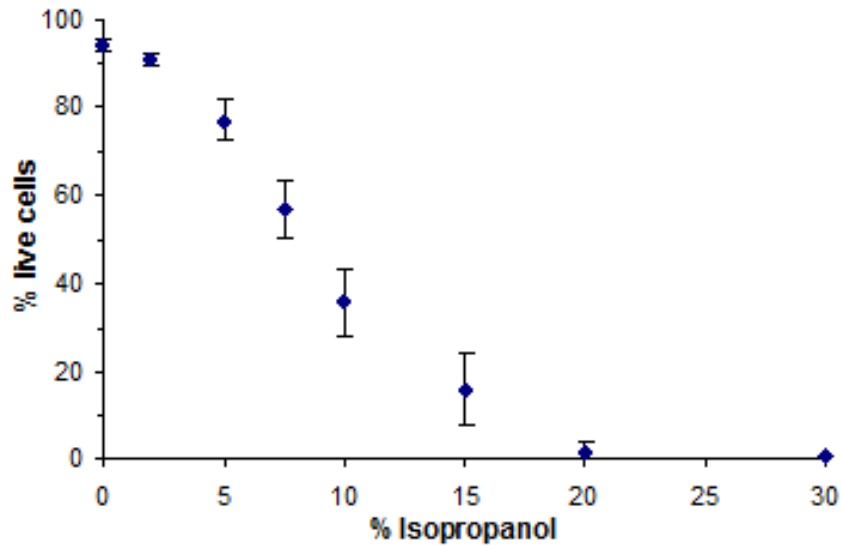


Figure 5.7. Titration of Live/Dead kit.

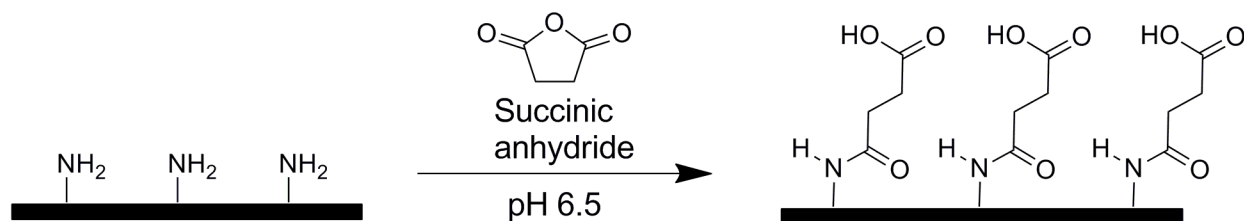
5.3. Results and Discussion

5.3.1. Surface characterization SAM-modified gold slides

The following alkanethiol SAMs on gold were used to test bacterial attachment and biofilm growth on surfaces terminating with CH₃ groups (hydrophobic), COOH and NH₂-terminated (charged hydrophilic), OH and PEG-terminated (uncharged hydrophilic). The surfaces were characterized by contact angle (Table 5.2). Surface reactions that were applied to glass surface were also performed on gold so that surface could be characterized each time by grazing IR spectroscopy.

Table 5.2. Contact angle and ellipsometry thickness of alkanethiol SAMs with various terminal groups on gold. The alkanethiols used were (in the order that they are listed on the table): dodecanethiol, 11-mercaptoundecanoic acid, 11-amino-1-undecanethiol, 11-mercaptoundecanol, triethylene glycol mono-11-mercaptoundecyl ether, and CH₃O-(CH₂CH₂O)₄₀-(CH₂)₂SH or mPEG-SH.

Surface (Full name or structure)	Terminal group	Contact angle of deionized water
DDT (Dodecanethiol)	CH ₃	98.7 ±1.2
MUA (11-Mercapto undecanoic acid)	COOH	14.1 ±1.5
AUT (11-Amino undecanethiol)	NH ₂	66.0 ±1.8
MUO (11-Mercapto undecanol)	OH	32.9 ±2.0
Short PEG Triethylene glycol mono-11- mercaptoundecyl ether	PEG (3-mer)	33.4 ±1.6
Long PEG CH ₃ O-(CH ₂ CH ₂ O) ₄₀ -(CH ₂) ₂ SH	PEG (40-mer)	34.7 ±1.6



Scheme 5.1. Modification of terminal amines to carboxyl groups on the surface. Under nucleophilic attack from the amino group the succinic anhydride ring opens to form an amide bond and a free carboxylic group.

Table 5.3. Contact angles of an amino-terminated surface before and after incubating with an aqueous solution of succinic anhydride overnight at room temperature. The NH₂-terminated surface was prepared by modifying the gold surface with cysteamine (NH₂CH₂CH₂SH). Solutions of 0.01 M H₂SO₄ and 0.01 M NaOH were used as pH 2 and pH 12 solutions, respectively.

Surface	Deionized water	pH 2	pH 12
NH ₂ -terminated	35.0 ±1.0	20.9 ±0.7	39.9 ±3.4
Modified with succinic anhydride	47.4 ±1.4	46.1 ±0.4	18.5 ±2.7

COOH-terminated SAMs are formed on gold surfaces by using carboxyl alkanethiols which are commercially available. However, alkoxy silane compounds containing free COOH groups are not stable, and they quickly form siloxane polymers in solution. Therefore, COOH-terminated glass surfaces were formed by modifying NH₂-terminated surfaces (Scheme 5.1). This is done by exposing NH₂-terminated surface to an aqueous solution of succinic anhydride. The modification of the surface with COOH groups was confirmed by contact angle (Table 5.3) and grazing IR spectroscopy (Figure 5.8). Prior to modification with succinic anhydride the pH 2 solutions provides the lowest contact angle values. The contact angle values of pH 2 and pH 12

solutions are reversed following modification with succinic anhydride. Grazing IR spectroscopy confirmed the presence of COOH groups after following surface modification with succinic anhydride and the ability to activate and add other groups to the surface *via* amide bonds.

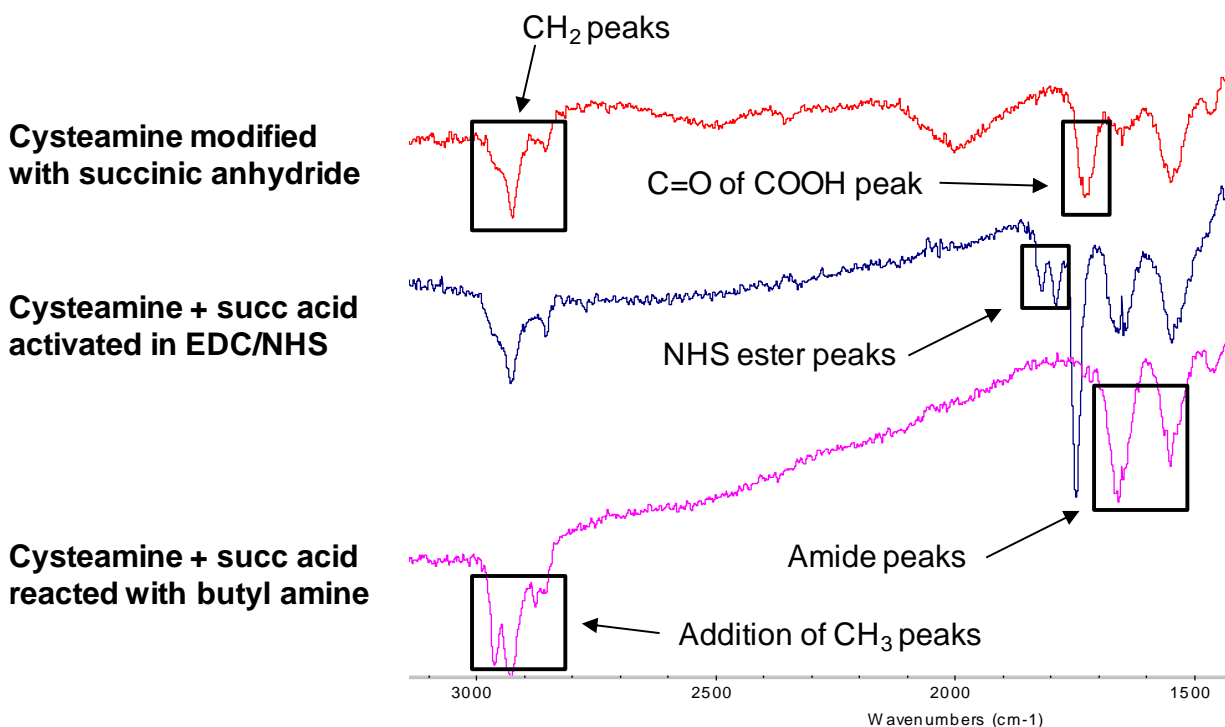
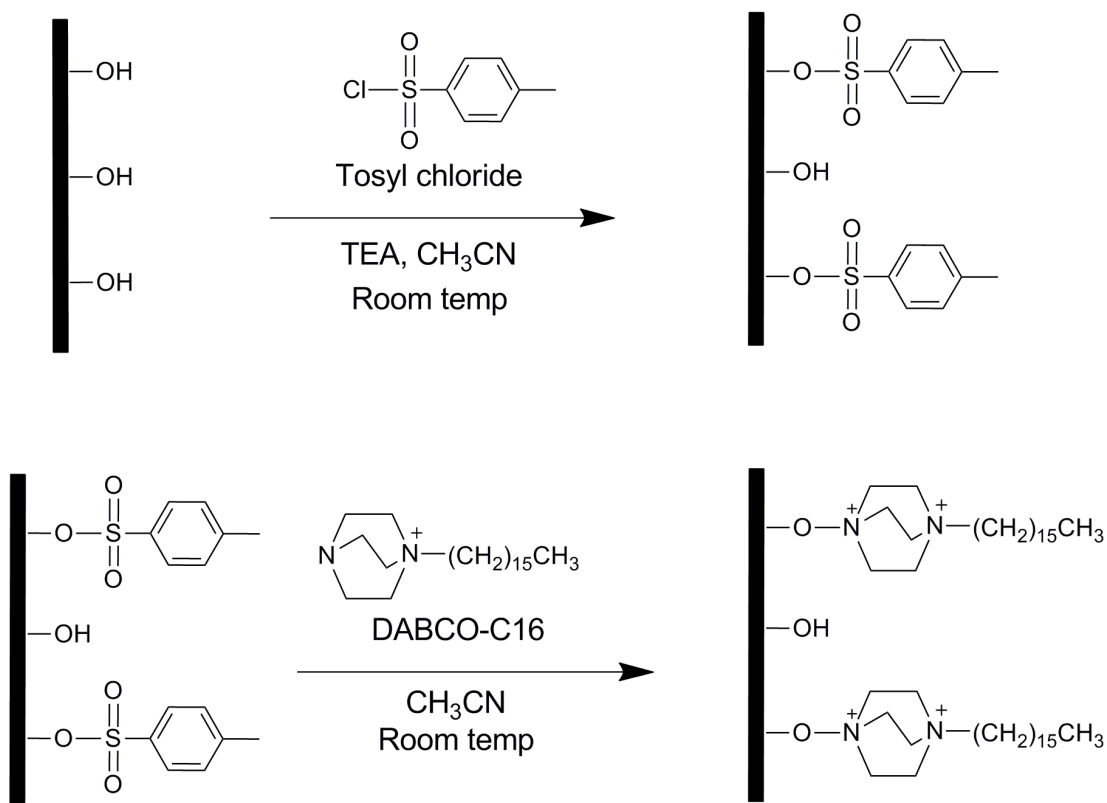


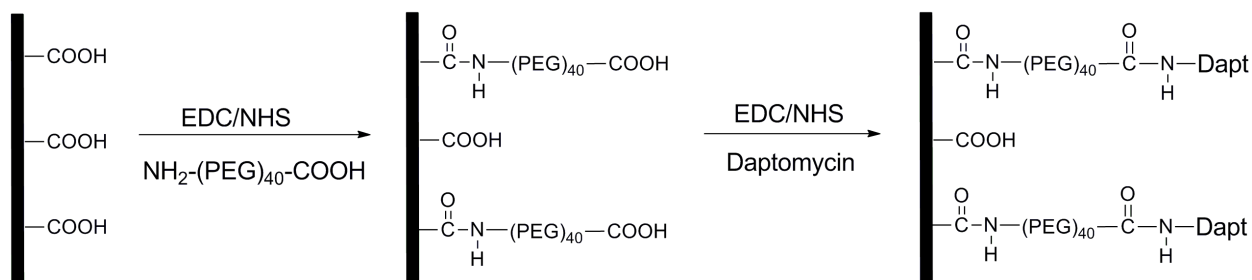
Figure 5.8. Confirmation of the formation of COOH on NH₂-terminated surface treated with succinic anhydride by grazing IR spectroscopy. To further confirm the presence of COOH groups, the surface was activated with EDC/NHS to show the formation of NHS esters and then reacted with butyl amine to show the disappearance of the carbonyl peak due to the formation of amide bonds. Note: amide bonds are already present after the reaction of succinic anhydride with the NH₂ groups on the surface.

Attachment of Dabco-C16 was performed on an OH-terminated surface (Scheme 5.2). The OH groups were activated by incubating with Tosyl chloride and then reacting with Dabco-C16. The wettability of the surface changed from hydrophilic ($33 \pm 2^\circ$) to hydrophobic ($84 \pm 3^\circ$). The only change in the grazing IR was an increase in the intensity of the methylene peaks.



Scheme 5.2. Covalent attachment of Dabco-C16 on OH-terminated surface. The OH-terminated surface on gold was obtained by forming a SAM of 11-mercaptoundecanol, whereas on glass it was formed by coating with n-(3-Triethoxysilylpropyl)gluconamide. The hydroxyl groups are activated with Tosyl chloride and then after exposure to DABCO-C16 solution in acetonitrile, the nitrogen forms a covalent bond with the surface oxygen. This reaction would apply to any amine containing compound.

Daptomycin was attached covalently *via* amide bond activation. Daptomycin was obtained from Cubist Pharmaceuticals, Inc. (Lexington, MA) as a yellow powder at 90% purity.¹⁴⁴ Daptomycin has four carboxylic and one primary amine residue on its structure. Both groups could be used to covalently attach daptomycin to a COOH or NH₂-terminated surface. However, attachment to the NH₂-terminated surface would require incubation of the surface in the presence of both daptomycin and the EDC/NHS activation agents. This would lead to amide bond formation



Scheme 5.3. Covalent attachment of daptomycin on the surface. The COOH-terminated surface on gold was generated by forming a SAM of 11-mercapto undecanoic acid, whereas on glass it was generated by coating the surface with 3-aminopropyltrimethoxysilane and then modifying the amino groups to COOH using Scheme 5.1. The COOH-terminated surface was activated with EDC/NHS and then incubated in a 10 mM solution of $\text{NH}_2\text{-(PEG)}_{40}\text{-COOH}$ in pH 9.6 buffer. The pegylated surface was also activated with EDC/NHS and then incubated in a 1 mM solution of daptomycin in pH 9.6 buffer.

between daptomycin molecules. The safest route is to activate the COOH-terminated surface with EDC/NHS, and then expose it to daptomycin so that it can form an amide bond through the ornithine amino acid residue. Prior to attachment of daptomycin a bifunctional PEG spacer is covalently bound to the activated COOH-terminated surface through its amino group and following another activation step daptomycin is attached to the COOH-terminated PEG surface (Scheme 5.3).

Contact angle measurements (Table 5.4) showed the presence of the COOH groups after modification of the gold surface with 11-mercapto undecanoic acid (MUA). Following the addition of the PEG spacer the contact angle values increased while there was still a difference between the pH 2 and pH 12 contact angles indicating the presence of COOH groups on the surface. Attachment of either daptomycin or butylamine caused the contact angle values to be constant between the different pH solutions. Grazing IR spectra (Figure 5.9) also indicated the

Table 5.4. Contact angles on gold after each modification step during the covalent attachment of daptomycin. Butylamine was initially attached on a different slide since it is smaller and it would be easier to observe its covalent attachment on the grazing IR spectrum. Solutions of 0.01 M H₂SO₄ and 0.01 M NaOH were used as pH 2 and pH 12 solutions, respectively.

Film components	Terminal group	Deionized water	pH2	pH 12
MUA	COOH	18.5 ±2.0	22.9 ±1.5	8.2 ±0.5
MUA + PEG	PEG-COOH	45.8 ±0.3	45.8 ±0.1	31.6 ±2.1
MUA + PEG + butylamine	(CH ₂) ₃ CH ₃	64.6 ±1.0	66.9 ±2.2	63.6 ±1.5
MUA + PEG + daptomycin	daptomycin	55.5 ±0.4	55.1 ±1.6	49.5 ±1.2

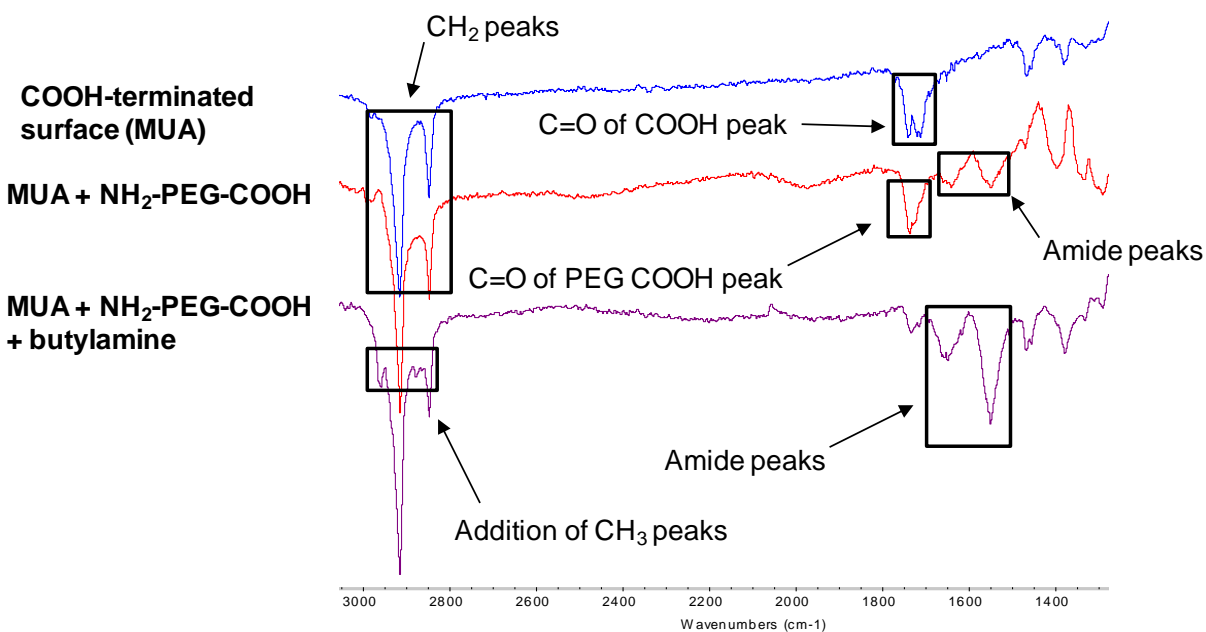


Figure 5.9. Grazing IR spectra showing the attachment of a PEG tether on the carboxyl terminated surface, followed by attachment of an amino containing compound, butylamine. Butylamine was used because it would be easily observed upon covalent attachment since it has a smaller size and contains only one functional group, compared to daptomycin which has several peptide bonds and functional groups. The formation of NHS ester peaks was observed after each activation step with EDC/NHS prior to the attachment of the PEG space or butylamine.

addition of the PEG spacer by the formation of amide peaks at 1640 and 1550 cm^{-1} . After the addition of butylamine the intensity of the amide peaks increased while the CH_3 peaks appeared at 2962 and 2881 cm^{-1} .

5.3.2. Surface characterization of SAM-modified glass slides

Glass slides were cleaned in piranha solution and then their surface was modified to be terminated with the compounds shown in Table 5.5. The modification was characterized by contact angle measurements.

5.3.3. Protein adhesion assay

As mentioned in the introduction, attachment of bacteria and biofilm formation on the surface of medical implants can be aided by the formation of conditioning films, derived from the nonspecific adsorption of bodily fluids proteins such as albumin, fibrinogen, fibronectin, and laminin. Therefore, we designed an assay that can be used to identify surfaces that prevent the formation of conditioning films and more specifically adsorption of plasma proteins. Gold slides modified with the SAMs listed in Table 5.6 were immersed in Dulbecco's Modified Eagle Medium (DMEM), which is a commonly used cell culture medium, supplemented with 15% fetal bovine serum. They were incubated for 24 hours at 37 °C. The contact angle and optical thickness of the surface was measured before and after the incubation. The results showed that the amino terminated surface had the highest thickness after incubation in medium with 15% serum. As expected, only the PEG terminated surfaces appear to have the same thickness after incubation in serum. Thus, the application of PEG terminated SAMs on the substrate should be able to prevent the formation of conditioning films and also the attachment of bacteria through

Table 5.6. Ellipsometry thickness (nm) of SAM modified gold slides before and after incubation in 15% fetal bovine serum in DMEM cell culture growth medium. The surfaces were incubated for 24 hours at 37 °C.

Surface	Terminal group	Before	After
DDT	CH ₃	1.4 ±0.4	2.8 ±0.7
MUA	COOH	1.0 ±0.2	3.6 ±0.3
AUT	NH ₂	0.9 ±0.2	5.6 ±0.5
MUO	OH	0.9 ±0.1	3.5 ±0.4
Short PEG	PEG (3-mer)	1.2 ±0.1	1.9 ±0.3
Long PEG	PEG (40-mer)	1.6 ±0.4	1.9 ±0.5

5.3.4. Bacterial attachment and biofilm assays

The same surfaces that were tested for protein adhesion underwent a bacterial attachment assay. Bacterial attachment or non-specific binding is the first stage of biofilm formation, unless the formation of the conditioning film occurs first. Therefore, an antifouling surface serves the dual function of preventing of bacterial attachment and the formation of conditioning films, which provide a larger variety of binding sites for bacteria. The bacterial suspension concentration was 2×10^7 bacteria/mL, which is 100 times dilution of the bacterial concentration in the mid-log phase of the growth curve. After 1 hour incubation at 37 °C the hydrophobic surface had the highest concentration of bacteria, followed by the charged hydrophilic surface. The hydroxyl terminated surface had relatively fewer bacteria than the other surfaces, while no cells were observed on the PEG-terminated surfaces (Table 5.7).

Table 5.7. Surface cell density on modified gold surfaces after exposing to a 2×10^7 bacteria/mL suspension of bacterial cells in Tris buffer at 37 °C for 1 hour.

Surface	Terminal group	Cells/mm ²
DDT	CH ₃	4,400
MUA	COOH	3,800
AUT	NH ₂	2,600
MUO	OH	950
Short PEG	PEG (3-mer)	no cells
Long PEG	PEG (40-mer)	no cells

A similar trend was observed for biofilm growth, where the PEG-terminated surfaces showed very little (3-mer) or no biofilm formation (Figures 5.10 & 5.11). The OH-terminated and 3-mer PEG surfaces also appeared to affect the growth biofilm matrix. The biofilm matrix for these surfaces was constrained only on the areas where the cells had been attached. This was uniformly observed on the 3-mer PEG surface, showing the resistance of the surface towards the biofilm matrix. The long PEG surface had very few signs of biofilm formation. This could be due to a better coverage of the longer PEG of the surface, resulting in prevention of bacterial adhesion and any proteins from the tryptic soy broth growth medium. In both cases the results indicate that the passive resistance to bacterial adhesion is able to prevent biofilm formation. Even in the cases when cells due stick to the surface the biofilm matrix growth was impeded and unlike the other surfaces the matrix growth is restricted only to the areas where cells are observed.

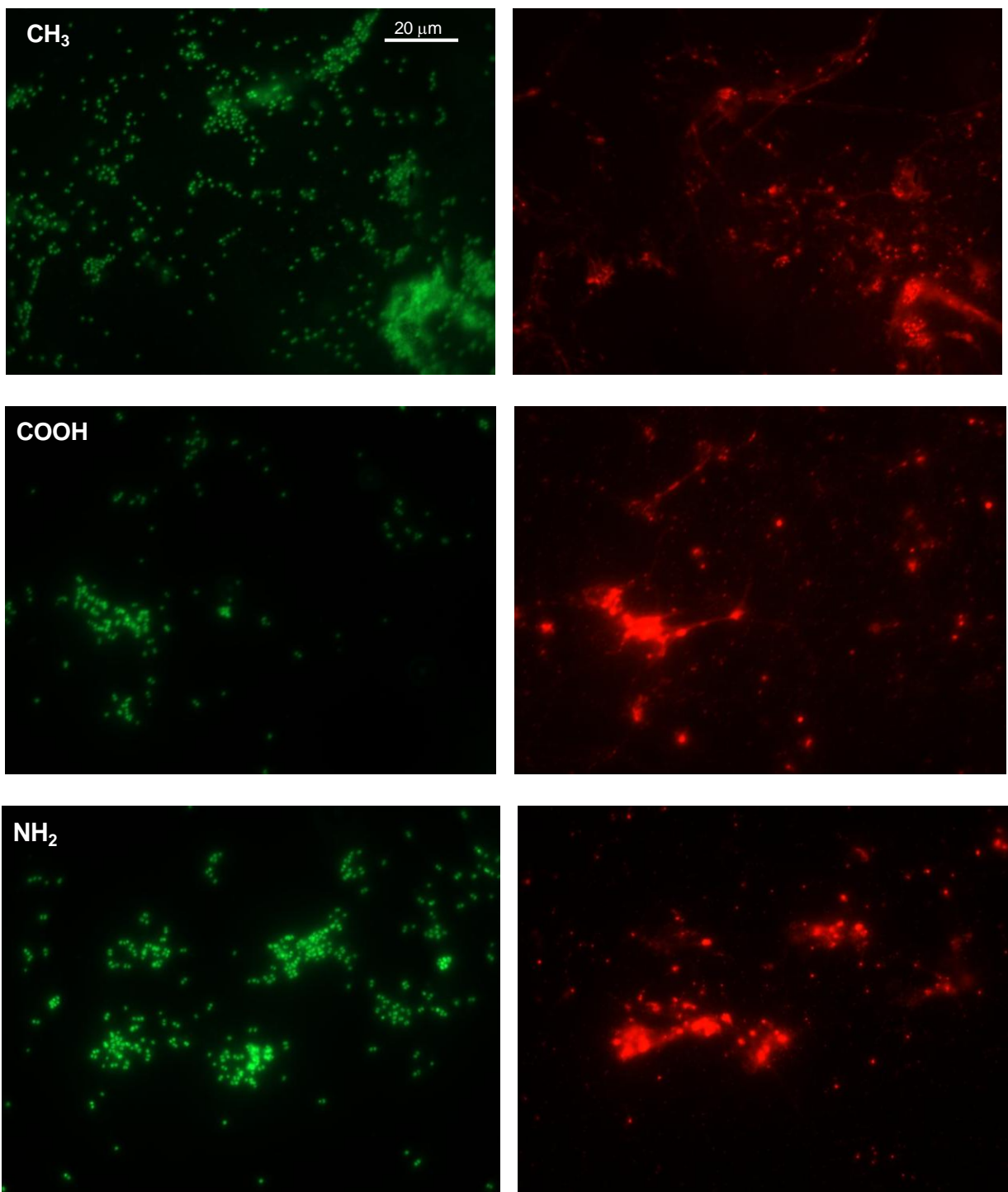


Figure 5.10. Fluorescent microscope images of *Staphylococcus epidermidis* biofilms grown on SAMs that favor cell attachment and biofilm formation. The surfaces were CH₃, COOH and NH₂-terminated. The cells were stained with both Syto 9 and propidium iodide and images were taken with the FITC and Texas Red filter cubes. Live cells fluoresce in green, whereas dead cells and biofilm mass fluoresce in red. As expected, most cells are alive (green).

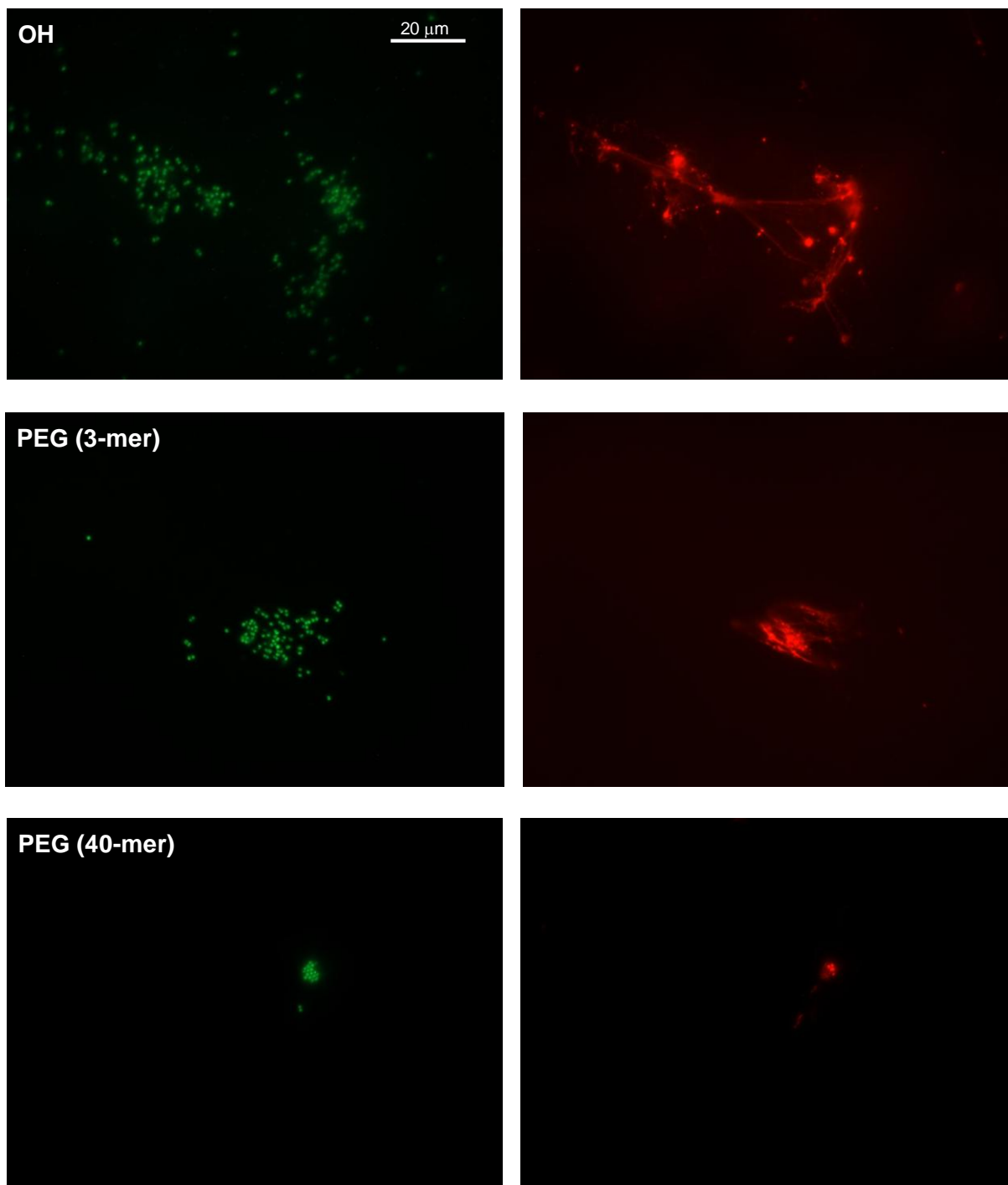


Figure 5.11. Fluorescent microscope images of *Staphylococcus epidermidis* biofilms grown on SAMs that do not favor cell attachment and slow or block biofilm formation. The surfaces were OH and PEG-terminated. The cells were stained with both Syto 9 and propidium iodide and images were taken with the FITC and Texas Red filter cubes. Live cells fluoresce in green, whereas dead cells and biofilm mass fluoresce in red. As expected, most cells are alive (green).

The bacterial attachment assay was also run on glass surfaces. Results are shown in Table 5.8. The ODTMS and APTMS showed results comparable to DDT and AUT surfaces on gold. The surfaces favored attachment of considerable numbers of bacteria in 1 hour from a relatively low solution concentration of bacteria (2×10^7 cells/mL). The PEGTMS surface had no cells bound to it, as expected. ODMA-terminated surface had also no cells on average. The fluorocarbon-terminated surface and Dabco-C16 had very few cells attached and in the case of Dabco-C16 the few cells that were observed were stained red.

Table 5.8. Surface cell density after exposing modified glass surfaces to a 2×10^7 cells/mL suspension of bacteria in Tris buffer for 1 hour at 37 °C.

Surface	Side group of alkoxy silane	Cells/mm ²
ODTMS	$-(\text{CH}_2)_{17}\text{CH}_3$	7,100
APTMS	$-\text{CH}_2\text{CH}_2\text{CH}_2\text{NH}_2$	5,200
PEGTMS	$-(\text{CH}_2)_3\text{NH}\overset{\text{O}}{\parallel}\text{C}(\text{CH}_2\text{CH}_2\text{O})_{4-6}\text{H}$	no cells
PFTMS	$-\text{CH}_2\text{CH}_2(\text{CF}_2)_5\text{CF}_3$	460
ODMA	$-(\text{CH}_2)_3-\overset{\text{CH}_3}{\underset{\text{CH}_3}{\text{N}^+}}-(\text{CH}_2)_{17}\text{CH}_3$	no cells
Dabco-C16	$-\text{N}^+(\text{CH}_2)_6\text{N}^+(\text{CH}_2)_{15}\text{CH}_3$	550

5.3.5. Covalent attachment of daptomycin

Under certain conditions bacteria with damaged membranes (red-stained with the Live/Dead kit) may be able to recover and multiply, or dead bacteria with intact membranes may score as

alive.¹⁴⁵ Furthermore, as the mechanism of action of daptomycin is not fully understood,¹⁴¹ the Live/Dead viability assay needed to be tested for cells killed from daptomycin, whether in

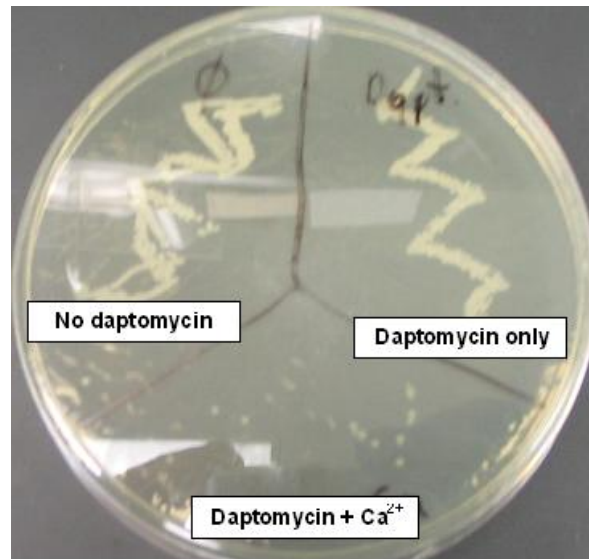
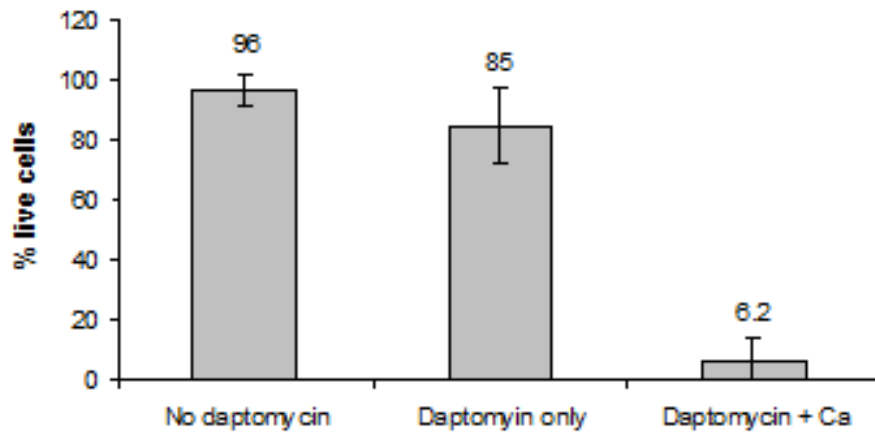


Figure 5.12. Viability of suspended cells to daptomycin in solution by (top) live/dead assay and (bottom) agar plating.

suspension or attached to a surface, and in each case the results from the viability assay would be checked by inoculating the treated cells on agar plates. The cells in suspension were diluted to 2×10^8 bacteria /mL in 0.85% NaCl solution, tenfold the bacterial concentration usually used.

The higher concentration was used because at 2×10^7 bacteria /mL suspensions, very few bacteria (less than five per field of view) were observed under the microscope. The cells were incubated in three different 0.85% NaCl solutions: without daptomycin, in 10 $\mu\text{g}/\text{mL}$ (or 6 μM) daptomycin, and 10 $\mu\text{g}/\text{mL}$ daptomycin with 50 $\mu\text{g}/\text{mL}$ (or 0.45 mM) CaCl_2 . After 2 hour incubation at 37°C, samples from each suspension were stained with the Live/Dead kit and observed under the fluorescent microscope (Figure 5.12 top). A second sample from each assay was inoculated on agar plates and incubated overnight at 37°C (Figure 5.12 bottom). Daptomycin was shown to be much more effective at killing cells when used with Ca^{2+} ions in both cases. More importantly, the Live/Dead assay was capable of scoring cells killed from daptomycin as dead. Cells attached on the surface slides were incubated under the same conditions in the three different solutions (Figure 5.13 top). Daptomycin killed more than 90% of the cells. This result was supported by growing cells on agar plates, too (Figure 5.13 bottom). The adhered cells were inoculated on the agar plates by pressing the slides face-down on the agar plate and then removing them. The plates were incubated overnight at 37°C. Therefore, if the modified gold surfaces have antibacterial properties, the assay will be able to determine the ratio of killed cells by the surface, when compared to the controls.

Since there were three different molecular layers under the daptomycin film, three controls were used when checking the viability of cells on daptomycin coated samples; bare glass, amino terminated, and daptomycin terminated. For each experiment the cells in suspension from the stock solution were kept under the same conditions as the adhered cells and then stained and viewed under the fluorescent microscope after all the other samples had been assayed. The Daptomycin coated surface showed high resistance to biofilm formation (Figure 5.14). This

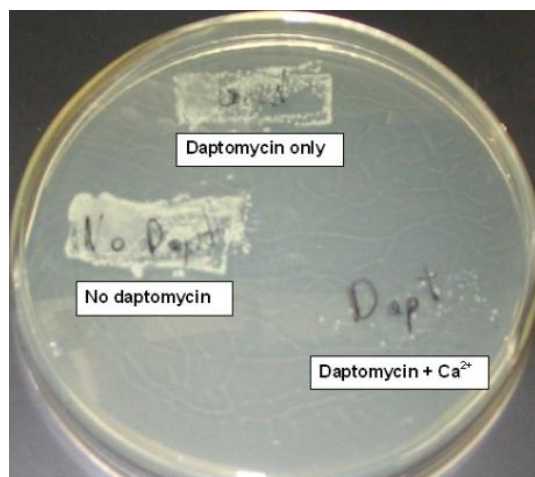
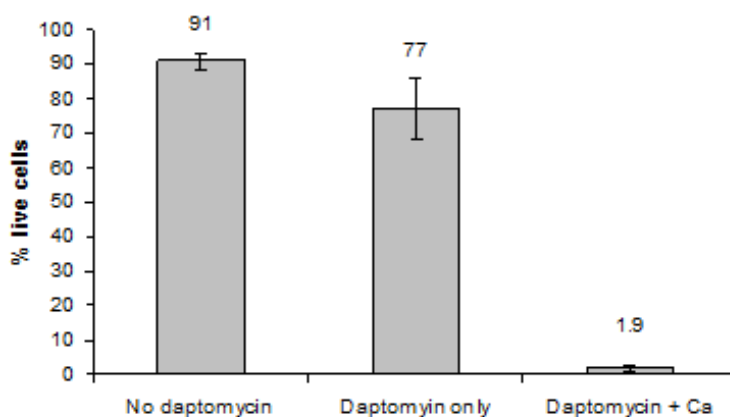


Figure 5.13. Viability of adhered cells to daptomycin in solution by (top) live/dead assay and (bottom) agar plating.

indicates that after by immobilizing daptomycin on the surface it still maintained its activity and ability to kill bacteria. The PEG tether would allow for daptomycin to achieve the correct orientation and insert in the bacterial cell membrane. In addition this result shows that a combination of passive and active coating would generate a surface that not only resists bacterial attachment, but also kills the few that due attach.

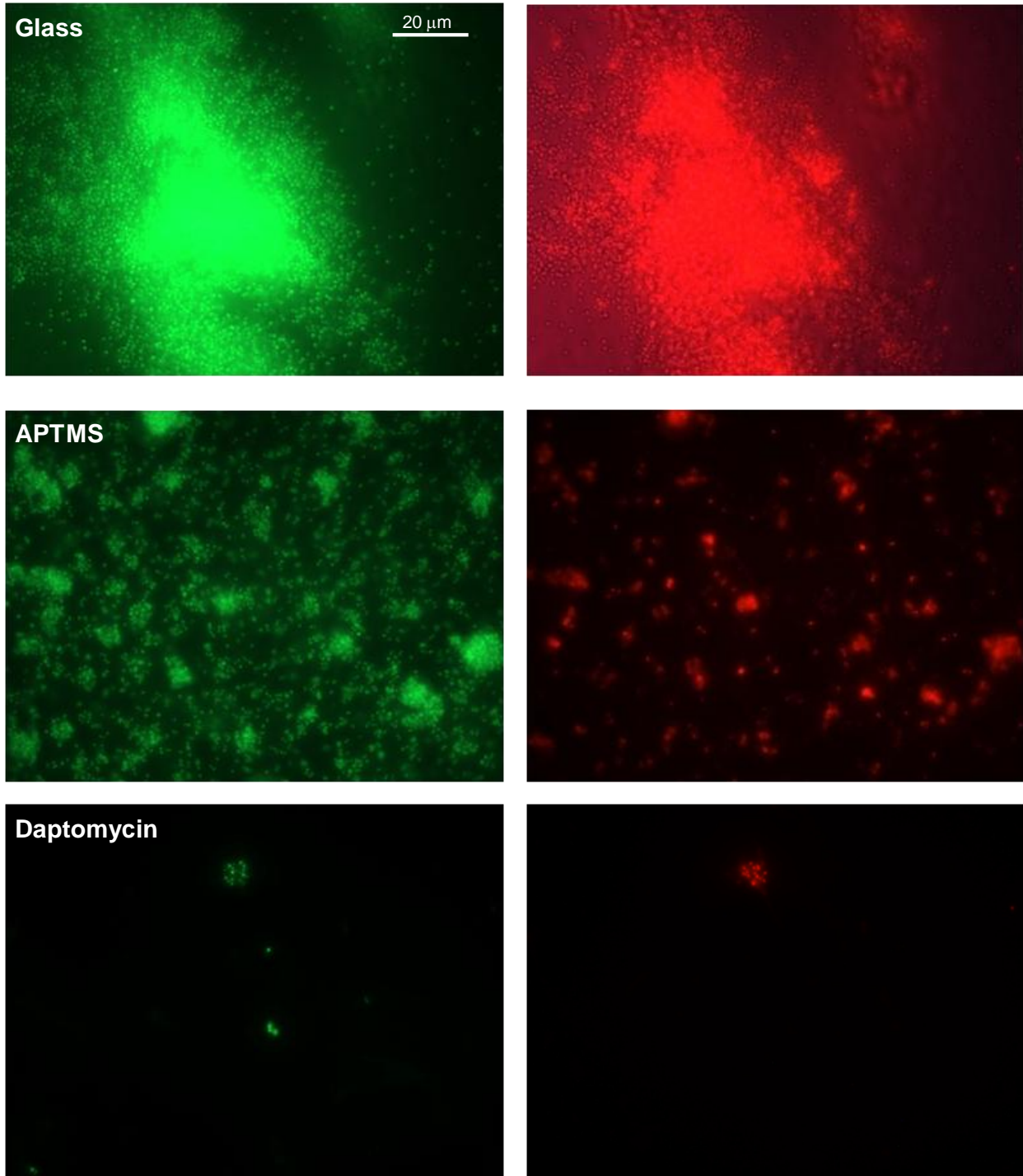


Figure 5.14. Fluorescent microscope images of *Staphylococcus epidermidis* biofilms grown on glass, APTMS, and daptomycin crosslinked to APTMS through a PEG spacer. The biofilm was grown by incubating the slides in tryptic soy broth with 0.25% glucose for 24 hours at 37 °C. The cells were stained with both Syto 9 and propidium iodide and images were taken with the FITC and Texas Red filter cubes.

5.4. Summary and Conclusions

Biofilm formation is a result of the availability of binding sites on man-made material implanted in patients and also the ability to grow a protective polysaccharide layer for self-protection once they attach to a surface. Bacteria have evolved special proteins, adhesins, in order to attach to an array of surfaces. At the same time the large variety of proteins in bodily fluids, especially blood, means that some proteins will bind specifically to a surface, thereby creating conditioning films that favour bacterial attachment better than the man-made material itself. Therefore, biofilm prevention has to include a combination of passive and active resistance. Surfaces such as poly(ethyleneglycol) are capable of providing inert surfaces on both gold and glass and using silane chemistry they can be applied to other substrates, such as polymers. Antimicrobial compounds that are able to kill microorganisms by binding to their membranes can provide the active resistance to the few bacteria that do attach. If the antimicrobial compound provided the only protection, their availability is limited so they could be overwhelmed by attaching bacteria and conditioning films. The combination of passive and active surfaces can be generated by the formation of mixed self-assembled monolayers. However in our construct we believe we have gone one step further by generating a mixed SAM not laterally but depth-wise. The long PEG tether served as the passive biofilm resistant layer, while also providing flexibility and anchoring daptomycin to the surface. The daptomycin was able to kill the few cells that did attach.

5.5. Practical Implementations and Future Work

The goal for the future experiments is to improve the viability assay so that there is no cell death in the negative controls and to obtain repeatable results, by using substrates other than glass, to

develop antifungal surfaces, to coat surfaces with other molecules known for their antimicrobial properties, and to study biofilm formation under laminar flow in a micro channel. The flow study has two applications; (1) it can be used to optimize coating in biosensors that will be used for detection of blood metabolites, and (2) it can be used as a model for studying biofilm formation in catheters inserted in blood vessels.

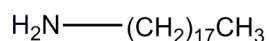
5.5.1. Polymeric, stainless steel and titanium surfaces

Most medical implants are made of polymers, and others are made of titanium and stainless steel. Intravascular devices, such as catheters, are usually made of silicone or polyurethane. Titanium is used as support for broken bones and is a material that is often used in prosthetic limbs. Stents are made of stainless steel. All these materials are suited for their respective functions, but the response of the host upon their insertion in the body can be unexpected and has risks due to the possible inflammation and/or bacterial infections (biofilm formation). Any surface modifications that can avoid these problems without affecting the physical properties of the bulk material are subject of high interest in the medical community. Samples consisting of materials with similar compositions to the ones used in the medical field will be coated with surfaces presenting antimicrobial and anti-adhesive properties, and bacterial attachment and biofilm formation will be assayed similar to the gold and glass surfaces.

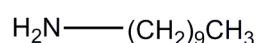
5.5.2. Effect of hydrophobic tail length compared to daptomycin

Daptomycin contains a nine carbon long hydrophobic chain attached *via* an amide bond to rupture the bacterial cell membrane. Although this is not done through the hydrophobic tail alone, it would be interesting to know if (1) long alkyl chains attached through amide bonds can

have a similar effect and (2) if the chain length has any effect in depolarizing the cell membrane. In order to answer these questions, long chain alkyl amines, Dabco, and alkoxy silanes of two different lengths will be attached to glass slides alongside daptomycin and their antimicrobial activity will be determined. The different compounds will be attached covalently to the surface.

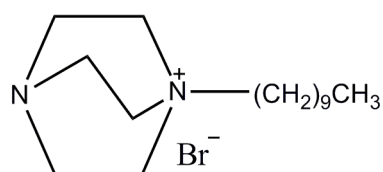
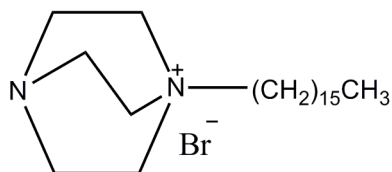


Octadecylamine

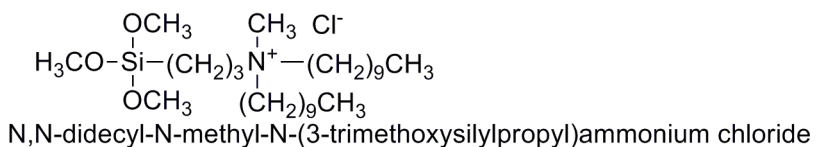
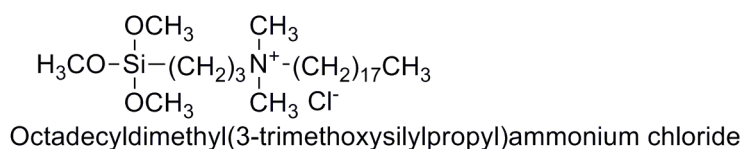


Decylamine

Amines (to be attached by amide bonds to COOH terminated surface)



DABCO



Quaternary amines

Figure 5.15. The different antimicrobial compounds that will be attached to the surface.

The carboxylic group in the Amphotericin B molecules will be used either to link it covalently through an amide bond to a SAM of 3-aminopropylsilane on glass substrate, which has the primary amine as the terminal group. Both tethering methods can be tried to determine which one provides the most antifungal effect. Molecular Probes FungaLight CFDA, AM/Propidium Iodide Yeast Vitality Kit, which works in a similar way to the bacterial Live/Dead kit, will be used to distinguish between live and dead cells, by using fluorescent images to count the live and dead cells.

Another approach to developing antimicrobial coatings will be to prepare surfaces with a mixed monolayer of two or more compounds which target various microorganisms. The ratio that shows an equal presence of both compounds during the characterization steps will be used to prepare the samples that will be tested with the viability assay.

5.5.4. Antibacterial surfaces comprising of quorum sensing autoinducers

In the last two decades microbiologists have discovered signaling pathways in bacteria that allow them to modulate their gene expression in response to changes in population density. This ability is known as quorum sensing. It involves production, release, and detection of small molecules called "autoinducers". When a threshold of autoinducer concentration is reached, a gene expression pathway is triggered that results in population-wide alteration in gene expression. It has been found that processes which require the combined action of numerous cells to be productive, such as bioluminescence, biofilm formation, or virulence factor expression, are controlled by quorum sensing.¹⁵⁰

Two predominant types of autoinducers have been discovered, acyl homoserine lactones (AHLs) and modified oligopeptides, are used by gram-negative and gram-positive bacteria, respectively.¹⁵¹ Targeting quorum sensing, the alga *Delisea pulchra* has evolved a way to prevent biofilm formation on its surface. It coats the surface of its leaves with a halogenated furanone that is structurally similar to (AHLs). This furanone blocks the signaling pathway by competing with the AHLs for the binding site of the AHL receptors (Figure 5.17).¹⁵² These inhibitors could have the same effect if they were immobilized on the surface, but the AHL receptors are found mostly inside the cells. However the receptors of gram-positive bacteria autoinducers are located in the cell membrane.¹⁵¹ These inducers range from 5 to 17 amino acids

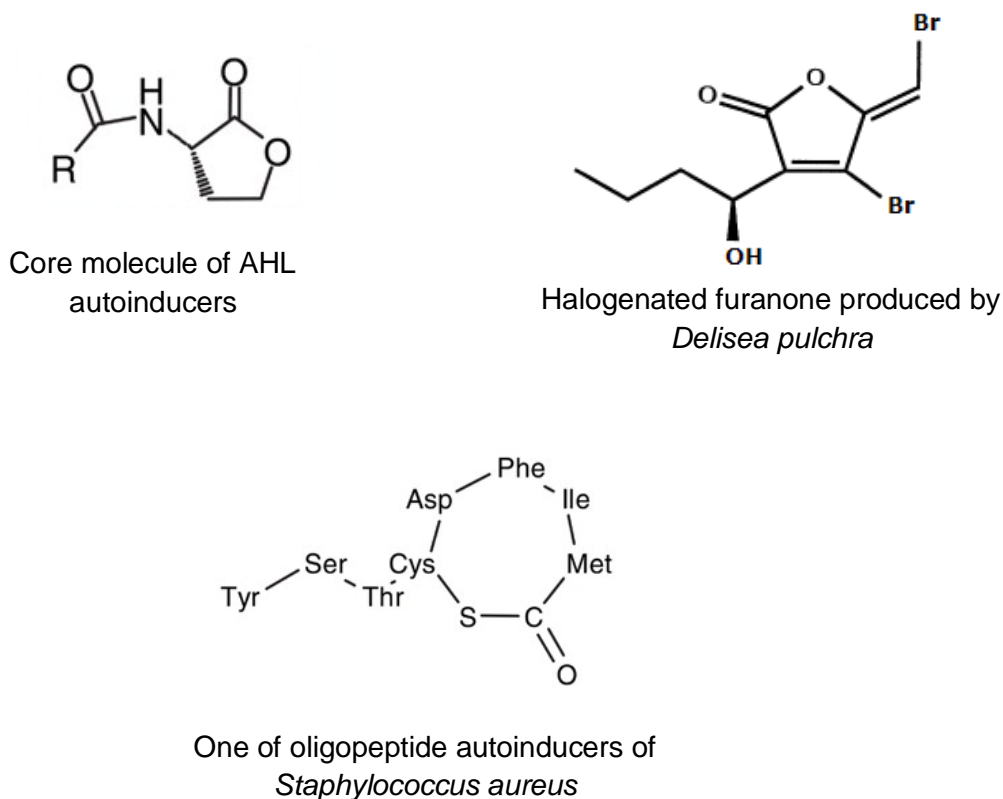


Figure 5.17. Several bacterial quorum sensing molecules.

in length and often contain thiolactone rings and have terminal amino groups (Figure 5.17). Recent evidence shows that replacement of sulfur in the thiolactone links with nitrogen or oxygen atoms can have inhibitory effects. The ring is also required for activation or inhibition, whereas the tail is required only for activation.¹⁵³ Therefore, if the inhibitory oligopeptide is tethered to the surface through its tail it will still have inhibitory effects. Potentially any bacteria that will bind to this surface will not be activated into biofilm formation. Since these oligopeptides have a terminal amine, they will be linked covalently to a SAM of 3-chloropropylsilane on ITO by incubating the SAM covered slides in an acetonitrile solution of the oligopeptide. After characterization of the oligopeptide film, the slides will be incubated in bacterial suspensions of different concentrations ($1 \times 10^5 - 1 \times 10^8$ bacteria /mL). The attached bacterial cells will be stained with SYTO 9, ten random pictures will be taken per slide at 1000x magnification, and the average number of cells per field will be compared to those of uncoated ITO slides.

5.5.5. Microfluidic study of biofilm formation

Prevention of biofilm formation is of interest for both reusable biosensors that detect analytes in blood, but also provides a model for studying biofilm formation under flow conditions similar to that of blood. In order to achieve this, a PDMS block containing a channel with $5 \times 1 \times 2$ mm dimensions is placed on top of a flat substrate of interest, creating a small channel (Figure 5.18). The channel is linked to tubing through holes made on the PDMS block on top of each end of the channel. A peristaltic pump will be used to generate laminar flow (at low flow rates). After introducing bacteria in the flow (at 1×10^7 cell/mL concentration), the whole system will be

placed at 37 °C at different time periods and the formation of biofilm will be assayed by staining with Syto 9[®] and propidium iodide.

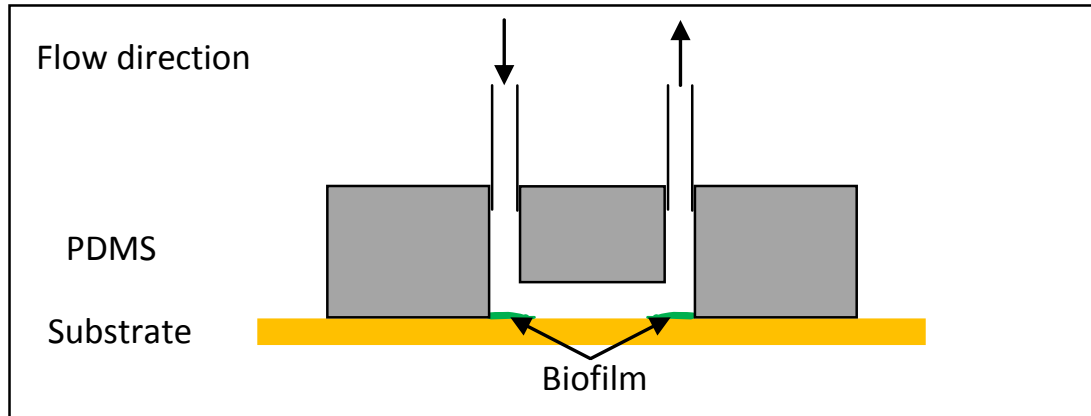


Figure 5.18. Depiction of the model that will be used to study biofilm formation in a microfluidic channel.

6. Interfacing Surfaces with Biological Systems

6.1. Introduction

Self-assembled monolayers (SAMs) are a well established method of functionalizing surfaces through selection of appropriate attachment chemistry.^{6, 154} Monolayers readily form on a variety of materials including metals, glass, and polymers. Common examples include alkanethiolates on gold and organosilanes on glass. However, numerous other substrates can be chemically modified, provided that the surface is appropriately prepared and the correct attachment chemistry is chosen. Chemically modified surfaces are highly stable, provide uniform surface properties, and offer virtually limitless possibilities in terms of applicability.

Although there is a large amount of literature that focuses on individual chemical surface modification techniques and specific applications, there is a limited amount that compiles functionalization methods for different types of surfaces. In this work we provide a comprehensive description of surface modification techniques for a variety of different types of surfaces including metals, metal oxides, silicates, and polymers. The utility of the methods demonstrated here are universal and only limited by the attachment chemistry that can be used for each substrate, the remaining portion of the molecule used for functionalization can be designed to suit whatever application is desired. Substrates examined in this study include; gold, glass, indium tin oxide (ITO), stainless steel, and a number of polymers (polydimethylsiloxane, polyurethane, polystyrene, and polytetrafluoroethylene). Functionalization of each type of surface will be described in a step-by-step approach that includes the substrate cleaning and activation process (if necessary), a description of the attachment chemistry, and the full

characterization of the modified surface. All these surface modifications apply to specific applications that include; controlled surface wettability, surface patterning, directed cell adhesion, biofilm resistance.

Cell culture is typically performed on flat two-dimensional surfaces. Although the coating of such surfaces can mimic the biochemical environment of the extracellular matrix of live tissues, the geometry of such a system confines both the ability to directly compare the behavior of these cells with those growing in living tissue and the ability to generate tissue.¹⁵⁵ Cells growing on a two-dimensional surface cannot interact with other cells in all directions as they would in any tissue of a living organism. Tissue engineering has become important in the replacement of damaged tissues and organs of patients due to either injury or disease.¹⁵⁶ However, growing cells on a three-dimensional porous substrate or scaffold has its own limitations.^{157, 158} Building of the scaffold either from processed natural products or biomaterials can be challenging especially when more than one cell type is required for tissue generation. When more than one type of cell or tissue is needed, directing and controlling of cell binding and growth in the correct formation on the same scaffold would be required. Once such a solid scaffold is exposed to the cells, cell growth or tissue generation cannot be controlled, often leading to unexpected and unwanted results.

If the scaffold or template was flexible or it was made of movable parts that could be removed, added or replaced, and whose movement could be controlled from the outside, then a system would be in place for controlling the binding and growth of the different cells and tissue layers in the correct formation. A magnetic support, such as magnetic beads, would allow for such a

template, and their movement can be controlled from an external magnetic field which can set and change the shape of the template without the need to directly intervene with the template and risk infection. Magnetic beads have been used in the past for several applications, such as enzyme immobilization and cell separation.¹⁵⁹ Magnetic beads are either coated with a thin film or are encapsulated in a polymer matrix.

The magnetic beads prepared and used in this work consist of iron oxide nanoparticles embedded in micrometer-size (10 – 100 micron) agarose gel beads. The agarose gel is a non-adherent substrate, which does not allow for bead aggregation. The surface of the beads can be coated with antibodies for specific cell-attachment or collagen for non-specific attachment. To show the ability of antibodies to immobilize cells, the antibodies were first attached to a flat surface and specific cell-immobilization on the surface was confirmed. The cells attached to magnetic beads can be arranged in various formations using an external magnetic field. By generating a homogeneous magnetic field the beads can be dispersed evenly in the medium creating a three-dimensional environment and allowing the cells to generate their own extracellular matrix without the need of a solid scaffold. A continuous flow of the growth medium over these beads will provide a fresh supply of nutrients and oxygen and provide the mechanical stress factor required, while at the same time removing waste products that will be adequate for the internal tissue layers.

A continuous flow bioreactor was constructed to culture three dimensional tissue stabilized by magnetic field in the solution medium. The continuous flow while the magnetic support is suspended in solution will provide the mechanical stress factor as well as freedom required for

enhanced proliferation of cells seeded on the magnetic beads. In addition to culturing cells and tissue, this bioreactor has high potential for a variety of industrial applications such as continuous production of biofuels, pharmaceuticals, and cellular metabolites.

6.2. Experimental Details

6.2.1. *Microcontact printing (μ CP)*

Clean gold slides are used as substrate for μ CP. The PDMS stamps are inked with a solution of dodecanethiol (DDT) in ethanol, dried with nitrogen and immediately placed on top the gold slide and removed after 1 min. In a second step the stamp is gently peeled off the gold surface and the gold slide is dipped in a solution of amino undecanethiol (AUT) in ethanol and incubated for 2 hours, in order to backfill the un-printed areas. The glass slide is rinsed with ethanol, dried with nitrogen and stored for further use in a sealed Petri dish at 4°C.

PDMS stamps are treated in a plasma cleaner and then dipped overnight in a solution of octadecyl trimethoxysilane (ODTMS) (in toluene), perfluorooctyl trimethoxysilane (PFTMS) (in tetracarbon chloride), or n-(Triethoxysilylpropyl)-o-polyethylene oxide urethane (PEG) (in ethanol). The PDMS are then rinsed with the same solvent where they were incubated and allowed to dry. Clean glass slides are used as substrate for μ CP. The passivated PDMS stamps are inked with a solution of n-(2-aminoethyl)-11-aminoundecyl trimethoxysilane (AUTMS) in ethanol, dried with nitrogen and immediately placed on top the glass slide. After making sure that the pattern has made contact with the glass surface, the glass slides with the stamp on them are sealed in a plastic Petri dish and allowed to incubate overnight. The stamp is gently peeled off the glass surface and the glass slide is dipped in a solution of PEGTMS in ethanol and

incubated overnight, in order to backfill the un-printed areas. The glass slide is rinsed with toluene, dried with nitrogen and stored for further use in a sealed Petri dish at 4°C.

6.2.2. Preparation of magnetic fluid

Dodecanoic acid (2 g) was added to a 200 mL aqueous solution of 0.12 M ferrous chloride and 0.24 M ferric chloride in a 600 mL beaker. The mixture was placed in a water bath at 50 °C and stirred at 1300 rpm with an overhead mixer from G. K. Heller Corporation (Floral Park, NY). After adding slowly 40 mL of 25% ammonia solution, the suspension was kept at 50 °C and stirred continuously at 1300 rpm. The process was allowed to run for 30 min, while removing any lather that was formed. The precipitate was recovered from the suspension by placing the beaker over a magnet and it was rinsed several times with 0.5% ammonia solution. The precipitate was then transferred into a 100 mL suspension of 1.0 g/L lauric acid (dodecanoic acid) in DI water (the acid was crushed into a fine powder prior to making the suspension). The suspension was heated to 80 °C and stirred continuously at 1300 rpm for 30 min. The magnetic fluid that was formed was left overnight to settle, and most of the clear liquid layer was then removed with a pipette. The magnetic fluid was stored at room temperature in a sealed container shielded from light until further use.

6.2.3. Preparation of magnetic agarose beads

A 10 mL volume of magnetic fluid was diluted with 10 mL of DI water, brought to pH 7.0 with 0.5% ammonia solution, and was then sonicated for 30 min. A 180 mL soybean oil solution containing 30 g/L of polysorbate was prepared in a 400 mL beaker. The oil solution was stirred at 630 rpm with the overhead mixer and heated to 90 °C in a water bath, while making sure that

the stirrer is submerged sufficiently so that no bubbles were created, which would disrupt the emulsion preparation. At the same time 10 mL of the magnetic fluid prepared above were heated to 90 °C in the water bath, while a 10 mL aqueous solution of 3% Seakem LE agarose was prepared in a 150 mL beaker by heating the mixture in a microwave oven for 50 seconds or until the solution turned clear indicating all the agarose had dissolved. The hot agarose solution was immediately added to the heated 10 mL of magnetic fluid and the mixture was stirred vigorously with a glass stirring rod, while keeping it in the 90 °C water bath.

Using a 3 mL syringe and an 18 gauge needle, the magnetic mixture was added dropwise to the oil solution while stirring at 600 rpm with the overhead mixer (the syringe was kept warm by squeezing the magnetic mixture in and out of the syringe a few times prior to transferring it to the oil mixture). The emulsion was stirred for 10 min at 90 °C. The water bath was then cooled down by carefully removing most of the hot water and adding ice to it until the temperature dropped to at least 15 °C and the emulsion was stirred for another 20 min. The magnetic agarose beads that were formed after the cooling were recovered from the oil phase by adding acetone to the emulsion mixture until it became clear, and placing it over a magnet. The magnetic beads were rinsed several times with acetone to remove any soybean oil and at the end they were thoroughly rinsed with deionized water. The magnetic beads were stored in deionized water at 4 °C until further use.

6.2.4. Chemical modification of magnetic agarose beads

The magnetic agarose beads underwent a modification step in order to increase the surface concentration of carboxyl groups, based on the procedure described in Section 2.4.2. The

magnetic beads were suspended in a freshly prepared 1 M chloroacetic acid solution in 3 M NaOH. The suspension was stirred for 70 min on an orbital shaker at room temperature. The reaction was stopped by adding 4 mg/mL of solid NaH_2PO_4 to the solution and then neutralized with 5 M HCl. The magnetic beads were recovered over a magnet and rinsed with deionized water.

In order to increase the flexibility of antibodies that would be attached to the surface, a PEG spacer was covalently attached to the carboxyl groups prior to antibody attachment, based on the procedure described in Section 2.4.7. The insertion of the spacer could make the antibodies more accessible to the antigen on the cell surface. Magnetic beads were transferred in a 1.5 mL centrifuge tube and suspended in a small volume (~ 0.5 mL) of freshly prepared solution of 100 mM EDC and 20 mM NHS in deionized water. The suspension was agitated on an orbital shaker for 15 min at room temperature. The beads were rinsed once with deionized water. This was done either by collecting the beads over a magnet or spinning the tube on a bench top centrifuge. A 100 μL solution of 100 mM $\text{NH}_2\text{-PEG}_{40}\text{-COOH}$ in pH 9.6 carbonate buffer was prepared and added to the magnetic beads. The suspension was incubated overnight at room temperature and was rinsed three times with deionized water.

6.2.5. Coating of agarose magnetic beads with protein

Beads were activated with EDC/NHS and coated with protein as described in Section 2.4.6. Prior to the activation step the magnetic agarose beads were sterilized by incubation in 70% ethanol for 1 hour at room temperature. The deionized water and all the solutions used after this step were sterile or were sterilized by filtering through a 0.2 μm HT Tiffryn membrane filter

from Pall Life Sciences (Port Washington, NY). The sterile beads were transferred to 1.5 mL centrifuge tubes and were rinsed three times with deionized water. A fresh solution of 100 mM EDC and 20 mM NHS in DI water was prepared and 0.5 mL were added to the magnetic beads. The suspension was allowed to sit at room temperature for 15 min. The beads were rinsed once with DI water. Subsequently, a 100 μ L solution of 100 μ g/mL of antibody in pH 9.6 buffer or 1 mg/mL of collagen in PBS was prepared and added to the magnetic beads. The solution was incubated overnight at 4 °C. The next day the beads were rinsed with PBS three times and stored at 4 °C until further use.

6.3. Result and Discussion Part I: Modification of Substrates

6.3.1. Gold

Substrate pretreatment is essential in order to subsequently form a highly ordered monolayer with minimal defects. The gold surface is easily contaminated. Organic molecules and other contaminants will readily adsorb to the surface if it is exposed to air even for a short period of time. The availability of various organic contaminants is higher in research laboratories where various volatile compounds are continuously used. Due to the high affinity of thiols for gold, alkanethiol monolayers will form on contaminated gold surfaces as the thiols will displace, at least to some degree, impurities on the substrate. However, resulting films fail to possess the same degree of order and reproducibility as those prepared on pretreated substrates. Piranha etching is a standard method of pretreatment of metal substrates prior to monolayer deposition. Piranha is an extremely strong oxidant and removes any organic contaminants present on the surface. The etchant is prepared from a mixture of 70 % concentrated (18 M) sulfuric acid and

30 % concentrated (35 % w/v) hydrogen peroxide. Following piranha cleaning, monolayer deposition is accomplished through exposure of the substrate to a 1 to 5 mM solution in an organic solvent (typically ethanol) overnight.

6.3.2. *Indium tin oxide*

Thin films of indium tin oxide (ITO) coated on glass substrates are useful due to their conductive and optically transparent properties.^{160, 161} In addition, ITO substrates provide a model for studying and characterizing the formation of alkoxy silane SAMs on an oxide surfaces, such as those on silicon, glass, other metal oxides, and polymers. Alkoxy silanes are the most commonly used of the organofunctional silanes for the formation of self-assembled monolayers on substrates presenting hydroxyl groups, due to easy handling, higher stability than chlorosilanes and non-corrosive byproduct formation. Alkoxy silanes used for SAM deposition consist of a trimethoxy or triethoxy silane molecules linked to a desired functional group (that will modify the surface properties of the substrate) through a hydrocarbon linker (Figure 6.1). Another advantage of using alkoxy silanes is the wide array of functional groups that can be incorporated into the molecule without affecting the overall stability of the silane.

Attachment of alkoxy silanes to oxide surfaces involves the formation of covalent bonds and occurs in two major steps. In the first step, the alkoxy groups are hydrolyzed to form silanols (Si-OH) and the corresponding alcohol of the alkoxy group. This requires the presence of trace amounts of water, which can come from the solution or adsorbed water on the surface. In the second step, the highly reactive silanols immediately form covalent bonds with hydroxyls on the surface by the elimination of a water molecule. The second step requires the presence of

hydroxyl groups on the substrate and therefore surface cleaning and preparation prior to coating is very critical.

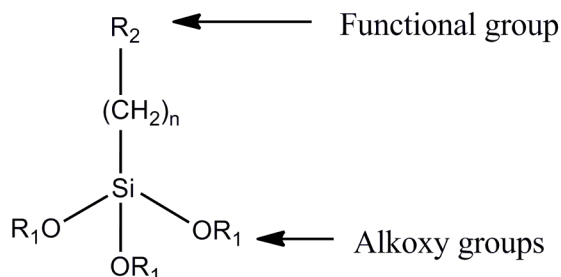


Figure 6.1. Chemical structure of a trialkoxy silane.

Similar to gold, ITO surfaces are easily contaminated during manufacture and handling, due to the adsorption of organic contaminants. Pretreatment of ITO surfaces involves a combination of wet chemical cleaning and oxygen plasma cleaning. Wet cleaning requires the use of a basic reagent, in combination with ultrasonication to remove any bulky contaminants. Acidic solutions will partially dissolve the ITO layer and damage the smoothness of the ITO film. In this work the wet cleaning was done in 20% (v/v) ethanolamine solution in deionized water (recommended by the supplier of the ITO slides, Delta Technologies, Ltd). The mixture is basic and mildly corrosive, but also acts as a degreaser. This cleaning method was compared to other wet cleaning methods reported in the literature. Contact angles measurements performed on slides cleaned with this method and other methods are shown in Table 6.1. The ethanol amine cleaning method provided the lowest contact angle value. A contaminant-free ITO surface should be very hydrophilic. Following oxygen plasma cleaning, the contact angle of deionized water decreased to less than 10° , indicating a very hydrophilic surface. Besides removing any residual organic contaminants, plasma cleaning also ensures the presence of hydroxyl groups on

the ITO surface.¹⁵⁴

Table 6.1. Contact angles of treated ITO substrates. All sonications are done for 15 min.

Surface treatment	Contact angle of deionized water
Untreated	89.5 ±3.1
Sonication in acetone	54.0 ±1.7
Sonication in EtOH/H ₂ O (50:50)	40.6 ±2.7
Sonication in 0.1 M NaOH	33.3 ±2.1
RCA*	47.0 ±1.5
Ethanolamine treatment	21.5 ±2.5

*RCA treatment involves mixing NH₄OH (30%) with H₂O₂ (35%) and heating the mixture to 60°C. Contact angle value is obtained from literature.¹⁶¹

Incubation in a toluene solution of a hydrophobic alkoxy silane, such as decyl trimethoxysilane (DTMS) or octadecyl trimethoxysilane (ODTMS), results in a drastic change of the contact angle value. This indicates that the alkoxy silane has deposited on the surface. In a timed study it was observed that the contact angle increased within 15 min of incubation in the DTMS solution and after 30 min the value was constant (Table 6.2). This shows that surface coating happens in a relatively short time. However, the surfaces are usually left overnight in the deposition solution to ensure full surface coverage and organization of the alkoxy silane SAM.

Formation of the alkoxy silane SAM on ITO was confirmed by cyclic voltammetry which is usually used to show the insulation properties of alkanethiol SAMs on gold slides (Figure 6.2).

Table 6.2. Contact angles of treated ITO substrates incubated at different times in a 1% (v/v) solution of decyl trimethoxy silane in anhydrous toluene containing 5 $\mu\text{L}/\text{mL}$ butylamine as catalyst.

Incubation time	Contact angle of deionized water (deg)
0 min	< 10
15 min	88.0 \pm 2.2
30 min	94.3 \pm 2.9
45 min	94.5 \pm 2.5
60 min	96.3 \pm 1.0

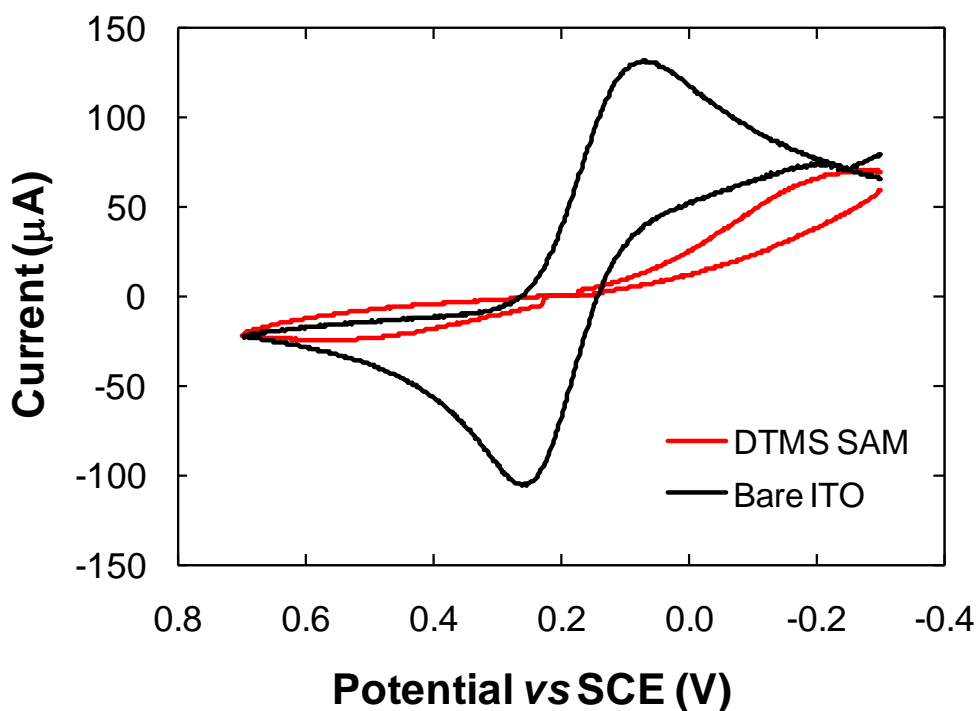


Figure 6.2. Cyclic voltammograms of bare and ITO coated with a decyltrimethoxy silane SAM. The measurement was conducted in a solution of 1 mM $\text{K}_3\text{Fe}(\text{CN})_6$ and 100 mM KCl in deionized water.

The bare ITO sample was conductive as shown by the redox peaks of the ferrocyanide ion, whereas the DTMS coated sample showed no redox peaks on the cyclic voltammogram. This has not been previously showed with a ten carbon alkyl chain SAMs on ITO. The grazing IR spectra also confirmed the presence of the alkyl chain of DTMS on the ITO surface, which are similar to those the DDT SAM on gold. The IR data seem to suggest that the methyl and methylene peaks of the alkyl chain of DTMS, unlike those of the DDT, are closer to the values observed for an alkane in liquid phase rather than in the crystalline phase. This is an agreement with the fact that the alkyl chains of silane SAMs tend to more randomly oriented than the alkyl chains of alkanethiol SAMs on gold surface.

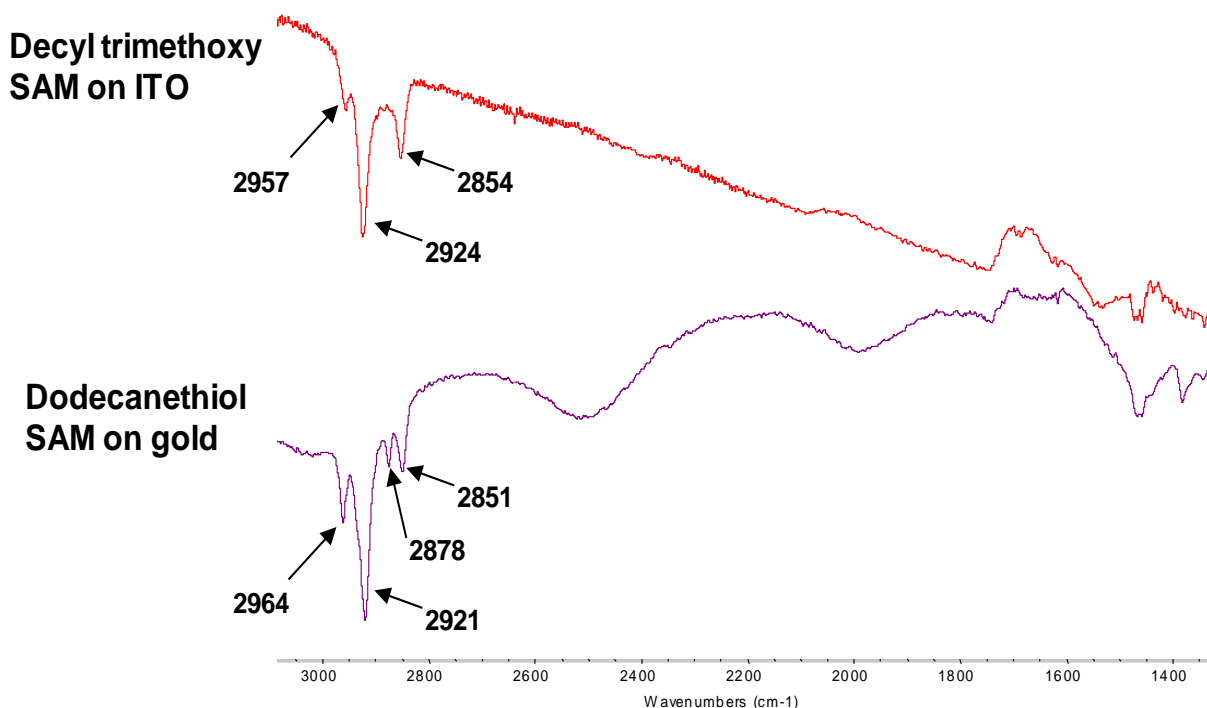
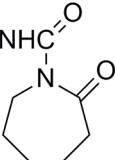


Figure 6.3. Grazing IR spectra of dodecethiol SAM on gold and decyl trimethoxysilane SAM on ITO. Both surfaces are highly hydrophobic with contact angle values larger than 90°. The spectra are in the same scale and appear to be identical. However, the peak values suggest that the SAM on gold is more organized than the one on ITO.

Table 6.3. Chemical structures of alkoxy silanes with simple functional groups.

Structure and name of alkoxy silane	Uses
$\begin{array}{c} \text{H}_3\text{CO} \\ \\ \text{H}_3\text{CO}-\text{Si}-(\text{CH}_2)_9\text{CH}_3 \\ \\ \text{H}_3\text{CO} \end{array}$ <p>Decyl trimethoxysilane (DTMS)</p>	<p>Provides hydrophobic surfaces. Alkyl chain length can vary. Octadecyl trimethoxysilane (ODTMS) was another hydrophobic silane used in this study.</p>
$\begin{array}{c} \text{H}_3\text{CO} \\ \\ \text{H}_3\text{CO}-\text{Si}-\text{CH}_2\text{CH}_2\text{CH}_2\text{NH}_2 \\ \\ \text{H}_3\text{CO} \end{array}$ <p>3-Aminopropyl trimethoxysilane (APTMS)</p>	<p>Used to form amino-terminated glass slides for the attachment of DNA, enzymes and antibodies <i>via</i> amide bond or glutaraldehyde coupling.</p>
$\begin{array}{c} \text{H}_3\text{CO} \\ \\ \text{H}_3\text{CO}-\text{Si}-\text{CH}_2\text{CH}_2\text{CH}_2\text{SH} \\ \\ \text{H}_3\text{CO} \end{array}$ <p>3-Mercaptopropyl trimethoxysilane (MPTMS)</p>	<p>Used for coating silica particles with metal scavenging properties. Used for the immobilization of enzymes <i>via</i> thiol reactive groups.</p>
$\begin{array}{c} \text{H}_3\text{CO} \\ \\ \text{H}_3\text{CO}-\text{Si}-\text{CHCH}_2\text{CH}_2-\text{N}^+\text{CH}_3 \\ \qquad \qquad \qquad \\ \text{H}_3\text{CO} \qquad \qquad \text{Cl}^- \text{CH}_3 \\ \qquad \qquad \qquad \\ \qquad \qquad \qquad \text{CH}_3 \end{array}$ <p>n-Trimethoxysilylpropyl-trimethylammonium chloride (TMA)</p>	<p>Used as anti-static coating. Provides ionic and hydrophilic surfaces.</p>
$\begin{array}{c} \text{H}_3\text{CH}_2\text{CO} \\ \\ \text{H}_3\text{CH}_2\text{CO}-\text{Si}-(\text{CH}_2)_3\text{NHCO}(\text{CH}_2\text{CH}_2\text{O})_{4-6}\text{H} \\ \\ \text{H}_3\text{CH}_2\text{CO} \end{array}$ <p>n-(Triethoxysilylpropyl)-o-polyethylene oxide urethane (PEG)</p>	<p>Provides PEG-terminated surfaces.</p>
$\begin{array}{c} \text{H}_3\text{CO} \\ \\ \text{H}_3\text{CO}-\text{Si}-\text{CH}_2\text{CH}_2(\text{CF}_2)_5\text{CF}_3 \\ \\ \text{H}_3\text{CO} \end{array}$ <p>1H, 1H, 2H, 2H-Perfluorooctyltriethoxysilane (PFTMS)</p>	<p>Provides fluorocarbon-terminated surfaces that have low surface energy.</p>

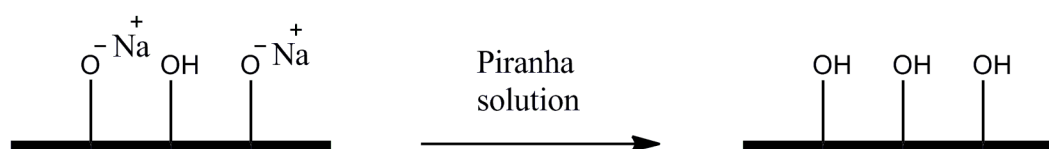
Table 6.4. Chemical structures of alkoxy silanes with complex functional groups.

Structure and name of alkoxy silane	Uses
$\begin{array}{c} \text{H}_3\text{CO} \\ \\ \text{H}_3\text{CO}-\text{Si}-(\text{CH}_2)_3\text{NH}(\text{CH}_2)_2\text{NH}(\text{CH}_2)_2\text{NH}_2 \\ \\ \text{H}_3\text{CO} \end{array}$ <p>(3-Trimethoxysilylpropyl) diethylenetriamine (DETA)</p>	<p>Used as coating for <i>in vitro</i> culturing of neuronal cell lines and primary neurons on glass surfaces. Present a surface similar to polylysine coatings.</p>
$\begin{array}{c} \text{H}_3\text{CO} \\ \\ \text{H}_3\text{CO}-\text{Si}-(\text{CH}_2)_{11}\text{NHCH}_2\text{CH}_2\text{NH}_2 \\ \\ \text{H}_3\text{CO} \end{array}$ <p>n-(2-Aminoethyl)-11-aminoundecyltrimethoxysilane (AUTMS)</p>	<p>Used in this work to coat surfaces for culturing and differentiating neuronal cell lines.</p>
$\begin{array}{c} \text{H}_3\text{CO} \\ \\ \text{H}_3\text{CO}-\text{Si}-\text{CH}_2\text{CH}_2\text{CH}_2\text{SCH}_2\text{CH}_2-\text{C}_5\text{H}_4\text{N} \\ \\ \text{H}_3\text{CO} \end{array}$ <p>2-(4-Pyridylethyl)thiopropyltrimethoxysilane (PYR)</p>	<p>Used as coating on glass surfaces for culturing neuronal cell lines and primary neurons. Also used as metal ion chelator.</p>
$\begin{array}{c} \text{H}_3\text{CO} \\ \\ \text{H}_3\text{CO}-\text{Si}-\text{CH}_2\text{CH}_2\text{CH}_2\text{NHC}(\text{O}) \\ \\ \text{H}_3\text{CO} \end{array}$  <p>n-[5-(Trimethoxysilyl)-2-aza-1-oxopentyl]caprolactam (LACTAM)</p>	<p>Used as a coating for culturing of primary neurons.</p>
$\begin{array}{c} \text{H}_3\text{CH}_2\text{CO} \\ \\ \text{H}_3\text{CH}_2\text{CO}-\text{Si}-(\text{CH}_2)_3\text{NH}-\text{C}(\text{O}) \\ \\ \text{H}_3\text{CH}_2\text{CO} \end{array}$ $\begin{array}{c} \text{H}-\text{C}-\text{OH} \\ \\ \text{HO}-\text{C}-\text{H} \\ \\ \text{H}-\text{C}-\text{OH} \\ \\ \text{H}-\text{C}-\text{OH} \\ \\ \text{CH}_2\text{OH} \end{array}$ <p>n-(3-Triethoxysilylpropyl)gluconamide (GLU)</p>	<p>Provides uncharged hydrophilic surfaces.</p>

6.3.3. Glass

Alkoxysilanes are commonly used to form monolayers on silica substrates, such as glass.

Surface cleaning and pretreatment prior to coating is also critical for glass. Besides organic contaminants, the glass surface contains alkali metal impurities, which occupy the hydroxyl binding sites. Cleaning glass surfaces involves immersion into piranha solution for at least one hour followed by thorough rinsing with deionized water. The piranha solution removes all organic contaminants and also allows for replacement of alkaline metal ions with hydrogen ions due to its acidity (Scheme 6.1).



Scheme 6.1. Modification of glass surface by piranha cleaning.

Deposition of different alkoxysilanes, listed in Tables 6.2 and 6.3 was characterized by contact angle (Table 6.5).

6.3.4. Stainless steel

Alkoxy silanes used in conjunction with the siloxylated StSt surfaces were the following:

ODTMS, APTMS, MPTMS, PFTMS, TMA, PEG and GLU. Non-siloylated surfaces were first tested for contact angles and compared to stainless steel. The freshly cleaned and passivated stainless steel surface was extremely hydrophilic ($<15^\circ$). The bare stainless steel samples soaked in ODTMS produced a relatively hydrophobic surface (contact angles 69.3 ± 6.0 degrees). This is in contrast to ODT SAMs on gold which produced contact angles of $112 \pm 1.0^\circ$. This clearly

Table 6.5. Contact angles of ITO and glass substrates coated with a number of alkoxy silanes. Deposition was done times in a 1% (v/v) solution of decyl trimethoxy silane in anhydrous toluene containing 5 $\mu\text{L}/\text{mL}$ butylamine as catalyst.

Incubation time	ITO	Glass
Bare Surface	< 10	< 10
DTMS	94.3 \pm 1.4	100.8 \pm 1.2
ODTMS	97.7 \pm 1.0	101.6 \pm 1.5
APTMS	24.9 \pm 3.7	31.3 \pm 3.7
AUTMS	72.4 \pm 1.7	68.3 \pm 2.3
MPTMS	72.4 \pm 1.6	61.7 \pm 2.4
PFTMS	116.9 \pm 1.5	104.4 \pm 1.1
DETA	28.1 \pm 2.4	21.7 \pm 2.9
TMA	34.2 \pm 3.1	16.3 \pm 1.0
PEG	43.2 \pm 0.8	32.9 \pm 2.3
PYR	55.5 \pm 1.6	50.1 \pm 1.8
GLU	41.5 \pm 2.6	30.2 \pm 2.0
LACTAM	71.8 \pm 4.3	78.8 \pm 1.5

indicates that the ODTMS did not react with the stainless steel surface and that the differences in contact angles are due to ‘dirtying’ of the substrates.

In order to form stable siloxane bonds the steel samples were dipped in neat tetramethoxy silane to coat the surface with a thin siloxane film. Following oxygen plasma treatment and incubation in ODTMS solution, the surface of steel became hydrophobic ($> 90^\circ$) and the value did not decrease after sonication in toluene. This leads us to conclude that the hydrophobicity observed here is due to the physisorption of ODTMS on the surface and not due to the formation

of a true self assembled monolayer. The results observed so far indicate that the oxide layer in stainless steel is not sufficiently active to form a sulfate/sulfite bond (with ODT) or possess sufficient density of OH groups to form a SAM with ODTMS.

6.3.5. Polymer substrates

Control over physical properties of polymers, such as biocompatibility, can be achieved through surface modification. Our strategy for modifying polymers surfaces is based on oxygen plasma treatment in order to generate hydroxyl groups on the surface. The polymer surfaces are then exposed to 3-aminopropyl trimethoxysilane (APTMS) to generate an amine terminated layer, which makes the surface hydrophilic and provides functionality for covalent attachment reactions to the surface as shown with gold and glass. The contact angles demonstrate the modification of the polymer surface (Table 6.6).

Table 6.6. Contact angles of PDMS, polyurethane and polystyrene coated with APTMS. Deposition was done times in a 1% (v/v) solution of decyl trimethoxy silane in anhydrous toluene containing 5 μ L/mL butylamine as catalyst.

Incubation time	PDMS	Polyurethane	Polystyrene
Untreated surface	106	94	97
After plasma cleaning	<10	<10	<10
APTMS coating	33	38	17

6.3.6. PTFE (Teflon)

The PTFE samples were immersed in acetone and sonicated for 30 min. After measuring contact

angles with deionized water, the cleaned samples were placed in a mixture of toluene and elemental sodium and the mixture was refluxed overnight. The samples were then rinsed with acetone, blow dried, and kept in a piranha solution at 90°C for 8 hours. Next they were thoroughly rinsed with water, blow dried and further treated in oxygen plasma for 2 minutes. The samples were incubated overnight in a 3% 3-aminopropyltrimethoxysilane ethanol solution, which was the last step of the treatment and coats the PTFE surface with amino groups. Contact angles were measured (Table 6.7). Next the slides underwent a simple surface reaction which converts amino groups to carboxyl groups, and should further decrease the contact angle or

Table 6.7. Contact angles of PTFE surfaces before and after surface modification.

Surface	Static	Advancing	Receding
Untreated PTFE	116.5	134.8	110.3
Amino-terminated PTFE	57.2	67.2	33.4
COOH-terminated PTFE	50.0	53.4	19.8

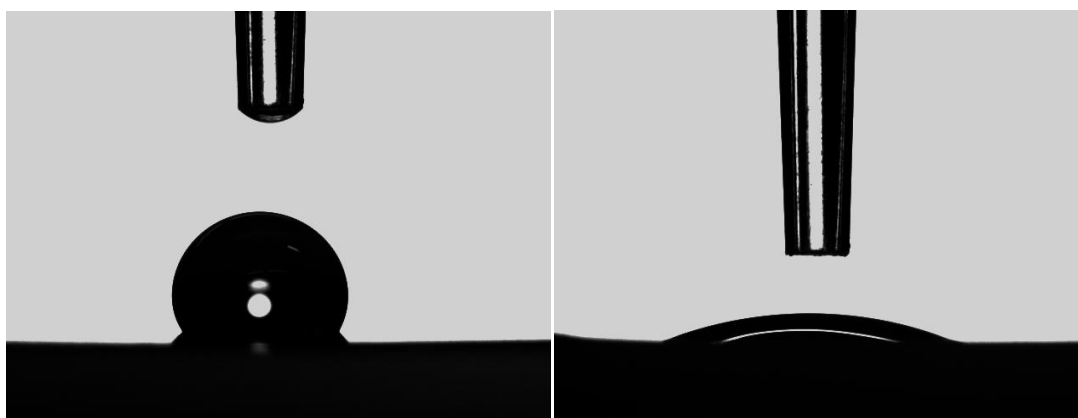


Figure 6.4. Receding contact angle of PTFE; before (left) and after (right) surface modification.

wettability of the surface. The most drastic changes in contact angle values were observed for the receding ones (Figure 6.4), due to the surface roughness of the PTFE sheet, which is visible with a naked eye.

6.4. Result and Discussion Part II: Differentiation of Neuronal Cells on Modified Surfaces

6.4.1 Microcontact printing

Microcontact printing is a soft lithography technique that allows a microstructure fabricated on an elastomer, such as PDMS, to transfer material to a flat surface.⁹⁷ With regard to SAM formation on gold for example the PDMS stamp is inked in an alkanethiol solution in ethanol, and after drying it is placed on a clean gold slide to print the pattern fabricated on the stamp. The unprinted area can be backfilled with an alkanethiol containing a different terminal group. In order to confirm our capability to perform microcontact printing, 40 μm squares of 11-mercaptoundecanoic acid were printed on a gold slide and backfilled with 11-mercapto undecanol. Then the COOH groups were activated with EDC/NHS and a fluorescent antibody was attached to visualize the pattern (Figure 6.5). The presence of the pattern can be visualized by other means, such as directed cell adhesion and growth, which is of more interest in cell biology and tissue regeneration. By being able to attach cells in a pattern, cells can be arranged in a predetermined formation leading to the generation of more complex cell structures similar to those in living tissues. For this to happen cell attachment and growth experiments were conducted using various coatings on glass to find coating that prevented or favored cell attachment, growth and differentiation.

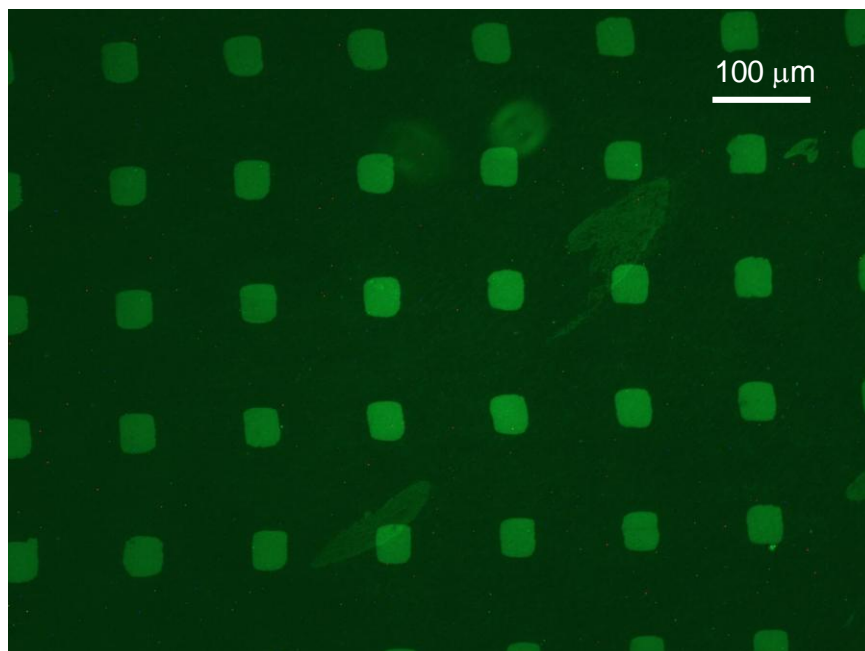


Figure 6.5. Microcontact printed pattern of a COOH-terminated alkanethiol on gold visualized with a fluorescent antibody. The antibody was attached *via* EDC/NHS activation method. After the covalent attachment of an Alexa Fluor 488 antibody (Invitrogen) a green fluorescent image of the pattern was taken.

Microcontact printing was also used to print an entire SAM using a flat piece of PDMS (Figure 6.5), demonstrating that both methods are valid in forming SAMs.

6.4.3 Differentiation of Neuroscreen-1 on a surface pattern

Neuroscreen-1 (a subclone of PC-12 cells) cells were cultured in RPMI medium supplemented with 10% horse serum (HS) and 5% fetal bovine serum (FBS) in an incubator at 37 °C and 5% CO₂. The cell were seeded on the surface at a concentration of 10,000 cells /mL and allowed to attach and grow in RPMI with 10% HS and 5% FBS over 2 – 3 days. The cells were differentiated by replacing the growth medium with RPMI + 10% HS and 5% FBS containing 100 ng/mL nerve growth factor (NGF). The differentiating medium was changed every 2 days.

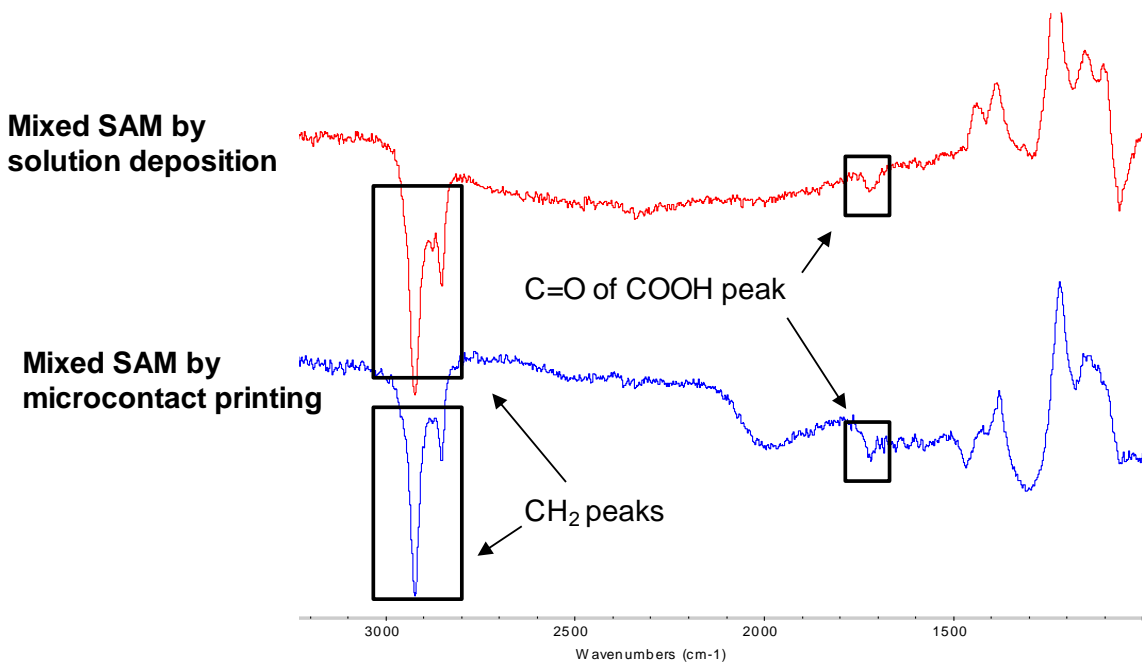


Figure 6.6. Grazing IR spectra of mixed SAMs of MUA and MUO at a 1 to 10 molar ratio in solution, prepared by solution deposition and microcontact printing. The spectra are identical.

Cells grew neurites within 48 hours and the images shown here were taken after 5 days. The cells were seeded on glass slides coated with the silanes shown in Tables 6.2 and 6.3. The AUTMS SAM provided the best surface for growing and differentiating Neuroscreen-1 cells. The coating provided similar results to collagen coatings, and the results were also reproducible on polystyrene (Figure 6.7). The collagen coating mimics ECM and this has been shown experimentally by trying various extra-cellular protein coatings on surfaces such as glass or polystyrene.¹⁶² Surface patterns were initially generated on gold slides, by using an amino-terminated alkanethiol SAM to adhere cells and a hydrophobic alkanethiol SAM to backfill the pattern (Figure 6.8). The experiment was initially performed on gold slides since contact printing is readily done on gold surfaces.⁹⁷ However, generation of patterns on glass surfaces is of more interest. AUTMS was used to generate patterns on glass and as expected cell grew only on the AUTMS coated pattern (Figure 6.9).

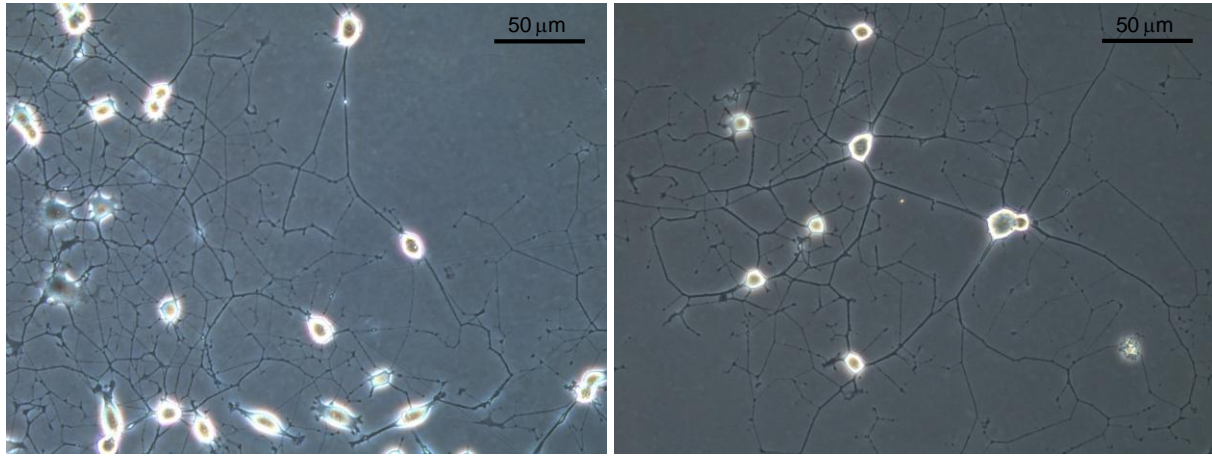


Figure 6.7. AUTMS coating (right) mimics collagen coating (left), which is typically used as substrate for growing and differentiating neuronal cell lines.

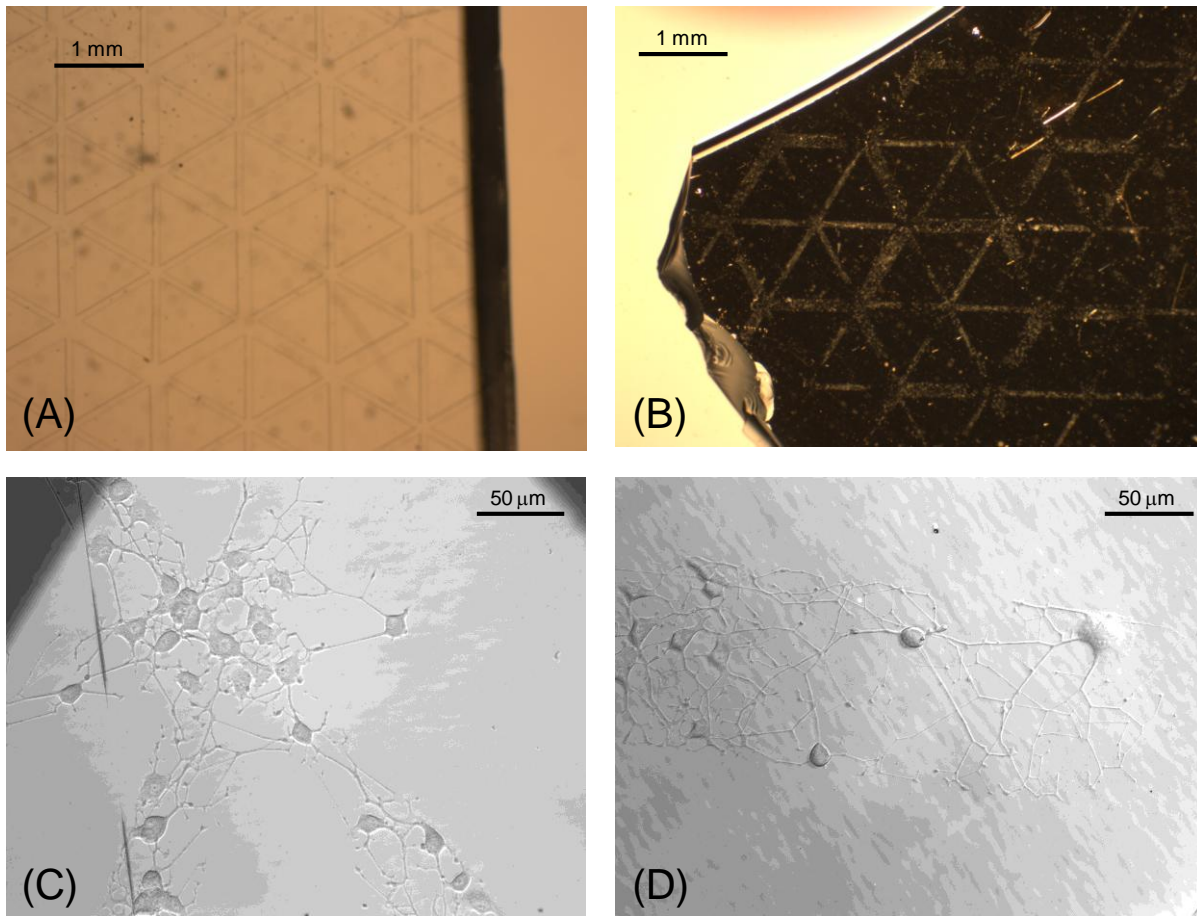


Figure 6.8. Neuroscreen-1 cells differentiated on an amino-terminated surface pattern on gold. (A) The PDMS stamp used to generate the pattern. (B, C & D) Optical images of the patterned cells on the gold slides.

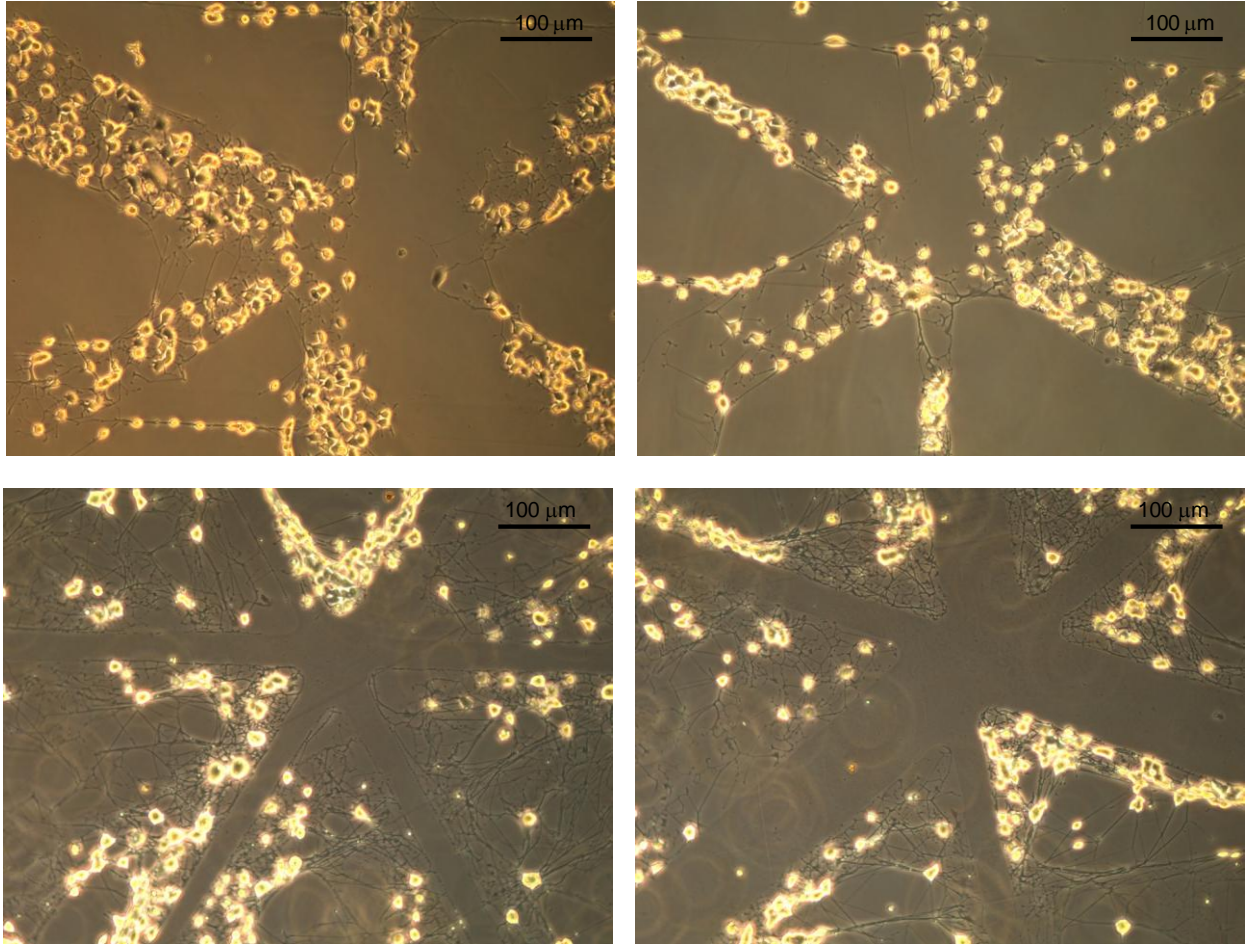


Figure 6.9. Neuroscreen-1 cells differentiated on AUTMS surface pattern on glass. The AUTMS pattern was either directly printed on the glass (top), or used as backfill after contact printing a hydrophobic alkoxy silane (DTMS) (bottom).

6.5. Result and Discussion Part III: Trapping Cells in Suspension with Magnetic Agarose Beads

6.5.1. Preparation of the magnetic agarose beads

The beads were prepared by emulsification of water in oil by using a surfactant to stabilize the emulsion. By dissolving agarose in water and keeping the emulsion mixture at high temperature (90 °C), the agarose solution was emulsified by stirring the mixture. Cooling of the emulsion

resulted in gelling of the agarose which obtained taking the spherical shape of the water emulsion. The agarose beads were formed with magnetic particles (Fe_3O_4) embedded in the gel (Figure 6.10). The size of the beads ranged from 30 – 445 μm , they were divided by decanting into two groups; small beads (30 – 150 μm) and large beads (150 – 445 μm). For most experiments the small beads were used. The beads were stored in 4 °C and they were stable for long time periods (at least one year).

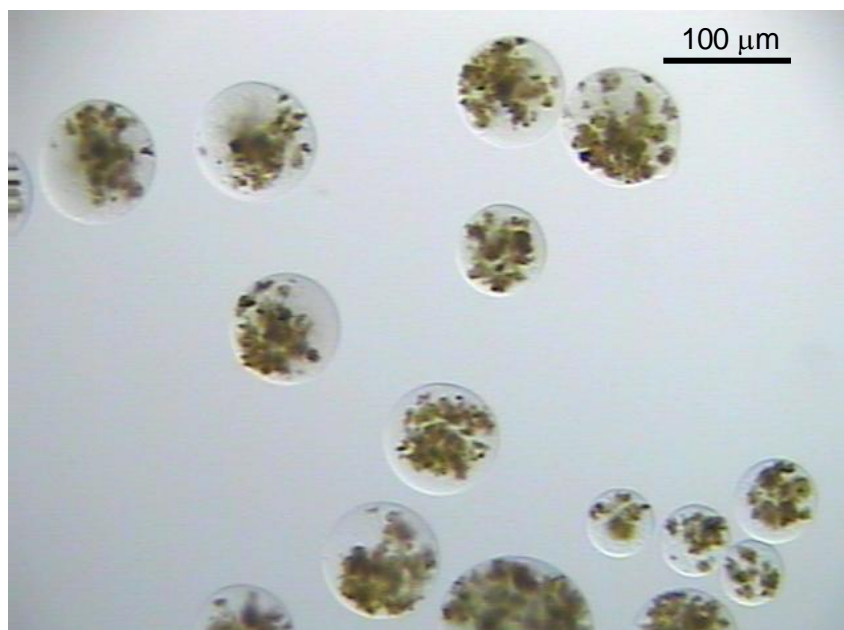
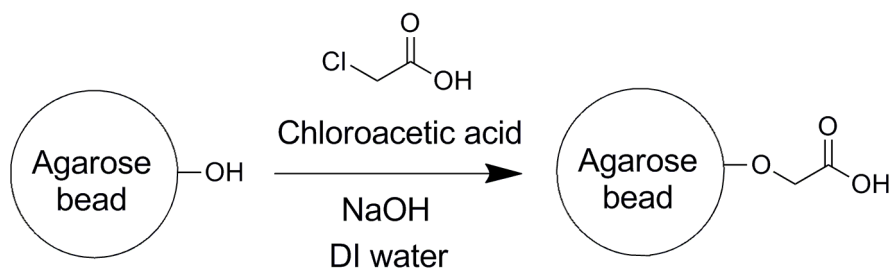


Figure 6.10. Phase contrast image of the magnetic agarose beads. The agarose gel appears clear while the magnetic particles have an orange-brown color. In large volumes the concentrated bead suspension has a reddish brown color.

6.5.2. Surface modification of agarose beads

Agarose is mainly composed of polysaccharides and therefore the surface is covered with hydroxyl groups. Activation of hydroxyl groups for protein attachment would require the use of organic chemicals that could damage the beads and be toxic to the cells, so the hydroxyls were

modified to COOH groups with a simple reaction that occurs in aqueous solutions. When hydroxyls are exposed to chloroacetic acid in the presence of a base catalyst, the oxygen of the hydroxyl binds to the α -carbon by replacing the chlorine atom (Scheme 6.2). Activation of the COOH groups for protein attachment can then be done in aqueous solutions *via* EDC/NHS without affecting the beads or the cells to trace amounts of organic solvents.



Scheme 6.2. Modification of hydroxyls to carboxyl groups on agarose beads.

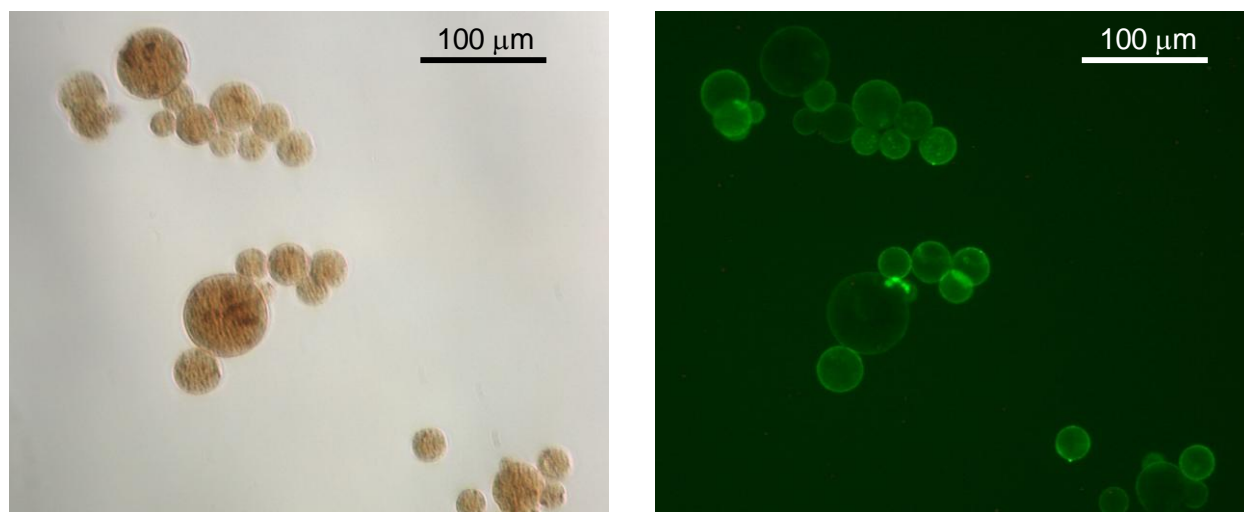


Figure 6.11. Agarose beads coated with a fluorescent antibody. The antibody was attached *via* EDC/NHS activation method. After the covalent attachment of an Alexa Fluor 488 antibody (Invitrogen) a phase contrast image (left) and green fluorescent image (right) of the magnetic agarose beads was taken. The higher intensity fluorescence at the rim of the beads indicates that the antibody has attached on the surface of the beads. The fluorescent image was obtained by using the FITC filter cube.

In order to confirm the attachment of an antibody to the beads, mouse derived antibodies (CD3 antibody) were attached to the magnetic agarose beads *via* the EDC/NHS activation method and then were incubated in the presence of a goat derived anti-mouse fluorescent antibody. After imaging in a fluorescent microscope the presence of the antibody was observed (Figure 6.11). The control with uncoated beads provided no fluorescence.

6.5.3. Using antibodies for cell immobilization

In order to confirm the ability of antibodies to immobilize cells, antibodies were attached to flat gold or indium tin oxide (ITO) surfaces. The cells used for this study, Jurkat cells, are derived from lymphoma (cancerous white blood cells). These cells do not adhere to surfaces and grow in suspension and therefore, if they attach to surfaces it would be due to the presence of a specific antibody on the surface. Since Jurkat cells are known to express the CD3 antigen on their membrane, the CD3 antibody was used to immobilize the cells. ITO slides were coated with CD3 IgG_{2a} antibody or non-specific IgG_{2a} antibody as a control (Figure 6.12). Cells were exposed to the surfaces overnight in the 37 °C incubator and then rinsed with growth medium. Only the CD3 antibody coated ITO surfaces had a significant number of cells attached to the surface. This showed the ability of the covalently attached antibody to immobilize cells.

Jurkat cells were also immobilized on gold slides (Figure 6.13). Gold surfaces allow for the formation of homogeneous mixed monolayers (with no island formations), as long as the alkyl chain of the alkanethiols is similar. The alkanethiols used were 11-mercapto undecanoic acid (MUA) and 11-mercapto undecanol (MUO), which terminate with a COOH or OH group, respectively. This would provide a model of the surface of agarose beads which is terminated

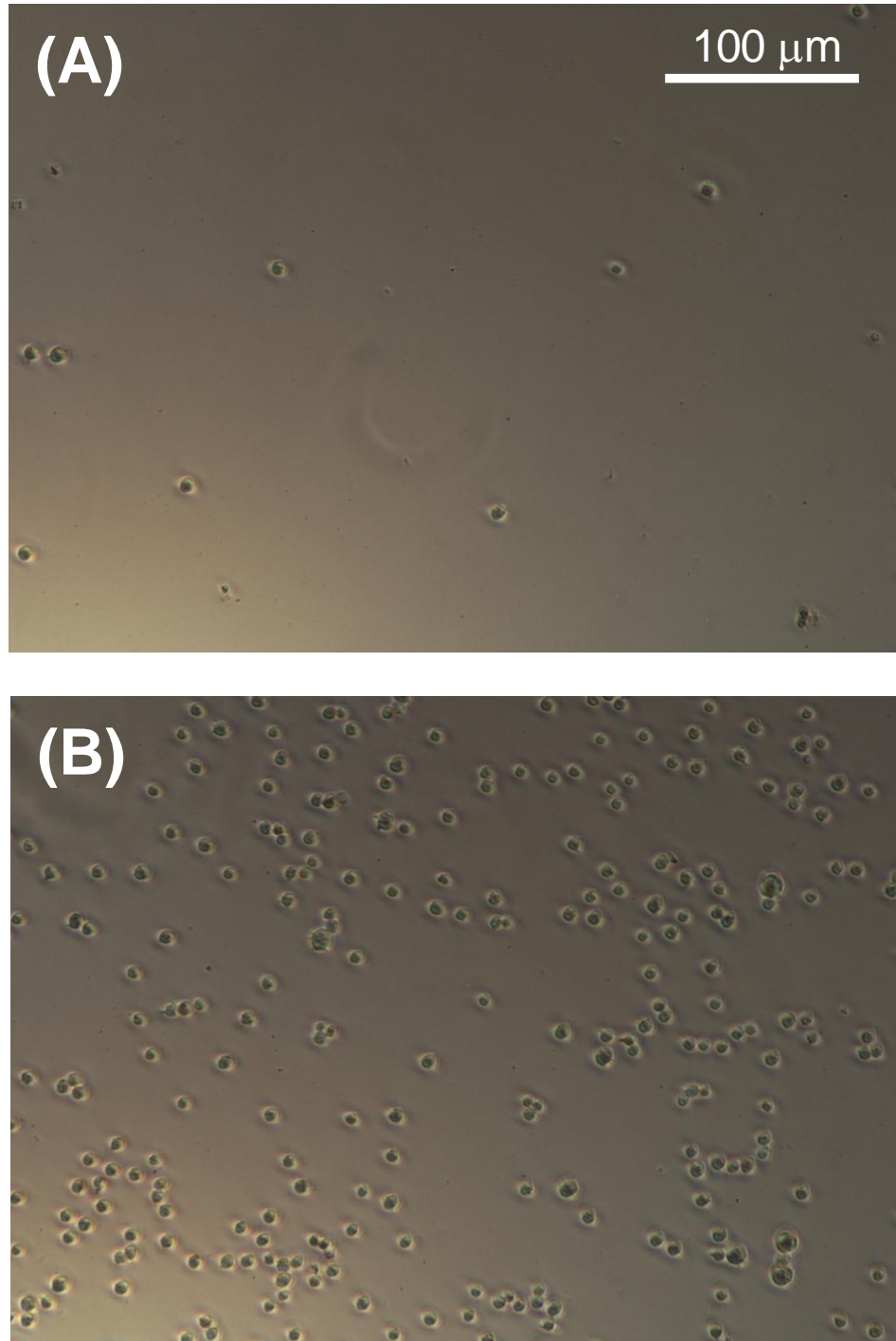


Figure 6.12. Immobilized Jurkat cells on ITO slides. ITO slides were derivatized with amino groups using 3-aminopropyl trimethoxysilane. After modification of amino groups to COOH with succinic anhydride, the surfaces were activated with EDC/NHS and coated with (A) non-specific antibody (mouse IgG_{2a}) and (B) mouse monoclonal antibody to human CD3. The surfaces were exposed overnight to a 1×10^5 cells/mL suspension of Jurkat cells at 37 °C, were carefully rinsed with growth medium and phase contrast images were obtained.

with OH and COOH groups. Mixed monolayers on gold surfaces are known to approximately follow their ratios in solution. SAMs were prepared in 100% MUA or MUO and MUA:MUO mixtures of 1:10 and 1:100. The surfaces prepared were activated with EDC/NHS and then

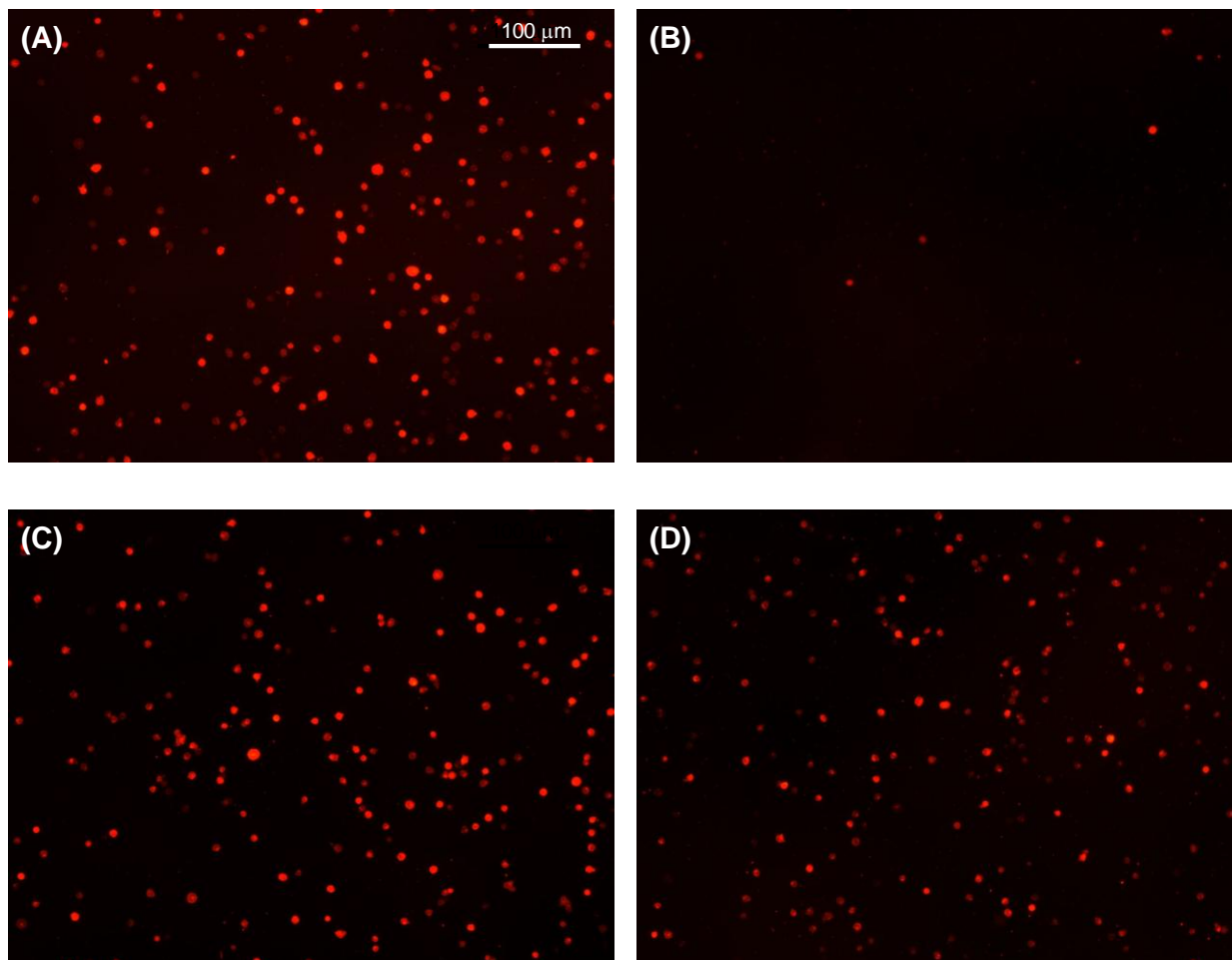


Figure 6.13. Immobilization of Jurkat cells on gold slides. Gold slides were derivatized with 11-mercapto undecanoic acid (MUA) and 11-mercapto-1-undecanol (MUO) at different ratios: (A) 100% MUA; (B) 100% MUO; (C) 1:10 MUA:MUO; (D) 1:100 MUA:MUO. The surfaces were then coated with CD3 antibody and exposed overnight to a 1×10^5 cells/mL suspension of Jurkat cells in the 37 °C incubator. After gently rinsing with growth medium the surfaces were stained for 15 min at 37 °C in serum-free growth medium containing 5 μ L/mL of DIO cell membrane fluorescent dye (Invitrogen). The surfaces were gently rinsed with growth medium and fluorescent images were obtained on a fluorescent microscope using the Texas Red filter cube.

coated with anti-CD3 antibody. The MUO SAM had very few attached cells, whereas all the other surfaces had immobilized cells on them. In addition there appeared to be no difference between the SAMs with different ratios of COOH groups. This means that only a small percentage (at least 1%) of hydroxyls on the surface of the agarose beads need to be modified to carboxyl groups in order to obtain immobilization of the Jurkat cells.

6.5.4 Attaching cells to agarose beads

Agarose beads that had been treated with chloroacetic acid were coated with CD3 antibodies and then were incubated overnight with Jurkat cells in the 37 °C incubator. The next day it was observed that most of the beads had cells attached to them, sometimes forming a corona of cells around the beads (Figure 6.14). The ability of the beads to immobilize or trap the cells over a long time period was determined. At the same time the different types of modifications, such as treatment with chloroacetic acid for adding COOH groups or insertion of a PEG (40-mer) spacer

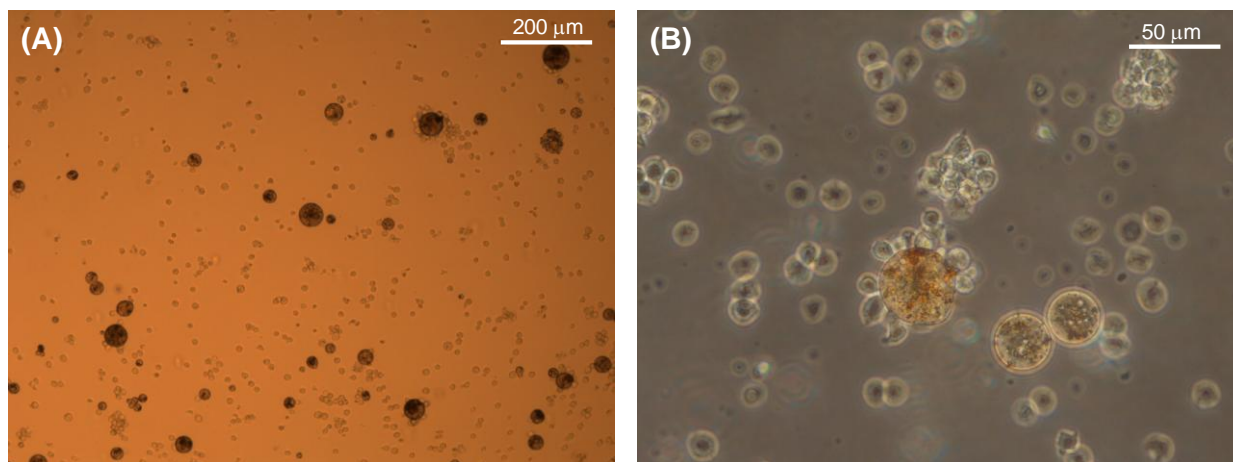


Figure 6.14. Phase contrast images at (A) 100X and (B) 400X magnification, showing the immobilization of Jurkat cells on magnetic agarose beads. The agarose beads were first treated with chloroacetic acid and then coated with CD3 antibody and exposed overnight to a 1×10^5 cells/mL suspension of Jurkat cells in growth medium in the 37 °C incubator. The images were obtained after 24 hours incubation.

to decrease non-specific binding and increase the flexibility of the antibodies were compared to each other. Four modifications and two different controls were studied:

- A – Beads modified with COOH groups, no PEG spacer, coated with CD3 antibody;
- B – Beads modified with COOH groups, with a PEG spacer, coated with CD3 antibody;
- C – Beads coated with CD3 antibody;
- D – Beads with a PEG spacer, coated with CD3 antibody;
- E – Beads, coated with non-specific antibody (control 1);
- F – Beads, with no antibody coating (control 2).

Each type of bead was incubated with Jurkat cells in cell culture flasks in the 37 °C incubator.

Type A beads seemed to have the most attachments of the beads with antibodies, of about 4 cells/bead in about 50% of beads in the flask after 6 days. This result was confirmed by two other repeats of this experiment. This appeared to indicate that modification of hydroxyl groups to COOH groups increases the number of attached antibodies and thus the number of immobilized cells (Table 6.8).

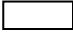
Two other stability experiments were conducted. In one experiment the stability of antibodies in 37 °C (old antibodies) was tested by pre-incubating the antibodies in PBS at 37 °C prior to attaching them to the beads. After this the attachments of beads with old antibodies to cell were compared to the attachments of beads with regular antibodies to cells. The number of attached cells per bead in the set of beads with old antibodies is very much the same as that of the ones with regular antibodies, but the percentage of beads coated with old antibodies with cell

Table 6.8. Jurkat cell immobilized on magnetic agarose beads in cell culture flasks over a 25-day period. After taking 15 random pictures (each containing 20 – 40 beads per field view) at different time points the percentage of beads with cells and average number of beads per cell was determined.

Coating	Days							
	1	4	6	7	12	14	21	24
A	54	61	86	91	84	71	77	-
	1.9	2.5	3.7	4.4	3.5	3.0	3.2	-
C	46	54	73	96	21	23	-	13
	2.4	2.3	2.6	3.0	1.7	1.8	-	1.5
E	19	34	76	93	18	14	43	12
	1.6	2.1	2.7	3.2	1.3	1.5	1.9	1.3
F	1	2	-	-	-	9	-	-
	1.4	1.3	-	-	-	1.12	-	-

Coating	Days						
	3	5	6	11	12	20	25
B	39	71	83	81	74	23	47
	1.5	2.5	3.0	3.3	2.5	2.1	1.6
D	32	46	84	21	28	4.5	25
	3.4	1.5	2.7	1.9	1.6	1.9	1.0

 % Beads with attachments

 Average number of cells attached per bead

attachments was significantly smaller than that of beads with fresh antibodies. In order to test the possibility that the pH 9.6 buffer could be denaturing the antibodies a stability experiment was carried out with beads that had been coated with antibody in pH 9.6 or 7.4 (PBS). After one experiment of using PBS instead of the pH 9.6 buffer, when the attachments were compared the beads with anti CD3 antibodies attached in PBS solution had a much smaller percentage of beads with cell attachment but a similar average number of cells attached to beads in that of the beads

with anti CD3 antibodies attached in the pH 9.6 buffer. The beads with control antibodies attached in PBS had almost no attachments of cells, which indicates that attachment of antibodies in pH 7.4 is not efficient, and most likely pH 9.6 does not denature the antibodies.

6.5.5. *Trapping cells in a magnetic flow-through bioreactor*

A continuous flow bioreactor was constructed to culture Jurkat cells in a chamber using an external magnetic field. The flow-through bioreactor contains the following components: the magnetic bioreactor system (Figure 6.15), the medium reservoir, the peristaltic pump, and the silicone conduit. The flow-through system was sterilized by flushing with 70% ethanol in water solution and then with D-PBS solution, prior to adding the growth medium (RPMI with 10% fetal bovine serum and 1 % penicillin/streptomycin). The growth medium was kept in a 250 ml

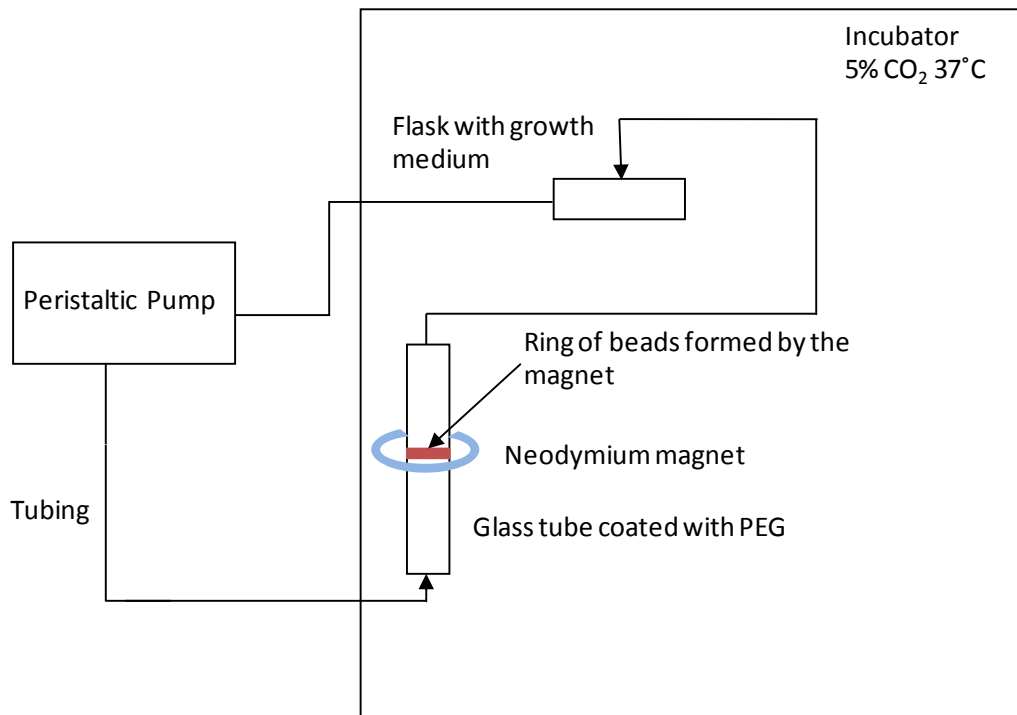


Figure 6.15. Schematic diagram of the flow-through bioreactor system.

plastic flask connected to silicon tubing with a 16G needle stuck into it and sealed on both ends. The growth medium was pumped through the system using a MasterFlex peristaltic pump (model 7518-00, Cole Palmer Instruments). The bioreactor chamber consisted of a sterilized glass tube (19 cm length and 8 mm diameter) coated with PEG.

The glass tube was connected with the silicone tubing on either side with a three-way valve linked to a 16G needle stuck through the rubber septum. In the middle of the glass tube, a circular neodymium magnet was attached with tape to keep it in place and attract and trap the magnetic beads, which form a ring around the inside of the glass tube (Figure 6.16). The cells

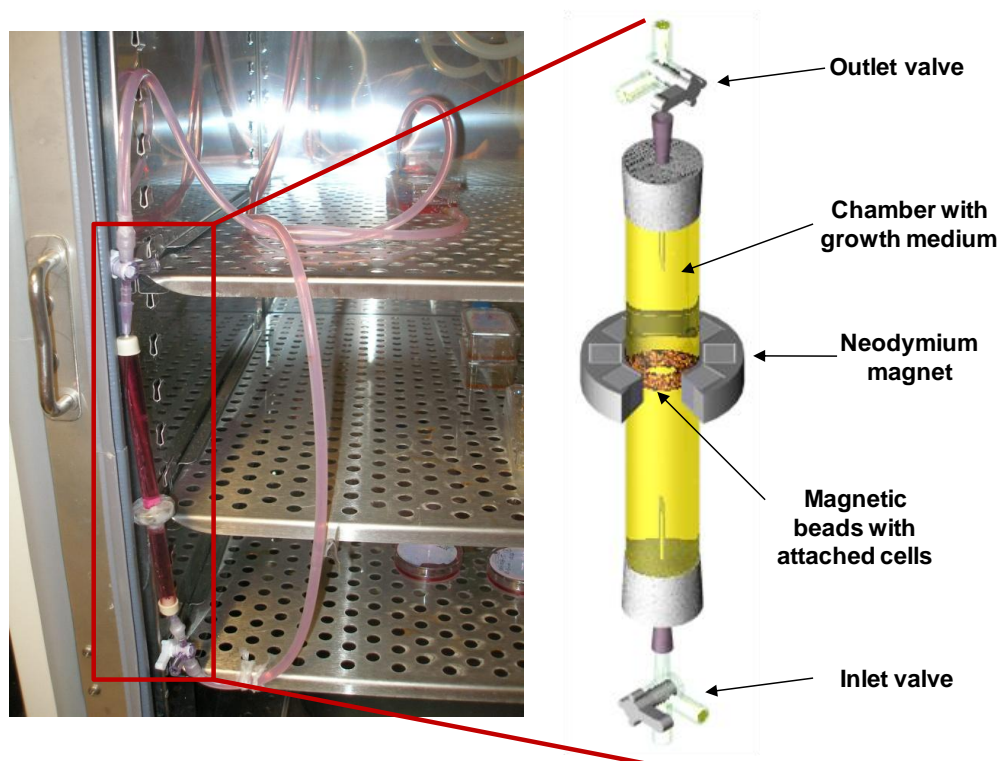


Figure 6.16. Continuous flow-through magnetic bioreactor system assembled in the incubator (left) and detailed drawing of continuous flow-through magnetic bioreactor chamber (right).

were seeded on the chemically modified magnetic agarose beads and the beads were trapped in a ring formed next to the magnetic field while the nutrient required for the cells was continuously provided by the flow of medium facilitated by peristaltic pump. The bioreactor and the reservoir were placed in a humidified 37°C with 5% CO₂ incubator and the pump was placed outside of the incubator. Besides serving as a source of growth medium the reservoir or 250 mL flask also allowed for gas exchange of the growth medium after it had passed through the bioreactor chamber.

The type A beads (modified with COOH groups and antibodies) were used for the flow-through bioreactor. During preliminary studies, the PEG coating on the inside of the glass chamber

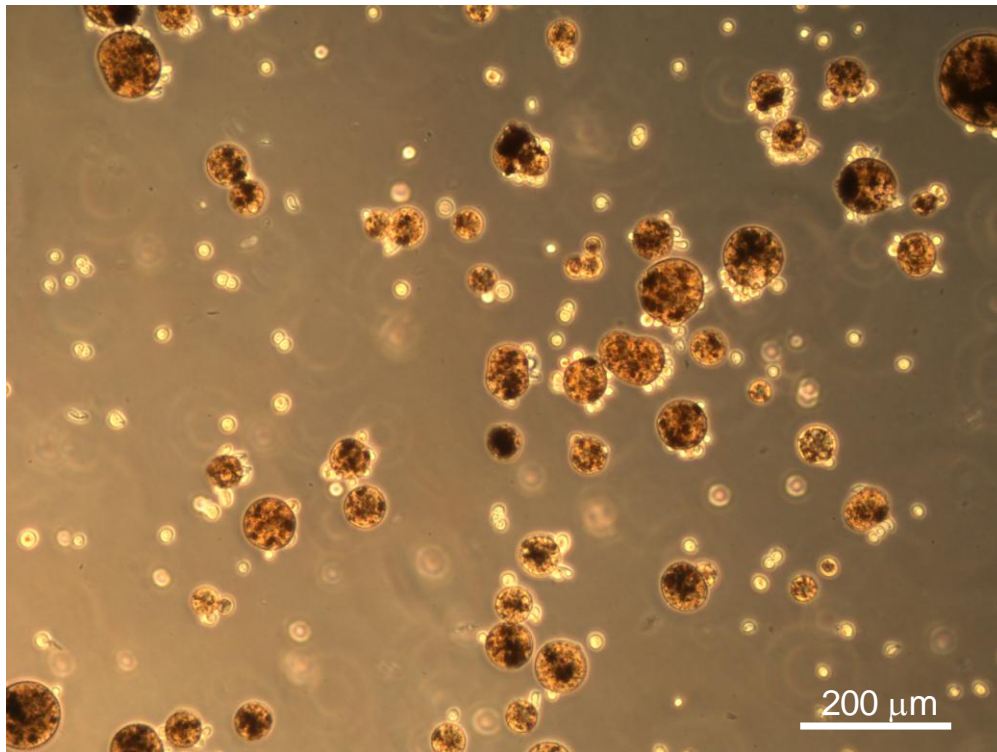


Figure 6.17. Phase contrast images showing the immobilization of Jurkat cells on magnetic agarose beads after 6 days incubation in the flow-through bioreactor. The agarose beads were treated with chloroacetic acid and then coated with CD3 antibody.

provided the best surface, showing no attachment of either cells or beads. The other coatings tried were hydrophobic and fluorocarbon. In both cases irreversible bead attachment was observed after forming the ring of beads with the circular neodymium magnet. Before the beads were put into the flow chamber (using a sterile syringe with a 16G needle) they were kept in flasks for a few days until some attachments were visible. The Jurkat cells/magnetic beads suspension was then transferred to the bioreactor chamber. Samples were taken from the bioreactor at different days using a sterile needle and plastic syringe. Cells stayed attached to the beads in consistent numbers for at least 6 days (Figure 6.17 and Table 6.9).

Table 6.9. Jurkat cells in the flow-through bioreactor. The ratio of beads with attached cells and average number of cells per bead was determined after taking at least 15 random images for each time point.

day	% beads with cells	Average number of beads per cell
1	47.9	2.2
4	70.4	3.3
6	65.4	3.3
8	21.4	1.9

6.5.6. *Growing tissue in suspension on a magnetically stabilized support*

Mouse fibroblasts produce extra-cellular matrix when induced with fibroblast growth factor (FGF). These cells readily adhere to surfaces and when growing on the surfaces they also flatten on them, which very likely it is not the way they look in the live tissue. The reason they were

chosen was their ability to grow extra-cellular matrix (ECM). If these cells adhered to a magnetized support and proliferated then this would result in ECM formation in the shape of the support. Cells were first allowed to proliferate in the culture flasks. The cells were then detached and suspended in growth medium solution containing magnetic beads coated with collagen.

The collagen coating mimics ECM and in addition would favor cell attachment as agarose itself and the shape of the beads would prevent the attachment and proliferation of the fibroblasts on the spherical beads. Allowing the suspension to incubate overnight in a flask as it was done for the Jurkat cells, resulted in all the cells had adhering to the bottom of the flask and no cells were observed on the beads. A new bead/cell suspension was immediately transferred into a 10 mm diameter glass test tube which had been coated with poly(ethylene glycol) (PEG) to prevent non-specific adhesion of proteins and fibroblasts. A magnet was placed around the tube in the middle to create a ring of magnetic beads and to trap the cells in suspension (Figure 6.18). Thus the only substrate that the cells would be like to adhere to was the ring of beads, and once the cells attached to the beads they would form a ring as well while producing extra-cellular matrix.

The tubes with the magnet were kept in the 37 °C incubator and the medium was changed every 2 days. After 1 week the medium was replaced with growth medium containing 4 ng/mL fibroblast growth factor (FGF) and the medium with FGF was replaced every 3 days. After 1 week the cells formed a gel-like membrane that appeared to follow the shape of the magnetic beads (Figure 6.19). The membrane was made of cells in close formation, which was possibly held together by extra-cellular matrix. In order to confirm the presence of the ECM, the

membrane was stained with H&E and picosirius red (Figure 6.20). The H&E staining confirms the presence of the cells. They appear to have grown while linked to each other and also some

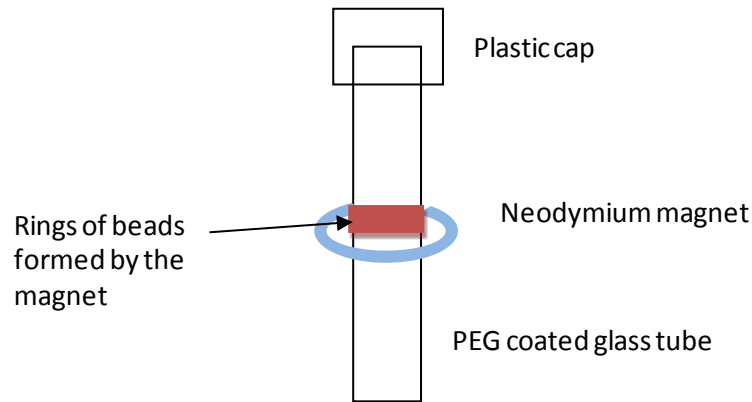


Figure 6.18. Schematic diagram of the beads suspended in a glass tube used for growing ECM.

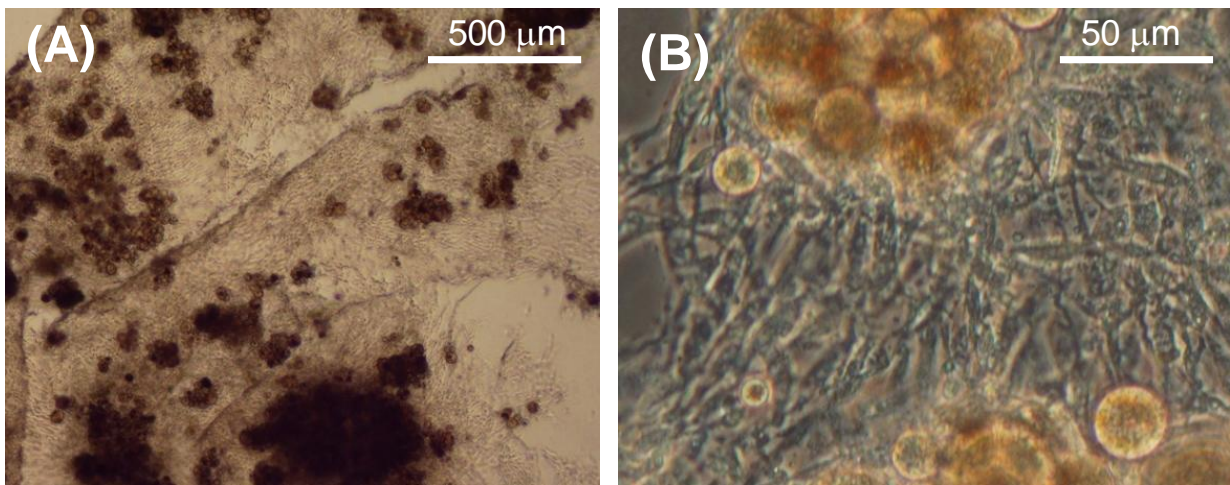


Figure 6.19. Phase contrast images at (A) 40X and (B) 400X magnification, showing the gel-like membrane grown on the magnetic bead ring and the individual cells, respectively. A suspension of fibroblasts and magnetic agarose beads coated with collagen were incubated in DMEM/F12 medium supplemented with 10% fetal bovine serum (FBS) in an incubator at 37 °C and 5% CO₂ in glass tube coated with PEG to prevent cell attachment. After one week the cells were exposed to 4 ng/mL of FGF in the growth medium and a week later the images shown above were taken.

are linked to the beads. The picosirius red staining gives the cells a green color whereas collagen is shown in pink. The pink color is usually associated with the green and outlines the green cells indicating that collagen was produced by the cells as they grew on the beads.

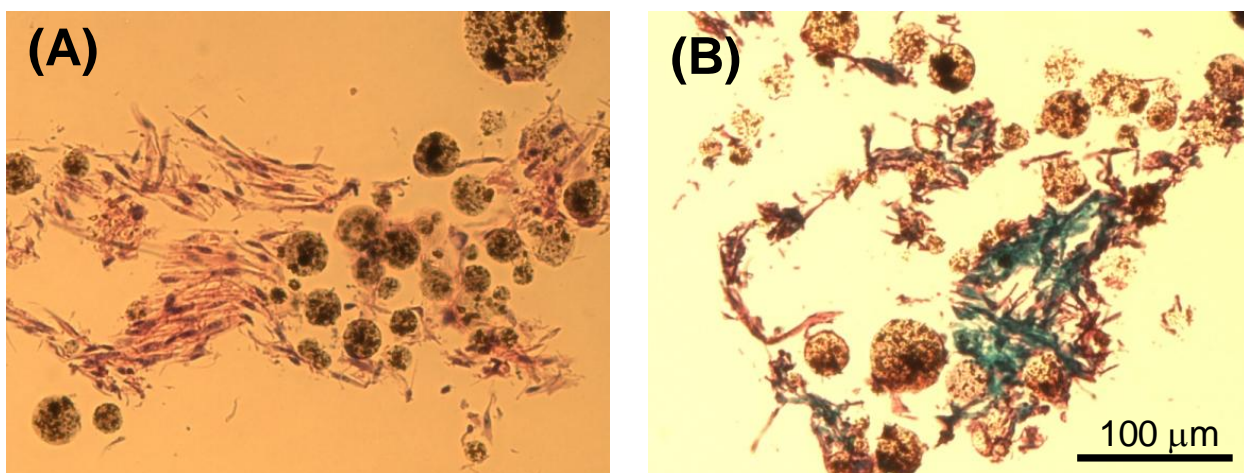


Figure 6.20. Histology staining of the fibroblast tissue grown in the test tube with a magnet. (A) H&E staining: cells and collagen are pink, while the nuclei are purple. (B) Picosirius red staining: cells are green, and the collagen stains pink. The beads have their natural orange-brown color. The image was taken at 100X magnification.

6.6. Summary and Conclusions

Different substrates were successfully coated with self-assembled monolayers. Surfaces such as glass, ITO, polyurethane and PDMS were coated by treating the surface to form free hydroxyl groups and then reacting the surface with trialkoxysilanes. Stainless steel required an additional treatment of its surface prior to forming trialkoxy silanes SAMs on its surface. The stainless steel surface was first treated with tetramethoxysilane to form a siloxane layer. This is due to the

composition of stainless steel which most likely does not allow for stable bonds to form with trialkoxy silanes. The nature of binding for the tetraalkoxysilane is not exactly known, but most likely it forms a conditioning layer on the surface of stainless steel. This is important because coating of stainless steel is crucial in the food industry where biofouling of surfaces needs to be prevented and in medicine where medical implants prepared out of stainless steel, such as stent are commonly used. For these medical implants the main requirement is prevention or retardation of tissue growth on the stent. Therefore the surface modification needs to provide a coating that mimics the surrounding tissue. The ability to modify the surface of PTFE or Teflon was also demonstrated. Since the fluorocarbon surface is chemically inert, the surface had to be modified to allow the introduction of functional groups such as hydroxyls. This was done by reducing the surface with elementary sodium to generate carbon double bonds. After two oxidizing steps, the surface was easily modified with silane chemistry.

Surface patterns that mimic ECM were successfully constructed on both gold and glass surfaces. After screening SAMs with different functional groups it was found that amino terminated SAMs with a long alkyl chain provided suitable surfaces for optimal growth and differentiation of neuronal cells. These SAMs were used to generate the surface patterns in combination with SAMs that have the opposite effect such as hydrophobic and PEG surfaces.

Growing cells in three-dimensional container versus on a two-dimensional surface, although not easy, has several advantages. It has the potential to culture a larger number of cells so whatever is extracted from the cells can be conducted in large industrial scales. Also, cell culture in a chamber versus a Petri dish can potentially lead to tissue and then organ culture and

reconstruction. The use of scaffolds is needed to direct tissue growth and the use of a scaffold whose shape can be controlled and changed without direct intervention would be a step forward. A magnetic scaffold or rather a magnetic support made of smaller magnetic parts would allow for this. Magnetic agarose beads were formed by the emulsification process. They consist of magnetic particles embedded in spherical agarose gel beads. The beads were successfully coated with a specific antibody to immobilize Jurkat cells which grow in suspension. Cell immobilization was stable for two weeks. It was later shown that incubation of antibodies in 37 °C does decrease their ability to immobilize cells, most likely due to degradation. In the presence of cells the antibodies degrade faster due to the presence of proteases.

A flow-through bioreactor was constructed to trap Jurkat cells attached to the agarose beads in a chamber, using an external magnet while flowing growth medium through the chamber. Jurkat cells were trapped in the chamber in stable numbers for at least 6 days. To show the feasibility of using the agarose beads as a support for tissue growth, mouse fibroblasts were suspended with collagen coated beads in a PEG coated glass tube, and after allowing them to proliferate for a week they were induced with FGF for another week in order to produce ECM. After a total of two weeks it was observed that cells had grown only on the ring of beads (formed by the external magnet) and that they had grown a gel-like membrane over the beads. Histology staining showed the membrane to be made of cells and extra-cellular matrix.

6.7. Practical Implementations and Future Work

Changing the surface chemical properties of materials without changing the chemical structure of

the bulk material is practical and advantageous over designing new materials simply to obtain a new surface structure. Changing surface properties has many uses. Just in the work described here knowing how to coat glass with an inert material such as poly(ethylene glycol) became useful when cells had to attach only to the beads but not the glass walls. Materials, such as stainless steel, need to be coated with anti-biofouling and antimicrobial. These coatings have practical uses in the food industry and in medicine. In medicine, stents have often to be removed because surrounding tissue can grow over them or they can become infected, in both cases impeding their function. They can be coated with anti-coagulating drugs which slowly diffuse out, but this provides only a temporary solution and it only retards blood clotting and tissue overgrowth. If the surface was coated with compounds that prevent adhesion of plasma proteins, such as PEG, or prevents coagulation of blood, such as heparin, then the stent would have a relatively longer life time. Before putting such coatings on stents their stability needs to be tested at 37 °C over time in a simple medium such as PBS and then using more complex media to simulate the composition and flow of blood. Another material of interest in the medical field is titanium. Experiments will be carried out to see what kind head group (alkoxy silane or carboxyl) provides the most stable coating.

The ideal medical device coating would be one that mimics the surrounding tissue. This means understanding the interactions of cells with man-made materials can allow the integration of these materials in tissues and organs without the risk of having to replace them. One part of this equation is knowing which surfaces cells prefer or do not prefer and why. In order to investigate why the Neuroscreen 1 cells they prefer the AUTMS terminated surface, a number of alkoxy silanes will be used to coat glass coverslips and the growth, differentiation and response of

various cell lines will be observed (Figure 6.21).

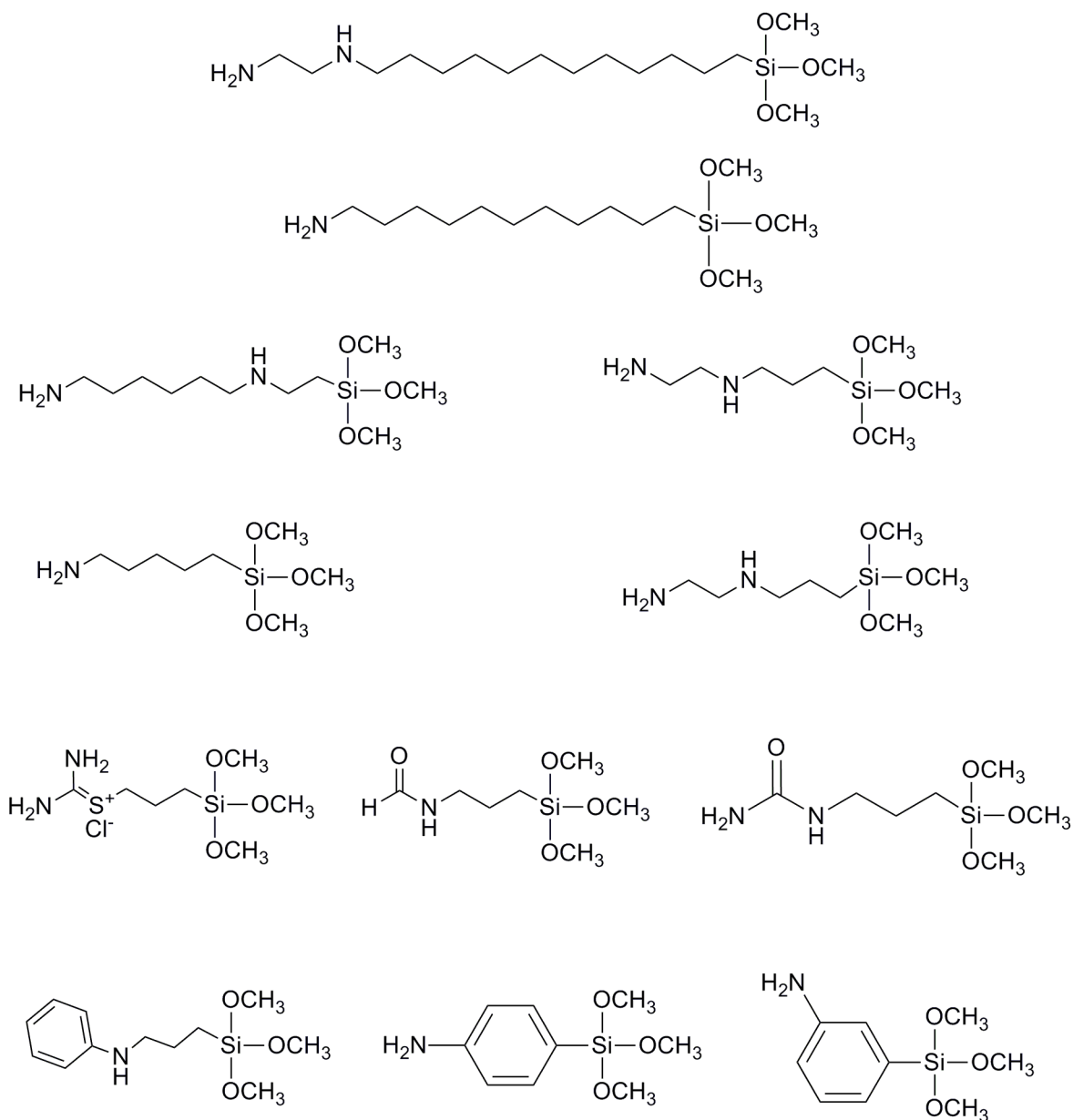


Figure 6.21. The chemical structures of the different trialkoxysilanes that will be used for coating glass coverslips.

The flow-through bioreactor has four practical uses; it can be used for the continuous production of (1) cell metabolites to be used as pharmaceuticals, (2) biofuels, (3) cell amplification, and (4)

tissue culture. With regard to the first use the bioreactor will be used to trap Jurkat cells and then they will be induced to produce interleukin (which is used as an anticancer drug). A second chamber will contain beads coated with interleukin antibodies to capture interleukin from the growth medium. Prior to this use, the lifetime of the antibody coated on the beads will be increased by using a cocktail of protease inhibitors which would prevent antibody degradation from proteases. Some preliminary experiments also showed that collagen coating was able to immobilize Jurkat cells. The possibility of using aptamers (DNA sequences that bind specifically to receptors on the cell membrane) will also be looked into as DNA is more stable than proteins. The ability of CD3 antibodies to promote interleukin production in Jurkat cells will also be investigated. If CD3 antibodies immobilized on beads promote interleukin production, then coating of magnetic beads with antibody will have the dual function of trapping beads and signaling them to produce interleukin.

The magnetic support system will also be improved by using a Halbach array of magnets. The Halbach array can generate a homogeneous magnetic field inside the chamber thus increasing the surface area available for cell binding. The flow-through reactor is also suitable for tissue growing. The continuous flow and suspension in the solution will provide the mechanical stress factor as well as freedom required for enhanced proliferation of cells seeded on the magnetic beads. The continuous flow will also provide fresh nutrients that will be suitable for the inner cells. Smooth muscle cells will be used to generate ring structures as that is the shape of the beads formed using a circular magnet. The number of the beads will also be decreased to find out what is the minimum density of beads to control the shape of the tissue grown.

7. Hybrid and Bilayer Membranes

7.1. Introduction

Cell membranes are the boundaries of living cells to their environment and at the same time they are portals that are essential to cell function. Cell membranes contain ion-channels and pumps for transport of electrolytes, small molecule transporters for carrying metabolites and nutrients, and receptors that allow cell signaling and communication. Signaling membrane proteins such as, tyrosine kinase receptors, cytokine receptors, neurotransmitters, and G protein-coupled receptors, are targets of roughly half of the 100 best-selling therapeutic drugs on the market¹⁶³ and furthermore, according to sequence homology of the human genes approximately 30% of all proteins are membrane proteins.¹⁶⁴ Discovery and screening of pharmaceuticals for these types of membrane proteins is challenging due to their hydrophobic nature.

Membrane receptor proteins contain hydrophobic domains that are embedded in the hydrophobic region of the cell membrane. Their purification requires the use of organic solvents and detergents and their conformation changes once they are extracted from the membrane, which means any screening assays for possible drug candidates in solution, may not apply to their real structures on the cell membrane. *In vivo* assays, involving mammalian cells, are not convenient and reliable to implement, especially with high-throughput screening (HTS) assays that test hundreds of samples at a time. One way to bypass using live cells is the reconstitution of these trans-membrane proteins in phospholipid vesicles and running *in vitro* HTS assays. The most abundant lipids in cell membranes are phospholipids, or glycerophospholipids, which consist of two fatty acyl groups esterified to the C1 and C2 position of a glycerol backbone and a hydrophilic molecule bound to the C3 position through a phosphate group. The phosphate and

another group attached to it make up the polar head of the phospholipid, whereas the acyl groups are the hydrophobic tails (Figure 7.1A).

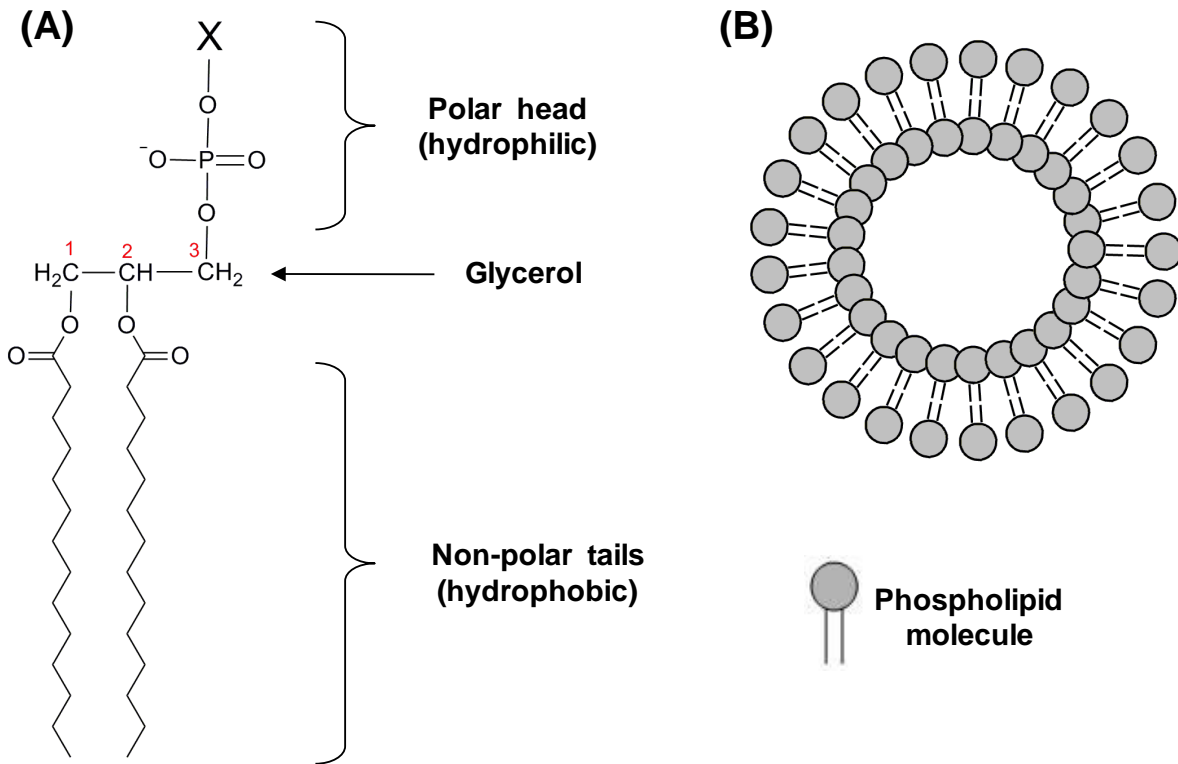


Figure 7.1. Schematic drawing of (A) a phospholipid and (B) a phospholipid vesicle. The two acyl groups bound to a glycerol in the 1,2 positions through ester bonds constitute the hydrophobic tails of the lipid. The hydrophilic head consists of the phosphate group covalently linked with another hydrophilic molecule (X), which usually is choline, serine, or ethanolamine.

Phospholipids are amphiphilic molecules that in aqueous solutions spontaneously form spherical lipid bilayers, also called lipid vesicles (Figure 7.1B). The polar heads of the phospholipids are exposed to the aqueous environment on both the inside and outside of the bilayer. Lipid vesicles have the same basic structure as cell membranes. The structure of membrane proteins and their activity can be assayed by reconstituting them in phospholipid vesicles. As mentioned earlier,

receptor proteins reconstituted in phospholipid vesicles would provide more practical constructs for high-throughput screening of drug candidates, compared to live cells. However, this method would still require purification of the membrane protein, and as reconstitution in vesicles has to be done by forming the vesicles in the presence of the membrane protein, detergents and glycerol (both used during purification and as stabilizers in aqueous solutions) impede the formation of phospholipid vesicles. Typical reconstitution or incorporation of purified membrane proteins in lipid vesicles is done with elaborate procedures requiring the removal of detergents and glycerol while making the vesicles.¹⁶⁵ These constructs may provide unreliable and non-reproducible results due to the presence of impurities, and other membrane proteins. In addition, protein activity and ligand-receptor interactions can be determined only with photometric and radioactive assays.

Another way to simplify the screening assay would be to clone the receptor protein without the hydrophobic domain, and use that as a construct without the need of vesicles and elaborate purification procedures. Unfortunately, this method provides binding sites for drug candidates that do not exist in the wild type protein, resulting in false leads, which would not apply to the receptor in live cells. A better construct would be one that contains the ligand-binding or cytoplasmic domain of the receptor together with the hydrophobic domain. The presence of the hydrophobic domain would allow for the correct orientation of the rest of the protein after incorporation in the phospholipid vesicle. Under the right conditions lipid vesicles are known to fuse with the surface and form planar membranes.¹⁶⁶⁻¹⁶⁸ Incorporation of membrane proteins on planar phospholipid membrane, where the proteins would be free to behave as if they were in a cell membrane, would represent a model system for studying membrane protein interactions such as ligand binding, protein folding, and phosphorylation, using a number of surface

characterization techniques, including Surface Plasmon Resonance, Electrochemical Impedance Spectroscopy, and Quartz Crystal Gravimetry, in addition to the standard protein activity assays. Most importantly this surface-based construct would provide an ideal platform for constructing high-throughput screening assays of therapeutic pharmaceuticals.

Formation of planar membranes requires the use of unilamellar lipid vesicles and substrates with known surface chemistry. Lipid vesicles or liposomes can be produced from phospholipids using a number of methods. Three general methods include, sonication, extrusion, and injection.¹⁶⁹ Sonication may lead to oxidation and deterioration of lipids during the formation of the vesicles. The injection method, is a rather simple method, and involves injection of ethanol solutions of lipids through a needle in an aqueous solution at temperatures above the phase transition temperature of the lipid. The phase transition temperature of the lipid refers to the specific temperature at which the acyl chains the lipid in the vesicles go from an ordered crystalline or gel phase to a more disorganized or liquid-crystalline phase. When heated to a temperature above that of the phase transition of the phospholipid, lipid vesicles spontaneously fuse with planar surfaces and form a lipid monolayer (one leaflet) or bilayer (both leaflets) on the surface (Figure 7.2).¹⁷⁰ The lipid monolayer is formed when vesicles are exposed to an alkyl terminated self assembled monolayer, resulting in the formation of a hybrid bilayer membrane.¹⁷¹ Lipid bilayer or bilayer membranes form when vesicles are exposed to hydrophilic surfaces. However, it has been reported that lipid bilayers form on silicon oxide but not on bare gold or titanium surfaces for unknown reasons.¹⁷⁰

The surface properties of the substrate are controlled by the formation of self-assembled

monolayers (SAMs). SAMs of alkanethiolates on gold substrates form well-ordered films that are stable and reproducible, and can be used to control the surface wettability and functionality of the gold surface.¹⁷² On glass, silicon, quartz, indium tin oxide, or polymer substrates alkoxy silanes SAMs can be used to control the surface chemistry. A SAM consisting of a long

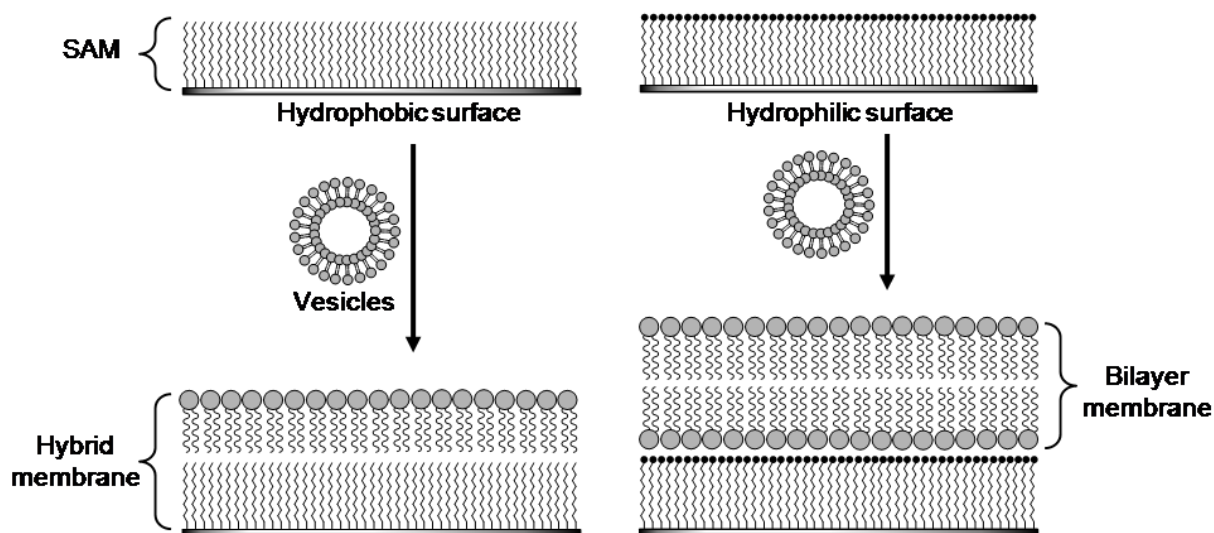


Figure 7.2. Schematic drawing of the formation of a hybrid membrane (left) or a bilayer membrane (right). Hybrid membranes are result from the fusion of lipid vesicles in aqueous solution onto hydrophobic self-assembled monolayer of alkyl chains. Bilayer membranes, on the other hand, tend to form in the presence of hydrophilic surfaces, and could also form on self-assembled monolayers terminating with hydrophilic groups.

hydrocarbon chain (C10 – C18) can be used to make hydrophobic surfaces. Plant and coworkers have demonstrated that exposing lipid vesicles to a hydrophobic SAM on gold causes vesicles to fuse with the surface, resulting in the formation of a hybrid membrane.¹⁷³ Silicon oxide surfaces, which are hydrophilic, have been shown to allow the formation of bilayer membranes on their surface, after exposure to a suspension of lipid vesicles.¹⁷⁴ A self-assembled monolayer that contains hydrophilic or charged terminal groups could be expected to provide a good substrate

for vesicle fusion and bilayer membrane formation.

Bilayer membranes are analogous to a cellular membrane permanently fixed to a surface. There are two other classes of membrane proteins besides the integral or trans-membrane proteins mentioned earlier; peripheral membrane proteins, and lipid-anchored membrane proteins.

Peripheral proteins are associated with one face of the cell membrane by hydrogen bonding or electrostatic interaction with the polar head groups of the membrane or integral proteins.

Lipid-anchored proteins, as the name says, are covalently bound to a lipid that is inserted in one of the leaflets of the cell membrane. Hybrid membranes can accommodate lipid-anchored membrane proteins or integral membrane proteins that span only to one leaflet of the cell membrane with their hydrophobic region (Figure 7.3).¹⁶⁴ The ability of hybrid membranes to accommodate full integral proteins has not been observed probably because SAMs on gold are expected to be more tightly packed (therefore less fluid) than the hydrophobic tails of the lipid monolayer, while their respective experimental dielectric constants have been reported to be similar. Bilayer membranes are expected to accommodate both lipid-anchored and integral membrane proteins (Figure 7.3). However, incorporation of the whole trans-membrane protein could be challenging if it contains domains on both sides of the membrane.

As mentioned earlier, if the protein construct contains the hydrophobic domain and only one outer domain (the ligand binding or the cytoplasmic domain), once inserted in the bilayer membrane, it is expected to interact with the surroundings and fold so that it has a conformation and function similar to the whole protein which resides in the cell membrane. Providing that the surface bound protein maintains its normal function, the hybrid or bilayer membrane could be

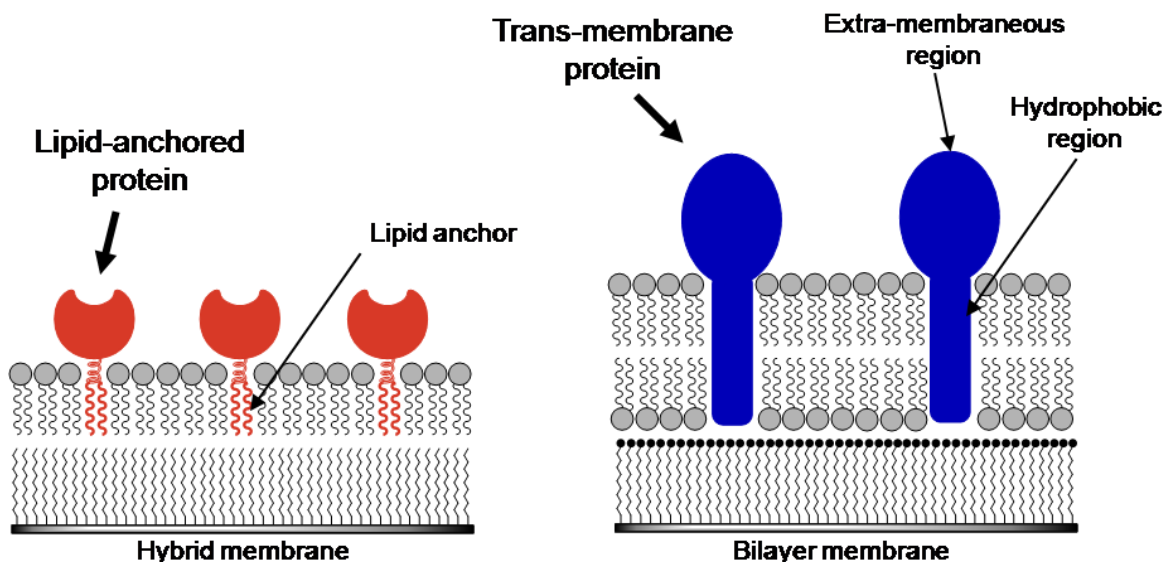


Figure 7.3. Diagram of lipid-anchored proteins on a hybrid membrane (left) and trans-membrane proteins on a bilayer membrane (right). Lipid-anchored proteins are found in both the cytoplasmic and extracellular face of the cell membrane. The trans-membrane protein depicted in this diagram has a very simplified structure. Many trans-membrane proteins in cells have more complicated structures usually with more than one hydrophobic domain spanning the membrane. The protein shown here would apply better to a cloned construct that contains the extra-membraneous region of interest from either face of the membrane and the hydrophobic domain which would allow for proper orientation and function or activity of the region of interest.

implemented in a surface based high-throughput screening system, to test activating or inhibiting agents against the protein of interest.

In this work, hybrid and bilayer membranes were formed using unilamellar lipid vesicles of DMPC (1,2-dimyristoyl-*sn*-glycero-3-phosphocholine), shown in Figure 7.4. Hybrid membranes were formed on hydrophobic alkanethiols of three different lengths and the formation of the membrane was monitored *in situ* using electrochemical impedance spectroscopy. The presence of the hybrid membrane was then confirmed by employing an acetylcholinesterase (AChE) with an amphiphilic tail and testing its activity with a standard photometric assay. Then, the same

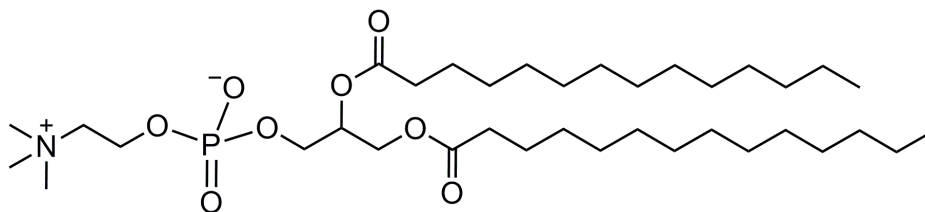


Figure 7.4. Chemical structure of DMPC (1,2-dimyristoyl-rac-glycero-3-phosphocholine).

protein was used to show the formation of bilayer membranes on hydrophilic surfaces prepared on gold substrates. Some of the hydrophilic surfaces contained alkyl chains to anchor the bilayer membrane. The activity of the enzyme in both solution and surface was determined and the maximum coverage was determined experimentally. This work demonstrates the ability to form hybrid or bilayer membranes on different SAMs, and also demonstrates the activity of a lipid-anchored protein on both surfaces on either membrane

7.2. Experimental Details

7.2.1. Preparation of lipid vesicles

Lipid vesicles were formed by the injection method reported by Batzri and Korn.¹⁷⁵ A 10 mL volume of Tris buffered saline (TBS), pH 7.0 or 7.5, was transferred in a 2 cm diameter glass tube and it was incubated in a temperature-controlled water bath at 37 °C, which is above the phase transition temperature (23 °C) of the phospholipid. While stirring the buffer in the glass tube, a solution of DMPC in absolute ethanol (12.5 mg in 0.5 mL) was slowly injected with a 22-gauge syringe needle into the buffer solution at a 17 $\mu\text{L}/\text{min}$ flow rate using a syringe pump. The injection took place approximately 2 cm below the surface of the TBS. The lipid vesicle suspension (at a final DMPC concentration of 2 mM) was used immediately after formation or

stored at 4 °C for later use.

7.2.2. Transmission electron microscopy (TEM) imaging

Samples were prepared by first centrifuging a solution of vesicles in PBS (1.0 mL) at 14,000 rpm for 5 min. Osmium tetroxide (0.4 mL of a 4% solution in DI water) was added to crosslink the vesicles for imaging. After 30 min of occasional shaking the solution was centrifuged again at 14,000 rpm for 30 min. The supernatant was removed, 1 mL of ethanol added, the solution mixed by a vortex for 30 sec, followed by centrifuging at 14,000 rpm for 30 min. This process was repeated once more using ethanol and then twice with propylene oxide. A 2:1 mixture of propylene oxide and resin was added let stand for 1 hour. The solution was removed by centrifugation, and the process was repeated using a 1:2 mixture of propylene oxide and resin. Finally, 100 % resin was added and cured overnight at 70 °C. Once cured, the resin was cut with a diamond blade into 50 to 60 nm slices, placed on formvar coated carbon grids and imaged.

7.2.3. Amide bond linkage on COOH and NH₂ terminated surfaces

Carboxyl terminated surfaces were activated with EDC/NHS. The samples were then rinsed with deionized water, dried, and immediately placed in 1 mM dodecylamine solution in anhydrous ethanol. Following overnight incubation at room temperature, the surfaces were rinsed with the ethanol and dried with nitrogen.

Amino terminated surfaces were immersed and incubated in an anhydrous ethanolic solution of 1 mM dodecanoic acid and 5 mM dicyclohexyl carbodiimide (DCC) overnight at room temperature. The surfaces were rinsed with ethanol and dried with nitrogen.

7.2.4. Electrochemical characterization of hybrid and bilayer membranes

Electrochemical impedance spectroscopy measurements were performed in TBS (0.150 mM NaCl and 20 mM Tris), pH 7.0, using the electrochemical setup described in Section 2.8.4. The surface area of the gold substrate dipped in solution was 1 cm² for all trials. The impedance measurements were carried out at a fixed potential of 0 V vs SCE and a 10 mV AC perturbation from 100 kHz to 1 Hz. The impedance spectra were recorded in the form of Nyquist plots and they were fitted to an equivalent circuit, based on the Randles model,^{55, 56, 176} using nonlinear least squares fitting to extrapolate values for monolayer capacitance (C_m), monolayer resistance (R_m), and solution resistance (R_s) (Figure 7.5). The temperature of the electrochemical cell was controlled by keeping the beaker containing the electrochemical cell immersed in a constant temperature circulating bath. The monolayer capacitance was monitored sequentially under

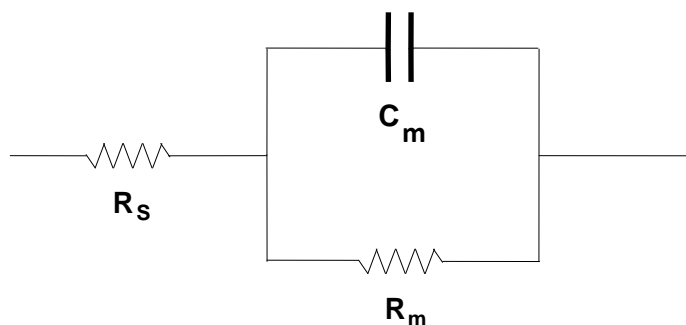


Figure 7.5. Diagram of the equivalent circuit used to fit the impedance spectroscopy data.

different temperatures or solution composition for each type of SAM. Impedance measurements were conducted every 5 – 6 min. For each change in the system the measurements were taken until a stable capacitance value was obtained for at least 15 minutes (or at least 3 consecutive measurements), meaning a capacitance change of less than 0.005 $\mu\text{F}/\text{cm}^2$ between two consecutive measurements. The impedance measurements were first carried out at room

temperature in TBS, pH 7.0. Then the solution temperature was heated to and held at 37 °C while measurements were still being carried out until the capacitance values stabilized. This was followed by replacing 10% of the volume of TBS serving as the electrochemical cell solution with TBS, pH 7.0, solution containing 5% (v/v) ethanol, resulting in a final ethanol concentration of 0.5%, in order to see if the ethanol addition would affect the capacitance of the monolayer, since the vesicle solution contains ethanol. The next change was the addition of vesicles by replacing 10% volume of the electrochemical cell solution with DMPC vesicle solution prepared in TBS, pH 7.0, for a final phospholipid concentration of 0.2 mM. Following the addition of vesicles, the impedance was measured over the course of 120 min in order to ensure the formation of the hybrid membrane.¹⁷⁷ The final change was the cooling down of the (0.2 mM) vesicle solution back to the initial room temperature, where capacitance measurements were again taken until they were stable. Each experiment was done in triplicate, using three different gold slides.

7.2.5. Formation of hybrid and bilayer membranes and protein incorporation

Hybrid and bilayer membranes were formed by incubating 1 cm² alkanethiol coated gold slides in the vesicle solution at 37 °C (above the phase transition temperature of DMPC). Prior to incubation with the gold slides, the vesicle suspension was spun at 100,000 ×g at room temperature for 15 min to remove any vesicle aggregates and then diluted four times with TBS, pH 7.5. The gold slides were placed individually in 12-well culture plates and 2.0 mL of vesicle solution was added on each well to ensure that the slides were completely submerged in the solution. The surfaces were incubated overnight at 37°C to allow formation of the hybrid and bilayer membranes. At the end of the incubation period, the slides were washed twelve times,

while keeping them submerged and not allowing the surface to dry or be exposed to air, which is known to destroy the hybrid membrane.¹⁷¹ This was done by exchanging 1.0 mL of vesicle solution on each well with 1.0 mL of plain buffer twelve times finally leaving 2.0 mL of TBS.

After the rinsing process, 2 μ L of red blood cell acetylcholinesterase (AChE) from the stock solution (0.22 mg/mL) were added to each well and the 12-well plate was agitated at room temperature on an orbital shaker for 4 hours to allow the insertion of the protein in the membrane. The surfaces were rinsed again 12 times by exchanging 1.0 mL volumes as described above. The 1.0 mL solution removed for 1st, 6th, and 12th rinse were saved in glass vials to test the effectiveness of successive rinses. The surfaces were kept submerged in the 2.0 mL TBS volume at 4 °C until further use.

7.2.6 Assessment of protein activity

AChE activity in solution was calibrated using Ellman's Reagent. First, stock solutions of acetylthiocholine iodide (100 mM) and DTNB (500 μ M) were prepared in TBS, pH 7.5. The DTNB solution was used to make an AChE solution at a concentration of 100 pmol/mL. Different amounts of AChE enzyme, 0 to 100 pmol, and 30 μ L of acetylthiocholine iodide solution were added to the DTNB solution for a final volume of 3.0 mL. Using an Evolution 300 UV-Visible double beam spectrophotometer from Thermo Scientific (Waltham, MA) facilitated with VISIONpro™ software, the absorbance measurements were recorded at a wavelength of 410 nm with one minute cycle time for 5 cycles. Calibration curves were generated in 1 min increments for up to 4 min reaction incubation time.

AChE activity on the surface was determined as follows. Following insertion of AChE in the membrane, the remaining 2.0 mL of TBS, pH 7.5, in each well was changed to 3.0 mL of 500 μ M solution of DTNB in TBS, pH 7.5. This was done by replacing 0.50 mL of TBS with 1.5 mL of 1 mM DTNB solution in TBS, pH 7.5. Then, 30 μ L of 100 mM acetyl thiocholine in TBS, pH 7.5, was added into each well (after removing 30 μ L of DTNB solution). The enzyme reaction was allowed to take place by agitating on the orbital shaker at room temperature. After 4 min, 1.5 mL was removed from each well and the absorbance was measured at 410 nm.

7.3. Results and Discussion

7.3.1. *Hydrophobic alkanethiol monolayer characterization*

Two of the hydrophobic alkanethiols used, dodecanethiol (DDT) and octadecanethiol (ODT), were selected since the phase transition temperature of the acyl group equivalents of their respective alkyl chains are well below or above the temperature range (21 – 37 °C) where the formation of hybrid membrane was monitored.¹⁷⁸ The acyl chains of the DMPC lipid, which is the equivalent of the alkyl chain of tetradecanethiol (TDT), have a phase transition temperature of 23 °C.

Self-assembled monolayers of alkanethiol on gold were characterized by contact angle goniometry, ellipsometry, and impedance spectroscopy. Contact angle (see Table 7.1) measurements confirmed the hydrophobic nature of the SAMs and are consistent with previously published results for these SAMs.¹⁷⁹ Ellipsometric measurements (Table 7.2) on the DDT SAM determined a film thickness of 1.6 nm \pm 0.4 nm, consistent with the theoretical thickness

and also consistent with published reports.¹⁷⁹⁻¹⁸¹ Electrochemical impedance spectroscopy was used to further confirm the presence of a well ordered SAM. Impedance measurements and subsequent equivalent circuit fitting determined the monolayer capacitance at room temperature to be 0.71 ± 0.13 , 0.67 ± 0.06 and 0.52 ± 0.06 $\mu\text{F}/\text{cm}^2$ for dodecanethiol (DDT), tetradecanethiol (TDT) and octadecanethiol (ODT), respectively, as shown in Table 7.3. The decrease in

Table 7.1. Average water contact angles of dodecanethiol (DDT), tetradecanethiol (TDT) and octadecanethiol SAMs.

Surface (Carbon chain length)	Contact angle
DDT (C12)	$102.2 \pm 1.9^*$
TDT (C14)	110.9 ± 0.8
ODT (C18)	111.0 ± 1.1

*Standard deviation, determined after making six measurements per slide for at least two different samples.

Table 7.2. Average film thickness measured by ellipsometry of dodecanethiol (DDT), tetradecanethiol (TDT) and octadecanethiol SAMs.

Surface	Theoretical thickness (nm)	Measured thickness (nm)
DDT (C12)	1.6	$1.6 \pm 0.4^*$
TDT (C14)	1.8	$1.7 \pm 0.2^\#$
ODT (C18)	2.2	$2.4 \pm 0.2^\#$

*Standard deviation, determined after making five measurements per slide for three different samples.

[#]Data reported in the literature.¹⁷⁹

capacitance between the DDT and ODT SAMs appears to be consistent with the increase in the SAM thickness. At 37 °C the capacitance values drop slightly to 0.70 ± 0.11 , 0.66 ± 0.04 and $0.49 \pm 0.09 \mu\text{F}/\text{cm}^2$ for dodecanethiol (DDT), tetradecanethiol (TDT) and octadecanethiol (ODT), respectively. These results indicate that the packing of the alkyl SAM is not affected by temperature, including TDT whose alkyl chains are the equivalents of the fatty acid tails of the DMPC phospholipid, which have a phase transition temperature of 23 °C. The elevated temperature could be expected to increase capacitance by reorganizing the alkanethiol molecules and promoting diffusion of electrolyte ions into the film. Although the changes in capacitance between room temperature and 37 °C are well within the experimental error range, the average values decrease for all three SAMs, showing that possibly the only change upon the temperature increase is better packing of the alkyl chains. The hydrophobic nature of these alkyl chains varying from 12 – 18 carbons, as the water contact angles show, ensures a stable SAM packing in the presence of water, which apparently is not affected by increasing the temperature to 37 °C. This observation is important because the formation of a hybrid bilayer membrane depends on interaction between the hydrophobic tails of the phospholipid with the hydrophobic alkyl chains of the SAM and the alkanethiol monolayer packing could affect the formation of the hybrid membrane.

7.3.2. *Lipid vesicles*

Liposome formation and size was confirmed by transmission electron microscopy (TEM), as shown Figure 7.6. Vesicles were measured against the scale and the average of 30 vesicles was 37 nm, ranging from 27 – 100 nm.

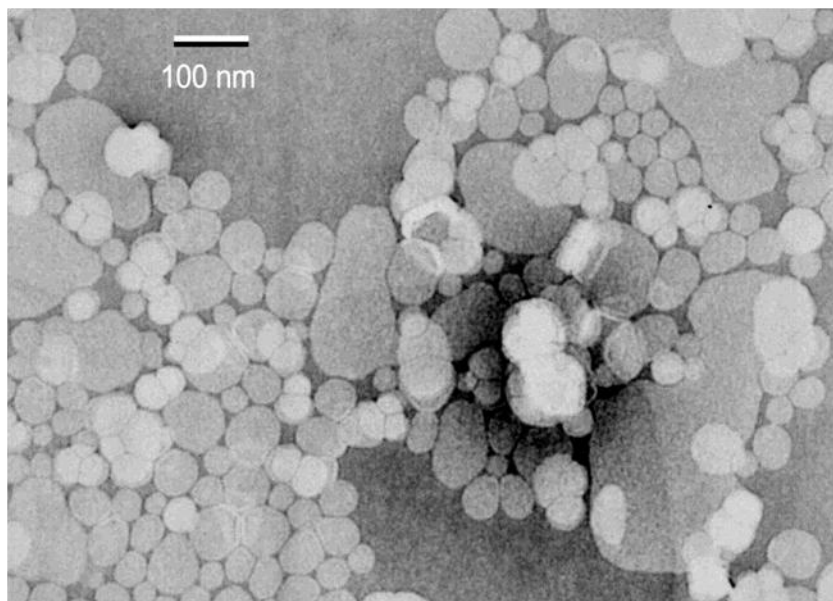


Figure 7.6. TEM image of the DMPC lipid vesicles. The vesicles were prepared by injecting an ethanol solution of DMPC (12.5 mg in 0.5 mL) in 10 mL of TBS at 37 °C while stirring the mixture.

7.3.3. Formation of hybrid membrane on hydrophobic alkanethiol SAMs

Due to the instability of the hybrid bilayer membrane if it is not submerged in solution (the surface tension of the liquid will rupture the membrane as it is removed from solution), characterization of the membrane was limited to experiments that could be performed while the SAM substrate remained in solution. Deposition of the hybrid membrane was monitored as it formed by electrochemical impedance spectroscopy, as described in Section 7.2.4. Since the DMPC lipid has a phase transition temperature of 23 °C, the alkanethiol modified gold substrates and the electrochemical cell were heated to 37 °C and vesicle fusion was carried out at 37 °C. The capacitance of the alkanethiol monolayer was monitored sequentially at room temperature and 37 °C, prior to addition of vesicles for each type SAM. After the addition of vesicles at 37 °C, the capacitance was monitored for over 120 min at 37 °C and then at room temperature

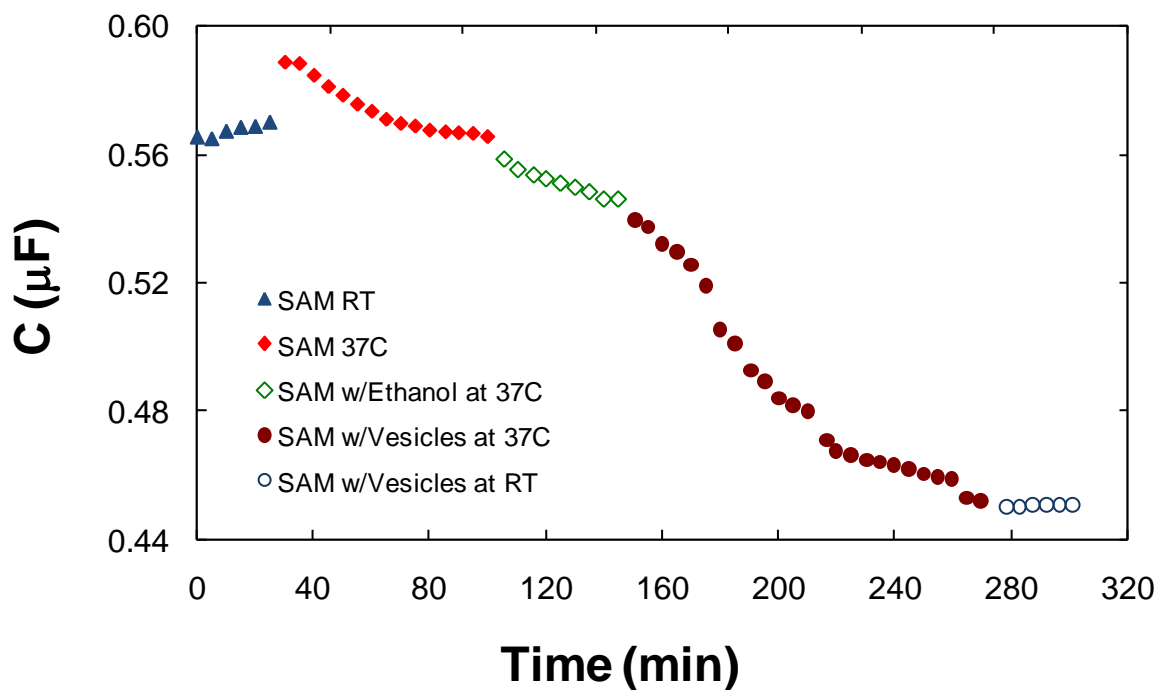


Figure 7.7. Capacitance of an octadecanethiol self-assembled monolayer (SAM) on the gold slide monitored sequentially over time: at room temperature; at 37 °C, in 0.5% (v/v) ethanol, in DMPC vesicle solution at 37 °C, and in DMPC vesicle solution at room temperature. Impedance measurements were conducted in TBS (150 mM NaCl and 20 mM Tris), pH 7.0. The spectra were obtained in the frequency range from 100 kHz to 1 Hz at a fixed DC potential of 0 V vs SCE and the modelling was done with Randles circuit.

again. Impedance data was modeled using an equivalent circuit to extrapolate values for monolayer capacitance, monolayer resistance, and solution resistance. After equivalent circuit fitting, the monolayer capacitance was plotted vs time, as shown in Figure 7.7. The results showed a significant decrease in capacitance after the addition of vesicles indicating the formation of a thicker film or the hybrid membrane onto the alkanethiol modified gold surface. This graph shows that a complete hybrid bilayer membrane is formed on the surface after at least 2 hours as indicated by a relatively constant film capacitance value after this time. The capacitance of the film decreases, as the hybrid bilayer membrane is formed, because the capacitance of a parallel plate capacitor (which is how an alkanethiol monolayer modified

working electrode immersed in electrolyte solution behaves) is inversely proportional to the distance between the plates, given by the equation:

$$C_m = \frac{\epsilon\epsilon_0 A}{d} \quad (7.1)$$

where C_m is capacitance of the film or monolayer on the electrode, ϵ is the relative permittivity of the capacitor (or the dielectric constant of the film on the electrode surface), ϵ_0 is the permittivity of vacuum, A is the surface area of the capacitor (area of the gold surface dipped in solution) and d is the distance between the plates (or film thickness, separating the gold surface from the electrolyte solution). The decrease in capacitance indicates an increase in the film thickness, d , on the working electrode as also reported by others.^{176, 182-184}

Decreasing the temperature from 37 °C to the initial room temperature (~22 °C) after formation of the hybrid membrane did not affect the capacitance values, similar to the result observed for the alkanethiol SAMs when the temperature was changed in the opposite direction. Since the area of the electrode is fixed at 1 cm², the only parameters that can affect the capacitance upon changes in temperature are the dielectric constant and thickness of the film on the gold surface. Any changes in dielectric constant would be attributed to changes in the packing of the alkanethiol SAM and/or lipid monolayer in the hybrid membrane, whereas changes in hybrid membrane thickness would only occur if the depth of interdigitation between the alkyl chains of the two monolayers was affected by temperature.

A reported study on hybrid membranes using surface enhanced Raman Spectroscopy and reflection-absorption infrared spectroscopy has indicated that changes in the alkanethiol are

subtle upon the formation of the hybrid membrane.¹⁷³ Therefore, according to these reports any changes in capacitance upon cooling of the system would indicate a change in the packing of the

Table 7.3. Average capacitance values for dodecanethiol (DDT), tetradecanethiol (TDT) and octadecanethiol SAMs measured in sequence before and after formation of the hybrid bilayer membrane as shown in Figure 7.4. The average and standard deviation values were obtained by performing the experiment on three different slides for each SAM.

SAM	SAM RT ($\mu\text{F}/\text{cm}^2$)	SAM 37°C ($\mu\text{F}/\text{cm}^2$)	SAM + EtOH ($\mu\text{F}/\text{cm}^2$)	Bilayer 37°C ($\mu\text{F}/\text{cm}^2$)	Bilayer RT ($\mu\text{F}/\text{cm}^2$)
DDT	0.71 \pm 0.13	0.70 \pm 0.11	0.65 \pm 0.09	0.53 \pm 0.04	0.52 \pm 0.04
TDT	0.67 \pm 0.06	0.66 \pm 0.04	0.62 \pm 0.05	0.53 \pm 0.06	0.52 \pm 0.06
ODT	0.52 \pm 0.06	0.49 \pm 0.09	0.48 \pm 0.08	0.41 \pm 0.08	0.40 \pm 0.08

lipid or alkanethiol monolayer in the hybrid membrane. Although the phase temperature of DMPC is 23 °C, the packing of either monolayer does not appear to be affected from the change in temperature. A decrease in capacitance was observed after incubation in vesicle solution for all three alkanethiol SAMs, DDT, TDT, and ODT, as it can be seen from Table 7.3. The change in capacitance upon the formation of the hybrid membrane is similar, while there is a steady decrease in capacitance compared to the alkanethiol chain length (Figure 7.8).

As discussed earlier, assuming that the alkanethiol monolayer does not change significantly with the addition of the lipid monolayer, the two monolayers can be considered to be capacitors in series, and the capacitance of the lipid monolayer can be determined as follows:

$$\frac{1}{C_{Lipid}} = \frac{1}{C_{HM}} - \frac{1}{C_{SAM}} \quad (7.2)$$

where C_{Lipid} , C_{HM} , C_{SAM} , are the capacitance of the lipid monolayer, hybrid membrane, and alkanethiol SAM, respectively. Using the capacitance values at room temperature from

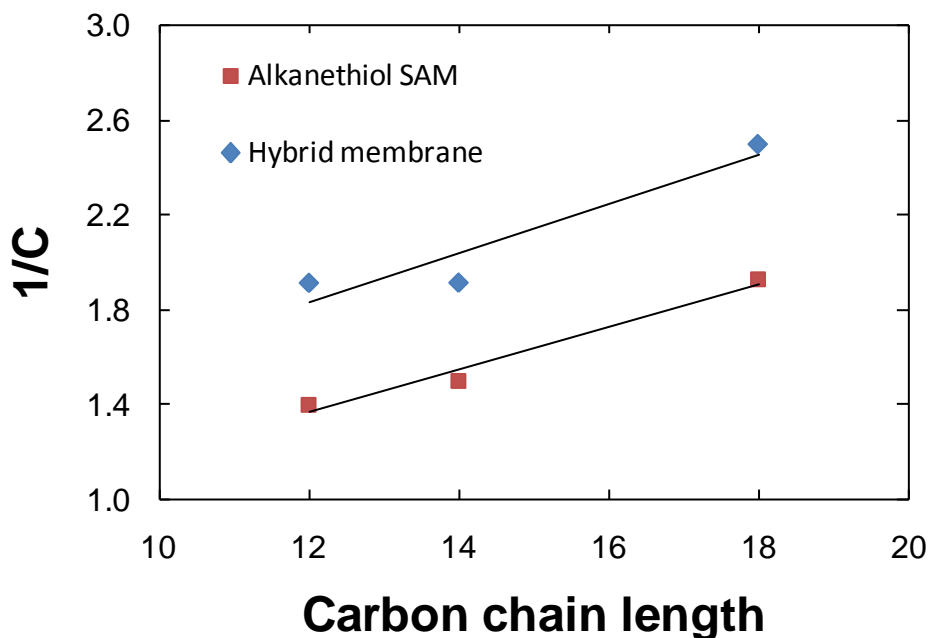


Figure 7.8. Alkanethiol chain length dependence of capacitance before and after the formation of the hybrid membrane.

Table 7.3 and equation (7.1), the capacitance and the thickness of the lipid layer were calculated for each alkanethiol SAM (see Table 7.4). The dielectric constant of the lipid was assumed to be 2.7 as reported previously.¹⁷¹ The lipid monolayer capacitance values are in accordance with other published results, which vary from 1.48 – 2.9 $\mu\text{F}/\text{cm}^2$.^{171, 176, 184-186} The thickness values are also consistent with the reported thickness of acyl chains in DMPC bilayers¹⁸⁷ and hybrid membranes formed with DMPC.¹⁸⁸ These values represent only the thickness of the

hydrophobic acyl group of the phospholipids as the polar head group is fully hydrated during the electrochemical impedance measurements. The discrepancy between the calculated thickness values of the lipid monolayer prepared on the different alkanethiol SAMs most likely is due to experimental error, although it could also be caused by slightly different interactions or interdigitation of the lipid layer with each SAM, as thicker SAMs are better packed and have more crystalline structures. Different packing would also lead to slightly different dielectric constants, and thus different calculated capacitance values for the capacitance of the lipid monolayer.

Table 7.4. Capacitance of the alkanethiol monolayer (C_{SAM}), hybrid membrane (C_{HB}) and the calculated capacitance (C_{Lipid}) and thickness of the lipid monolayer.

SAM	C_{SAM} ($\mu\text{F}/\text{cm}^2$)	C_{HB} ($\mu\text{F}/\text{cm}^2$)	C_{Lipid} ($\mu\text{F}/\text{cm}^2$)	Lipid layer thickness (nm)
DDT	0.71	0.53	1.94	1.2
TDT	0.67	0.53	2.40	1.0
ODT	0.52	0.41	1.75	1.4

7.3.4. Formation of bilayer membrane on the COOH-terminated SAM

Fusion of DMPC vesicles was also examined in the presence of a COOH terminated SAM and changes in capacitance were monitored by electrochemical impedance spectroscopy, as shown in Figure 7.9. The 11-mercapto undecanoic acid (MUA) SAM is very hydrophilic, indicated by a water contact angle smaller than 10° . Therefore, vesicle fusion cannot happen through one leaflet as with hydrophobic alkanethiol SAMs, but instead vesicle fusion is expected to result in

the formation of a bilayer membrane. The capacitance of the MUA SAM decreases after the addition of vesicles, similar to the hydrophobic alkanethiol SAMs. The capacitance the COOH-terminated SAM is larger than those obtained for the hydrophobic SAMs, due to the presence of the hydrophilic COOH group and the capacitance of the MUA samples varied from 2.62 – 3.53 $\mu\text{F}/\text{cm}^2$. These results indicate that the carbon chains of MUA are not as well packed as those of the alkane thiols due to the presence of the COOH groups. This is also the cause of the variance in capacitance values between the different samples. The drop in capacitance after the addition of vesicles (1.88 – 2.55 $\mu\text{F}/\text{cm}^2$) was in the range of 28 – 35% compared to the

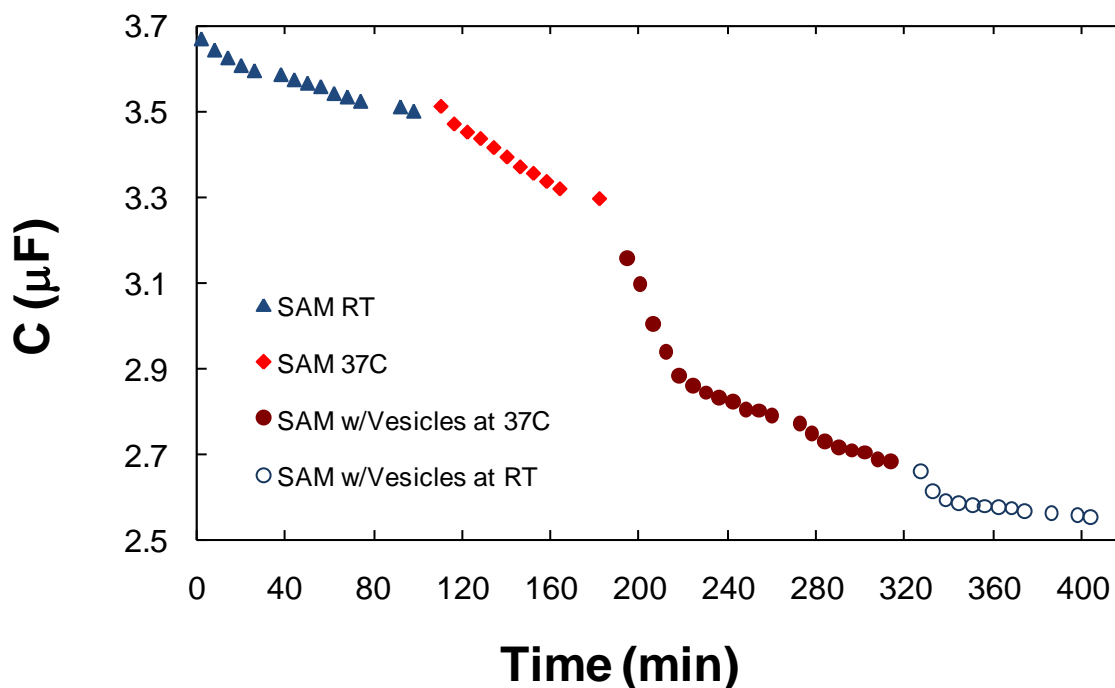


Figure 7.9. Capacitance of an 11-mercapto undecanoic acid (MUA) SAM on the gold slide monitored sequentially over time: at room temperature; at 37 °C, in DMPC vesicle solution at 37 °C, and in DMPC vesicle solution at room temperature. Impedance measurements were conducted in TBS (150 mM NaCl and 20 mM Tris), pH 7.0. The spectra were obtained in the frequency range from 100 kHz to 1 Hz at a fixed DC potential of 0 V *vs* SCE.

MUA capacitance. This drop is comparable to that of the alkanethiol SAMs after the formation of the hybrid membrane. Bilayer membranes are known to have a capacitance of $2 \mu\text{F}/\text{cm}^2$.¹⁶⁸ This means that based on equation (7.2) and the capacitance of the MUA SAMs of the capacitance values for the MUA + bilayer membrane film should be in the range of $1.1 - 1.3 \mu\text{F}/\text{cm}^2$. The experimental values based on the Randles circuit fitting are higher than those expected. This could indicate that the bilayer membrane has not fully formed yet and that there are still defects (or MUA only areas) on the surface.

7.3.5. Incorporation of a lipid-anchored protein into the hybrid and bilayer membrane

Many eukaryotic lipid-anchored proteins are linked to a molecule of glycosyl phosphatidylinositol, also known as a GPI anchor, which contains a 1,2-diacyl-glycerol linked to a glycan as the membrane anchor. The protein used for these experiments was an acetylcholinesterase (AChE) that is purified from human red blood cells (RBC) which contains a GPI anchor and is known to be present only on the outer leaflet of red blood cells. RBC acetylcholinesterase is derived from the same gene that encodes the AChE sitting on neuronal and neuro-muscular junctions. The role of AChE present in RBC is not exactly known, but there is increasing evidence that it may be involved in the proliferation and differentiation of hematopoietic cells from which RBCs are formed.¹⁸⁹

The AChE presence can be determined with a photometric assay using Ellman's reagent. Calibration curves of enzyme activity were obtained by adding varying the concentration of AChE and measuring the absorbance of the yellow product. The activity was measured in the presence or lack of detergent in the activity assay buffer (Figure 7.10). The detergent used and

its concentration were the same as in the original solution AChE. The calibration curves given in Figure 7.10 are those obtained after 4 min reaction incubation time. The activity of AChE in detergent is twice as high compared to the enzyme activity in detergent-free buffer. This result shows that the enzyme is less active in plain buffer due to the presence of the amphiphilic GPI anchor, indicating that the enzyme is more active, therefore more stable, when the lipid tail is inserted into the detergent micelles. This means that when the amphiphilic AChE is introduced in a detergent-free buffer it is expected to spontaneously anchor itself onto the hybrid membrane by inserting its lipid tail into the lipid layer once it comes into contact with it. Incorporation of

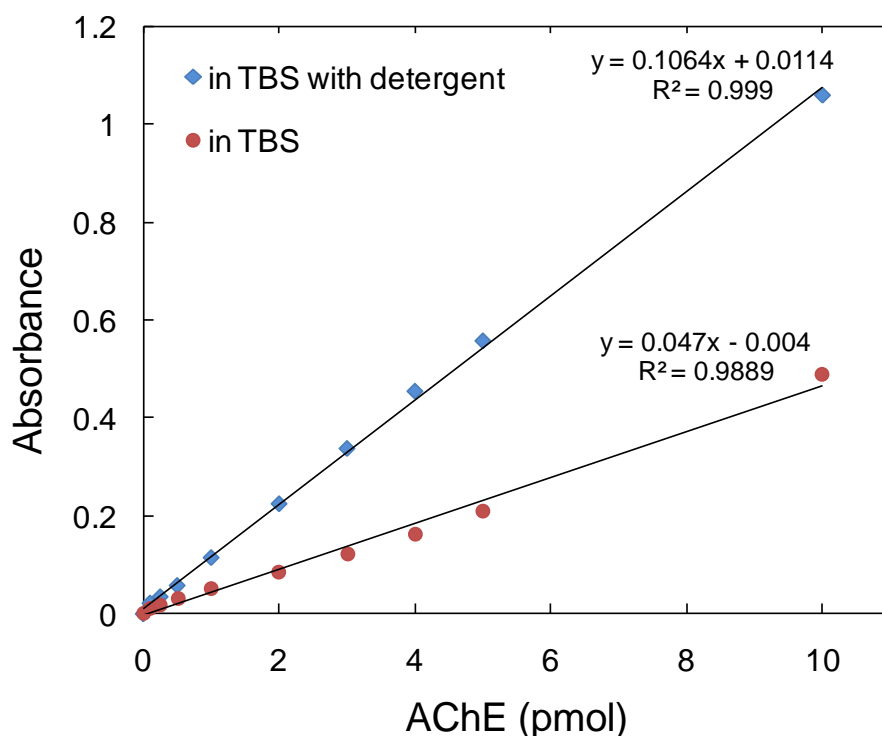


Figure 7.10. Calibration of GPI-anchored AChE (from human red blood cells) activity in solution with or without 0.1% (v/v) Triton X-100 detergent. Absorbance was measured at 410 nm after 4 min incubation for different amounts of amphiphilic AChE in the activity assay solution (1 mM acetylthiocholine iodide and 500 μ M DTNB in TBS, pH 7.5).

the AChE enzyme on the surface would allow for determination of enzyme activity on the surface, thus indirectly confirming the presence of a planar membrane on the surface.

Different SAMs prepared on 1 cm² gold substrates were used to form hybrid or bilayer membranes, incubated in the presence of AChE and then exposed to AChE activity solution to observe the formation of the yellow product. All SAMs were incubated in vesicle solution overnight at 37 °C, in order to allow for formation of the hybrid or bilayer membrane, since the electrochemical measurements on the COOH terminated SAM appeared to show that 2 hours might not be long enough to form a complete bilayer membrane. In addition, others have reported that even though the formation of the hybrid membrane happens within 2 hours, overnight incubation ensures better organization of the lipid membrane. After thorough rinsing (see Experimental Details, Section 7.2.5), the surfaces were exposed to AChE solution in detergent-free TBS, pH 7.5, and were agitated for 4 hours at room temperature to allow the enzyme to come into contact with the surface and anchor itself on the membrane (Figure 7.11A).

After thoroughly rinsing the surfaces again, in order to remove all enzymes present in solution, they were exposed to the activity assay solution. Octadecanethiol (ODT) SAMs were used for the formation of the hybrid membrane. As shown in Figure 7.11B, the ODT surfaces exposed to vesicles (hybrid membrane) and then to amphiphilic AChE, contain the enzyme, indicated by the formation of yellow product. The control wells containing the ODT SAMs and hybrid membrane that were not exposed to AChE solution, and ODT SAMs that were exposed to AChE, did not turn the solution yellow even after 1 hour incubation in the activity assay solution. The hybrid membrane samples exposed to AChE turned the solution yellow within 10 min. The

rinse samples obtained during the rinsing process after incubation in enzyme solution (see Section 7.2.5) showed that only the 1st rinse had enzyme present, whereas the 6th and 12th rinse

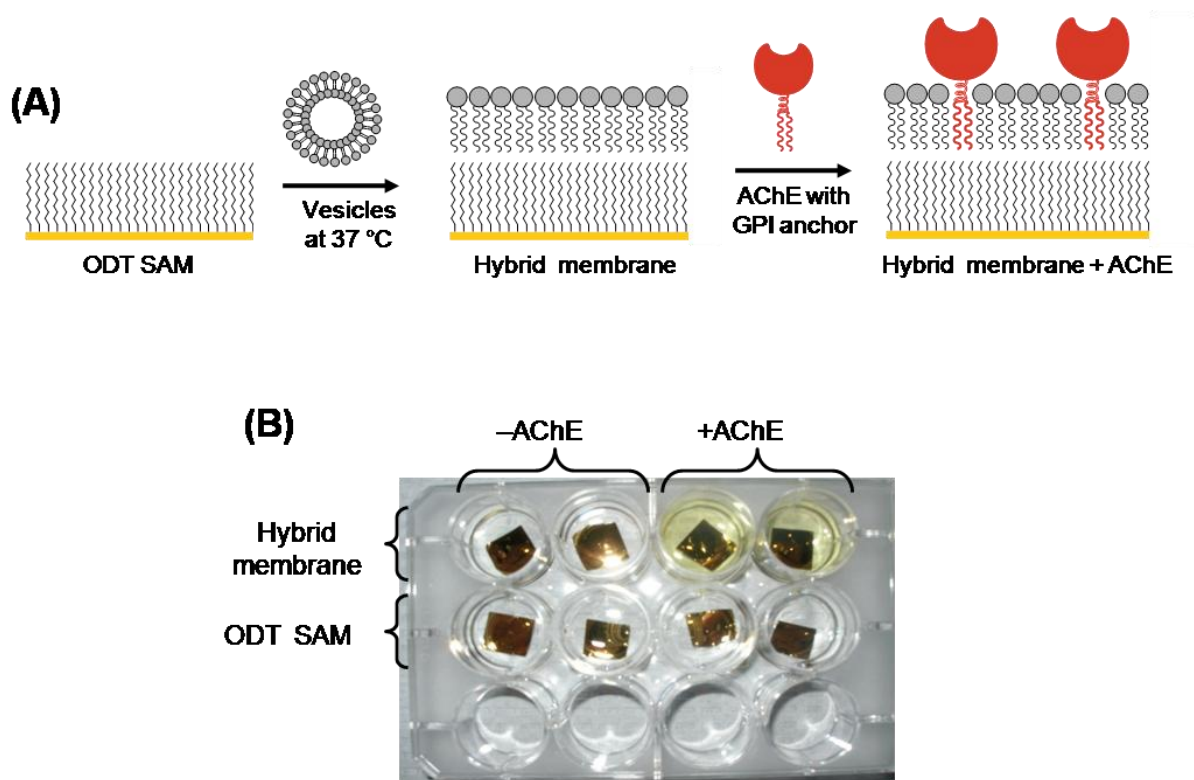


Figure 7.11. Strategy for insertion of a lipid-anchored AChE enzyme on a hybrid membrane and confirmation of the presence on the surface using an AChE activity assay. (A) Diagram of the incorporation of the amphiphilic AChE on a hybrid membrane formed on an octadecanethiol (ODT) SAM. (B) Determination of AChE activity, thus presence on the surface, as an indirect indicator for the formation of the hybrid membrane. ODT SAMs on gold slides (1 cm²) were incubated in a 12-well plate submerged in vesicle solution overnight and after thorough rinsing they were incubated in 3 pmol/mL AChE for 4 hours at room temperature with agitation on an orbital shaker. The slides were thoroughly rinsed again and subsequently incubated in AChE activity solution with agitation on an orbital shaker. During all the rinsing and incubation steps the slides were kept submerged in solution. The hybrid membrane exposed to amphiphilic AChE turned the solution yellow (top right) within 10 min. Hybrid membrane (top left) and ODT (bottom left) samples which were not exposed to amphiphilic AChE did not turn the solution yellow. Most important, no yellow color was observed on ODT surfaces exposed to AChE (bottom right). The picture was taken after 10 min incubation in the activity assay solution (1 mM acetylthiocholine iodide and 500 μ M DTNB in TBS, pH 7.5).

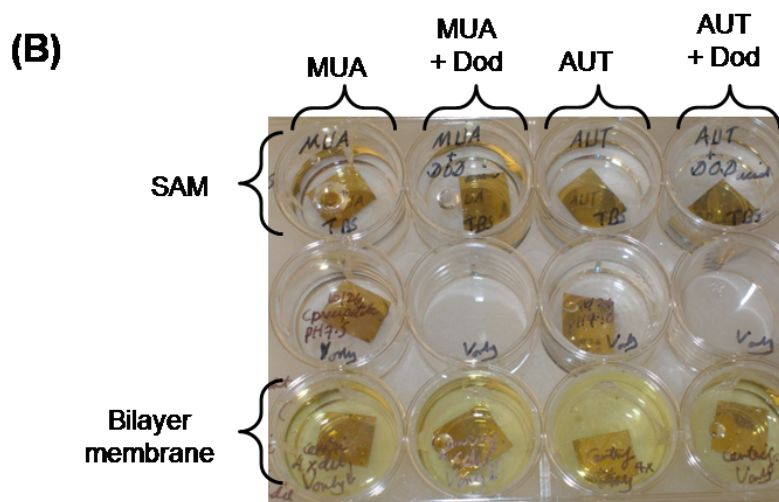
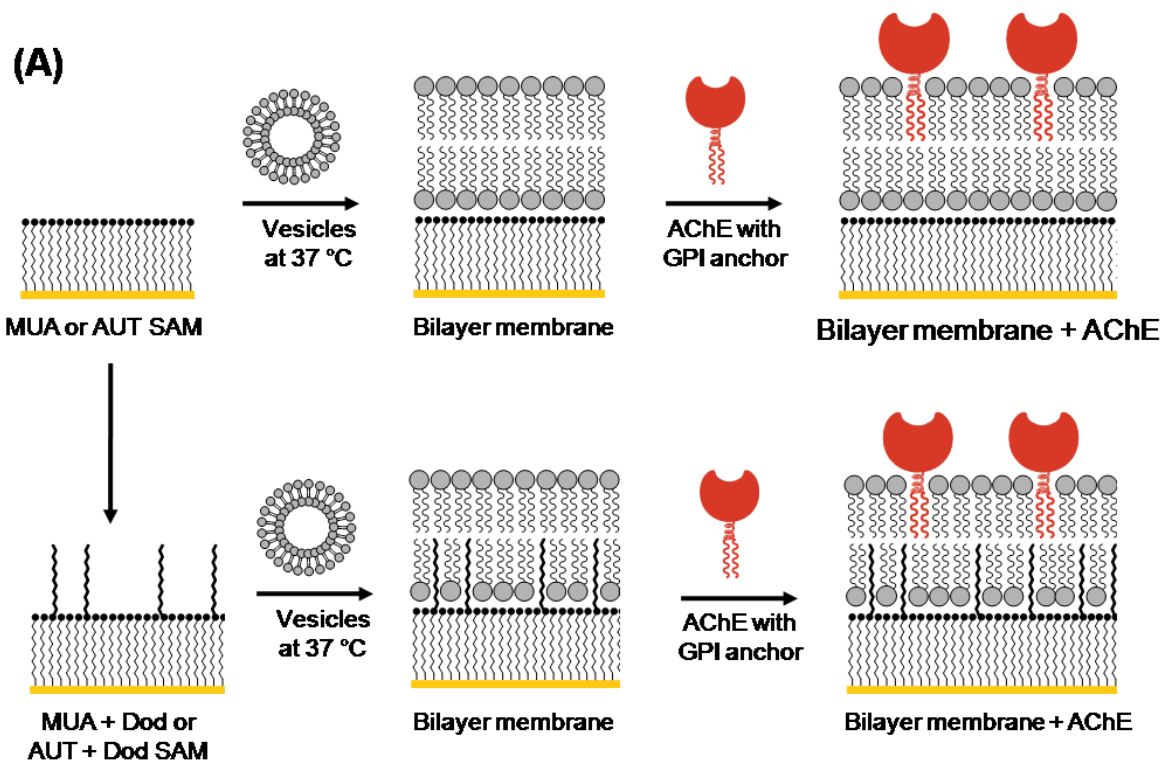


Figure 7.12. Insertion of AChE on a bilayer membrane. (A) Diagram of the incorporation of the amphiphilic AChE on a bilayer membrane formed on different SAMs. (B) AChE activity, was observed for all SAMs exposed to vesicle solution (bottom row), but not those that were not (top row). The SAMs are: 11-mercaptop undecanoic (MUA), MUA reacted with 1 mM dodecyl amine (MUA + Dod), 11-amino-1-undecanethiol (AUT), and AUT reacted with 1 mM dodecanoic acid (AUT + Dod). Membrane preparation, incubation in AChE and activity procedures were the same as the one followed for the ODT SAMs. The picture was taken after 10 min incubation.

did not show yellow coloration for at least 1 hour. This experiment clearly confirms the formation of hybrid membranes on a hydrophobic SAM and indicates the incorporation onto the membrane of a lipid-anchored enzyme in its active form.

Bilayer membranes can be used to accommodate trans-membrane proteins. Hydrophilic SAMs were used as substrate for the formation of bilayer membranes, using the same procedure as for the formation of hybrid membranes. Two different hydrophilic SAMs were used, 11-mercapto undecanoic acid (MUA), and 11-amino-1-undecanethiol (AUT). In aqueous solutions the MUA and AUT SAMs have negatively and positively charged surfaces, respectively. As it can be seen from the chemical structure, the polar head of the DMPC lipid is a zwitterion (Figure 7.4), therefore DMPC vesicles can be expected to fuse with either surface.

Lipids and their respective vesicles can be made with any desired charge, but phosphatidyl choline lipids are one of the most common ones in mammalian cell membranes, therefore they would provide a favorable substrate for the incorporation and normal conformation and function of membrane proteins. Some of the MUA and AUT surfaces were modified by surface chemistry so they contained alkyl chains sticking out of the charged surface (see Figure 12A). Since some lipid-anchored proteins are anchored on membranes with one fatty acyl chain linked to an amino acid residue by an amide or ester bond, these alkyl chains are expected to anchor the bilayer membrane once it formed on the hydrophilic surface and make it more stable. The modification of the MUA and AUT surface was done by reacting the terminal group of the SAM with dodecylamine and dodecanoic acid, respectively, resulting in alkyl terminated surfaces (MUA + Dod and AUT + Dod, respectively) by the formation of amide bonds. These kinds of

surface reactions are known to result in approximately 50 % surface coverage at 1 M solution concentration of reactants,¹⁹⁰ therefore at a 1 mM concentration few alkyl chains are expected to bind on the surface.

The activity assay experiment showed yellow coloration for all surfaces exposed to vesicle solution (Figure 12B) within 10 min incubation, whereas the corresponding controls that were not exposed to vesicles did turn the solution yellow. However, after approximately 1 hour incubation these controls also showed yellow coloration. This means that the hydrophilic surfaces either contain physisorbed AChE due to electrostatic interactions, or that some AChEs are anchored on these hydrophilic SAMs. The second explanation is plausible because these hydrophilic SAMs are similar in structure to a lipid monolayer. They have a charged and hydrated terminal group and a hydrophobic alkyl chain, which correspond to the polar head and acyl chains of the phospholipid, respectively. As the electrochemical impedance measurements showed, the MUA SAM had a capacitance that was six times larger than the one of dodecanethiol (DDT) SAM, meaning that the packing of the MUA was less dense or less organized than that of DDT. This could be indicating that since well packed SAMs are too rigid to accommodate membrane proteins, by controlling the size of the terminal group, the SAM can be potentially be tailored to provide a more fluid, cell membrane-like substrate for the incorporation of membrane proteins. The approach for this consideration will be discussed in the future work section.

All hydrophilic surfaces tested showed the presence of active AChE on the surface, regardless of the charge of the terminal group. These experiments also showed that using the amphiphilic

AChE and its activity assay provided a rapid test for verification of membrane formation, and it can be used to confirm the presence of the membrane on other surfaces, such as glass and polymers, which are difficult to characterize with standard surface characterization techniques.

7.3.6. Determination of AChE coverage on the hybrid membrane.

Lipid-anchored proteins are expected to have the same activity on the artificial membrane as their solution counterparts inserted in detergent micelles. In addition, all the enzymes attached on that membrane are expected to be active, because the lipid anchor ensures their correct orientation. In order to determine the maximum amount of enzyme that can be incorporated on the surface, several ODT coated gold slides that were exposed to a vesicle solution to form hybrid membranes, were incubated in different solution concentrations of AChE in detergent-free TBS, pH 7.5. Using the calibration curve obtained in activity assay with detergent (see Figure 7.10C), the amount of enzyme on the surface can be correlated with the incubating solution concentration of AChE.

In the 1 – 10 pmol/mL concentration range, AChE incorporation on the membrane appears to have a linear dependence on solution concentration and at 50 pmol/mL solution concentration the surface coverage appears to be at or near the saturation point or maximum coverage (see Figure 7.13). This linear range applies to the incubation parameters used in this experiment: room temperature, 4 hour incubation time, and agitation. Under a different set of parameters the linearity range could be changed. This means that the amount of lipid-anchored protein on the surface can be controlled by setting the solution concentration in the linear range (of surface density dependence on solution concentration) for a desired set of parameters.

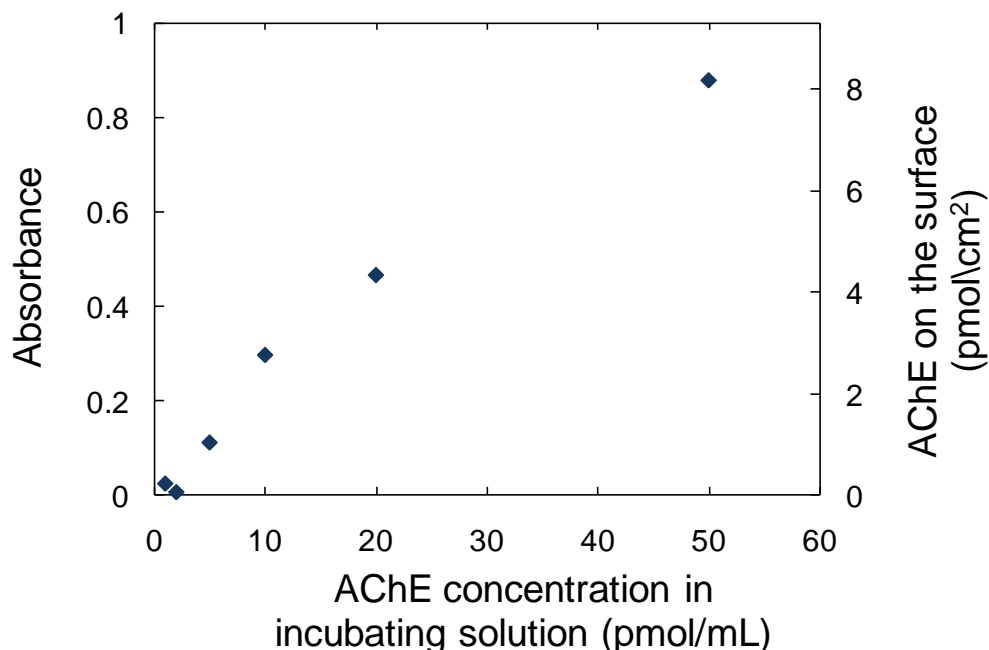


Figure 7.13. Red blood cell AChE activity assay on the surface. ODT SAMs on gold slides (1 cm^2) were incubated in a 12-well plate were exposed overnight to a DMPC vesicle solution and after thorough rinsing they were incubated in 1, 2, 5, 10, 20, and 50 pmol/mL AChE solution in detergent-free TBS, pH 7.5, for 4 hours at room temperature with agitation on an orbital shaker. The slides were thoroughly rinsed again and subsequently incubated in AChE activity solution with agitation on an orbital shaker at room temperature. After 4 min incubation 1.5 mL volume samples were taken from each well and the absorbance was measured at 410 nm. The absorbance values at each concentration represent the average obtained from two samples.

7.4. Summary and Conclusions

Artificial planar membranes provide practical platforms for the reconstitution of membrane proteins. By controlling the surface chemistry of the substrates artificial membranes can potentially be formed on any type of substrate. The formation of hybrid and bilayer membranes was monitored electrochemically by impedance spectroscopy. The results indicated the formation of the membrane by a decrease in capacitance. Testing of different hydrophobic

surfaces showed that different SAM thickness did not affect the formation of hybrid membrane or the ability to detect its formation. The electrochemistry results also seem to suggest that the packing of the SAM could be denser than that of the lipid monolayer, but neither was affected by the change in temperature. However, the phase transition of DMPC is at room temperature, so it is possible that if impedance of hybrid or bilayer membranes was monitored at temperatures below room temperature, than it could result in detectable changes, due to the transition to a gel phase.

A lipid anchored enzyme was successfully incorporated in both types of membranes, opening the way for further research that could lead to the incorporation of trans-membrane proteins on this surfaces and their use in high-throughput screening assays. Unlike mammalian cells, these artificial membranes can allow for the screening of either extra or intracellular protein domains. The use of the amphiphilic AChE also showed that this lipid-anchored enzyme can be used for rapid testing and conformation of the presence of artificial membranes on a surface.

7.5. Practical Implementations and Future Work

7.5.1. Practical implementations

Many important and therapeutic drug target membrane proteins require bilayer membrane support to function properly. Even though the receptor domain of the membrane protein can be cloned separately, it is widely believed that its interaction with potential drugs will not be similar to the interaction of the full protein inserted in the membrane. Nevertheless insertion of receptor domains that still contain their hydrophobic region would be a closer model to the full protein in

a real cell membrane. As mentioned in the Introduction, cells are not a convenient substrate for running reliable large scale high-throughput screening assays. The hybrid and bilayer membranes formed in this work can be applied for high-throughput screening in three different formats: (1) by running activity assay with multiple wells whose bottom has been coated with a thin gold layer for the formation of the artificial membrane with incorporated protein; (2) by using gold nanoparticles as substrates for the formation the assay can be run in solution without the need to coat the bottom of the wells with gold; (3) surface characterization techniques which can monitor changes in discrete portions of the surface, such as surface plasmon resonance, can be employed for the development of sensors that will not need the use of activity assay, but can indirectly detect binding of analytes.

7.5.2. Incorporation of a trans-membrane protein construct into a bilayer membrane

Incorporation of a trans-membrane protein in a bilayer membrane would lead to its application in the discovery and high-throughput screening of potential pharmaceuticals. One trans-membrane of interest is the insulin receptor tyrosine kinase (IRTK). The insulin receptor tyrosine kinase is responsible for initiating the intracellular signaling pathway upon binding of insulin (Figure 7.14.). Binding of insulin on the extracellular domain causes dimerization of two receptors and activation of the tyrosine kinase domains. The final outcome is cross-phosphorylation or autophosphorylation of the two receptors. The dimerization and autophosphorylation of the tyrosine kinase (TK) is of interest because it is crucial in initiating a series of metabolic pathways

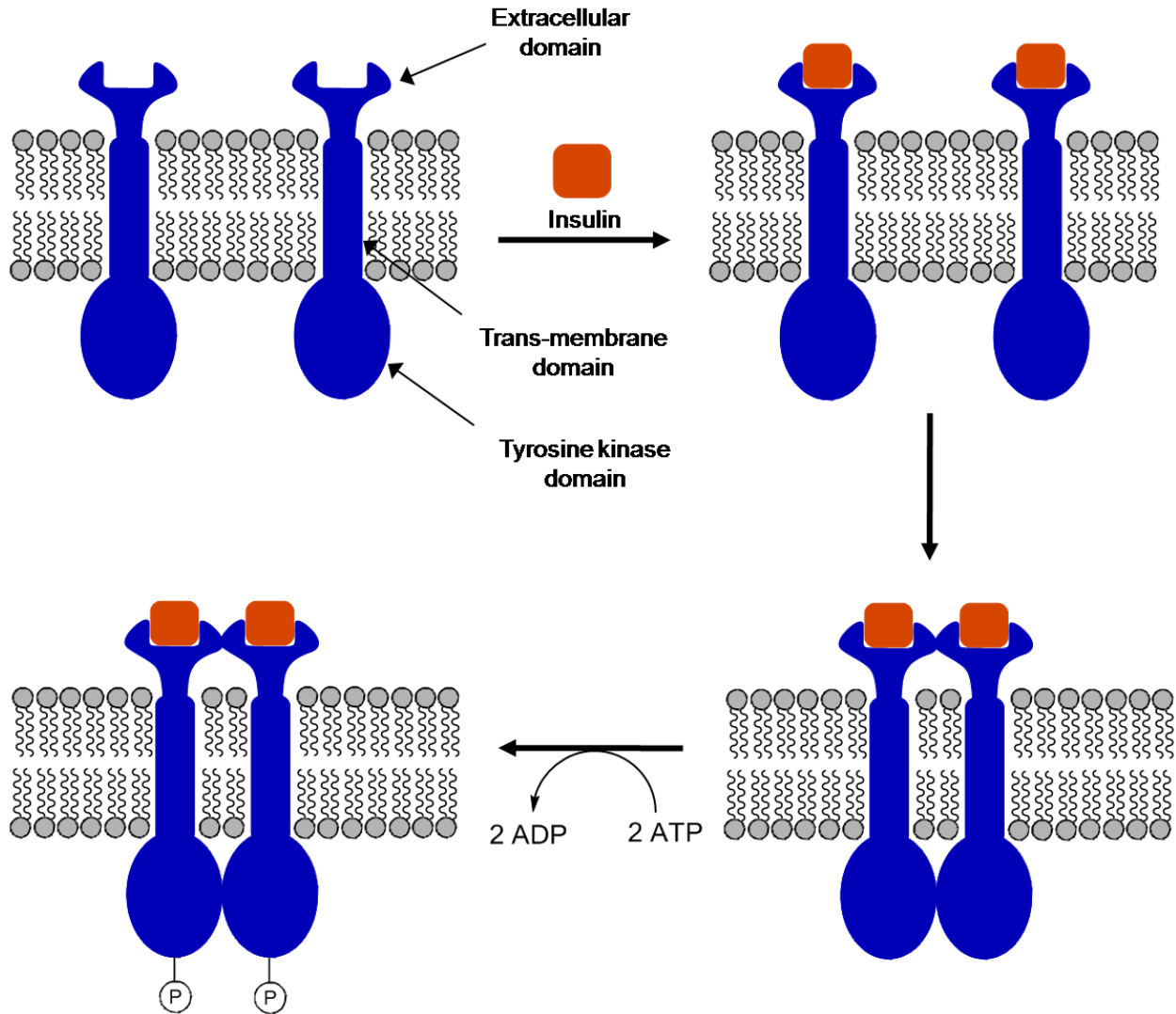


Figure 7.14. Activation of insulin receptor tyrosine kinase. Binding of insulin to the extracellular domain triggers a change in conformation and activation of the catalytic centers in the intracellular part of tyrosine kinase. This results in the dimerization of two adjacent receptors, followed by cross-phosphorylation (phosphorylation of the other partner), a process called *autophosphorylation*.

due to insulin binding. Therefore therapeutic drugs enhancing or inhibiting this process can help people with diabetes. The tyrosine kinase domain containing the hydrophobic trans-membrane region was cloned and amplified, so that it would make it easier for incorporation in either vesicles or planar bilayer membranes (Figure 7.15).

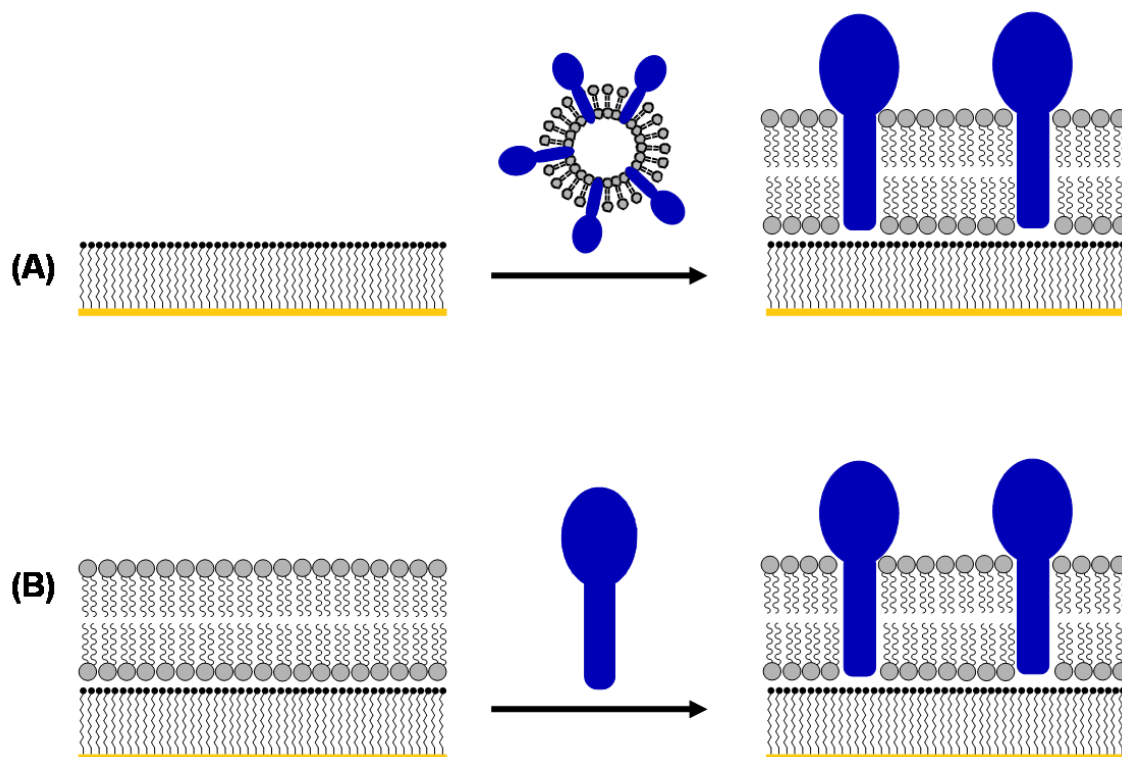


Figure 7.15. Strategies for incorporation of tyrosine kinase (TK) construct on a planar bilayer membrane. (A) TK is incorporated initially in vesicles and then vesicle fusion is expected to result in the formation of a bilayer membrane with TK in it. (B) A bilayer membrane is exposed to TK in detergent-free solution similar to incorporation of AChE in hybrid membranes. This method will be successful if the protein does not precipitate in detergent-free buffer and there are no residual detergent molecules bound to the hydrophobic region of the kinase.

The tyrosine kinase construct was expressed and purified based on the process described as follows. Expression of the recombinant VEGF will be optimized in *E. coli* and protein production verified by a combination of SDS-PAGE (Coomassie stain) and Western blot (anti-His). A multistep enrichment process was developed that included the following: high pressure homogenization, isolation of inclusion bodies, denaturation and refolding (urea), affinity chromatography, ion exchange chromatography, and endotoxin removal. The enriched proteins were analyzed by SDS-PAGE (Silver stain) and Western blot, mass spectrometry, and N-terminal sequencing.

The kinase activity assay can be determined with a non-radioactive method for measuring the activity of kinases by quantifying the amount of ATP remaining in solution after the kinase reaction. It specifically determines the decrease in luminescence due to ATP consumption from the kinase catalyzed phosphorylation of tyrosine residues or cross-phosphorylation of the tyrosine kinase domains in insulin receptors. The cloned tyrosine kinase receptor's activity was first measured both with the protein in a buffer solution only, and also after incorporating the protein into lipid vesicles. The results showed that the kinase was slightly active in TBS without MgCl₂, which is expected as magnesium ions stabilize the negatively charged ATP (Figure 7.16). Even though the protein concentration was the same the kinase incorporated in vesicles was less

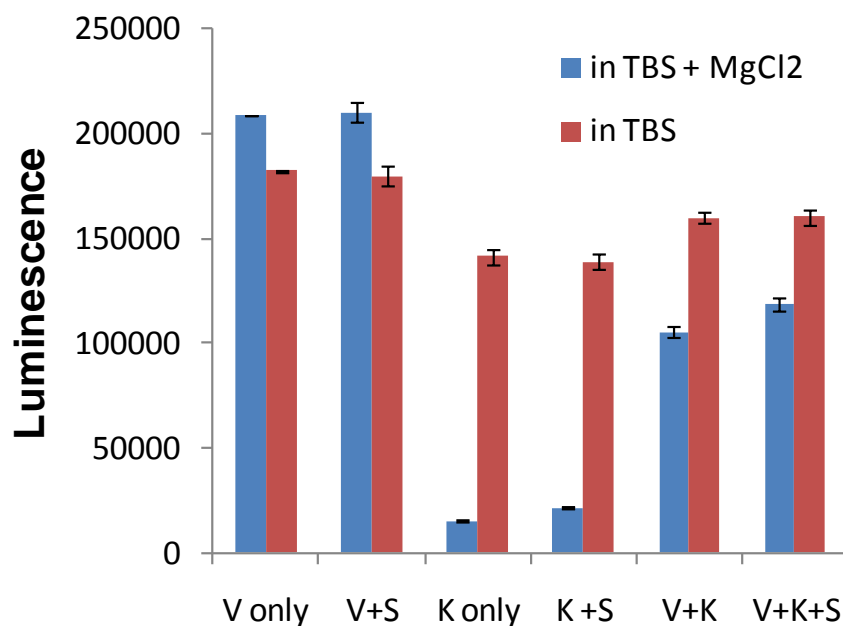


Figure 7.16. The tyrosine assay activity determined with the free protein (K only), vesicles with no protein (V only), and protein incorporated in vesicles (V+K). Kinase concentration in either case was 100 µg/mL. Assay was run in TBS with 1 µM ATP at 37 °C, with or without 10 mM MgCl₂. 'S' represents addition of substrate to the reaction mixture.

active. This could indicate that some of the proteins are deactivated during the process of insertion in vesicles. Also, the substrate did not decrease ATP concentration or luminescence, thus showing that the protein could be already dimerized and thus could not undergo multiple turnovers, meaning cross-phosphorylation happens faster (or is more favored) than phosphorylation of the substrate due to the protein existing as a dimer. Other trials confirmed that the kinase did not consume more ATP in the presence of substrate and that kinase inserted in vesicles was less active than free kinase, as shown in Figure 7.17. In addition, the amount of ATP consumed follows closely the kinase concentration (Table 7.5).

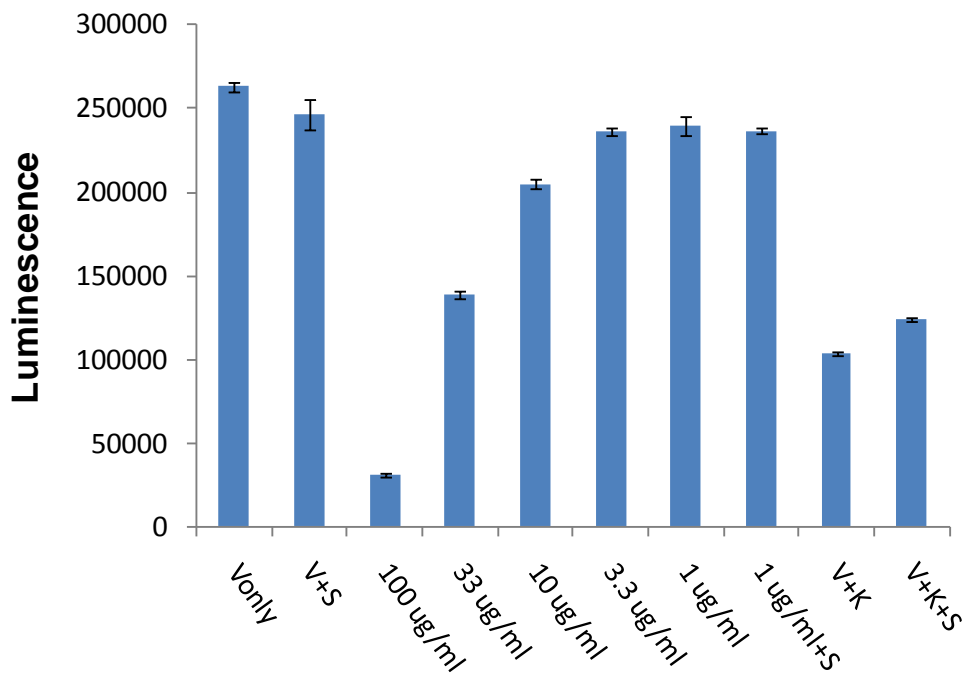


Figure 7.17.

The tyrosine assay activity determined with the free protein (concentrations given on the x-axis), vesicles with no protein (V only), and protein incorporated in vesicles (V+K). Kinase concentration in V+K was 100 $\mu\text{g}/\text{mL}$. Assay was run in TBS with 10 mM MgCl_2 and 1 μM ATP at 37 $^\circ\text{C}$. 'S' represents addition of substrate to the reaction mixture.

Table 7.5. Luminescence decrease and ATP consumption for the kinase concentrations used in

Figure 7.17 (from 100 – 3.3 $\mu\text{g/mL}$). The values clearly show that the amount of ATP used matches the amounts of kinase present, assuming one phosphorylation per kinase. The molecular weight of the tyrosine kinase construct is 58,134 Da.

K conc. ($\mu\text{g/mL}$)	100	33	10	3.3
K conc. (μM)	1.7	0.57	0.17	0.057
1 μM ATP used	87%	44%	17%	4%

Since the expected amount of tyrosine kinase on the 1 cm^2 substrate surfaces was approximately $1\ \mu\text{g}$ or $20\ \text{pmol}$, assuming the slide was dipped in $1\ \text{mL}$ solution, then the kinase activity on the surface would be similar to that of $1\ \mu\text{g/mL}$ or $17\ \text{nM}$ kinase in solution. Therefore a calibration of the free kinase was carried out in $10\ \text{nM}$ ATP to test the detection limit of the luminescence assay (Figure 7.18). The $10\ \text{nM}$ ATP concentration was chosen due to the previous results showing that the tyrosine kinase undergoes one turnover and thus the concentration of ATP has to be in the same range as that of the kinase in order to be able to detect the kinase activity. The kinase assay showed a 15% decrease in luminescence for $1.5\ \mu\text{g/mL}$ kinase concentration in the presence of $10\ \text{nM}$ ATP, therefore concentrations as low as $1\ \mu\text{g/mL}$ of tyrosine kinase can be detected with the luminescence assay.

Before attempting to measure the activity of the tyrosine kinase on the surface, the activity of the free kinase was compared to that incorporated in vesicles at $15\ ^\circ\text{C}$ and $37\ ^\circ\text{C}$. If the kinase is

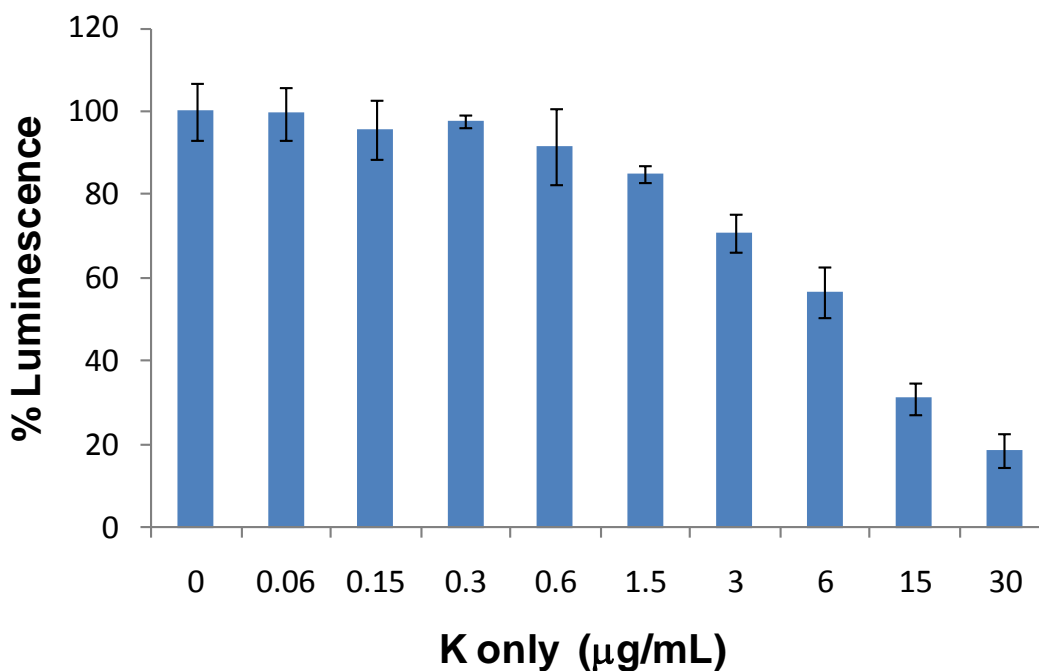


Figure 7.18. The tyrosine assay activity determined with the free protein (K only). Assay was run in TBS with 10 mM MgCl₂ and 10 nM ATP at 37 °C.

inserted in the membrane through its hydrophobic part than its activity would be affected from the temperature, since the phase transition of the DMPC vesicles is 23 °C (Figure 7.19). At 15 °C the vesicles would be in the gel phase and thus protein folding would be more difficult, whereas at 37 °C, when the vesicles are in the liquid phase, the protein would be free to fold during dimerization and/or phosphorylation. The results showed that the incorporated kinase activity was affected by temperature, and as expected, it was more active at 37 °C. However the activity of V+K was approximately only 10% higher at 37 °C compared to 15 °C. This would be consistent with the assumption that some of the tyrosine kinases are not active and can't undergo phosphorylation after their insertion in vesicles, as observed in this assay and previous assays.

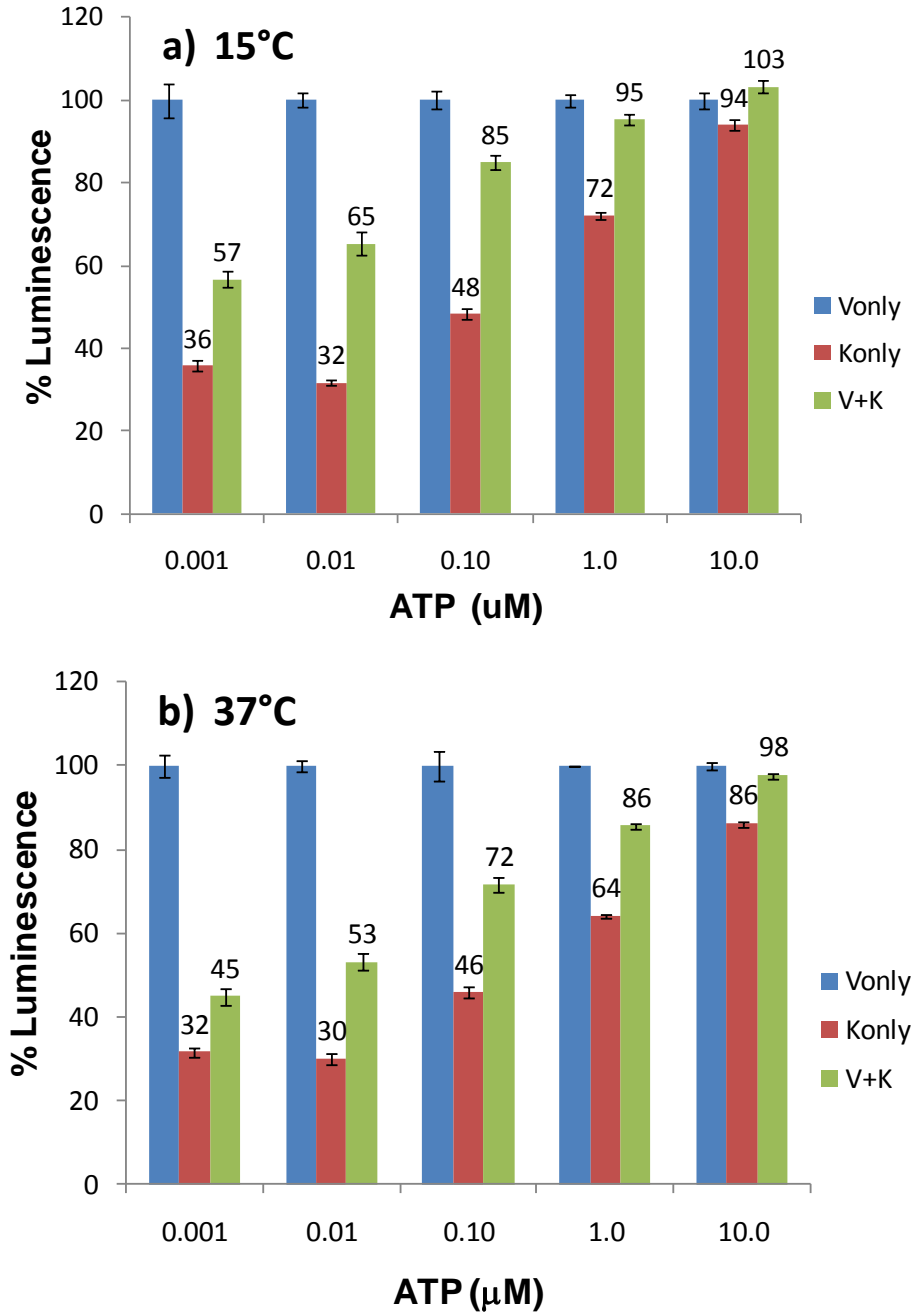


Figure 7.19. The tyrosine assay activity determined with no kinase in solution (**V only**), the free protein (**K only**) and the protein incorporated in vesicles (**V+K**) at different temperatures. Protein concentration for **K only** and **V+K** was 10 μg/mL. Assay was run in triplicate in TBS with 10 mM MgCl₂ and different ATP concentrations at: a) 15 °C and b) 37 °C. The error bar represents the standard deviation of the triplicate measurements. The luminescence result for **K only** and **V+K** were normalized with the **Vonly** measurements. The activity of the free kinase (**K only**) was not affected by temperature, whereas the activity of the kinase in vesicles was clearly affected by temperature at the lower ATP concentrations.

7.5.3. One-step formation of a membrane-like surface by self-assembly using a thiol-modified phospholipid.

The artificial membranes made in this work showed that they were valid substrates for the incorporation of lipid-anchored membrane proteins and possibly trans-membrane proteins. However, they required a two-step formation method (SAM formation followed by incubation in vesicle solution) and afterwards an elaborate and long rinsing method in order not to keep the surface submerged in buffer during the whole time, including after the incorporation of the AChE enzyme. These types of membranes would be impractical to be used for real applications and stored for long time periods. In the experiment involving the formation of bilayer membranes on hydrophilic SAMs (see Section 7.3.5) it was mentioned that some enzyme activity was observed when the MUA and AUT SAMs were exposed to the AChE solution. Since the ODT SAM exposed to AChE did not show any activity and electrochemical impedance measurements suggested that the MUA SAM is more disorganized than the ODT SAM, it is possible that some AChE enzymes were able to insert their hydrophobic tails into the MUA and AUT SAMs. These SAMs can be viewed as a lipid monolayer with their charged terminal group polar head acting as the polar head and the alkyl chain as the acyl chains of the lipid (Figure 7.20A).

From the other point of view, a phospholipid such as DMPC is similar in the overall structure to an alkane thiol, such as MUA, with a rather large hydrophilic terminal group and two hydrophobic alkyl chains instead of one. The synthesis of phospholipids modified with thiols at the end of the acyl groups has been reported in the literature.¹⁹¹ This thiol-modified lipid (thiolipid) can be used to form a monolayer by dipping gold slides in an ethanol solution of the

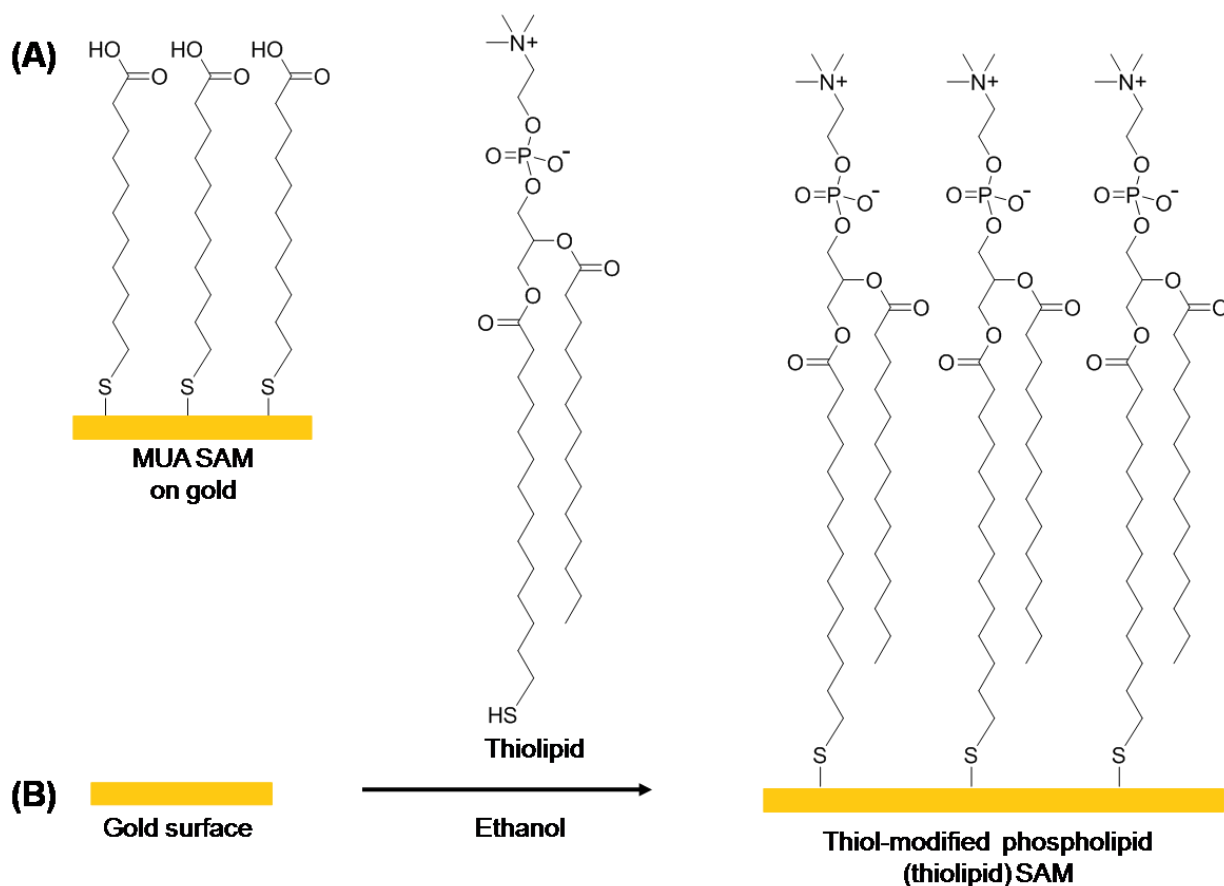


Figure 7.20. Strategy for the formation of a phospholipid self-assembled monolayer on gold. (A) Schematic drawing of MUA SAM on gold. (B) A thiol-modified phospholipid (thiolipid) is synthesized containing a thiol group at the end of one of the acyl chains. A solution of the thiolipid in ethanol is used to form a self-assembled monolayer on gold surfaces, similar to alkanethiol monolayers. The presence of the polar head would ensure that the packing of the hydrophobic acyl chains would be similar to those on hybrid and bilayer membranes.

thiolipid (Figure 7.20B). Modification in only one of the acyl chains is expected to allow the thiolipids and the monolayer overall to be more fluid, compared to both acyl groups linking to the gold surface with thiol groups. This method has three advantage points compared to other methods for making artificial membranes: (1) it requires only one step for membrane preparation; (2) the thiolipid film would be stable if exposed to air, and (3) the surface would be

stable for a long time periods, in terms of shelf storage. The thiolipid SAM would be easily applied to high-throughput screening and detection systems. Using longer acyl chains could potentially allow for incorporation of integral membrane proteins with long trans-membrane regions that span both leaflets of the cell membrane.

8. Final Conclusions

The work described in this dissertation has showed the successful modification of surfaces with direct applications in biosensors, surface control, and product manufacturing. Surface control refers to the development of bio-compatible and bio-mimicking surfaces that will be used to couple biological systems to artificial materials or *vice versa*. Product manufacturing refers to the development of a flow-through bioreactor that will be used for the continuous production of pharmaceuticals, biofuels and generation of tissue and more complex structures.

The immobilization of DNA oligonucleotides on the gold surface, while still maintaining their ability to hybridize allowed for the construction of a SPR-based nucleic acid sensor capable of detecting DNA and RNA sequences. The sensor was able to detect single nucleotide mismatches in 21-base long synthetic DNA sequences at various concentrations. The sensor was reusable and its ability to detect mismatches was not affected over a wide range in buffer concentration, flow rate and temperature. This will allow for the detection of single nucleotide mismatches in genomic DNA amplified by asymmetric PCR and treated with restriction nucleases.

The same SPR-based sensor, but coupled with an enzyme, was used for the detection of pharmaceutical drugs (or inhibitors) that are used to treat muscle weakness and Alzheimer's disease symptoms. Besides the potential to be used as a high-throughput screening platform for similar drugs, this result also showed that our biosensor is detecting changes in conformation of the enzyme rather than detecting the mass binding of the inhibitors.

The ability to detect changes in conformation of proteins via a real-time sensing platform such as SPR has great potential in the high-throughput screening of drug candidates for membrane proteins or receptors, such as tyrosine kinases. This will be achieved by generating artificial phospholipid membranes and coupling them with the SPR sensor. To show this ability, hybrid lipid membranes (containing one leaflet) and bilayer lipid membranes (containing two leaflets) were generated on gold slides, and both were capable of hosting a lipid anchored membrane protein and maintain its activity.

Bio-mimetic surface were formed on gold and glass substrates that were capable of favoring or preventing adhesion of proteins, bacterial cells, and/or mammalian cells to these modified surfaces. Several synthetic compounds were screened on glass substrates to find a replacement for traditional coatings such as collagen. An alkoxysilane terminating with a diamine ethylene linked to the surface via an 11 carbon chain showed a remarkable ability in favoring the attachment, growth and differentiation of Neuroscreen-1 cells on both glass and polystyrene substrates. By using a combination of this coating and a coating with the opposite affect patterned surfaces were generated, which resulted in cells growing on the desired pattern. With regard to neuronal growth and differentiation on patterned surfaces, this ability will lead to the development of interfaces that will accommodate neuroprosthetic devices.

A similar goal is behind the development of a flow through bioreactor containing a magnetic support that will be used for generation of tissue and eventually organs, as it provides a three-dimensional environment for cell growth. Magnetic agarose beads, which will provide the magnetic support in the bioreactor, were successfully formed and the ability to modify their

surface and immobilize cells on them was also shown. The same beads have the potential to be used in trapping mammalian, yeast, or bacterial cells in order to continuously collect the desired product, without the need to shut down the bioreactor and reseed it with cells.

9. REFERENCES

- (1) Rodriguez-Mozaz, S.; Lopez de Alda, M. J.; Marco, M.-P.; Barcelo, D. *Talanta* **2005**, *65*, 291-297.
- (2) Whitesides, G. M.; Grzybowski, B. *Science* **2002**, *295*, 2418-2421.
- (3) Gaines, G. L. *Insoluble Monolayers at Liquid-Gas Interfaces*; Interscience Publishers: New York, 1966.
- (4) Adamson, A. W. G., A. P. *Physical Chemistry of Surfaces, 6th ed.*; Wiley-Interscience: New York, **1997**.
- (5) Nuzzo, R. G.; Allara, D. L. *J. Am. Chem. Soc.* **1983**, *105*, 4481-4483.
- (6) Love, J. C.; Estroff, L. A.; Kriebel, J. K.; Nuzzo, R. G.; Whitesides, G. M. *Chem. Rev.* **2005**, *105*, 1103-1169.
- (7) Wang, H.; Chen, S.; Li, L.; Jiang, S. *Langmuir* **2005**, *21*, 2633-2636.
- (8) Klotz, I. M. *Methods Enzymol.* **1967**, *11*, 576-580.
- (9) Plotz, P. H.; Rifai, A. *Biochemistry* **1982**, *21*, 301-308.
- (10) Brunswick, M.; Finkelman, F. D.; Highet, P. F.; Inman, J. K.; Dintzis, H. M.; Mond, J. J. *J. Immunol.* **1988**, *140*, 3364-3372.
- (11) Chechik, V.; Stirling, C. J. M. *The chemistry of organic derivatives of gold and silver*; John Wiley & Sons: New York, 1999.
- (12) Douglass, E. F., Jr.; Driscoll, P. F.; Liu, D.; Burnham, N. A.; Lambert, C. R.; McGimpsey, W. G. *Anal. Chem.* **2008**, *80*, 7670-7677.
- (13) HapMap *Nature* **2003**, *426*, 789-796
- (14) King, R. A.; Rotter, J. I.; Motulsky, A. G. *The Genetic Basis of Common Diseases Vol. 20*; Oxford Univ. Press: Oxford, 1992.
- (15) HapMap *Nature* **2005**, *437*, 1299-1320
- (16) The International HapMap Project website: <http://www.hapmap.org>.
- (17) The Pharmacogenetics and Pharmacogenomics Knowledge Base (PharmGKB) website: <http://www.pharmgkb.org>.
- (18) Moulin, G. *Rev Sci Technol.* **2005**, *24*, 101-107.
- (19) Grishok, A.; Pasquinelli, A. E.; Conte, D.; Li, N.; Parrish, S.; Ha, I.; Baillie, D. L.; Fire, A.; Ruvkun, G.; Mello, C. C. *Cell* **2001**, *106*, 23-34.

- (20) Hwang, H. W.; Mendell, J. T. *Br. J. Cancer* **2006**, *94*, 776-780.
- (21) Lee, R. C.; Feinbaum, R. L.; Ambros, V. *Cell* **1993**, *75*, 843-854.
- (22) Cissell, K. A.; Shrestha, S.; Deo, S. K. *Anal. Chem.* **2007**, *79*, 4754-4761.
- (23) Homola, J. *Anal. Bioanal. Chem.* **2003**, *377*, 528-539.
- (24) Kukanskis, K.; Elkind, J.; Melendez, J.; Murphy, T.; Miller, G.; Garner, H. *Anal. Biochem.* **1999**, *274*, 7-17.
- (25) Van der Merwe, P. A. *Surface Plasmon Resonance in Protein-Ligand Interactions: Hydrodynamics and Calorimetry*; Oxford University Press, 2001.
- (26) Schuck, P. *Annu. Rev. Biophys. Biomol. Struct.* **1997**, *26*, 541-566.
- (27) Miura, N.; Ogata, K.; Sakai, G.; Uda, T.; Yamazoe, N. *Chem. Lett.* **1997**, 713-714.
- (28) Minunni, M.; Mascini, M. *Anal. Lett.* **1993**, *26*, 1441-1460.
- (29) Koubova, V.; Brynda, E.; Karasova, L.; Skvor, J.; Homola, J.; Dostalek, J.; Tobiska, P.; Rosicky, J. *Sens. Actuators B* **2001**, *B74*, 100-105.
- (30) Drummond, T. G.; Hill, M. G.; Barton, J. K. *Nat. Biotechnol.* **2003**, *21*, 1192-1199.
- (31) Homola, J.; Yee, S. S.; Gauglitz, G. *Sens. Actuators B* **1999**, *B54*, 3-15.
- (32) Beattie, K. L.; Beattie, W. G.; Meng, L.; Turner, S. L.; Coral-Vazquez, R.; Smith, D. D.; McIntyre, P. M.; Dao, D. D. *Clin. Chem.* **1995**, *41*, 700-706.
- (33) Jin, W.; Lin, X.; Lv, S.; Zhang, Y.; Jin, Q.; Mu, Y. *Biosens. Bioelectron.* **2009**, *24*, 1266-1269.
- (34) Ladd, J.; Taylor, A. D.; Piliarik, M.; Homola, J.; Jiang, S. *Anal. Chem.* **2008**, *80*, 4231-4236.
- (35) Kai, E.; Sawata, S.; Ikebukuro, K.; Iida, T.; Honda, T.; Karube, I. *Anal. Chem.* **1999**, *71*, 796-800.
- (36) Persson, B.; Stenhag, K.; Nilsson, P.; Larsson, A.; Uhlen, M.; Nygren, P.-A. *Anal. Biochem.* **1997**, *246*, 34-44.
- (37) Yang, N.; Su, X.; Tjong, V.; Knoll, W. *Biosens. Bioelectron.* **2007**, *22*, 2700-2706.
- (38) Mark, S. S.; Sandhyarani, N.; Zhu, C.; Campagnolo, C.; Batt, C. A. *Langmuir* **2004**, *20*, 6808-6817.
- (39) Vaisocherova, H.; Zitova, A.; Lachmanova, M.; Stepanek, J.; Kralikova, S.; Liboska, R.; Rejman, D.; Rosenberg, I.; Homola, J. *Biopolymers* **2006**, *82*, 394-398.

- (40) Nelson, B. P.; Grimsrud, T. E.; Liles, M. R.; Goodman, R. M.; Corn, R. M. *Anal. Chem.* **2001**, *73*, 1-7.
- (41) He, L.; Musick, M. D.; Nicewarner, S. R.; Salinas, F. G.; Benkovic, S. J.; Natan, M. J.; Keating, C. D. *J. Am. Chem. Soc.* **2000**, *122*, 9071-9077.
- (42) Nabok, A.; Tsargorodskaya, A.; Davis, F.; Higson, S. P. J. *Biosens. Bioelectron.* **2007**, *23*, 377-383.
- (43) Nabok, A.; Tsargorodskaya, A.; Gauthier, D.; Davis, F.; Higson, S. P. J.; Berzina, T.; Cristofolini, L.; Fontana, M. P. *J. Phys. Chem. B* **2009**, *113*, 7897-7902.
- (44) Nakatani, K.; Kobori, A.; Kumasawa, H.; Saito, I. *Bioorg. Med. Chem. Lett.* **2004**, *14*, 1105-1108.
- (45) Hagihara, S.; Kumasawa, H.; Goto, Y.; Hayashi, G.; Kobori, A.; Saito, I.; Nakatani, K. *Nucleic Acids Res.* **2004**, *32*, 278-286.
- (46) Jiang, T.; Minunni, M.; Wilson, P.; Zhang, J.; Turner, A. P. F.; Mascini, M. *Biosens. Bioelectron.* **2005**, *20*, 1939-1945.
- (47) Tawa, K.; Knoll, W. *Nucleic Acids Res.* **2004**, *32*, 2372-2377.
- (48) Dell'Atti, D.; Tombelli, S.; Minunni, M.; Mascini, M. *Biosens. Bioelectron.* **2006**, *21*, 1876-1879.
- (49) Cai, H.; Lee, T. M.-H.; Hsing, I. M. *Sens. Actuators B* **2006**, *B114*, 433-437.
- (50) Gong, P.; Lee, C.-Y.; Gamble Lara, J.; Castner David, G.; Grainger David, W. *Anal. Chem.* **2006**, *78*, 3326-3334.
- (51) Peterson, A. W.; Heaton, R. J.; Georgiadis, R. M. *Nucleic Acids Res* **2001**, *29*, 5163-5168.
- (52) Wong, E. L. S.; Mearns, F. J.; Gooding, J. J. *Sens. Actuators B* **2005**, *B111-B112*, 515-521.
- (53) Herne, T. M.; Tarlov, M. J. *J. Am. Chem. Soc.* **1997**, *119*, 8916-8920.
- (54) Ito, T.; Hosokawa, K.; Maeda, M. *Biosens. Bioelectron.* **2007**, *22*, 1816-1819.
- (55) Randles, J. E. B. *Discuss. Faraday Soc.* **1947**, *No. 1*, 11-19.
- (56) Park, S.-M.; Yoo, J.-S. *Anal. Chem.* **2003**, *75*, 455A-461A.
- (57) Katz, E.; Willner, I. *Electroanalysis* **2003**, *15*, 913-947.
- (58) Macdonald, J. R. *Impedance Spectroscopy*; Wiley/Interscience: New York, 1987.
- (59) Bardea, A.; Katz, E.; Willner, I. *Electroanalysis* **2000**, *12*, 1097-1106.

- (60) Savitri, D.; Mitra, C. K. *Bioelectrochem. Bioenerg.* **1999**, *48*, 163-169.
- (61) Patolsky, F.; Lichtenstin, A.; Willner, I. *Nat. Biotechnol.* **2001**, *19*, 253-257.
- (62) Long, Y.-T.; Li, C.-Z.; Sutherland, T. C.; Kraatz, H.-B.; Lee, J. S. *Anal. Chem.* **2004**, *76*, 4059-4065.
- (63) Liu, J.; Tian, S.; Nielsen, P. E.; Knoll, W. *Chem. Commun.* **2005**, 2969-2971.
- (64) Gautier, C.; Cougnon, C.; Pilard, J.-F.; Casse, N.; Chenais, B.; Lauhier, M. *Biosens. Bioelectron.* **2007**, *22*, 2025-2031.
- (65) Li, A.; Yang, F.; Ma, Y.; Yang, X. *Biosens. Bioelectron.* **2007**, *22*, 1716-1722.
- (66) Paproth, A.; Wolter, K.-J.; Herzog, T.; Zerna, T., Calimanesti-Caciulata, Romania, May 5-9, 2001.
- (67) Erickson, D.; Li, D.; Krull Ulrich, J. *Anal. Biochem.* **2003**, *317*, 186-200.
- (68) Okahata, Y.; Kawase, M.; Niikura, K.; Ohtake, F.; Furusawa, H.; Ebara, Y. *Anal. Chem.* **1998**, *70*, 1288-1296.
- (69) Park, H.; Germini, A.; Sforza, S.; Corradini, R.; Marchelli, R.; Knoll, W. *Biointerphases* **2007**, *2*, 80-88.
- (70) Yamasaki, R.; Kim, J.; Jung, H.; Lee, H.; Kawai, T. *Biochem. Eng. J.* **2006**, *29*, 125-128.
- (71) Lenigk, R.; Liu, R. H.; Athavale, M.; Chen, Z.; Ganser, D.; Yang, J.; Rauch, C.; Liu, Y.; Chan, B.; Yu, H.; Ray, M.; Marrero, R.; Grodzinski, P. *Anal. Biochem.* **2002**, *311*, 40-49.
- (72) Noerholm, M.; Bruus, H.; Jakobsen, M. H.; Telleman, P.; Ramsing, N. B. *Lab Chip* **2004**, *4*, 28-37.
- (73) Yuen, P. K.; Li, G.; Bao, Y.; Mueller, U. R. *Lab Chip* **2003**, *3*, 46-50.
- (74) Bishop, J.; Blair, S.; Chagovetz, A. *Biosens. Bioelectron.* **2007**, *22*, 2192-2198.
- (75) Bloomfield, V. A.; Crothers, D. M.; Tinoco, I. *Nucleic Acids - Structures, Properties, and Functions*; University Science Books: Sausalito, CA, 2000.
- (76) Thiel, A. J.; Frutos, A. G.; Jordan, C. E.; Corn, R. M.; Smith, L. M. *Anal. Chem.* **1997**, *69*, 4948-4956.
- (77) Fiche, J. B.; Buhot, A.; Calemczuk, R.; Livache, T. *Biophys. J.* **2007**, *92*, 935-946.
- (78) Levicky, R.; Horgan, A. *Trends Biotechnol.* **2005**, *23*, 143-149.
- (79) Stenberg, E.; Persson, B.; Roos, H.; Urbaniczky, C. *J. Colloid Interface Sci.* **1991**, *143*, 513-526.
- (80) Vainrub, A.; Pettitt, B. M. *Phys. Rev. E* **2002**, *66*, 041905/041901-041905/041904.

- (81) Vainrub, A.; Pettitt, B. M. *J. Am. Chem. Soc.* **2003**, *125*, 7798-7799.
- (82) Wang, R.; Minunni, M.; Tombelli, S.; Mascini, M. *Biosens. Bioelectron.* **2004**, *20*, 598-605.
- (83) Zuo, L.; van Dyck, C. H.; Luo, X.; Kranzler, H. R.; Yang, B.-z.; Gelernter, J. *Behav. Brain Funct.* **2006**, *2*, No pp given.
- (84) Brunton, L. B.; LazoJohn, J. S. a. K. L.; Parker, K. L. *Goodman & Gilman's The Pharmacological Basis of Therapeutics*, 2008.
- (85) Schumacher, M.; Camp, S.; Maulet, Y.; Newton, M.; MacPhee-Quigley, K.; Taylor, S. S.; Friedmann, T.; Taylor, P. *Nature* **1986**, *319*, 407-409.
- (86) Sussman, J. L.; Harel, M.; Frolow, F.; Oefner, C.; Goldman, A.; Toker, L.; Silman, I. *Science* **1991**, *253*, 872-879.
- (87) Froede, H. C.; Wilson, I. B. *Enzymes, 3rd Ed.* **1971**, *5*, 87-114.
- (88) Summers, W. K.; Majovski, L. V.; Marsh, G. M.; Tachiki, K.; Kling, A. *N. Engl. J. Med.* **1986**, *315*, 1241-1245.
- (89) Giacobini, E.; Cuadra, G. *Alzheimer Dis.* **1994**, 155-171.
- (90) Fambrough, D. M.; Drachman, D. B.; Satyamurti, S. *Science* **1973**, *182*, 293-295.
- (91) Katzman, R.; Jackson, J. E. *J. Am. Geriatr. Soc.* **1991**, *39*, 516-525.
- (92) Ellman, G. L.; Courtney, K. D.; Andres, V., Jr.; Featherstone, R. M. *Biochem. Pharmacol.* **1961**, *7*, 88-95.
- (93) Moris, P.; Alexandre, I.; Roger, M.; Remacle, J. *Anal. Chim.* **1995**, *302*, 53-59.
- (94) Roda, A.; Rauch, P.; Ferri, E.; Girotti, S.; Ghini, S.; Carrea, G.; Bovara, R. *Anal. Chim. Acta* **1994**, *294*, 35-42.
- (95) Guenther, A.; Bilitewski, U. *Anal. Chim. Acta* **1995**, *300*, 117-125.
- (96) Flentge, F.; Venema, K.; Koch, T.; Korf, J. *Anal. Biochem.* **1992**, *204*, 305-310.
- (97) Whitesides, G. M.; Ostuni, E.; Takayama, S.; Jiang, X.; Ingber, D. E. *Annu. Rev. Biomed.* **2001**, *3*, 335-373.
- (98) Li, X.-M.; Huskens, J.; Reinhoudt, D. N. *J. Mater. Chem.* **2004**, *14*, 2954-2971.
- (99) Ferretti, S.; Paynter, S.; Russell, D. A.; Sapsford, K. E.; Richardson, D. J. *Trends Anal. Chem.* **2000**, *19*, 530-540.
- (100) Lahiri, J.; Isaacs, L.; Grzybowski, B.; Carbeck, J. D.; Whitesides, G. M. *Langmuir* **1999**, *15*, 7186-7198.

- (101) Patel, N.; Davies, M. C.; Hartshorne, M.; Heaton, R. J.; Roberts, C. J.; Tendler, S. J. B.; Williams, P. M. *Langmuir* **1997**, *13*, 6485-6490.
- (102) Bain, C. D.; Whitesides, G. M. *Langmuir* **1989**, *5*, 1370-1378.
- (103) Creager, S. E.; Clarke, J. *Langmuir* **1994**, *10*, 3675-3683.
- (104) Driscoll, P. F.; Milkani, E.; Lambert, C. R.; McGimpsey, W. G. *Langmuir*, *26*, 3731-3738.
- (105) Darder, M.; Takada, K.; Pariente, F.; Lorenzo, E.; Abruna, H. D. *Anal. Chem.* **1999**, *71*, 5530-5537.
- (106) Darder, M.; Casero, E.; Pariente, F.; Lorenzo, E. *Anal. Chem.* **2000**, *72*, 5753.
- (107) Wilson, I. B.; Harrison, M. A.; Ginsburg, S. *J. Biol. Chem.* **1961**, *236*, 1498-1500.
- (108) Ariel, N.; Ordentlich, A.; Barak, D.; Bino, T.; Velan, B.; Shafferman, A. *Biochem. J.* **1998**, *335*, 95-102.
- (109) Elwing, H. *Biomaterials* **1998**, *19*, 397-406.
- (110) Costerton, J. W.; Geesey, G. G.; Cheng, G. K. *Sci. Am.* **1978**, *238*, 86-95
- (111) Costerton, J. W.; Lewandowski, Z.; Caldwell, D. E.; Korber, D. R.; M., L.-S. H. *Annu. Rev. Microbiol.* **1995**, *49*, 711-745.
- (112) Anwar, H.; Costerton, J. *ASM News* **1992**, *58*, 665-668.
- (113) Donlan, R. M.; Costerton, J. W. *Clin. Microbiol. Rev.* **2002**, *15*, 167-193.
- (114) www.uweb.engr.washington.edu/research/tutorials/introbiomat.html.
- (115) The Williams dictionary of Biomaterials, D. W., 1999.
- (116) Chen, X.; Stewart, P. S. *Microbiol. Biotechnol.* **2002**, *59*, 718-720.
- (117) Mayer, C.; Moritz, R.; Kirschner, C.; Borchard, W.; Maibaum, R.; Wingender, J.; Flemming, H. C. *Int. J. Biol. Macromol.* **1999**, *26*, 3-16.
- (118) Pasmore, M.; Costerton, J. W. *J. Ind. Microbiol. Biotechnol.* **2003**, *30*, 407-413.
- (119) Davies, D. G.; Geesey, G. G. *Appl. Environ. Microbiol.* **1995**, *61*, 860-867.
- (120) Dunne, M. W. *Clin. Microbiol. Rev.* **2002**, *15*, 155-166.
- (121) Maki, D. G. *Ann. Intern. Med.* **1994**, *127*, 257-266.
- (122) Raad, I. *Lancet* **1998**, *351*, 893-898.
- (123) Stewart, P. S.; William Costerton, J. *Lancet* **2001**, *358*, 135-138.
- (124) Hojo, S.; Komatsu, M.; Okuda, R.; Takahashi, N.; Yamada, T. *J. Den. Res.* **1994**, *73*, 1853-1857.

- (125) Perea, E. *Int. J. Antimicrob. Agents* **2001**, *18*, S29.
- (126) Drenkard, E.; Ausubel, F. M. *Nature* **2002**, *416*, 740-743.
- (127) Gilbert, P. *Adv. Microb. Physiol.* **2002**, *46*, 202.
- (128) <http://www.altcorp.com/AffinityLaboratory/biofilms.htm>.
- (129) Anaissie, E.; Samonis, G.; Kontoyiannis, D.; Costerton, J.; Sabharwal, U.; Bodey, G.; Raad, I. *Eur. J. Clin. Microbiol. Infect. Dis.* **1995**, *14*, 135-137.
- (130) Raad, I. *Lancet* **1998**, *351*, 893-898
- (131) Stickler, D. J. *Biofouling* **1996**, *94*, 293-305.
- (132) Tunney, M. M.; Jones, D. S.; Gorman, S. P. *Methods Enzymol.* **1999**, *310*, 558-566.
- (133) Gristina, A. G. *Science (Washington, DC, United States)* **1987**, *237*, 1588-1595.
- (134) Bach, A.; Darby, D.; Bottiger, B.; Bohrer, H.; Motsch, J.; Martin, E. *Int. Care Med.* **1996**, *22*, 1066-1069.
- (135) Becker, R. O. *Met.-based Drugs* **1999**, *6*, 297-300.
- (136) Silver, S. *FEMS Microbiol. Rev.* **2003**, *27*, 341-353.
- (137) Fukai, R.; Dakwa, P. H. R.; Chen, W. J. *Polym Sci., Part A: Polym Chem* **2004**, *42*, 5389-5400.
- (138) Prime, K. L.; Whitesides, G. M. *Science (Washington, DC, United States)* **1991**, *252*, 1164-1167.
- (139) Mrksich, M.; Sigal, G. B.; Whitesides, G. M. *Langmuir* **1995**, *11*, 4383-4385.
- (140) Carpenter, C. F.; Chambers, H. F. *Clin. Infect. Dis.* **2004**, *38*, 994-1000.
- (141) Silverman, J. A.; Perlmutter, N. G.; Shapiro, H. M. *Antimicrob. Agents Chemother* **2003**, *47*, 2538-2544.
- (142) The growth curve was determined by Yatao Liu, Department of Chemical Engineering, Worcester Polytechnic Institute.
- (143) Handbook of fluorescent probes and research chemicals, Molecular Probes.
- (144) Courtesy of Stephen Heard, M.D., Department of Anesthesiology, UMass Medical School, Worcester, MA.
- (145) Roszak, D. B.; Colwell, R. R. *Microbiol. Rev.* **1987**, *51*, 365.
- (146) Kumamoto, C. A.; Vines, M. D. *Annu. Rev. Microbiol.* **2005**, *59*, 113-133.
- (147) Gudlaugsson, O.; Gillespie, S.; Lee, K.; Vande Berg, J.; Hu, J.; Messer, S.; Herwaldt, L.; Pfaller, M.; Diekema, D. *Clin. Infect. Dis.* **2003**, *37*, 1172-1177.

- (148) Kojic Erna, M.; Darouiche Rabih, O. *Clin. Microbiol. Rev.* **2004**, *17*, 255-267.
- (149) Terrell, C. L.; Hughes, C. E. *Mayo Clin. Proc. Mayo Clinic* **1992**, *67*, 69-91.
- (150) Waters, C. M.; Bassler, B. L. *Ann. Rev. Cell Dev. Biol.* **2005**, *21*, 319-346.
- (151) Camilli, A.; Bassler, B. L. *Science (Washington, DC, United States)* **2006**, *311*, 1113-1116.
- (152) Manefield, M.; Rasmussen, T. B.; Henzter, M.; Andersen, J. B.; Steinberg, P.; Kjelleberg, S.; Givskov, M. *Microbiology (Reading, United Kingdom)* **2002**, *148*, 1119-1127.
- (153) Novick, R. P. *Mol. Microbiol.* **2003**, *48*, 1429-1449.
- (154) Goddard, J. M.; Hotchkiss, J. H. *Prog. Polym. Sci.* **2007**, *32*, 698-725.
- (155) Elsdale, T.; Bard, J. J. *Cell Biol.* **1972**, *54*, 626-637.
- (156) Griffith, L. G.; Swartz, M. A. *Nat. Rev. Mol. Cell Biol.* **2006**, *7*, 211-224.
- (157) Atala, A. *J. Tissue Eng. Regen. Med.* **2007**, *1*, 83-96.
- (158) Dutta, R. C.; Dutta, A. K. *Biotechnol. Adv.* **2009**, *27*, 334-339.
- (159) Hristov, J.; Ivanova, V. *Recent Res. Dev. Ferment. Bioeng.* **1999**, *2*, 41-94.
- (160) Hillebrandt, H.; Tanaka, M. *J. Phys. Chem. B* **2001**, *105*, 4270-4276.
- (161) Besbes, S.; Ben Ouada, H.; Davenas, J.; Ponsonnet, L.; Jaffrezic, N.; Alcouffe, P. *Mater. Sci. Eng. C* **2006**, *26*, 505-510.
- (162) Spector, D. L.; Goldman, R. D.; Leinwand, L. A. *Cells: Culture and Biochemical Analysis of cells*; Cold Spring harbor Laboratory Press, 2002.
- (163) Terstappen, G. C.; Reggiani, A. *Trends Pharmacol. Sci.* **2001**, *22*, 23-26.
- (164) Cooper, M. A. *J. Mol. Recognit.* **2004**, *17*, 286-315.
- (165) Rigaud, J.-L.; Pitard, B.; Levy, D. *Biochim. Biophys. Acta, Bioenerg.* **1995**, *1231*, 223-246.
- (166) McConnell, H. M.; Watts, T. H.; Weis, R. M.; Brian, A. A. *Biochim Biophys Acta* **1986**, *864*, 95-106.
- (167) Tero, R.; Takizawa, M.; Li, Y.-J.; Yamazaki, M.; Urisu, T. *Langmuir* **2004**, *20*, 7526-7531.
- (168) Mueller, P.; Rudin, D. O.; Tien, H. T.; Wescott, W. C. *Nature* **1962**, *194*, 979-980.
- (169) Szoka, F., Jr.; Papahadjopoulos, D. *Annu. Rev. Biophys. Bioeng.* **1980**, *9*, 467-508.
- (170) Reimhult, E.; Hooeok, F.; Kasemo, B. *Langmuir* **2003**, *19*, 1681-1691.
- (171) Plant, A. L. *Langmuir* **1993**, *9*, 2764-2767.

- (172) Ulman, A. *Chem. Rev.* **1996**, *96*, 1533-1554.
- (173) Plant, A. L. *Langmuir* **1999**, *15*, 5128-5135.
- (174) Keller, C. A.; Glasmaster, K.; Zhdanov, V. P.; Kasemo, B. *Phys. Rev. Lett.* **2000**, *84*, 5443-5446.
- (175) Batzri, S.; Korn, E. D. *Biochim. Biophys. Acta, Biomembr.* **1973**, *298*, 1015-1019.
- (176) Plant, A. L.; Gueguetchkeri, M.; Yap, W. *Biophys. J.* **1994**, *67*, 1126-1133.
- (177) Plant, A. L.; Brigham-Burke, M.; Petrella, E. C.; Oshannessy, D. J. *Anal. Biochem.* **1995**, *226*, 342-348.
- (178) Silvius, D. R. *Thermotropic Phase Transitions of Pure Lipids in Model Membranes and Their Modifications by Membrane Proteins.*; John Wiley & Sons, Inc.: New York, 1982.
- (179) Bain, C. D.; Troughton, E. B.; Tao, Y. T.; Evall, J.; Whitesides, G. M.; Nuzzo, R. G. *J. Am. Chem. Soc.* **1989**, *111*, 321-335.
- (180) Porter, M. D.; Bright, T. B.; Allara, D. L.; Chidsey, C. E. D. *J. Am. Chem. Soc.* **1987**, *109*, 3559-3568.
- (181) Peterlinz, K. A.; Georgiadis, R. *Langmuir* **1996**, *12*, 4731-4740.
- (182) Diao, P.; Jiang, D.; Cui, X.; Gu, D.; Tong, R.; Zhong, B. *Bioelectrochem. Bioenerg.* **1999**, *48*, 469-475.
- (183) Lingler, S.; Rubinstein, I.; Knoll, W.; Offenhaeusser, A. *Langmuir* **1997**, *13*, 7085-7091.
- (184) Ding, L.; Li, J.; Dong, S.; Wang, E. *J. Electroanal. Chem.* **1996**, *416*, 105-112.
- (185) Terrettaz, S.; Stora, T.; Duschl, C.; Vogel, H. *Langmuir* **1993**, *9*, 1361-1369.
- (186) Rao, N. M.; Plant, A. L.; Silin, V.; Wight, S.; Hui, S. W. *Biophys. J.* **1997**, *73*, 3066-3077.
- (187) Lewis, B. A.; Engelman, D. M. *J. Mol. Biol.* **1983**, *166*, 211-217.
- (188) Florin, E. L.; Gaub, H. E. *Biophys. J.* **1993**, *64*, 375-383.
- (189) Chan, R. Y. Y.; Jasmin, B. J. *Gene Ther. Mol. Biol.* **1999**, *3*, 347-354.
- (190) Yan, L.; Marzolin, C.; Terfort, A.; Whitesides, G. M. *Langmuir* **1997**, *13*, 6704-6712.
- (191) Fabianowski, W.; Coyle, L. C.; Weber, B. A.; Granata, R. D.; Castner, D. G.; Sadownik, A.; Regen, S. L. *Langmuir* **1989**, *5*, 35-41.